

LIGAND BINDING AND CATALYSIS IN SELECTED SIRTUIN ISOZYMES

A Dissertation  
Submitted to the Graduate Faculty  
of the  
North Dakota State University  
of Agriculture and Applied Science

By

Junru Yu

In Partial Fulfillment of the Requirements  
for the Degree of  
DOCTOR OF PHILOSOPHY

Major Department:  
Chemistry and Biochemistry

June 2016

Fargo, North Dakota

North Dakota State University  
Graduate School

---

**Title**

LIGAND BINDING AND CATALYSIS IN SELECTED SIRTUIN  
ISOZYMES

---

**By**

Junru Yu

---

The Supervisory Committee certifies that this *disquisition* complies with North Dakota State University's regulations and meets the accepted standards for the degree of

**DOCTOR OF PHILOSOPHY**

SUPERVISORY COMMITTEE:

D. K. Srivastava

---

Chair

Gregory Cook

---

Wenfang Sun

---

Lawrence Reynolds

---

Approved:

07/06/2016

---

Date

Gregory Cook

---

Department Chair

## ABSTRACT

Due to their intimate roles in survival, longevity as well as pathogenesis via “epigenetic” and “metabolic” regulatory mechanisms, sirtuins have gained considerable interest toward undertaking detailed biochemical/biophysical studies. The present study was designed to ascertain the mechanistic details of ligand binding and catalysis in selected sirtuin isozymes (viz., SIRT1 and SIRT5) from the point of view of designing isozyme selective inhibitors as potential therapeutics. By screening of the in-house synthesized compounds, two barbiturate derivatives were identified as the SIRT5 selective inhibitors. These, along with some of known inhibitors of SIRT1 and SIRT5, namely, MH5-75, nicotinamide, suramin were investigated by a combination of spectroscopic, kinetic, and thermodynamic techniques. The influence of the sirtuin inhibitors in modulating the structural features of the enzymes were ascertained by CD spectroscopic, lifetime fluorescence, and thermal denaturation studies using wild-type and selected site-specific mutant enzymes. The experimental data revealed that the substrate selectivity and inhibitory features in SIRT5 were manifested via the mutual cooperation between Y102 and R105 residues of the enzyme, and the overall catalytic feature of the enzyme was modulated by changes in the protein structure. Whereas the stoichiometry of SIRT1 to suramin remained invariant as 1:1, that of SIRT5 to suramin increased from 1:1 to 2:1 upon increase in the molar ratio of the enzyme to the ligand. A comparative account of the experimental data presented herein sheds light on the structural-functional differences SIRT1 and SIRT5, leading to the design of isozyme selective inhibitors as therapeutic tools for the treatment of sirtuin associated diseases.

## ACKNOWLEDGEMENTS

I am extremely thankful to many people for their support throughout the adventure of my Ph.D. I would like to first thank my advisor, Dr. D.K. Srivastava, for giving me the opportunity to obtain my degree in his lab. I am grateful for his mentorship and the time and energy he devoted to me so that I may be successful. I greatly admire his enthusiasm, discipline and attitude for research and hope I can emulate these traits in my future career.

I am grateful to my thesis advisory committee members, Dr. Gregory Cook, Dr. Wenfang Sun, and Dr. Lawrence Renoys for their guidance and generous support without which it would have been impossible to complete my graduate studies. I am particularly appreciative of the collaborations with the laboratories of Dr. Cook, Dr Yanki and Dr. Mallik, and members of their labs. I was fortunate to participate in numerous collaborative efforts throughout my thesis work and am grateful for the interactions I shared with other researchers.

I would like to thank the past and present members of DK's lab for their scientific insight, suggestions and friendship. I would especially like to thank former lab members Dr. Raushan Singh, Dr. Nitesh Sule and Ruchi Gupta for the training they provided. I have had the pleasure of mentoring Abbas Sedigh, Dustin Mueller, Joseph Omlid and Jerrod Strode, with whom many friendships developed in the past years. I am also grateful for having the opportunity to mentor former undergraduate Abby McGillivray who contributed to the effort of screening novel inhibitors for SIRT5, and is now pursuing her own PhD at University of Maryland.

Finally, Typesetting and formatting this document would not have been accomplished without the guidance provided by graduate school staff through workshops.

## **DEDICATION**

To

my parents Huamin Ding and Wanning Yu

for being always supportive!

To

my husband Wei Sun

Our story began when I received the offer from NDSU. Thank you for your love and patience

through the years!

## TABLE OF CONTENTS

ABSTRACT.....	iii
ACKNOWLEDGEMENTS.....	iv
DEDICATION.....	v
LIST OF TABLES.....	xi
LIST OF FIGURES.....	xii
LIST OF ABBREVIATIONS.....	xviii
1. INTRODUCTION.....	1
1.1. Post-translational Lysine Acetylation.....	1
1.1.1. Post-translational modification.....	1
1.1.2. Lysine acetylation and acylation.....	1
1.2. Discovery of Sirtuins as NAD <sup>+</sup> Dependent Deacylases.....	2
1.2.1. History of sirtuins.....	2
1.2.2. Classification of sirtuins.....	3
1.3. Structure and Chemistry of Sirtuins.....	5
1.3.1. Structural features of sirtuins.....	5
1.3.2. Catalytic mechanism of sirtuins.....	19
1.3.3. ADP-ribosyl transferase activity.....	28
1.4. Cellular Regulation of Sirtuin Activity.....	29
1.4.1. Post-translational modifications (PTM).....	29
1.4.2. Role of NAD <sup>+</sup> .....	30
1.5. Physiological and Pathological Roles of Human Sirtuins.....	30
1.5.1. Cellular localizations of seven human sirtuins.....	31
1.5.2. Substrate specificity of sirtuins.....	31
1.5.3. Physiological roles of human sirtuins.....	33

1.5.4. Pathological roles of human sirtuins .....	40
1.6. Activators of Sirtuins .....	46
1.6.1. Sirtuin activators and their physiological effects .....	46
1.6.2. Controversy over the STACs.....	48
1.6.3. Other sirtuin activators .....	50
1.7. Inhibitors of Sirtuins.....	51
1.7.1. Mechanism-based sirtuin inhibitors .....	51
1.7.2. Sirtuins inhibitors discovered through high-throughput screening .....	55
2. STATEMENT OF PROBLEM.....	64
3. MATERIALS.....	65
4. METHODS .....	66
4.1. Cloning, Expression and Purification of Recombinant Human Sirtuin Isoforms .....	66
4.1.1. Sub-cloning of human SIRT1 and SIRT5 .....	66
4.1.2. Site-directed mutagenesis of SIRT5 .....	68
4.1.3. Expression and purification of SIRT1 .....	69
4.1.4. Expression and purification of SIRT5 wild type and mutants .....	70
4.1.5. Purity of proteins .....	71
4.1.6. Estimation of protein concentrations.....	72
4.2. Electronic Spectroscopic Methods .....	72
4.2.1. Spectrophotometric studies .....	72
4.2.2. Measurements of protein emission spectra.....	72
4.2.3. Measurements of time-resolved fluorescence spectra.....	73
4.2.4. Measurements of circular dichroism (CD) spectra.....	74
4.3. Steady-state Kinetic Methods.....	74
4.3.1. Trypsin-coupled enzyme activity assay.....	74

4.3.2. Bi-substrate kinetic analysis of the sirtuin catalyzed reactions .....	75
4.3.3. Screening of sirtuin effectors.....	76
4.3.4. $K_i$ measurement .....	76
4.3.5. $IC_{50}$ measurement .....	77
4.3.6. Inhibition mode .....	78
4.4. Transient Kinetic Methods .....	79
4.5. Thermodynamic Studies.....	80
4.5.1. Binding isotherms of suramin to SIRT1 and SIRT5 .....	80
4.5.2. Isothermal titration calorimetry .....	81
4.5.3. Size exclusion chromatographic studies.....	82
4.5.4. Thermal stabilities .....	83
4.6. Atomic Force Microscope Size Measurements.....	84
4.7. Molecular Modeling.....	85
5. RESULTS .....	87
5.1. Cloning, Expression, Purification, and Physiochemical Properties Characterization of Recombinant Human SIRT1 and SIRT5 .....	87
5.1.1. Cloning, expression, purification of SIRT1, SIRT2 and SIRT5 .....	87
5.1.2. Cloning, expression and purification of SIRT5 mutants.....	92
5.1.3. Physiochemical properties characterization of SIRT1, SIRT2 and SIRT5 .....	97
5.2. Steady-state Kinetics of SIRT1 and SIRT5 Variants .....	107
5.2.1. Trypsin coupled enzyme reaction of sirtuins.....	107
5.2.2. Bisubstrate kinetic studies of the wild-type and mutant sirtuin catalyzed reactions.....	110
5.3. Inhibition Studies of SIRT1 and SIRT5 Variants .....	120
5.3.1. Screening of inhibitors of SIRT1 and SIRT5 .....	120
5.3.2. Steady-state kinetics for the inhibition of SIRT5 by MH5-75 .....	160



5.3.3. Inhibition of selected sirtuins by suramin .....	163
5.3.4. Inhibition mode of SIRT5 desuccinylase activity by suramin .....	167
5.3.5. Inhibition of sirtuins by nicotinamide .....	169
5.3.6. Effects of isonicotinamide on sirtuin catalysis and inhibition.....	178
5.3.7. Inhibition of sirtuins by EX527.....	183
5.4. Spectroscopic, Kinetic, and Thermodynamic Basis for the Binding of Selected Inhibitors to Sirtuins.....	187
5.4.1. Binding of MH5-75 to SIRT5 .....	187
5.4.2. Binding studies of SIRT1 and suramin .....	189
5.4.3. Binding of nicotinamide to SIRT5 .....	228
5.4.4. Binding of EX527 to SIRT5 variants .....	232
5.5. Thermal Stabilities of SIRT1 and SIRT5 Variants .....	235
5.5.1. Thermal unfolding of SIRT1 and SIRT5 variants.....	235
5.5.2. Thermal stability of SIRT5 in the presence of suramin .....	241
6. DISCUSSION.....	244
6.1. Contribution of Y102 and R105 Residues of SIRT5 in Catalysis.....	244
6.2. Inhibition of Desuccinylase Activity of SIRT5.....	246
6.2.1. Inhibition of nicotinamide.....	246
6.2.2. Inhibition of EX527.....	248
6.2.3. Inhibition of suramin .....	251
6.3. Mutation Induced Changes in the Secondary Structural Features of SIRT1 and SIRT5 and Its Mutant Variants .....	253
6.4. Barbiturate Derivative as Sirtuin Inhibitors .....	255
6.5. Suramin-mediated Changes in the Structural Features of SIRT5 .....	259
6.5.1. Suramin-mediated changes in the conformational states of SIRT5 .....	259
6.5.2. Suramin-mediated changes in the oligomeric states of SIRT5 .....	263

REFERENCES ..... 268

## LIST OF TABLES

<u>Table</u>	<u>Page</u>
1.1. Summary of Sirtuin Structures .....	7
1.2. Selected Human Sirtuin Substrates .....	33
1.3. Summary of representative sirtuin inhibitors.....	63
5.1. Steady-state kinetic parameters of SIRT5 variants and SIRT1 on acetyl and succinyl substrates.....	113
5.2. Summary of screening of thiolated compounds for SIRT1 and SIRT5.....	122
5.3. Summary of screening of thiourea derivatives for SIRT1 and SIRT5.....	127
5.4. Summary of screening of hydroxybenzoic, hydroxypicolinic and nicotinic group containing compounds for SIRT1 and SIRT5 .....	133
5.5. Summary of screening of hydrazine/hydrazide derivatives as potential inhibitors/activators for SIRT1 .....	141
5.6. Summary of screening of barbiturate/thiobarbiturate derivatives as potential inhibitors/activators for SIRT1 and SIRT5.....	145
5.7. Summary of screening of miscellaneous compounds as potential inhibitors/activators for SIRT1 and SIRT5.....	154
5.8 Inhibition potency of suramin against SIRT1 and SIRT5 variants.....	167
5.9. Nicotinamide inhibition against SIRT1 and SIRT1 variants .....	178
5.10. Isonicotinamide (iNAM) effect on the nicotinamide inhibition of SIRT1 and SIRT5 .....	183
5.11. Thermodynamic parameters for binding of suramin/half suramin to SIRT5 .....	205
5.12. Melting temperatures of SIRT1 and SIRT5 variants .....	239

## LIST OF FIGURES

<u>Figure</u>	<u>Page</u>
1.1. Molecular phylogeny of the sirtuins.....	4
1.2. Overall Structure of Sirtuin represented by Hst2.....	6
1.3. Three-dimensional structure of several representative sirtuin proteins that has been determined.....	9
1.4. Zinc coordination in SIRT5.....	11
1.5. The substrates-binding cleft.....	12
1.6. Binding of peptide substrate.....	14
1.7. Binding of NAD <sup>+</sup> .....	15
1.8. Structure of <i>H. sapiens</i> SIRT1.....	18
1.9. Overall deacylation reactions catalyzed by sirtuins.....	19
1.10. Schematic representation of the sirtuin catalyzed reaction mechanism.....	20
1.11. Mechanisms of reaction of NAD <sup>+</sup> with acetyllysine nucleophile.....	23
1.12. Structure of a Sir2Tm-S-Alkylamidate intermediate complex.....	26
1.13. Structure of a SIRT5-bicyclic intermediate complex.....	27
1.14. Structures of SIRT1-activating compounds (STACs).....	48
1.15. Mechanism-based sirtuin inhibitors.....	54
1.16. Overall structure of the SIRT5 suramin complex.....	57
1.17. Sirtuin inhibitors discovered through high-throughput screening (suramin and indole analogs).....	61
1.18. Sirtuin inhibitors discovered through high-throughput screening (continued, other inhibitors).....	62
4.1. The ligation independent cloning strategy for the sub-cloning of the human SIRT1 and SIRT5 gene.....	68
4.2. Schematic representation of the trypsin-coupled assay to measure the initial rate of the sirtuin catalyzed reaction.....	75

5.1. The vector map of the pLIC-His vector used for cloning human SIRT5 gene. ....	88
5.2. The agarose gel electrophoresis showing the PCR amplified SIRT1 gene using the pLIC compatible forward and reverse primers.....	89
5.3. SDS-PAGE analysis of purified SIRT1 by Ni <sup>2+</sup> -IDA affinity chromatography. ....	90
5.4. SDS-PAGE analysis of SIRT5 fractions eluted from the Ni <sup>2+</sup> -IDA affinity column.....	92
5.5. Comparative structural features in the catalytic domains of SIRT5 and SIRT1 .....	94
5.6. SDS-PAGE analysis of SIRT5 Y102A fractions eluted from the Ni <sup>2+</sup> -IDA affinity column .....	95
5.7. SDS-PAGE analysis of SIRT5 R105I fractions by Ni <sup>2+</sup> -IDA affinity column.....	96
5.8. SDS-PAGE analysis of SIRT5 Y102A/R105I fractions by Ni <sup>2+</sup> -IDA affinity column .....	97
5.9. UV-visible spectrum of the recombinant human SIRT1 .....	98
5.10. UV-visible spectrum of the recombinant human SIRT5.....	99
5.11. CD spectra of SIRT1 and SIRT5 variants .....	100
5.12. Ribbon Diagram of SIRT1 Catalytic Core Showing Seven Tyrosine Residues (Pink) .....	102
5.13. Steady-state fluorescence emission spectra (black color traces) of 1 μM SIRT1 in 25 mM Tris-Cl, pH 7.5, 100 mM NaCl, 10 % glycerol and 1 mM TCEP) upon excitation at 280 nm .....	102
5.14. Ribbon diagram of SIRT5 showing the tryptophan (red) and tyrosine residues (blue) .....	103
5.15. Steady-state fluorescence emission spectra of 1 μM SIRT5 in 25 mM Tris-Cl, pH 7.5, 100 mM NaCl, 10 % glycerol and 1 mM TCEP) upon excitation at 280 nm .....	103
5.16. Fluorescence lifetime decay of SIRT1 .....	105
5.17. Fluorescence lifetime decay of SIRT5 .....	106
5.18. The excitation and the emission spectra of the fluorogenic substrate (Fluoro-de-Lys <sup>®</sup> ) and the final product of the trypsin-coupled assay. The excitation spectra were obtained at the emission wavelength of 500 nm.....	109
5.19. Real-time progress curve for SIRT5-catalyzed desuccinylation reaction. ....	110
5.20. Standard plot the increase in fluorescence (RFU; λ <sub>ex</sub> = 360 nm, λ <sub>em</sub> = 460 nm) as a function of fluorophore concentration.....	114

5.21. Two substrates reactions of SIRT1 .....	115
5.22. Two substrates reactions of SIRT5 .....	116
5.23. Two substrates sesuccinylation reactions of SIRT5 Y102A .....	117
5.24. Two substrates deacetylation reactions of SIRT5 Y102A .....	118
5.25. Two substrates reactions of SIRT5 R105I .....	119
5.26. Two substrates reactions of SIRT5 Y102A/R105I.....	120
5.27. Dose-response of SIRT5 desuccinylase activity in the presence of 150 $\mu$ M Ac-Suclys-AMC, 50 $\mu$ M NAD <sup>+</sup> , and increasing concentration of MD-3-16 (from 0 to 100 $\mu$ M) .....	159
5.28. Dose-response of SIRT5 desuccinylase activity in the presence of 150 $\mu$ M Ac-Suclys-AMC, 50 $\mu$ M NAD <sup>+</sup> , and increasing concentration of MH5-75 (from 0 to 400 $\mu$ M) .....	160
5.29. Steady-state kinetics for the inhibition of SIRT5 by compound MH5-75 .....	162
5.30. K <sub>i</sub> determination of SIRT1 and SIRT5 by suramin .....	165
5.31. K <sub>i</sub> determination of SIRT5 Y102A by suramin .....	166
5.32. K <sub>i</sub> determination of SIRT5 Y102A/R105I by suramin .....	167
5.33. Steady-state kinetics for the inhibition of SIRT5 desuccinylase activity by suramin.....	169
5.34. Proposed nicotinamide inhibition as a result of reversible cleavage of glycosidic bond of NAD <sup>+</sup> .....	172
5.35. Inhibition of nicotinamide on SIRT5 with varying concentrations of Ac-Suclys-AMC .....	173
5.36. Inhibition of nicotinamide on SIRT5 with varying NAD <sup>+</sup> .....	174
5.37. Inhibition of nicotinamide on SIRT1 with varying NAD <sup>+</sup> .....	175
5.38. Inhibition of nicotinamide on SIRT5 Y102A with varying NAD <sup>+</sup> .....	176
5.39. Inhibition of nicotinamide on SIRT5 Y102A/R102A with varying NAD <sup>+</sup> .....	177
5.40. Effects of isonicotinamide on SIRT1 and SIRT5 catalyzed reactions .....	180
5.41. Effects of nicotinamide on SIRT1 catalyzed reaction in the absence (A) and presence (B) of isonicotinamide .....	181

5.42. Effects of nicotinamide on SIRT5 catalyzed reaction in the absence (A) and presence (B) of isonicotinamide .....	182
5.43. Effects of EX527 on SIRT5 variants catalyzed reactions .....	185
5.44. Steady-state kinetics for the inhibition of SIRT1 activity by EX527.....	186
5.45. Steady-state kinetics for the inhibition of SIRT5 Y102A/R105I activity by EX527.....	186
5.46. Time-dependent changes in the UV/Vis absorption spectra of MH5-75 in the presence of SIRT5 .....	188
5.47. Binding isotherm for the interaction of suramin with SIRT5 .....	191
5.48. Binding isotherm for the interaction of suramin with SIRT1 .....	192
5.49. The time resolved fluorescence decay curve of the tryptophan residues of 5 $\mu$ M SIRT5 in the absence and presence of 1 $\mu$ M suramin .....	194
5.50. The representative stopped flow trace for the association of SIRT5 and suramin.....	196
5.51. Dependence of the observed rate constants on suramin concentrations for the association of suramin to SIRT5 .....	197
5.52. Crystal structure of SIRT5-suramin complex showing hydrogen bond between the urea (NH-CO-NH) group and Y225 .....	200
5.53. ITC profiles of SIRT5 titrated with suramin showing two binding sites .....	201
5.54. ITC profiles of SIRT5 titrated with suramin showing one binding sites .....	202
5.55. ITC profiles of SIRT1 titrated with suramin in 50 mM HEPES, pH 7.5 containing 100 mM NaCl, 10 % glycerol and 1 mM TCEP at 25 $^{\circ}$ C .....	204
5.56. ITC profile of SIRT5 R105I titrated with suramin in 50 mM HEPES, pH 7.5 containing 100 mM NaCl, 10 % glycerol and 1 mM TCEP at 25 $^{\circ}$ C.....	208
5.57. ITC profile of SIRT5 Y102A titrated with suramin in 50 mM HEPES, pH 7.5 containing 100 mM NaCl, 10 % glycerol and 1 mM TCEP at 25 $^{\circ}$ C.....	209
5.58. ITC profile of SIRT5 Y102A/R105I titrated with suramin in 25 mM HEPES, pH 7.5 containing 100 mM NaCl, 10 % glycerol and 1 mM TCEP at 25 $^{\circ}$ C.....	210
5.59. Structure of half-suramin.....	212
5.60. Binding isotherm for the interaction of half-suramin with SIRT5 .....	213
5.61. ITC profile of SIRT5 titrated with half-suramin .....	214

5.62. Effects of half-suramin on SIRT1 and SIRT5 catalyzed reactions .....	215
5.63. Calibration curve for the column superdex 200 using five known proteins as standards.....	217
5.64. Size exclusion chromatography profile and multiple peaks analysis for 26 $\mu$ M SIRT5 the absence and presence of suramin.....	220
5.65. Molar ratios of monomer/total and dimer/total are plotted against different concentrations of suramin from size exclusion chromatography profiles.....	221
5.66. AFM images of SIRT5 on a mica surface at various concentrations of Sumarin .....	224
5.67. Size distributions of SIRT5 at various concentrations of sumarin.....	225
5.68. Molecular modeling of SIRT5 with suramin .....	227
5.69. Molecular modeling of SIRT5 with energy minimized suramin .....	228
5.70. ITC profile for the binding of nicotinamide to SIRT5 .....	230
5.71. ITC profile for the binding of nicotinamide to SIRT5-substrate complex.....	231
5.72. ITC profile for the binding of EX527 to SIRT5 Y102A/R105I in the absence (A) and presence (B) of 10 mM NAD <sup>+</sup> .....	233
5.73. ITC profile for the binding of EX527 to SIRT5 in the absence (A) and presence (B) of 10 mM NAD <sup>+</sup> .....	234
5.74. Thermal denaturation SIRT5.....	237
5.75. Thermal denaturation of SIRT5 Y102A.....	237
5.76. Thermal denaturation of SIRT5 R105I .....	238
5.77. Thermal denaturation of SIRT5 Y102A/R105I.....	238
5.78. Thermal denaturation of SIRT1 .....	239
5.79. CD spectra of wild-type (black) and R105I (red) and Y102A (blue) mutants of SIRT5 after completion of the melting phases .....	240
5.80. CD Spectra of SIRT5 in the absence and presence of suramin.....	242
5.81. Thermal denaturation of SIRT5 in the presence of suramin .....	243
6.1. Structure of EX527, the analogue, and the catalytic domain of SIRT1 bound with EX527 analog and NAD <sup>+</sup> .....	250



6.2. Superimposition of SIRT1 and SIRT5 showing the binding site of EX527 .....	251
6.3. Coordination of Y102 and R105 with the sulfonate group of suramin. Hydrogen bonds are shown as dashed orange lines .....	253
6.4. Binding and Inhibition mechanism of MH5-75 against SIRT5 .....	257
6.5. Sirtuin inhibitors with a barbiturate or thiobarbiturate scaffold. ....	257
6.6. Docking result for one representative thiobarbiturate at SIRT5 active site pocket. Hydrogen bonds are shown as dashed orange lines .....	259
6.7. Crystal structures of SIRT5 in complex with suramin or substrates .....	261
6.8. Two-step binding mechanism for the binding of suramin to SIRT5.....	262
6.10. Proposed SIRT5-suramin binding mechanism.....	266

## LIST OF ABBREVIATIONS

AceCS .....	Acetyl-CoA synthetase
ALDH2 .....	Aldehyde dehydrogenase 2
AMC .....	7-amino-4-methylcoumarin
BSA.....	Bovine serum albumin
CD.....	Circular dichroism
CDK9 .....	Cyclin-dependent kinase 9
DMSO .....	Dimethylsulfoxide
CPS1 .....	Carbamoyl-phosphate synthase 1
CPT-1 .....	Carnitine palmitoyltransferase-1a
CREB .....	cAMP response element-binding protein
CRTC2 .....	CREB-regulated transcription co-activator 2
CtIP .....	C-terminal-binding protein-interacting protein
GDH.....	Glutamate dehydrogenase
GLUT1 .....	Glucose transporter 1
GNAT .....	The Gcn5 related N-acetyltransferase
HDAC .....	Histone deacetylase
HEPES .....	4-(2-hydroxyethyl)-1-piperazineethanesulfonic acid
HIV .....	Human immunodeficiency virus
HMGCS2 .....	3-hydroxy-3-methylglutaryl CoA synthase 2
IDA .....	Iminodiacetic acid
iNAM .....	Isonicotinamide
IPTG.....	Isopropyl thio- $\beta$ -galactopyranoside
ITC .....	Isothermal titration calorimetry
LCAD.....	Long-chain acyl coenzyme A dehydrogenase

LIC .....	Ligation Independent Cloning
MAR1 .....	Mating-type regulator 1
MCAD.....	Medium chain acyl-CoA dehydrogenase
min .....	Minute
MnSOD.....	Manganese superoxide dismutase
NAM .....	Nicotinamide
OAADPr .....	2'-O-acetyl-ADP-ribose
PAGE .....	Polyacrylamide gel electrophoresis
PDB.....	Protein Data Bank
PEPCK .....	Phosphoenolpyruvate carboxykinase
PFK1 .....	Phosphofructokinase 1
Pfu .....	<i>Pyrococcus furiosus</i>
PGC-1 $\alpha$ .....	Peroxisome proliferator-activated receptor gamma coactivator 1-alpha
PTM .....	Post-translational modification
ROS.....	Reactive oxygen species
s.....	Second
SdhA .....	Succinate dehydrogenase flavoprotein
SDHA.....	Succinate dehydrogenase A
SDS .....	Sodium dodecyl sulfate
SIRT .....	Sirtuin
TCA.....	Tricarboxylate acid
$\Delta G$ .....	Change in the Gibbs free energy
$\Delta H$ .....	Change in enthalpy
$\Delta S$ .....	Change in entropy

$\theta$ .....Degree of ellipticity

# 1. INTRODUCTION

## 1.1. Post-translational Lysine Acetylation

### 1.1.1. Post-translational modification

The complexity of the human proteome well exceeds that of the human genome, with the estimated 1 million-member proteome encoded by just 25,000 genes (1). This complexity partially arises from transcriptional regulation in the forms of alternative splicing, recombination events, differential transcriptional activation and termination, and post-translational modifications. Post-translational modifications (PTMs) are chemical modifications of proteins, including phosphorylation, methylation, acetylation, acylation, N-linked and O-linked glycosylation, ADP-ribosylation, ubiquitination, SUMOylation and biotinylation. PTM regulates protein structure and stability, protein cellular localization, protein-DNA/protein-protein interactions and consequently, they modulate a variety of cellular processes, such as gene expression, DNA damage, apoptosis, cell-cycle regulation, metabolism and stress response (2-5).

### 1.1.2. Lysine acetylation and acylation

Lysine is one of the most commonly modified amino acid residues in proteins, and the positive charge it carries enables it to accommodate different PTMs, including acetylation, non-acetyllinse acylation, methylation, and ubiquitination. Reversible acetylation on  $\epsilon$ -amino group of lysine residues was first discovered in histones by Allfrey et al in 1964 (6). Later on, lysine acetylation/deacetylation were also found in a variety of important non-histone proteins, such as p53, estrogen receptor, Hsp90, tubulin, etc (7). Enzymes that catalyze the addition of acetyl group to proteins are classified as histone/lysine acetyltransferases (HAT/KAT) (8). These enzymes are grouped into three major protein families, including the MYST family, the GNAT

family (Gcn5 related N-acyltransferase) and CBP/p300 family (9). Enzymes that remove the acetyl group from proteins are classified as histone/lysine deacetylases (HDAC/KDAC), which include HDAC1 to HDAC8 and SIRT1 to SIRT7 (NAD<sup>+</sup> dependent deacetylases). Recently, several new types of non-acetyllysine acylation have also been identified, including succinylation, malonylation (10), glutarylation (11), myristoylation, palmitoylation (12), butyrylation, and propionylation (13). It has been well demonstrated that SIRT1-SIRT6 all possess the potential to catalyze the deacylation reactions of fatty acyl-lysine conjugates in peptides/proteins (14, 15).

## **1.2. Discovery of Sirtuins as NAD<sup>+</sup> Dependent Deacylases**

### **1.2.1. History of sirtuins**

Sirtuins (Sir2 proteins) belong to an ancient family of proteins, which are highly conserved in various organisms ranging from bacteria to humans. About 30 years ago, the first sirtuin gene encoding for Sir2 enzyme was identified in budding yeast (*Saccharomyces cerevisiae*) as MAR1 (mating type regulator 1) (16). Later on in 1987, Herskowitz started to use SIR (Silent Information Regulators) nomenclature (17). In 1995, Boeke and his colleagues identified 4 homologs of Sir2 genes (HST1-4) from *Saccharomyces cerevisiae* and concluded that the sir2 genes, conserved in both prokaryotes and eukaryotes, involve in gene silencing, cell-cycle regulation and chromosome stability (18). In 1999, Frye identified 5 human Sir2 homologs (SIRT1-5) and named the Sir2 protein family as “sirtuins”. Based on the dependence of NAD<sup>+</sup>, he also speculated that the sir2 proteins were ADP-ribosyltransferases (19). In the same year, Moazed et al demonstrated that human SIRT2 and E.coli cob proteins possessed ADP-ribosyltransferase activity (20). In 2000, two research groups reported independently that

sir2 and its homologs are NAD<sup>+</sup> dependent deacetylases (21, 22). Since then, sirtuins have increased researchers' interest as to their physiological roles especially their correlations with life-span expansion process (23). In recently years, novel activities of sirtuins have been identified. Hence, the sirtuins are more appropriately names as NAD<sup>+</sup> dependent deacylases.

### **1.2.2. Classification of sirtuins**

Sirtuins are found in all three domains of life (from bacteria to mammals). General speaking, the more complicated the organisms are, the more sirtuins they possess. Most prokaryotic genomes only encode one sirtuin, while eukaryotes possess multiple sirtuins. For instance, yeast encodes 5 (Sir2 and HST1-4), *Drosophila* encodes 6, and human genome encodes 7 sirtuins. Based on the molecular phylogenetic analysis of 60 sirtuins, the family is divided into five classes by Frye (I-IV and U) (24). Class I includes yeast Sir2, HST1, HST2, mammalian SIRT1, SIRT2 and SIRT3. Class II is composed of the mammalian SIRT4 and the fruitfly D.mel3. Most bacterial sirtuins are included in class III, which also includes mammalian SIRT4, SIRT5 and some other eukaryotic orthologs from *Candida albicans* and *Plasmodium falciparum*. Class IV is eukaryotic specific, which includes mammalian SIRT6 and SIRT7, and are further subdivided into class IVa (SIRT6, D.mel4, C.ele4, P.Fal2, O.sat, and A.tha) and class IVb (SIRT7 and D.mel5). Class U is composed of prokaryotic sirtuins with gene sequence motifs as being intermediate between classes I, II and classes III, IV.

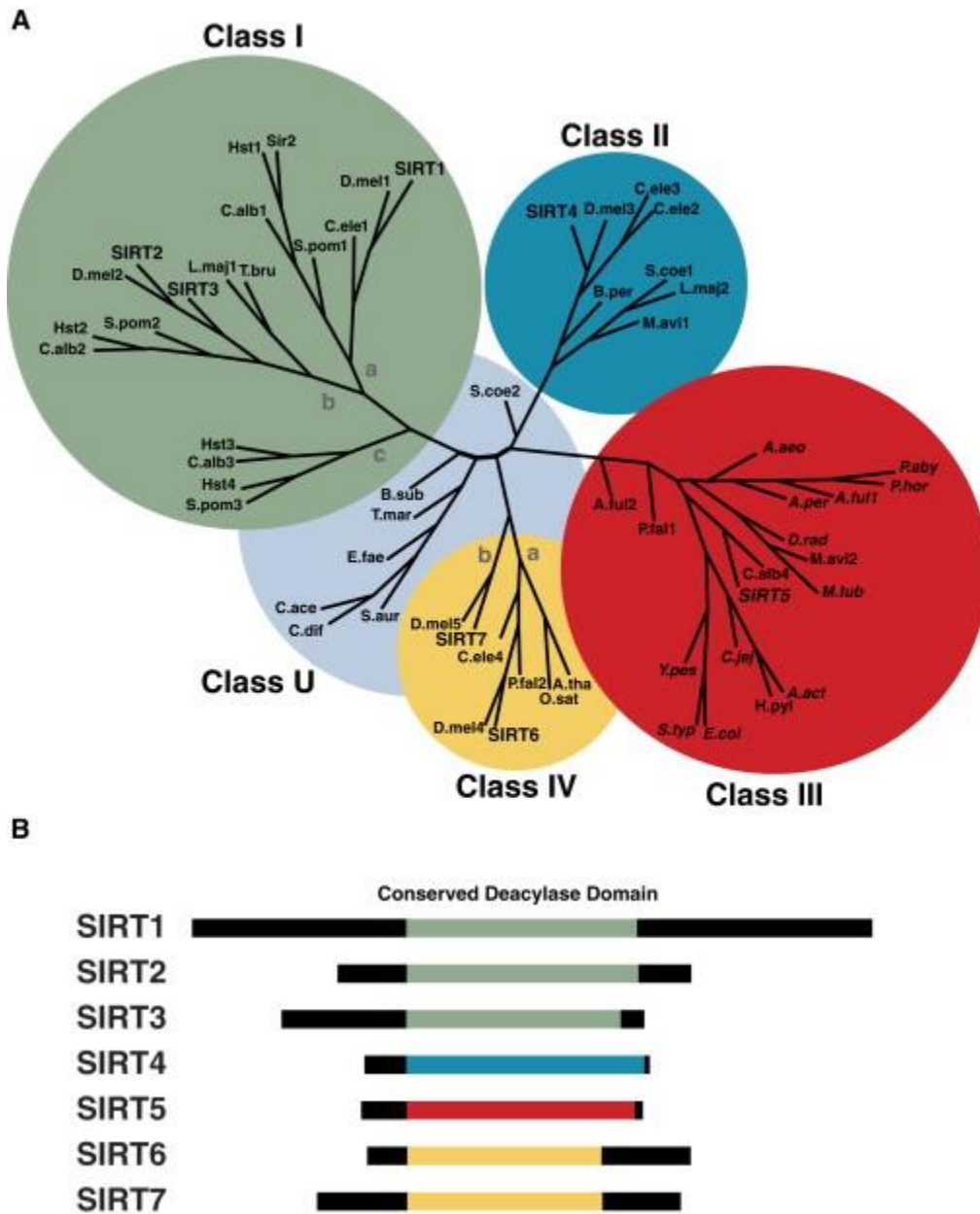


Figure 1.1. Molecular phylogeny of the sirtuins. (A) An unrooted tree diagram of a phylogenetic analysis of sirtuins based on the sequences of their conserved core deacylase domain. Sirtuins are divided into class I, II, III, IV, and U groups; classes I and IV are further divided into subclasses indicated by lowercase letters. (B) Scheme of the conserved catalytic core domains in human SIRT1–7, color coded to match the phylogenetic class from (A) are indicated in green, blue, red and yellow, respectively. The extended N-terminal and C-terminal regions are indicated in black. The figure is adapted from reference (25)



### 1.3. Structure and Chemistry of Sirtuins

#### 1.3.1. Structural features of sirtuins

Structural information of sirtuins is crucial for understanding the catalytic mechanism, substrate specificity, and inhibition/activation mechanisms. Of the 60 sirtuin proteins, the crystal structures of several ones have been solved (Table 1.1) , including two Sir2 homolog from bacteria (CobB from *Escherichchia coli*, Sir2Tm from *Thermatoga maritima* ) (26-28), two from archaea (Sir2Af1 and Sir2Af2 from *Archaeoglobus fulgidus* (29, 30)), one from yeast (Hst2 from *Saccharomyces cerevisiae* (31)), and five out of seven human sirtuins (SIRT1, SIRT2 (32), SIRT3 (33), SIRT5 (10, 34) and SIRT6 (12, 35)) have been solved. All these above structures share a highly conserved catalytic core consisting of approximately 275 amino acids. Additionally, some sirtuin proteins have extended N-terminal and C-terminal flanking regions at various length and amino acids sequences. The overall catalytic core consists of a large Rossmann-fold domain, a small zinc-binding domain, and a cleft consisting of several loops between the two domains where the peptide substrate and NAD<sup>+</sup> enter (Figure 1.2.).

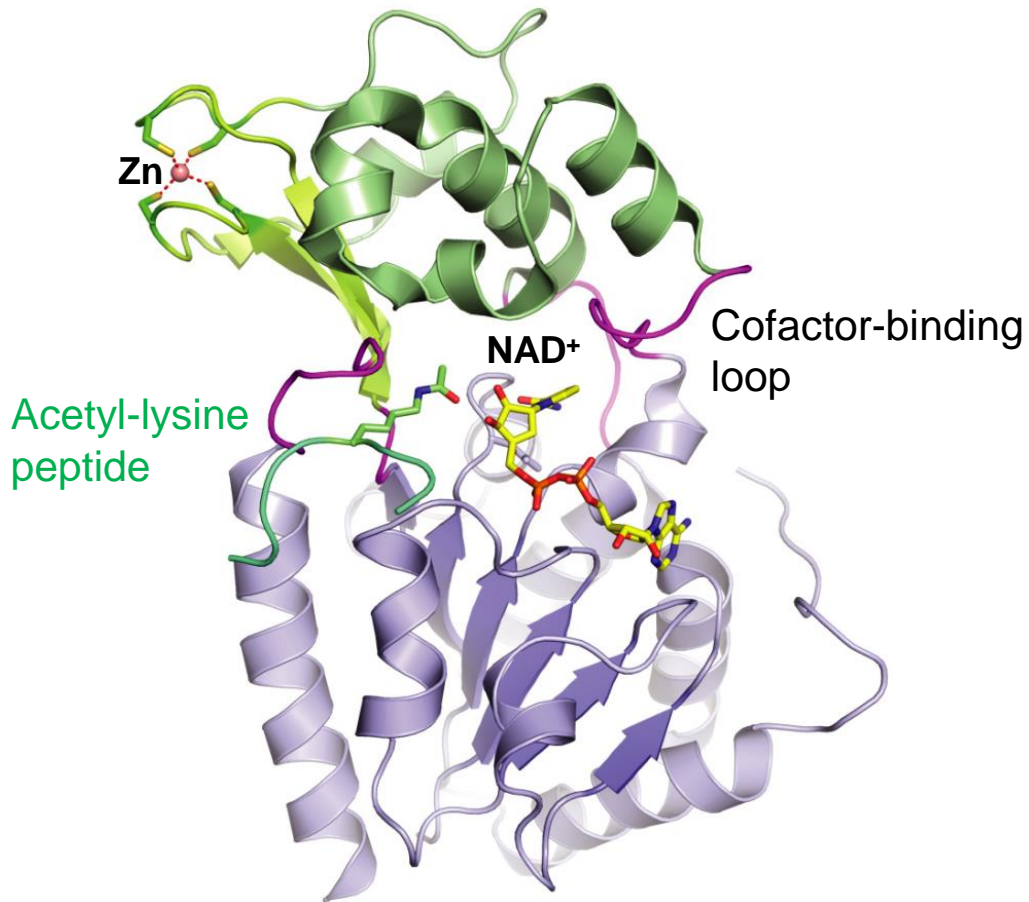


Figure 1.2. Overall Structure of Sirtuin represented by Hst2. Crystal structure of the protein bound to acetyllysine and carba-NAD<sup>+</sup> substrates represented in stick model (PDB code 1SZC). The small domain is shown in green, the large domain in blue, and the four linking loops in purple. The figure is adapted from reference (36).

Table 1.1. Summary of Sirtuin Structures (36)

Protein	PDB ID	Major Findings	Reference
Sir2Af1 + NAD <sup>+</sup>	1ICI	Overall sirtuin fold and NAD <sup>+</sup> binding site	Xu et al, 2001 (29)
SIRT2 (human) apo	1J8F	Overall sirtuin fold	Finnin et al., 2001(32)
Sir2Af2 + p53K382Ac peptide	1MA3	Mode of p53 substrate binding	Wolberger et al., 2002 (37)
Hst2 (yeast)	1Q14	Overall Hst fold. C- and N-terminal extensions interact with NAD <sup>+</sup> and acetyllysine binding sites, respectively to autoregulate the enzyme	Marmorstein et al., 2003, (38)
Hst2 + NAD <sup>+</sup>	1Q17	Cofactor binding loop becomes ordered compared to apo structure	
Hst2 + NAD <sup>+</sup> + H4K16Ac peptide	1Q1A	Model for 2'-OAADPr product and acetyllysine substrate binding in the same structure	
CobB (E.coli) + H4K16Ac peptide	1S5P	Model of acetyllysine peptide substrate binding	Marmorstein et al, 2004 (26)
Sir2Af2 + NAD <sup>+</sup> + NAM	1YC2	Free nicotinamide binding observed in the C pocket	Wolberger et al, (39)
Sir2Tm + p53K382Ac peptide	2H2D	Residues at -1 and +2 positions of the peptide make side chain interactions with Sir2Tm	Avalos et al, 2006 (37)
Sir2Tm + p53K382 peptide	2H2F		
Hst2 + ADP-HPD + H4K16Ac peptide	2OD7	Binding model of an oxocarbenium intermediate mimic	Marmorstein et al, 2007
Hst2 + ADP-HPD + H4K16Ac peptide +NAM	2OD9	Nicotinamide is observed to bind in the D pocket	
SIRT5 (human) + NAD <sup>+</sup>	2B4Y	SIRT5 fold	Plotnikov et al, 2007 (34)
SIRT5 + suramin	2NYR	Suramin binding model	
Sir2Tm + DADMe-NAD <sup>+</sup> + p53K382Ac peptide	3D4B	Binding model of a dissociative intermediate	Hawse et al., 2008 (40)
Sir2Tm + S-alkylamidate	3D81	Binding model of an O-alkylamidate intermediate mimic	
Sir2Tm + p53 peptide	3JR3	Putative nucleophilic attack from Arg at +2 of acetyllysine peptide for ADP-ribosylation	Wolberger et al., 2009 (41)

Table 1.1. Summary of Sirtuin Structures (36) (continued)

Protein	PDB ID	Major Findings	Reference
SIRT3 (human) apo	3GLS	Sirtuin fold	Perni et al., 2009 (33)
SIRT3 + AceCS2-K <sub>ac</sub>	3GLR	Model of acetyllysine binding	
SIRT3 + AceCS2-K <sub>s-ac</sub> -ADPR	3GLT	Binding model of an S-alkylamidate intermediate	
SIRT3 + AceCS2-K	3GLU	Binding model of a dethioacetylated AceCS2	
SIRT5 + NAD <sup>+</sup> + H3K9(N-succinyl) peptide	3RIY	Binding model of a succinyl-lysine peptide to SIRT5	Du et al., 2010 (10)
SirTm + p53K382(propionyl) peptide	3PDH	Binding model of propionyl-lysine	Wolberger et al, 2011 (42)
SIRT6 (human) + NAD <sup>+</sup>	3K35	SRIT6 fold	Pan et al, 2011 (35)
SIRT6 + 2'-N-acetyl-ADPr	3PKJ	Sirtuin bound to 2'-N-acetyl-ADP-ribose, a non-hydrolyzable analog of O-acetyl-ADP-ribose	
SIRT5 + such3K9	4F4U	Binding mode of SIRT5 with bicyclic intermediate	Zhou et al., 2011 (43)
SIRT5 + bicyclic intermediate	4F56		
SIRT1 + EX527 analog + NAD <sup>+</sup>	4I5I	Binding mode of EX527 to SIRT1	Zhao et al., 2013 (44)
Sir2Tm + EX527 + NAD <sup>+</sup>	4BV3	EX527 occupies the nicotinamide site and a neighboring pocket and contacts the ribose of NAD <sup>+</sup> or of the product 2'-OAADPr, stabilizing the closed enzyme conformation preventing product release.	Gertz et al., 2013 (45)
Sir2Tm + p53 peptide + OAADPr + EX527	4BV2		
SIRT3 + EX527 + ADPr	4BVB		
SIRT3 + thioalkylimidate + EX527	4BVF		
SIRT3 + alkylimidate + EX527	4BVG		
SIRT3 + 2'-OAADPR + EX527	4BVH		
SIRT1 <sup>CAT</sup> + CTR + ADPR + substrate (open state)	4IG9	Overall SIRT1 fold; regulatory role of C-terminal segment	Davenport et al, 2014 (46)
SIRT1 <sup>CAT</sup> + CTR (closed state)	4KXQ		

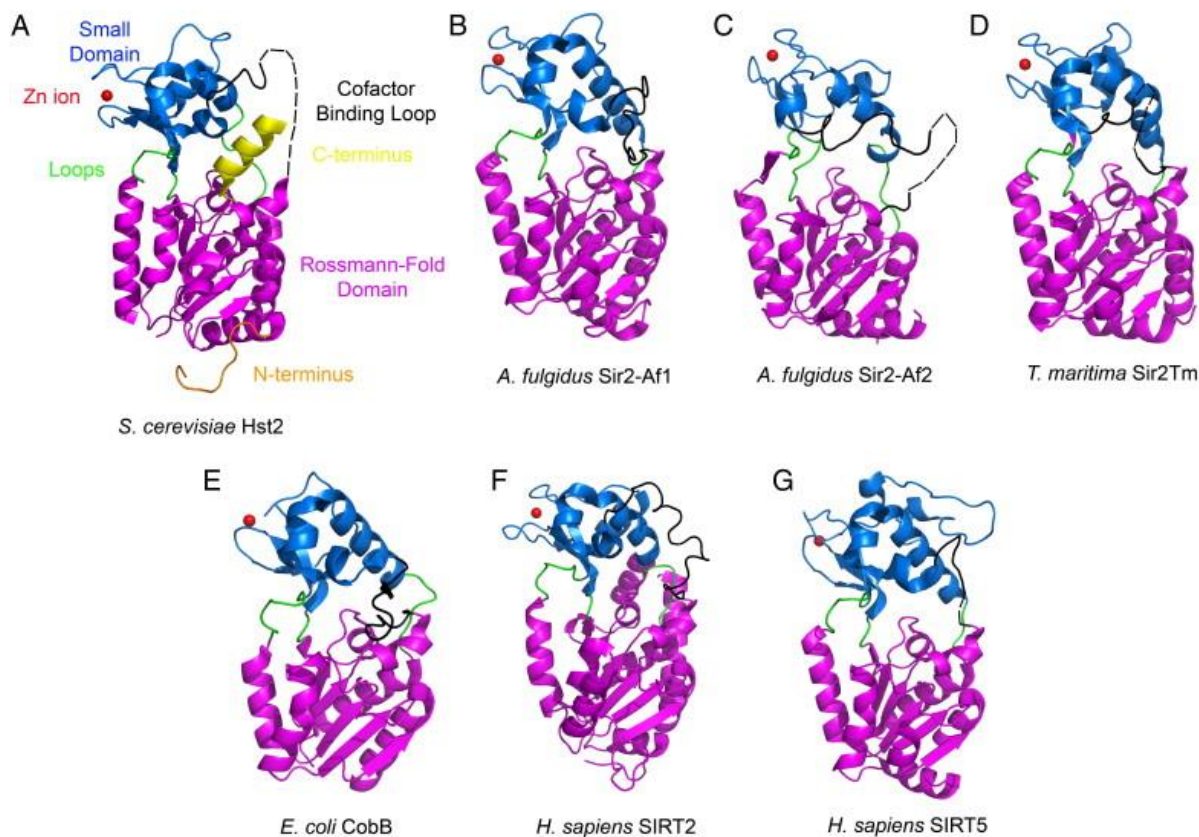


Figure 1.3. Three-dimensional structure of several representative sirtuin proteins that has been determined. The enzymes are shown without bound ligands. (A) *S. cerevisiae* Hst2 (PDB code 1Q14). (B) *A. fulgidus* Sir2-Af1 (1ICI). (C) *A. fulgidus* Sir2-Af2 (1MA3). (D) *T. maritima* Sir2Tm (2H4J). (E) *E. coli* cobB (1S5P). (F) *H. sapiens* SIRT2 (1J8F). (G) *H. sapiens* SIRT5 (2B4Y) Figures are adapted from reference (47).

#### 1.3.1.1. The large domain

The large domain adopts a characteristic  $\alpha/\beta$  Rossmann-fold, consisting of 6 parallel  $\beta$  strands that are sandwiched between several  $\alpha$  helices. The number of  $\alpha$  helices varies in different sirtuins. For instance, in human SIRT2, the 6  $\alpha$  helices pack against the 6  $\beta$  strands; but in SIRT5, the number of  $\alpha$  helices is 9. The Rossmann-fold has characteristic hallmarks of  $\text{NAD}^+/\text{NADH}$  binding proteins, such as Gly-X-Gly sequence important for binding of the  $\text{NAD}^+$  phosphate, the small hydrophobic pocket, and polar residues (Asn, Asp/Glu) that hydrogen-bond to the adenine ribose 2' and 3' OH groups. Interestingly, the Rossmann-fold

domain of sirtuin enzymes resembles the inverted Rossmann-fold enzymes, which means the NAD<sup>+</sup> molecule is oriented in an inverted manner as compared to other NAD<sup>+</sup>-linked dehydrogenases (48): the adenine base of NAD<sup>+</sup> binds to the C-terminal half and the nicotinamide group of NAD<sup>+</sup> binds to the N-terminal half of the  $\beta$  sheet.

### ***1.3.1.2. The small domain***

The small domain is comprised of a zinc-binding module and a helical module with three or four helices. This domain is the most diverse region among sirtuin family members for which structures have been determined, in terms of secondary structure and the position relative to the Rossmann-fold. A conserved salt-bridge (Arg217 and Glu215 in SIRT5) seems to be important for positioning the small zinc-binding domain with respect to the large domain (29, 34) (Figure 1.3).

The zinc-binding ribbon module is composed of three antiparallel  $\beta$  strands with the conserved motifs Cys-X<sub>2-4</sub>-Cys-X<sub>15-40</sub>-Cys-X<sub>2-4</sub>-Cys (X is any amino acid). In most sirtuin structures, the zinc molecule is bound with two pairs of Cys, which are highly conserved among sirtuins, forming a tetrahedral geometry. The only exception is CobB, which contains only three Cys residues expected for the zinc coordination based on sequence alignment (47). The three stranded metal-binding ribbon module resembles the zinc-ribbon structure of transcription factors TFIIS (49), TFIIB (50), and the RNA polymerase II subunit RPB9 (51). Unlike Class I and II HDACs, of which the zinc-binding module is involved in the catalysis by coordinating with the substrate, the zinc in sirtuins locates apart from the active site and does not participate in the catalysis directly. Charkrabarty et al demonstrated that depletion of zinc in *Plasmodium falciparum* Sir2 by mutating the cysteines or using chelating reagent partially denatures the protein structure and knocks down the enzyme activity. The enzyme activity is

partially/completely restored by supplementing the enzyme by zinc, suggesting that the zinc is critical for maintaining the three dimensional structures of sirtuins (52).

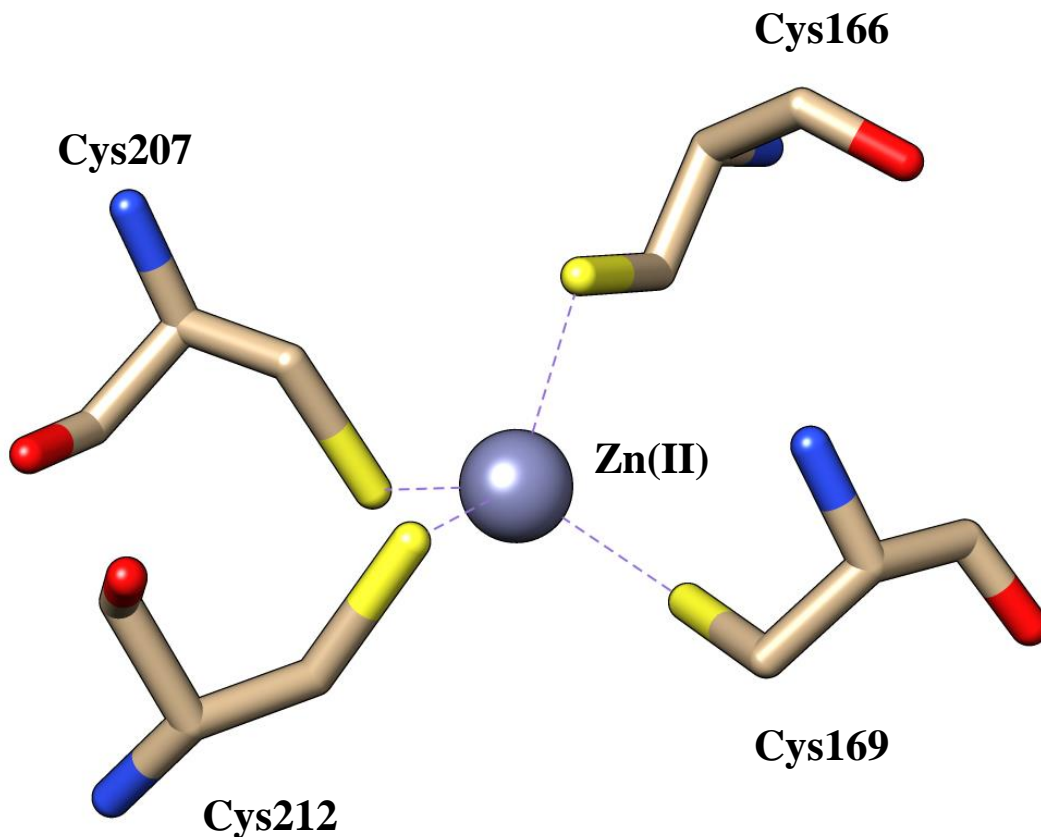


Figure 1.4. Zinc coordination in SIRT5. The zinc molecule is bound with two pairs of Cys, which are highly conserved among sirtuins, forming a tetrahedral geometry.

### *1.3.1.3. The large active site groove*

Four loops connect the large and small domains and form a cleft where both the peptide substrate and  $\text{NAD}^+$  enter, thereby acting as the enzyme's active site. The residues of these four loops are highly conserved. It has been found that mutations in the large groove blocked the deacetylase activity of some sirtuins. The residues of these four loops are highly conserved. It has been found that mutations in the large groove blocked deacetylase activity of some sirtuins

(32). Three hydrophobic residues (Phe223, Leu227, Val254 in SIRT5), which are highly conserved within the sirtuin family, define the entrance of the acyl-lysine binding pocket (Figure 1.5). Recent studies have suggested that the size of the hydrophobic pocket varies among sirtuin enzymes. The substrate binding site in SIRT6 possesses a relatively larger hydrophobic pocket, which enables it to accommodate long-chain fatty-acid modified lysine (12). The substrate binding pocket in SIRT5 is also larger as compared to other sirtuin enzymes that possess robust deacetylase activity. In addition to the hydrophobic residues, two non-hydrophobic residues (Tyr102 and Arg105) locate in the deep end of the substrate-binding pocket, enabling the enzyme to bind negatively charged acyl groups (succinyl, malonyl, glutaryl) and act as a desuccinylase, demalonylase and deglutarylase enzymes (10, 11).

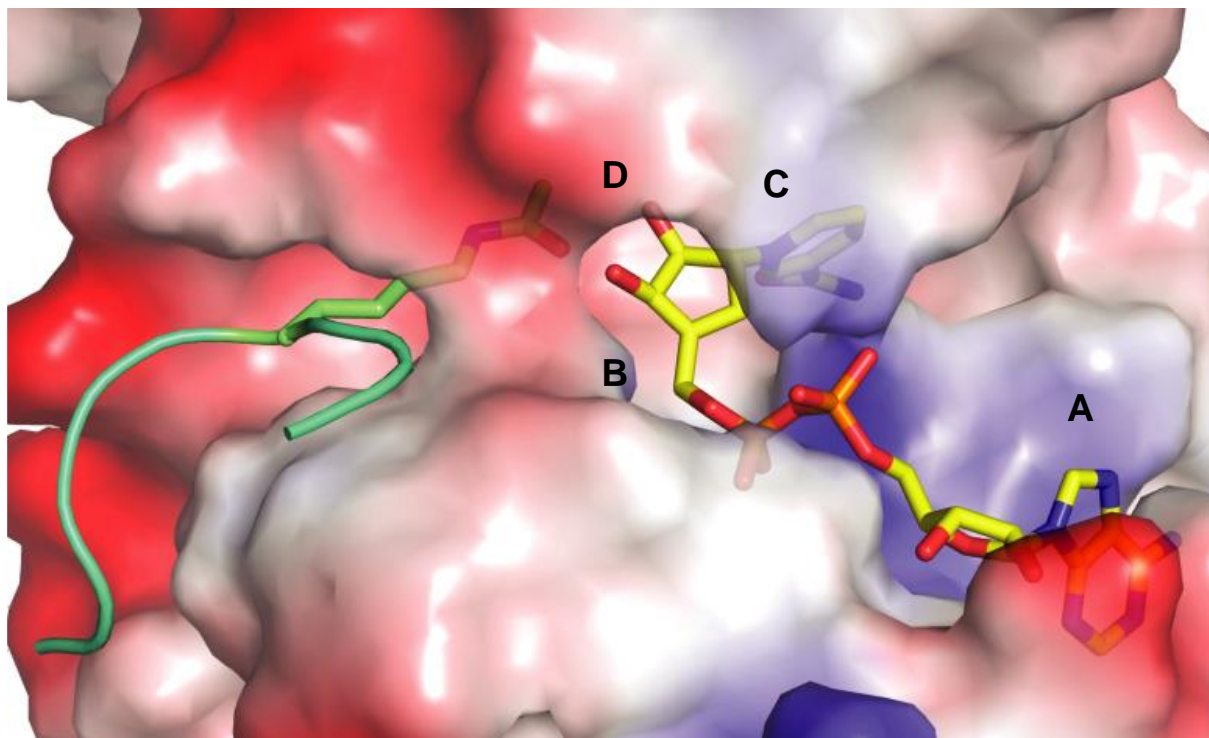


Figure 1.5. The substrates-binding cleft. The substrates-binding cleft is shown in surface representation and is colored red for negative charge and blue for positive charge. The NAD<sup>+</sup>-binding region is divided into sites A-D. Figure is adapted from reference (36).



#### ***1.3.1.4. NAD<sup>+</sup> binding pocket***

The NAD<sup>+</sup> binding pocket locates at the bottom of the large Rossmann-fold domain and the loop region (particularly the cofactor binding loop) at the interface between the large domain and small domain. It consists of three different regions (Figure 1.5): site A, where the adenine-ribose moiety of NAD<sup>+</sup> is bound; site B, where the nicotinamide ribose is bound; site C that lies deep inside the pocket, where the nicotinamide moiety is bound. The site A is mostly hydrophobic, providing van der Waals interactions with the adenine ribose moiety via several conserved Gly residues. A conserved Asn (Asn248 in Hst2 and Asn275 in SIRT5) forms hydrogen bonds with the 3'-OH and 2'-OH group of the adenine ribose. Other functionally conserved residues participate in the hydrogen bond interactions with the pyrophosphate group. In the site B, a conserved His residue (His158 in SIRT5) forms hydrogen bond with the 3'-OH groups of the nicotinamide ribose, acting as a general base during catalysis (discussed in the latter section). The electron density of the nicotinamide moiety of NAD<sup>+</sup> is usually not observed in the sirtuin structures, which are crystallized in the presence of NAD<sup>+</sup>, presumably due to the slow non-enzymatic hydrolysis of NAD<sup>+</sup> or the disorder of nicotinamide moiety upon binding.

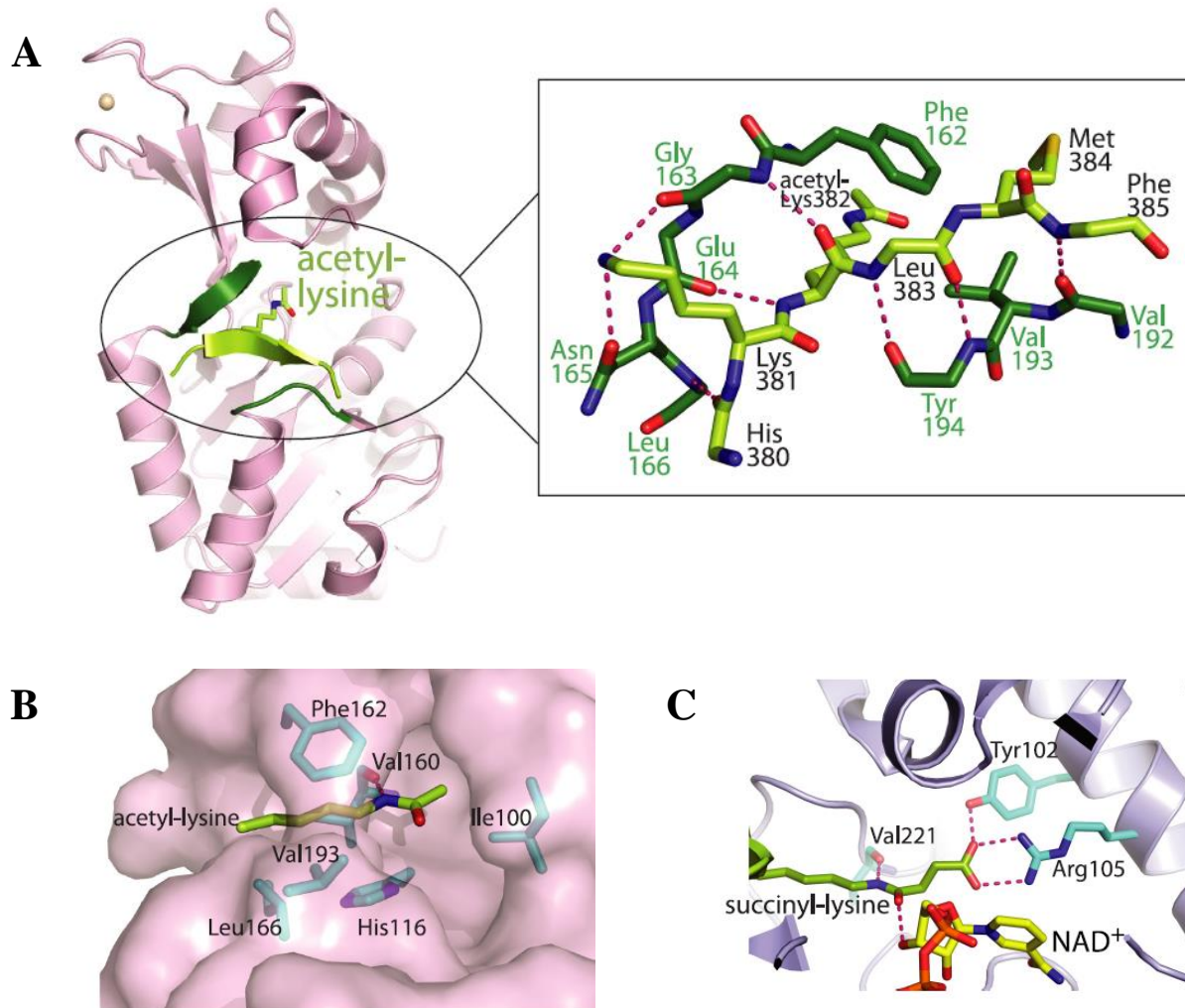


Figure 1.6. Binding of peptide substrate. Binding of acetyllysine-containing p53 peptide to Sir2Tm are shown in A and B. (A) The acetyllysine peptide (light green) forms a  $\beta$ -staple with sirtuin residues (dark green). Only the backbone of the residues is shown except for where side chain interactions are made: Lys-381 (+1 position) forms hydrogen bonds with Asn165 and Gly163, and Met384 (+2 position) makes van der Waals interactions with Phe162 and Val193. (B) The acetyllysine side chain is buried in a hydrophobic tunnel and makes van der Waals interactions with sirtuin residues (blue stick). (C) Succinyllysine (green) forms hydrogen bonds with NAD<sup>+</sup> and SIRT5 residues Tyr102 and Arg105. Figures are adapted from reference (36).

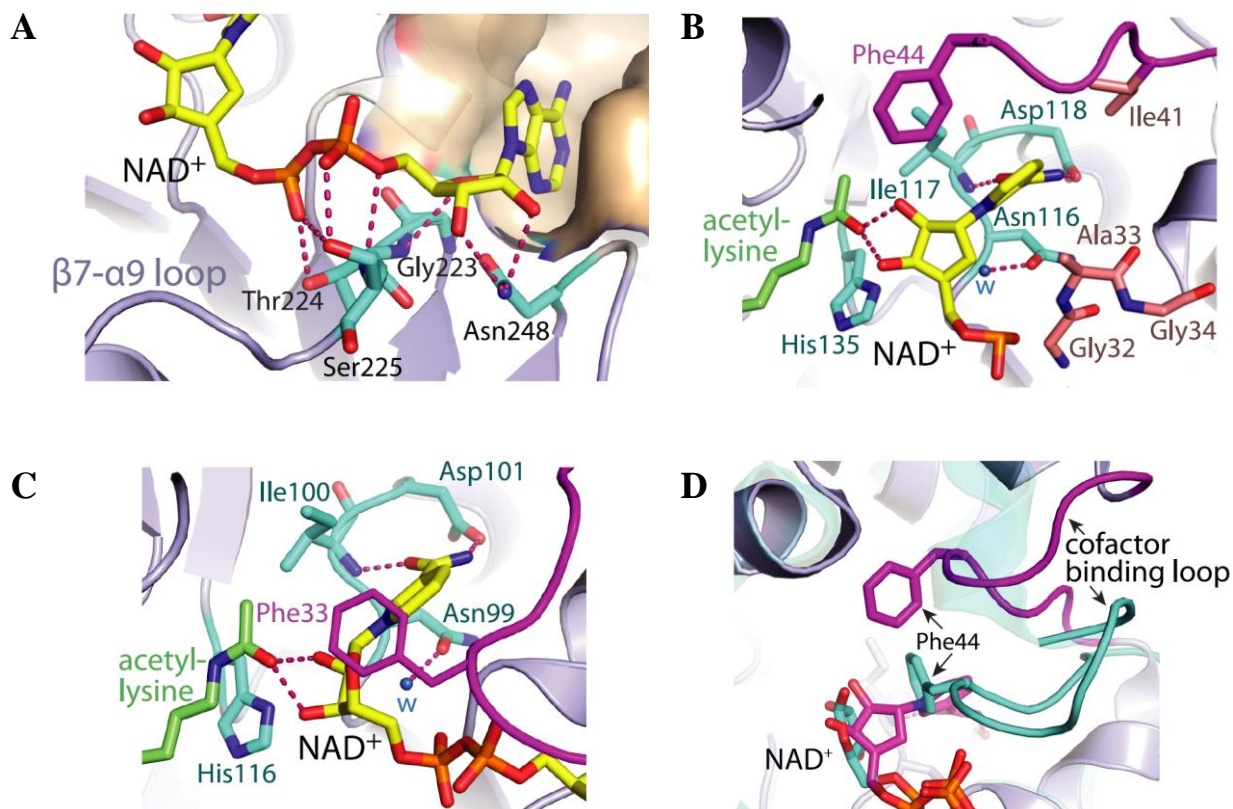


Figure 1.7. Binding of NAD<sup>+</sup>. (A) Site A of the NAD<sup>+</sup> binding pocket. Residues represented in blue stick form hydrogen bonds (dashed lines) with NAD<sup>+</sup>. The adenine base sits in a hydrophobic pocket shown in surface representation. yHst2, yeast Hst2. (B) Sites B and C. NAD<sup>+</sup> forms hydrogen bonds with Ile117, Asp118, and acetyllysine. Gly32, Ala33, Gly34, Ile41, and Phe44 make van der Waals interactions with NAD<sup>+</sup>. Asn116 forms a hydrogen bond with an ordered water molecule (indicated as w; blue sphere). (C) Sites B and C of the NAD<sup>+</sup> binding pocket represented by the Sir2Tm-NAD<sup>+</sup>-acetyllysine complex. The nicotinamide ribose is rotated by ~90 °C compared with B. (D) Different conformations of the cofactor-binding loop. Hst2 bound to carba-NAD<sup>+</sup> (purple) is superimposed on Hst2 bound to ADPR (green), showing the different positions of Phe44. Figures are adapted from reference (36).

### 1.3.1.5. N-terminal and C-terminal extensions

Outside the catalytic core, sirtuins possess divergent N-terminal and C-terminal extensions that vary in length, amino acids sequence and secondary structure. These two domains are absent in most of the solved sirtuin structures. The few structures that include the N-terminal and/or C-terminal domains, as well as molecular modeling based design of

minimally functional construct have provided useful information of the roles of these two regions in sirtuin catalysis and regulation (31, 53-55).

In yeast Hst2, seven residues of the N-terminal domain form an extended loop that interacts with the active site of a symmetry-related molecule, mediating the formation of a homotrimer that blocks the entry of acetylated substrate. In the ternary complex of Hst2/NAD<sup>+</sup>/Histone H4 which is not a trimer, the N-terminal region is disordered and the substrate replaces it in the active site, suggesting that the N-terminal region of Hst2 is involved in both maintaining the oligomerization state and autoregulating the binding of the substrate (31). In human SIRT2 and yeast HST2, an additional  $\alpha$ -helix packs against the Rossmann-fold; however, this helix is absent in bacterial sirtuins SirTm and CobB, archaeal sirtuins Sir2Af1 and Sir2Af2, and human SIRT5 (Figure 1.3.). It has been proposed that this packing autoregulates the NAD<sup>+</sup> binding as evident by the following facts: (1) the helix interacts with the residues in the Rossmann-fold that also contact with NAD<sup>+</sup>, and (2) removal of the C-terminal region reduces the  $K_m$  of NAD<sup>+</sup> (38).

SIRT1, which is composed of 747 amino acids, possesses an unusually long extended N-terminal and C-terminal regions. The attempt to solve the structure of the above enzyme in the presence of both N-terminal and C-terminal regions has not been successful due to the conformational flexibility of these two regions. It has been shown that N-terminal contributes to the catalytic rate, independent of the nature of the acetyl-lysine peptide substrate, while the C-terminal lowers the  $K_m$  for NAD<sup>+</sup> (which is contrary to that observed with yeast Hst2) (56). In 2013, Davenport et al. identified residues 641-665 as the C-terminal regulatory segment (CTR) and crystallized SIRT1 catalytic core in complex with this CTR (46). The CTR forms a  $\beta$  hairpin loop that complements the parallel  $\beta$  sheet of the Rossmann-fold where NAD<sup>+</sup> is bound (Figure

1.4). Two residues, Arg276 and Glu656 form a salt bridge between the catalytic core and the CTR. This CTR-mediated “augmentation” seems to stabilize the active site.

The N-terminal region of SIRT1 has also been demonstrated to be critical for the binding of sirtuin-activating compounds (STACs). Recently, Dai et al. engineered and characterized a mini SIRT1 construct containing only the minimal structural elements required for the catalysis and activation of STACs, including the catalytic core, the STAC-binding domain (SBD) and the CTR (55). Their structural and biochemical studies demonstrated that STACs bind to the N-terminal domain (will be discussed into detailed in the latter section).

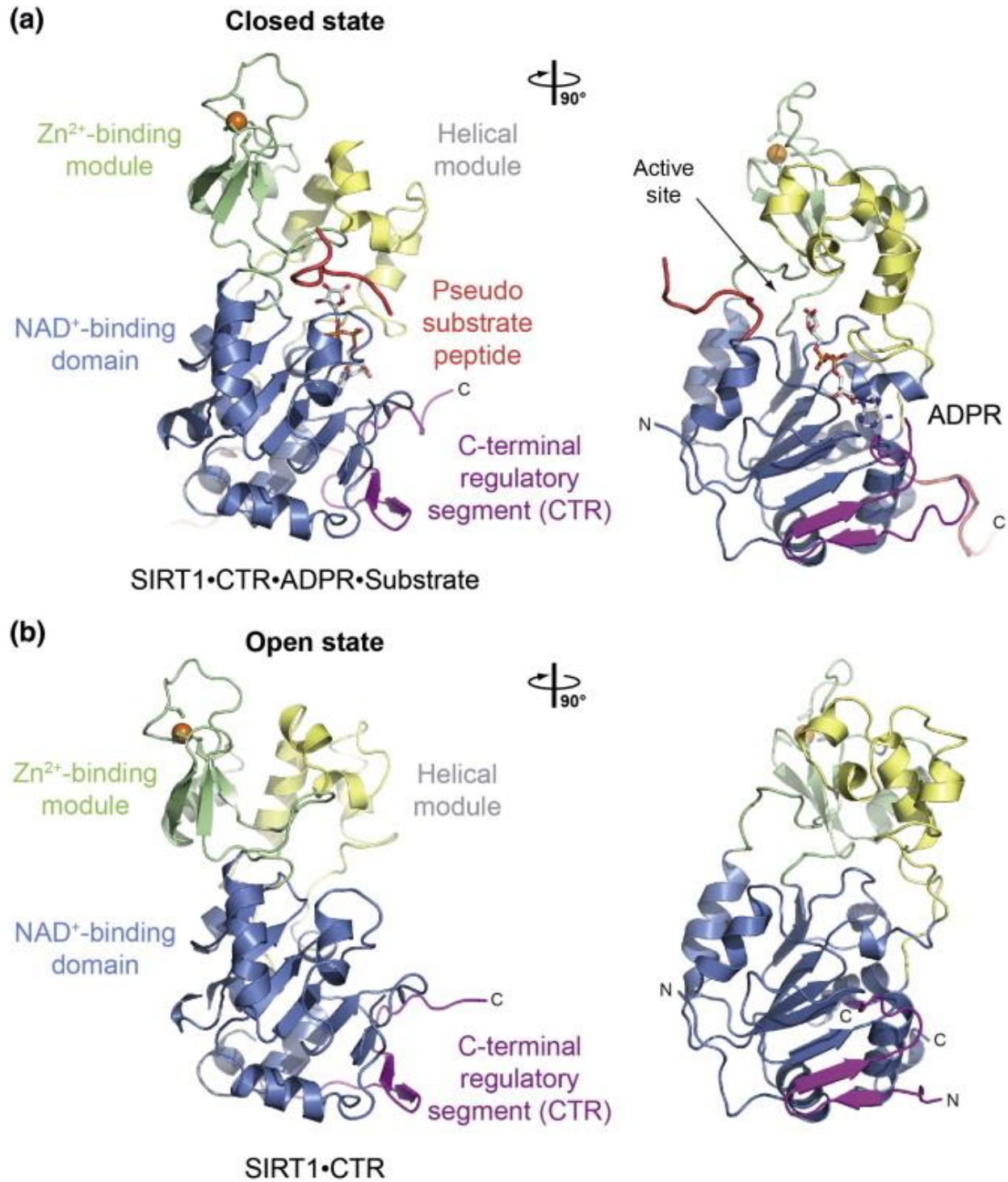


Figure 1.8. Structure of *H. sapiens* SIRT1. (a) Crystal structure of the quaternary SIRT1<sup>CAT</sup>.CTR·ADPR·Substrate complex in ribbon representation. (b) Crystal structure of the SIRT1<sup>CAT</sup>.CTR heterodimer, displayed in the same orientation as in (a). Views rotated 90° are shown on the right. Figures are adapted from reference (46).



### 1.3.2. Catalytic mechanism of sirtuins

The most common reaction catalyzed by sirtuin enzymes is  $\text{NAD}^+$  dependent protein deacetylation, resulting in the formation of deacetylated lysine, nicotinamide, and 2'-O-acetyl-ADP-ribose (OAADPr) (Figure 1.10) (57). The overall reaction couples amide hydrolysis to ester synthesis with the help of  $\text{NAD}^+$ . Structural studies of sirtuins, in conjunction with other biochemical approaches, such as isotope-labeling and chemical probes, provide insights into the catalytic mechanism of sirtuins. In general, the reaction proceeds via the nucleophilic attack of the carbonyl oxygen of the acylated substrate to the C1' ribose of  $\text{NAD}^+$ , resulting in the cleavage of the nicotinamide moiety of  $\text{NAD}^+$  and formation of C1'-O-alkylimidate intermediate (Figure 1.11). The alkylimidate intermediate undergoes the cyclization reaction followed by hydrolysis, generating the deacetylated product and 2'-O-acetyl-ADP-ribose (OAADPr) species. The latter is slowly isomerized (non-enzymatically) to form 3'-OAADPr.

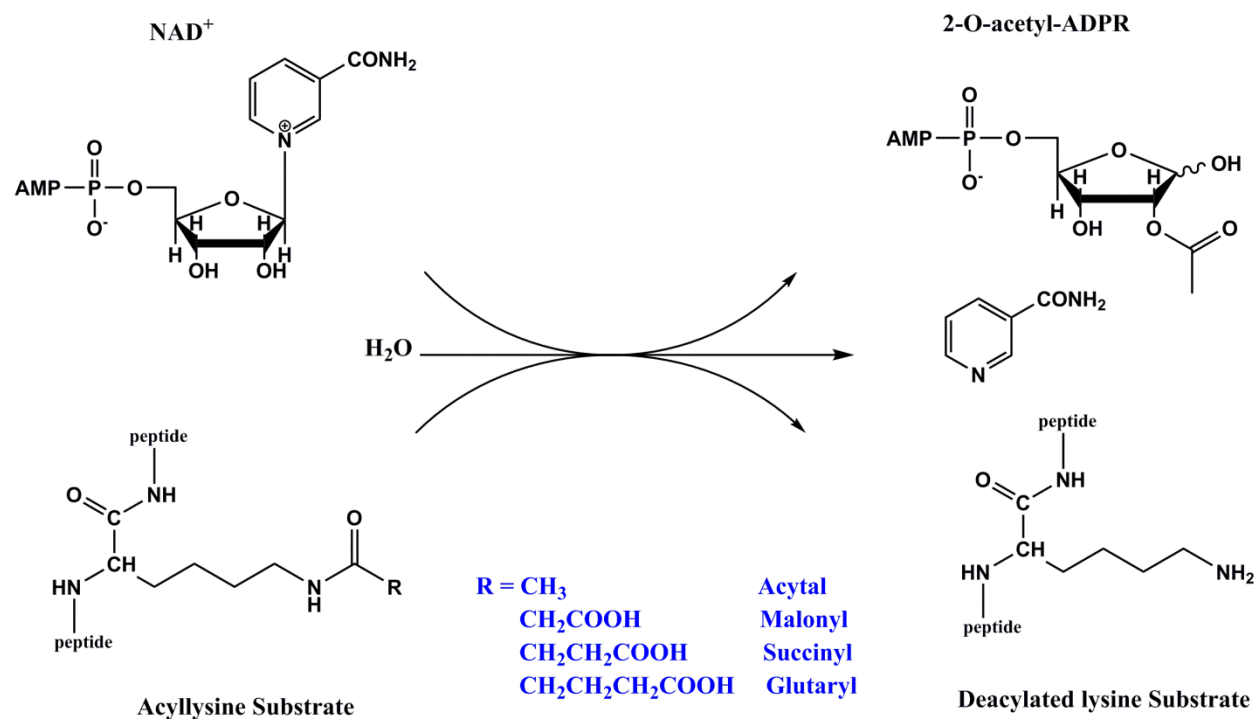


Figure 1.9. Overall deacetylation reactions catalyzed by sirtuins.

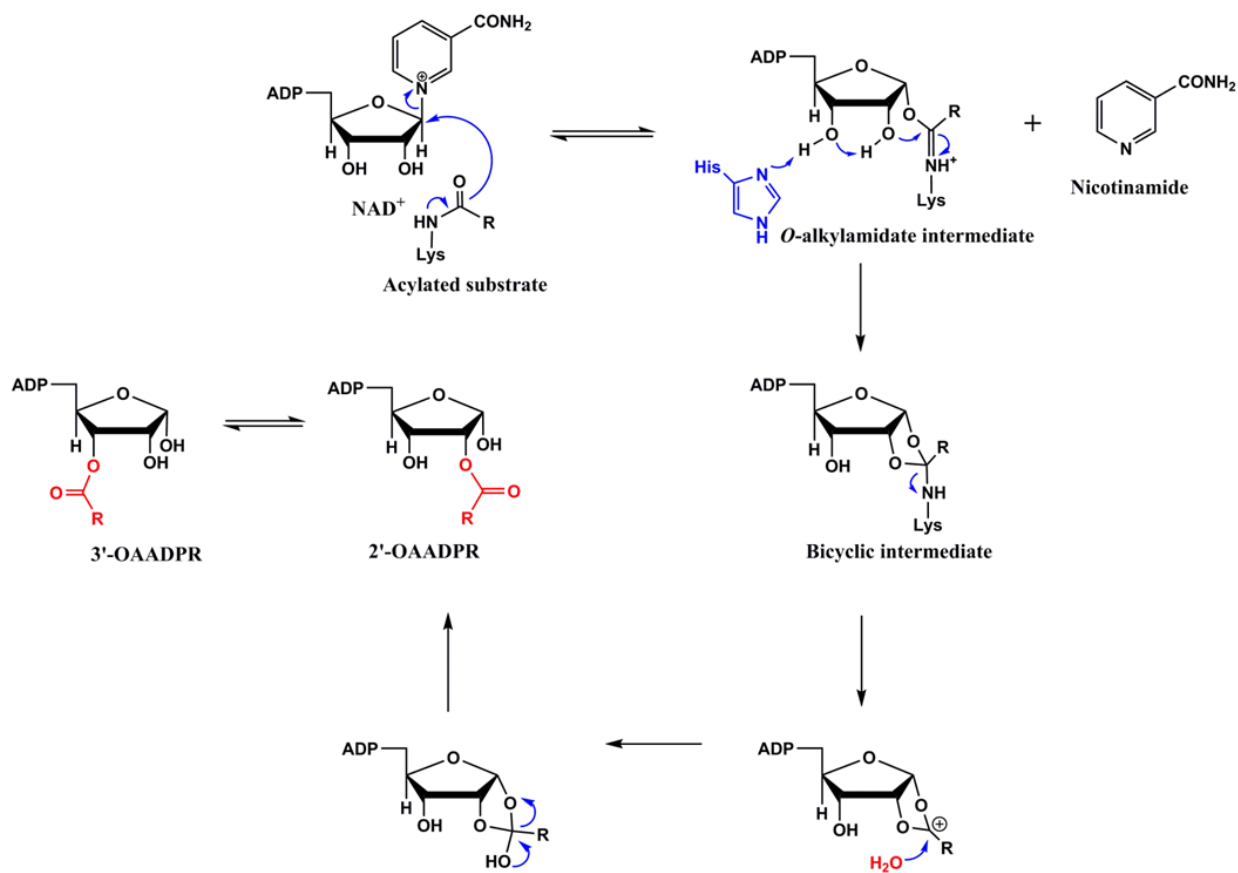


Figure 1.10. Schematic representation of the sirtuin catalyzed reaction mechanism. The sirtuin catalyzed reaction proceeds via the nucleophilic attack of the carbonyl oxygen of the acylated substrate to the C1' ribose of NAD<sup>+</sup>, resulting in the cleavage of the nicotinamide moiety of NAD<sup>+</sup> and formation of C1'-O-alkylimidate intermediate. The alkylimidate intermediate undergoes the cyclization reaction followed by hydrolysis, generating the deacylated product and 2'-O-acyl-ADP-ribose (OAADPr) species. The latter is slowly isomerized (non-enzymatically) to form 3'-OAADPr.



### ***1.3.2.1. Cleavage of the glycosidic bond***

The deacetylation reaction of sirtuins is initiated by the binding of both acetyllysine and NAD<sup>+</sup> to the catalytic site. The first chemical step of the sirtuin reaction involves the cleavage of the glycosidic bond of NAD<sup>+</sup> and addition of the acetyl oxygen to C1' of the nicotinamide ribose, forming a C1'-O-alkylamidate intermediate. It has been debated as to how the cleavage of the glycosidic bond occurs, and three mechanisms have been proposed in literature, including stepwise S<sub>N</sub>1, S<sub>N</sub>2, or highly asynchronous S<sub>N</sub>2 mechanism (Figure 1.11) (58). The S<sub>N</sub>1 mechanism requires the full dissociation of the nicotinamide to form an enzyme-stabilized oxacarbenium ion prior to nucleophilic attack of the acetyl oxygen of acetyllysine at the 1'-carbon of the nicotinamide ribose. Zhao et al. crystallized a non-active ternary complex of the yeast Sir2 homolog Hst2 with an acetyl-lysine peptide and a nonhydrolyzable NAD<sup>+</sup> analog (carba-NAD<sup>+</sup>). This observed conformation precluded attack of the acetyl oxygen at the 1'-carbon of the nicotinamide ribose and thus appears to support the stepwise S<sub>N</sub>1 mechanism (39). However, a different NAD<sup>+</sup> conformation was also observed in the ternary complex structure of Sir2Tm bound with native substrates acetyllysine and NAD<sup>+</sup> (59). The acetyl oxygen was placed 3.2 Å from the 1'-carbon on the α face of the nicotinamide ribose in this NAD<sup>+</sup> conformation, which seemed to satisfy the positioning requirements for acetyl oxygen attack without the formation of the an oxacarbenium intermediate. Biochemical studies by Smith and Denu proposed a S<sub>N</sub>2 mechanism (60), in which the association of the nucleophile (acetyllysine) at the transition state is required. By performing single-turnover kinetics of Hst2 monitoring nicotinamide formation with acetyl-lysine analogues containing electron withdrawing groups (monofluoroacetyllysine, difluoroacetyllysine, trifluoroacetyllysine, etc), Smith and Denu revealed that the nicotinamide formation rate decreased with decreasing nucleophilicity of the

amide oxygen. Importantly, the  $K_d$  values for these acetyllysine analogues to the enzyme was not diminished, thus the reduced formation rates observed was not due to the reduced binding affinity. Their results appeared to rule out the stepwise  $S_N1$  mechanism, in which nicotinamide formation should be independent on the nucleophilicity of the amide oxygen. As an alternative to either  $S_N1$  or  $S_N2$  mechanism, the asynchronous  $S_N2$  mechanism appears to be more attractive, in which an oxocarbenium ion is formed at the transition state during the time of both extensive bond cleavages to the leaving group and weak bond formation to the nucleophile (Figure 1.7, middle). More recently, ab initio QM/MM computational studies on TmSir2 by Hu et al. support this mechanism (61). The results of molecular dynamic simulations suggest that no stable oxocarbenium intermediate needs to be formed during the reaction. Instead, the calculated transition state is very loose and dissociative and requires the participation of the acetyl-lysine, indicating that the nicotinamide cleavage reaction employs “a highly dissociative and concerted displacement mechanism”. Kinetic isotope effects and computational studies on AfSir2 catalyzed reaction by Cen et al. also reached at a similar conclusion, providing additional support for the asynchronous  $S_N2$  mechanism (62). Despite of the intensive studies in past years, several important questions regarding the nicotinamide cleavage still remain unanswered. Do all sirtuin isozymes follow the identical mechanism? Is substrate destabilization required prior to the nucleophilic attack? Answers to the above questions are expected to assist a more comprehensive understanding of sirtuin chemistry.

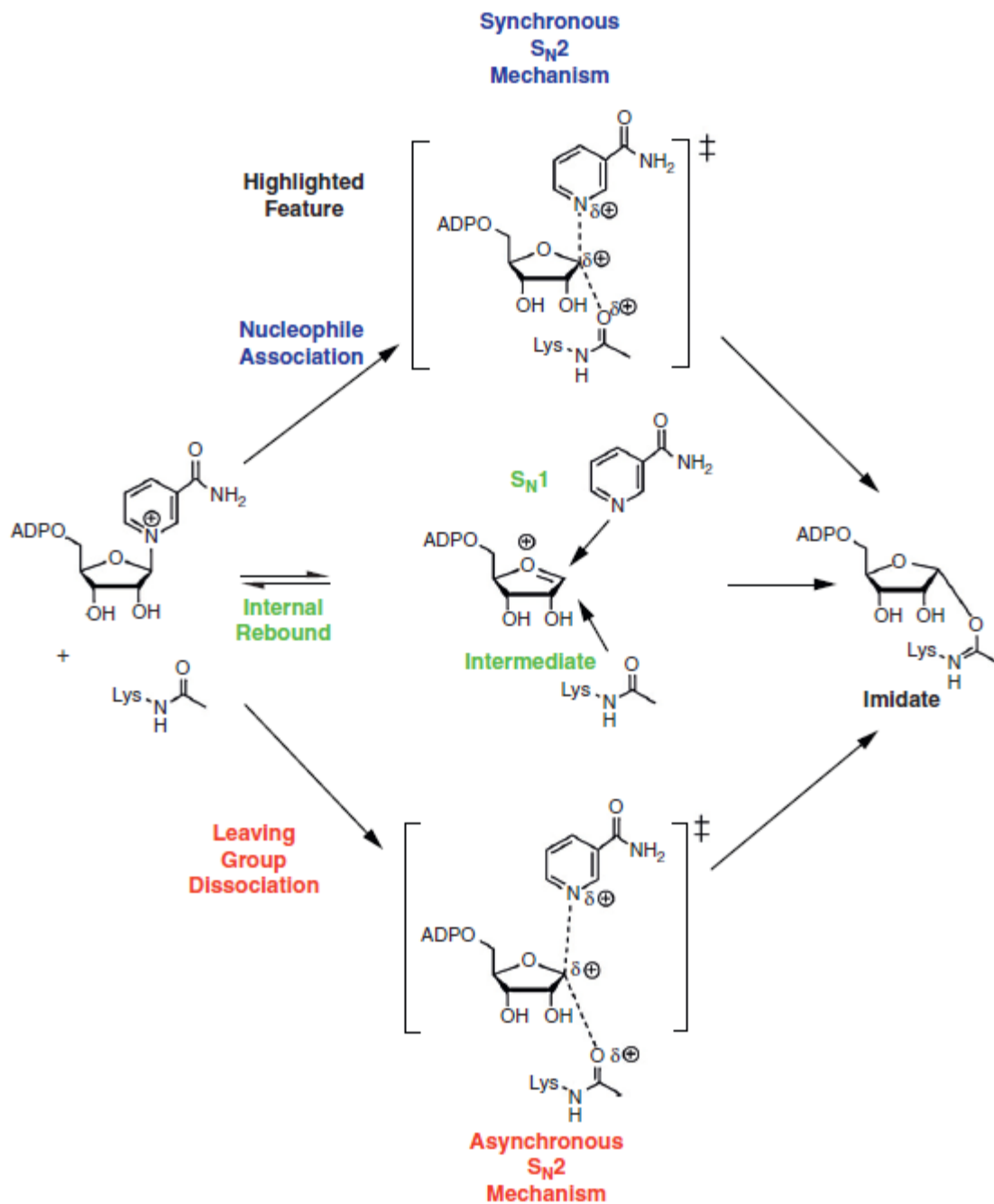


Figure 1.11. Mechanisms of reaction of NAD<sup>+</sup> with acetyllysine nucleophile. Three mechanistic possibilities can be considered for reaction of acetyllysine with NAD<sup>+</sup>, as shown by top (S<sub>N</sub>2), middle (S<sub>N</sub>1) and bottom (asynchronous S<sub>N</sub>2) reaction pathways. Figure is adapted from reference (63).

### ***1.3.2.2. From imidate intermediate to products***

C1'-*O*-alkylamidate intermediate is formed after the cleavage of the glycosidic bond linking nicotinamide to the N-ribose and the transfer of the ADP-ribose to the acetyllysine. Isotope labeling by Sauve et al. and Kinetic experiments by Smith et al. support the existence of this intermediate (64-66). The most direct support of the above mechanism emerges from the crystal structure of Sir2Tm in complex with an S-alkylamidate intermediate, which is an analog of the naturally occurring *O*-alkylamidate intermediate (Figure 1.12) (28). The imidate intermediate is proposed to have two fundamental reaction pathways. The first pathway is the reversal to NAD<sup>+</sup> via  $\beta$ -face attack of nicotinamide on the anomeric carbon (so called "base exchange" reaction). This base exchange mechanism has been implicated in the inhibition of enzyme reaction in the presence of nicotinamide (67, 68). The other pathway is to proceed to complete the sirtuin deacetylation reaction. After formation of the *O*-alkylamidate, the 2'-OH of the nicotinamide ribose is activated by deprotonation of the conserved histidine residue (His135 in Hst2) at the active site of the enzyme followed by the attack the *O*-alkylamidate carbon to form a 1',2'-intermediate (58). Mutation of His135 to Ala does not affect the base-exchange reaction, but slows down the overall deacetylation reaction, suggesting that the above His residue is involved in the chemical steps after the formation of *O*-alkylamidate and nicotinamide (65). Moreover,  $\beta$ -2'-deoxy-2'-fluororibo-NAD<sup>+</sup>, which lacks the 2'-OH group, also reacts with Hst2 to form a similar imidate intermediate, but only results in the release of acetate when the reaction is quenched with alkaline solution, suggesting that the 2'-OH is required to complete the sirtuin deacetylation reaction (27). The 1',2'-cyclic intermediate has yet to be directly observed in sirtuin deacetylation reactions, although kinetic and mass spectrometry experiments suggests its existence (65, 66). Zhou et al. obtained the crystal

structure of SIRT5 (which catalyzes desuccinylation reaction faster than deacetylation) in complex with 1',2'-cyclic intermediate by incubating SIRT5-H3K9 with the thiosuccinyl peptide and NAD<sup>+</sup> (Figure 1.13), providing the first bicyclic intermediate for a sirtuin-catalyzed deacylation reaction (43).

To complete the reaction, the bicyclic intermediate is further hydrolyzed to a free lysine and 2'-acetyl-*O*-ADPR (2'-OAADPR). Following release from the sirtuin active site, OAADPR undergoes nonenzymatic interconversion between 2'-OAADPR and 3'-OAADPR (69).

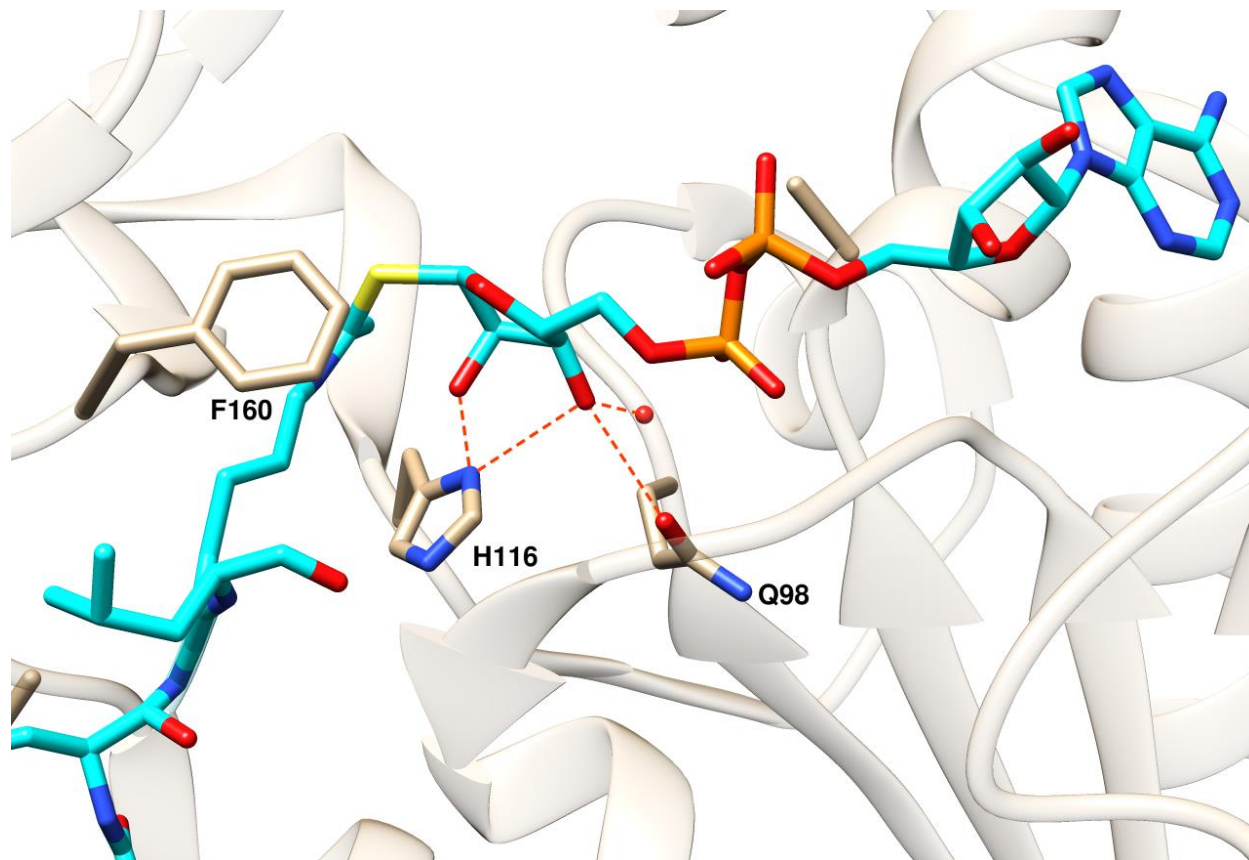


Figure 1.12. Structure of a Sir2Tm-S-Alkylamidate intermediate complex. Hydrogen bond network between side chains in Sir2Tm (grey) and the S-alkylamidate intermediate (cyan). Hydrogen bonds are shown in orange (40).

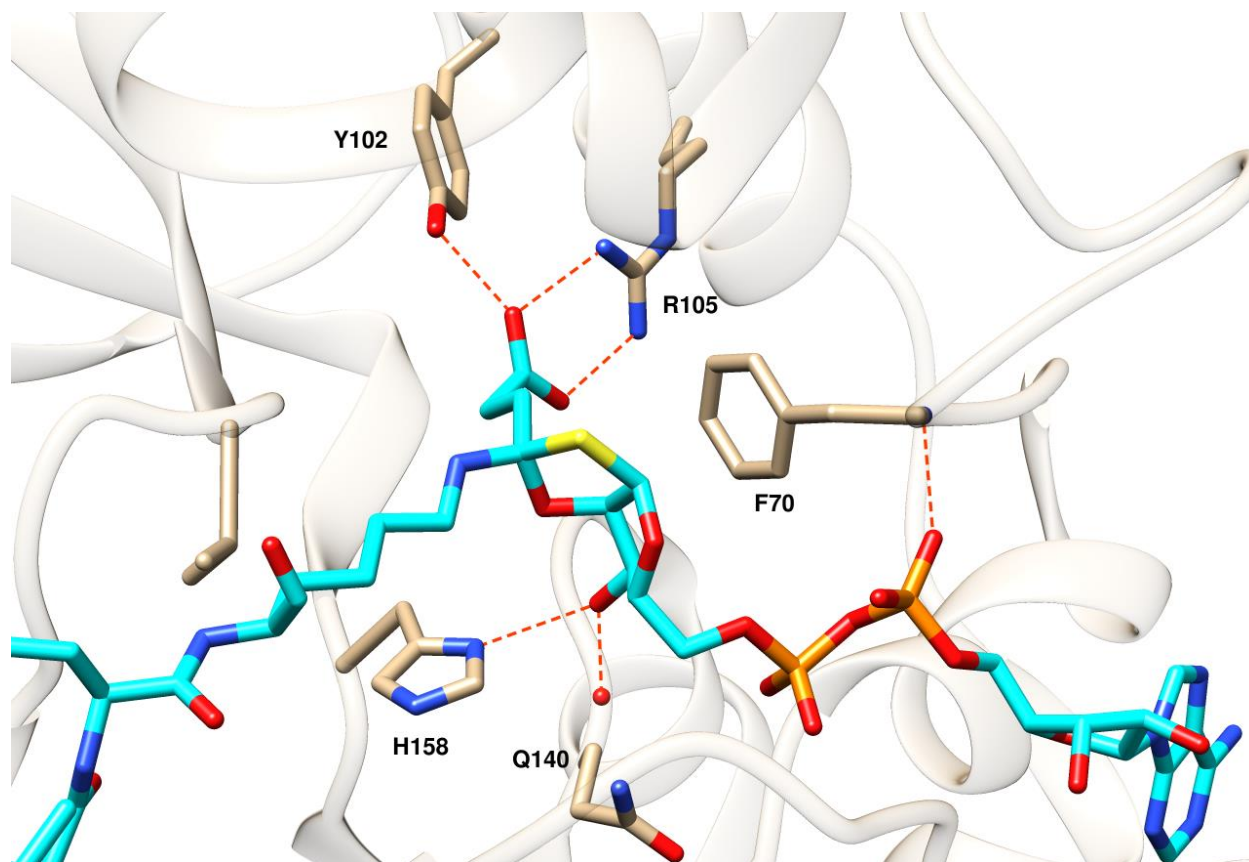


Figure 1.13. Structure of a SIRT5-bicyclic intermediate complex. Bicyclic intermediate interacts with SIRT5 via hydrophobic interaction and hydrogen bonding. The hydrogen bonds are shown in orange (43).

### 1.3.3. ADP-ribosyl transferase activity

Although protein deacetylation is thought to be the primary activity displayed by sirtuins, several reports have suggested that some sirtuins (e.g., SIRT4 and SIRT6) exhibit ADP-ribosyltransferase activity (70-72), the possible mechanism of NAD<sup>+</sup>-dependent protein ADP-ribosylation has not been explicitly demonstrated, and the nature of the linkage, the site of modification and the final products remain unclear. Kowieski et al. has proposed two distinct ADP-ribosylation mechanisms, both of which require an acetyl-lysine substrate (73). In one mechanism, acetyl-lysine reacts with NAD<sup>+</sup> to form the *O*-alkylamidate intermediate. Importantly, Smith et al. demonstrated that the *O*-alkylamidate intermediate is able to react with other exogenous alcohol nucleophiles, such as methanol or ethanol (65), indicating that an amino acid side chain nucleophile from bound histone might intercept and react with the *O*-alkylamidate intermediate, resulting in ADP-ribosylation instead of deacetylation. In a second ADP-ribosylation mechanism, the acetyl-lysine substrate and NAD<sup>+</sup> bind to the active site and follow the deacetylation process to form OAADPr, which then interacts and reacts with the protein substrate possibly nonenzymatically, resulting in the ADP-ribosylation reaction. However, it has also been suggested that Pfsir2 catalyzes the ADP-ribosyltransfer to protein nucleophiles directly in the absence of an acetyl-lysine substrate and/or in a nicotinamide-insensitive manner, though the acetyllysine independent hydrolysis activity was much less than the acetyllysine-dependent hydrolysis activity (74). <sup>32</sup>P blots demonstrated that SIRT4 might also possess ADP-ribosyltransferase activity in the absence of acetyl-lysine substrates (70, 71). However, the specific residue that is ADP-ribosylated during the catalysis has not been determined. In this case, it is possible that some amino acid residues such as Asn or Gln replace acetyl-lysine to form a similar *O*-alkylamidate intermediate.



## 1.4. Cellular Regulation of Sirtuin Activity

In cells, sirtuin activity may be affected by the quantity of sirtuin molecules, reversible post-translational modifications (PTM) of sirtuin, availability of NAD<sup>+</sup> and nicotinamide.

### 1.4.1. Post-translational modifications (PTM)

Post-translational modifications (PTM) of sirtuins, including phosphorylation, sumoylation, methylation and transnitrosylation, usually occur in N-terminal and C-terminal extensions (so-called regulatory regions). Phosphorylation sites have been identified in all sirtuins, but the biological outcome associated with phosphorylation has only been studied in SIRT1 and SIRT2 (75). Phosphorylation activates SIRT1, but inhibits SIRT2. Multiple phosphorylation sites located in N- and C-terminal domains of SIRT1 have been reported, and several kinases that regulate the activity of SIRT1 have been identified, including DYRK (dual specificity tyrosine phosphorylation-regulated kinase), JNK1 (c-Jun N-terminal kinase 1), cyclin B/Cdk1 (cyclin-dependent kinase 1) and protein kinase A (PKA) (76-78). Sasaki et al. identified 13 phosphorylation sites in SIRT5 and cyclinB/Cdk1 as a cell cycle-dependent kinase that phosphorylates and activates SIRT1 (76). Gerhart-Hines et al. demonstrated that cAMP/PKA pathway activates SIRT1 activity and promote fatty acid oxidation (78). The cAMP-dependent phosphorylation at Ser434 of SIRT1 increases its deacetylase activity, presumably by reducing the  $K_m$  for NAD<sup>+</sup> (78). However, the detail mechanism of SIRT1 activation via phosphorylation remains unclear. SIRT2 is phosphorylated at Ser331 and Ser335 within the C-terminal region by cyclin E-Cdk2, cyclin A-Cdk2, and p35-Cdk5 both in vitro and in cells (79). Phosphorylation of Ser331 is catalyzed by cyclin-dependent kinase and inhibits the activity of SIRT2, whereas the enzyme and effect of phosphorylation of Ser335 remain unknown.

### **1.4.2. Role of NAD<sup>+</sup>**

The catalytic activities of sirtuins are ascribed to be strictly regulated by the levels of intracellular co-substrate NAD<sup>+</sup> and product nicotinamide. The unique catalytic consumption of NAD<sup>+</sup> indicates that sirtuins might be sensitive to changes in intracellular NAD<sup>+</sup> concentration. Generally speaking, decrease in the NAD<sup>+</sup> level, that accompanies organismic aging, has been found to downregulate the sirtuin activity. On the other hand, increase in NAD<sup>+</sup> level that occurs during exercise, fasting, and caloric restriction, due to multiple ways of cellular regulations, can activate sirtuin activity (80). It has been suggested that increasing NAD<sup>+</sup> synthesis through the NAD<sup>+</sup> salvage pathway could increase sirtuin activity. For example, nicotinamide phosphoribosyltransferase (NAMPT) catalyzes the formation of NMN by the addition of 5-phosphoribosylpyrophosphate to nicotinamide (81). NMN is then converted to NAD<sup>+</sup> by NMN adenylyltransferase. Small molecules that inhibit NAMPT have been demonstrated to decrease SIRT2 activity, providing evidence that sirtuin activity could be regulated by changes in the cellular NAD<sup>+</sup> concentration (82). Moreover, AMP activated kinase (AMPK), which is stimulated by decrease in the energy status, nutrient and oxygen deprivation, and increased energy expenditure, have been demonstrated to activate NAD<sup>+</sup> synthesis through stimulated transcription of NAMPT (83).

### **1.5. Physiological and Pathological Roles of Human Sirtuins**

There are seven homologous sirtuins in humans (SIRT1-SIRT7), most of which catalyze the deacetylation reactions. Sirtuins exhibit their functional roles both via “epigenetic” and “metabolic” regulatory pathways, which are manifested in promoting longevity by modulating cytoskeletal formation/rearrangement, stress factors, energy metabolism, DNA repair and silencing, inflammation, differentiation, among others. The biological functions SIRT isozymes

are different due to their subcellular localizations, expression pattern, binding partners, and substrate specificity in terms of recognizing and cleaving the acyl-moieties from their cognate protein surfaces. Due to their involvement in such diverse biological processes, sirtuins play important pathological roles, thereby becoming attractive targets for drug design.

### **1.5.1. Cellular localizations of seven human sirtuins**

The functional diversification of seven human sirtuins is clearly illustrated by their different cellular locations and their ability to shuttle between organelles. Three of them, SIRT1, SIRT6 and SIRT7 mainly localize in the nucleus. SIRT2 is the only isozyme that mainly localizes to cytoplasm. Recent finding suggests that SIRT2 shuttles to the nucleus during certain conditions such as mitosis and bacterial infection (84, 85). SIRT3, SIRT4, and SIRT5 are mainly localized in mitochondria. The localization of SIRT3 has been debated (86-88). SIRT3 is also found in the nucleus under normal condition (87). SIRT4 is exclusively located in mitochondria, whereas SIRT5 is present both mitochondrially and extramitochondrially (5, 89, 90).

### **1.5.2. Substrate specificity of sirtuins**

The number of reported sirtuin substrates is continually increasing in recent years (Table 1.2). SIRT1, the most studied member of the sirtuin family so far, deacetylates more than 20 of histone and non-histone proteins, including, but not limited to, histone H1, H3, H4, p53, p300, PGC-1 $\alpha$  and a number of transcriptional factors. SIRT2 also deacetylates histone H4 (H4K16) (91), p53, p300, and a number of other non-histone substrates, such as  $\alpha$ -tubulin (92), p53, p300 (93), CDH1 (94), CDC20 (94). SIRT3 deacetylates H3, H4, and a number of metabolic enzymes. No deacetylation substrate for SIRT4 has yet been found. However, SIRT4 has been reported to inhibit the activity of glutamate dehydrogenase (GDH) by ADP-ribosylation (71).

SIRT5 deacetylates, desuccinylates and deglutarylates carbamoyl phosphate synthase 1 (CPS1) (10, 11, 95); It also desuccinylates a number of other metabolic enzymes, including pyruvate dehydrogenase complex (PDC) and succinate dehydrogenase (SDH)(5). SIRT6 was recently found to deacetylate histone H3 and C-terminal-binding protein-interacting protein (CtIP) (96, 97). The only substrate that has been explicitly identified for SIRT7 is H3 (H3K18)(98), while indirect evidence suggests that SIRT7 deacetylates p53 (99). A more detailed account of the roles sirtuins plays in the physiological system is reviewed in the next section.

Although a thorough understanding of the protein substrate selectivity of sirtuins is lacking, recent structural and computational studies shed light on the peptide sequence preferences of sirtuins. Initial structural studies on sirtuins bound with non-native substrates revealed that the binding of acetyllysine peptide to sirtuins is dominated by the peptide backbone hydrogen bonding, forming an enzyme-substrate  $\beta$  sheet ( $\beta$  staple; Figure 1.5) (37). These findings suggested that sirtuins possess relatively little substrate specificity. Some other studies also supported this conclusion: peptide library screening and steady-state kinetic studies by Blander et al. indicated that SIRT1 had no substrate specificity (100); in vitro deacetylation assays using a variety of acetylated substrate by Khan et al. suggested that Hst2 employed conformational rather than sequence specificity for substrate recognition (101). However, other later studies led to different conclusions. Garske et al. investigated substrate specificity of SIRT1 using a one-bead, one-compound (OBOC) acetyl-peptide library followed by mass spectroscopy and in-solution deacetylase assay and found that SIRT1 displayed considerable preference for some substrate sequences (102). Structural studies of Sir2Tm bound with five different substrates suggested that the first residue N-terminal to the acetyllysine (position -1) and the second residue C-terminal to the acetyllysine (position +2) are important for sirtuin

substrate binding (103). Rauh et al. used an acetylome peptide microarray to identify several sirtuin substrates and also characterized the substrate preferences of the human sirtuins by statistical analysis (104). Such unbiased methods are important for identifying the *in vivo* substrates of sirtuin isoforms, especially SIRT4 and SIRT7.

Table 1.2. Selected Human Sirtuin Substrates

	Histone Substrates	Non-histone Substrates
SIRT1	H1 (105), H3 (105), H4 (105)	p53 (106), p300 (107), AceCS1 (108), PCG1- $\alpha$ (109), Ku70 (110), FOXO 1 (111) and 4 (112), NF- $\kappa$ B (113), Tat (114), CRTC2, CREB (115), etc.
SIRT2	H4 (91)	$\alpha$ -tubulin (92), p53, p300 (93), CDH1 (94), CDC20 (94), RIP1 (116),PEPCK, CDK9 (117), etc.
SIRT3	H3 (118), H4 (87)	p53, AceCS2 (108, 119), GDH (120), Ku70 (121), SdhA (122), MnSOD (123), ALDH2 (124), CypD (125), LCAD (126), etc.
SIRT4	N/A	GDH (71)
SIRT5	N/A	CPS1 (95), PDC (5), SDH (5)
SIRT6	H3 (96)	CtIP (97, 127)
SIRT7	H3 (98)	p53 (99)

N/A: No histone substrate has been identified for the corresponding enzyme.

### 1.5.3. Physiological roles of human sirtuins

In 2000, Sir2, the first sirtuin enzyme identified in budding yeast, was found to increase the life span of yeast (23). Since then more than 1000 peer-reviewed publications have shown the importance of sirtuin involved in promoting health span (128). Extensive studies cemented the roles of sirtuins in various biological processes, including transcriptional regulation, DNA repair, metabolism, aging, and cancer development.

### ***1.5.3.1. Transcription regulation***

In eukaryotic cells, the chromatin is composed of DNA and histone that pack together other via electrostatic interaction. Reversible acetylation is a common way to regulation gene expression by modulating the compact state of chromatin (129). Acetylation of lysine residues in histone tail neutralizes the positive charge and loosens the compact state of chromatin, making it accessible for gene transcription and protein expression. To the contrary, deacetylation of histone inhibits the gene transcription. Indeed, the histone deacetylase activity of sirtuins has been linked to transcription regulation both directly and indirectly (130).

In mammals, except for SIRT4 and SIRT5, all other sirtuins (SIRT1-SIRT3, SIRT6 and SIRT7) have been reported to deacetylate histones (Table 1.2.). SIRT1 deacetylates H1, H3 lysine and H4 lysine, with the preference for H4K16 (105). SIRT1 initiates gene repression through deacetylation of H4K16, recruitment of H1 and loss of methylated H3-K7. SIRT2 also deacetylates H3 and H4. SIRT3 and SIRT7 have been recently found to deacetylate H3K18 and promote transcriptional regression.

Sirtuins also regulate transcription by acting on a number of transcriptional factors (p53, FOXO1, PGC1 $\alpha$ , etc.) which regulate a set of gene expressions that play important roles in biological functions, including DNA repair, metabolism and cancer. SIRT1 also deacetylates and activates the human immunodeficiency virus (HIV) transactivator Tat, leading to the Tat-mediated transactivation of HIV promoter (114).

### ***1.5.3.2. Metabolism***

Sirtuin activity is linked to multiple metabolic pathways for two reasons. First, sirtuin catalyzed reactions require NAD<sup>+</sup>, which is a cofactor of various enzymes involved in metabolic pathways in cells (131). Second, many substrates of sirtuins are themselves metabolic enzymes

(Table 1.2.) Indeed, sirtuins are involved in a number of different metabolic pathways, including lipid, glucose and glutamine metabolism, ketone body synthesis, and urea cycle. Specifically, most sirtuins play roles in regulating metabolism and energy homeostasis to help the cell adapt to low-energy conditions like fasting and CR environment (132).

(a) Glucose metabolism

Glucose is a primary resource for cell survival and proliferation, so its level is strictly regulated via a number of different biological processes. Sirtuins have been found to modulate some of these processes, including glycolysis, gluconeogenesis and insulin secretion (133). SIRT1 modulates both glycolysis and gluconeogenesis by regulating several important metabolic factors. PGC1 $\alpha$  is a key regulator of mitochondria biogenesis in vertebrates (134). Activation of PGC1 $\alpha$  by SIRT1 induces gluconeogenic genes and represses glycolytic genes during fasting, thereby inducing glucose production (134). On the other hand, Liu et al. demonstrated that in liver during late fasting, SIRT1 could also suppress glucose production by deacetylating CRTC2 and promoting its ubiquitin-dependent degradation (135). SIRT2, SIRT3 and SIRT4 are also involved in regulating gluconeogenesis, which plays an important role when energy level is limited. SIRT2 deacetylates and stabilizes PEPCK, the rate-limiting enzyme of gluconeogenesis, to promote glucose production during fasting. SIRT3 and SIRT4 regulate the activity of GDH a mitochondria enzyme that converts glutamate to  $\alpha$ -ketoglutarate in the TCA (tricarboxylic acid) cycle, in an opposite manner (71, 120). SIRT3 deacetylates GDH in vivo and the activity of GDH is found to be increased in the presence of SIRT3 in vitro, although the physiological role of GDH acetylation has not been conclusively established. SIRT4 ADP-ribosylates and inhibits GDH, leading to reduced insulin secretion in response to amino acids. SIRT5 has regulatory effects on glucose metabolism by desuccinylating and inhibiting pyruvate

dehydrogenase (PDH), succinate dehydrogenase (SDH), leading to decreased mitochondrial respiration in mouse liver and embryonic fibroblasts. Recently, SIRT6 is also found to assist maintain glucose homeostasis through deacetylation of histone H3K9 which control the expression of multiple glycolytic genes, such as PFK1 and GLUT1 (*136*). SIRT6 deficiency causes a pronounced increase in glucose uptake both in muscle and brown adipose tissues.

#### (b) Lipid metabolism

Lipid metabolism, comprising of lipids synthesis, storage and expenditure, is tightly regulated in the cells. The role SIRT1 plays in lipid metabolism is complicated. It has been elegantly demonstrated that SIRT1 plays an important role in regulating lipid metabolism under extreme conditions, such as fasting or high fat diet. SIRT1 activation in high fat fed mice enhances fat oxidation and protects the mice against metabolic disorders (*137, 138*).

Hepatocyte-specific deletion of SIRT1 increases susceptibility to body weight gain upon high fat feeding, while the whole-body SIRT1 knock out mice fed on high fat diet impairs glycerolipid/free fatty acid cycle (*139, 140*). It has also been suggested that SIRT1 inhibits lipid synthesis and stimulates fatty-acid oxidation in response to fasting (*141*). SIRT1 deacetylates and activates PGC1 $\alpha$ , which upregulates the expression of several enzymes involved in fatty acid oxidation, including medium chain acyl-CoA dehydrogenase (MCAD) and carnitine palmitoyltransferase-1a (CPT-1a) (*109, 141*). During fasting, SIRT1 helps in maintaining the energy balance via sequential induction of CRTC2 and FOXO1 (*135*). For example, it induces the expression of the rate-limiting lipolytic enzyme adipose triglyceride lipase (ATGL) via deacetylating FOXO1 (*142*). SIRT1 also deacetylates and inhibits sterol regulatory element-binding protein (SREBP), a transfactor that is a critical regulator of lipid and sterol homeostasis in eukaryotes, resulting in decreased expression of lipogenic genes, lipid synthesis and fat



storage (143, 144). The above studies seem to show clear evidence of SIRT1's role in lipid metabolism. However, some studies yield contradictory conclusions. For example, Pfluger et al. showed that SIRT1-overexpressing mice were protected from hepatic steatosis under high-fat diet (145), while Qiang et al. found the opposite result, attributing the outcome to SIRT1 inhibition of cAMP-responsive element-binding protein, a transcription factor that normally activates fatty acid metabolism and gluconeogenesis (115). Moreover, overexpression of SIRT1 in the forebrain of female mice increased fat mass and increased expression of adipogenic genes in white adipose tissue, leading to increased fat accumulation and decreased physical activity (146). Based on these contradicted results, it has been proposed that SIRT1 mediated decomposition or adipogenesis may be tissue specific and dependent on expression the level of the enzyme (132).

The expression of SIRT3 is upregulated during fasting in liver and brown adipose tissues. It has been demonstrated that SIRT3 deacetylates and activates long-chain acyl Coenzyme A dehydrogenase (LCAD) under fasting condition, leading to the upregulation of long-chain fatty acids oxidation (126). SIRT3-deficient mice exhibits reduced ATP levels and intolerance to cold exposure during fasting, suggesting that SIRT3 also plays an important role in regulation of fatty acid oxidation (147). By contrast, SIRT4 seems to negatively regulate fatty-acid oxidation in liver and muscle cells (148). SIRT6 is implicated in both lipid synthesis and fatty acid oxidation. Liver-specific deletion of SIRT6 in mice leads to reduced fatty-acid oxidation and triglyceride synthesis (149).

#### (c) Other metabolism

Sirtuins are also involved in other metabolism that specifically associates with fasting and limited nutrient supply. For example, SIRT3 upregulates the electron transport chain via

deacetylating succinate dehydrogenase A (SDHA) (150). During fasting, SIRT3 deacetylates and activates mitochondria 3-hydroxy-3-methylglutaryl-CoA synthase 2(HMGCS2), the rate-limiting enzyme in ketone body synthesis (151). It also deacetylates and stimulates ornithine transcarbamoylase (OTC), promoting the urea cycle during calorie restriction (CR). SIRT3 knockout mice exhibits a failure to reduce orotic acid levels, a known outcome of OTC deficiency (152). SIRT5 deacetylates and activates CPS1, the rate-limiting enzyme of the urea cycle (95). As mentioned in the previous section, SIRT5 has recently been defined as a lysine demalonylase, desuccinylase and deglutarylase, and further studies suggest that the above activities are involved in the deacylation of CPS1 (10, 11).

#### ***1.5.3.3. DNA repair***

Our cells are susceptible for environmental conditions which often lead to the DNA damages via single (SSB) and double-strand breaks (DSB). Eukaryotes have evolved to circumvent/repair DNA damage via four major pathways: (1) homologous recombination (HR), (2) non-homologous end joining (NHEJ), (3) base-excision repair (BER), and (4) nucleotide-excision repair (NER). Studies in model organisms suggest that some members of sirtuin family (SIRT1-SIRT3, SIRT4 and SIRT6) play important roles in maintaining genomic integrity by regulating DNA repair (153, 154). Some of them regulate DNA repair factors directly via their deacetylation, whereas the other influence DNA repair by preventing DNA damage indirectly via modulating the cell cycle and preventing oxidative stress (154).

SIRT1 plays a pivotal role in DNA repair via regulating different pathways. SIRT1 null embryos exhibits impaired DNA damage response and reduced the ability to repair the DNA damage (155). It has been demonstrated that SIRT1 regulates a number of proteins important for HR repair, such as NBS (156), Rad51 (157), and the DSB sensing protein WRN (158).

SIRT1 regulates NHEJ via cooperative action with ataxia telangiectasia mutated (ATM) and HDAC1 in the neuronal DSB response (159). In postmitotic neurons, after being recruited to DSBs, SIRT1 stimulates the activity of ATM, which primes the cellular DSB signaling cascade for DNA repair. On the other hand, SIRT1 also deacetylates and stimulates HDAC1, which is crucial for DSB repair through NHEJ. SIRT1 also plays key roles in NER by deacetylating xeroderma pigmentosum group A and C (XPA and XPC) and recruiting them to the sites of DNA damage (160, 161).

SIRT2 links to DNA repair mainly via its regulatory roles in cell cycle and replication stress response. During G2/M phase of mitosis, SIRT2 enters nuclei and deacetylates histone H4K16Ac (85), facilitating H4K20 methylation and regulating mitotic entrance (162). The loss of SIRT2 is associated with greater genome instability and DNA damage. The replication stress response is one of the DNA damage response (DDR) pathways that recognizes challenges to DNA replication and mobilizes diverse DNA repair and cell cycle checkpoint pathways (163). SIRT2 is found to promote the replication stress response by deacetylating and activating the activity of cyclin-dependent kinase 9 (CDK9) (117).

The mitochondria sirtuins, SIRT3, 4 and 5 are not involved directly in DNA repair. However, their roles in regulating metabolism and preventing the accumulation of reactive oxygen species (ROS) enable them to regulate DNA repair indirectly. Failure to activate MnSOD by SIRT3 leads to high level of ROS (164). SIRT4 inhibits glutamine metabolism by deacetylation induced inhibition of GDH, leading to the cell cycle arrest which provides sufficient time for cells to repair their DNA. Cells lacking SIRT4 continue to proliferate following the DNA damage and thus promoting genomic instability (165, 166).

Accumulative studies have demonstrated the role for SIRT6 in numerous DNA repair pathways, even before the discoveries of its substrates. SIRT6 knockout cells exhibit hypersensitivity to genotoxic agents and genomic instability (167). It has been demonstrated that SIRT6 is required to stabilize DNA-dependent protein kinase in response to induced DSB to promote NHEJ repair (168). Moreover, SIRT6 protects telomeric regions of chromatin by deacetylation of H3K9 and H3K56 (96, 169). CtIP, which is recently identified as a SIRT6 substrate, is a DNA damage response protein which facilitates the resection of DSBs and DNA repair by HR (97). SIRT6 ADP-ribosylates PARP, resulting in an enhanced DSB repair by both NHEJ and HR (170). SIRT6 promotes chromatin remodeling which also plays a crucial role in DSB repair (171).

#### **1.5.4. Pathological roles of human sirtuins**

Since sirtuins are involved in controlling multiple biological processes, especially in DNA repair and metabolism, it is not surprising that they are associated with a number of human diseases such as metabolic disorders, inflammation, type 2 diabetes, cardiovascular disease, Alzheimer's disease, and cancers. Most of the above diseases are age-related, and they are intimately correlated with the sirtuin activities. For example, chronic inflammation impairs metabolic homeostasis, which in turn leads to the the pathogenesis of type 2 diabetes. The implication of sirtuins in various human diseases has led to the identification of sirtuins as potential therapeutic targets.

##### ***1.5.4.1. Inflammation***

Inflammation is an important factor in the pathogenesis of several metabolic and age-related degenerative diseases. Emerging studies have demonstrated that there is a close molecular coordination between different phases of inflammation and the energy metabolism

(172). Since sirtuins play regulatory roles in metabolism, it is not surprising that they are linked to inflammation. Indeed, SIRT1, SIRT2, SIRT3, and SIRT6 have shown anti-inflammation effect.

Several studies have suggested that SIRT1 protects organisms against inflammation via inhibiting the effects of inflammatory factors, such as NF- $\kappa$ B and tumor necrosis factor TNF- $\alpha$ (173, 174). NF- $\kappa$ B, which governs an ancient signaling pathway in insects and vertebrates, is the master regulator of innate immunity (175). NF- $\kappa$ B is a heterodimeric complex of p50 and p65 (RelA) and it controls several genes involved in inflammation, and its activity increase with age in many mammalian tissues and stem cells. The NF- $\kappa$ B signaling pathway in conjunction with SIRT1 integrate energy metabolism to immune responses, contributing to the maintenance of cellular homeostasis (175). SIRT1 deacetylates the p65 subunit of NF- $\kappa$ B and inhibits its signaling pathway, which stimulate glycolytic energy flux during acute inflammation. Macrophages play an important role in initiating obesity-related tissue inflammatory responses (176). It has been demonstrated that SIRT1 represses the inflammatory pathway activity and release of TNF $\alpha$  from LPS-stimulated macrophages (174). Moreover, SIRT1 stimulates oxidative energy production via the activation of AMPK, PPAR $\alpha$  and PGC1- $\alpha$ , which also inhibit NF- $\kappa$ B signaling and suppress inflammation. During inflammation, the transcription of SIRT1 is also suppressed by the pro-inflammatory cytokine IFN- $\gamma$  (177), whereas SIRT1 activator resveratrol restores this decline (178).

NF- $\kappa$ B is also regulated by other sirtuins, including SIRT2 and SIRT6. SIRT2 deacetylates NF- $\kappa$ B subunit p65 at Lys-310, leading to the suppression of NF- $\kappa$ B level and inflammation(179). In SIRT2 knock-out mouse embryonic fibroblasts, Lys310 of p65 is acetylated, leading to an increased expression of NF- $\kappa$ B target genes. In mouse models, SIRT6

is found to bind to NF- $\kappa$ B subunit RelA and destabilize it via deacetylation of H3K9, possibly leading to anti-inflammatory features of SIRT1 and SIRT2 (180, 181). Another study by Van Gool et al. suggests that TNF- $\alpha$  translation is enhanced by increased intracellular NAD<sup>+</sup> in a SIRT6 dependent manner (182). However, the molecular mechanism underlying this opposite effect is not yet clear. Finally, SIRT7-deficient mice develop inflammatory cardiomyopathy, indicating that it also has an anti-inflammatory role (99).

#### ***1.5.4.2. Cardiovascular disease***

Cardiovascular disease is one of the most life threatening diseases of human beings. SIRT1, SIRT3, SIRT6 and SIRT7 have been reported as regulators of cardiac hypertrophy (abnormal enlargement or thickening of heart muscle), which is one of the main causes of heart failure.

Early studies demonstrated that SIRT1 play a protective role against cardiac hypertrophy by deacetylating and modulating p53 activity (ref). Recently, the protective role of SIRT1 has been extended to its ability to regulate fatty acid oxidation (as discussed in the previous section). Cardiac hypertrophy is accompanied by a metabolic shift to glycolysis and impaired fatty acid oxidation. Thus, SIRT1 alleviates cardiac hypertrophy by inhibiting glycolysis and promoting fatty acid oxidation. However, some other studies suggest that SIRT1 might play a detrimental role in cardiac function. For example, Kawashima et al. found that moderate overexpression of SIRT1 impaired cardiac diastolic function without causing heart failure in mice (183). Sundareen et al. demonstrated that the overexpression of SIRT1 in mice heart led to an increased phosphorylation and deacetylation of Akt and consequently caused cardiac hypertrophy, as well as increased the extent of Akt deacetylation leading to reduction in tumor development (184). Studies by Alcendor et al. might provide some explanation for such oppose

results. Their findings suggest that low (2.5 fold) to moderate (7.5 fold) overexpression of heart-specific SIRT1 attenuates age-dependent increases in cardiac hypertrophy and cardiac dysfunction, while high level (12.5 fold) of SIRT1 overexpression increases hypertrophy and decreases cardiac function (185).

SIRT3 is involved in preventing cardiovascular diseases due to its mitochondrial localization and ability to regulate reactive oxygen species (ROS). SIRT3 deficient mice develop cardiac hypertrophy, whereas transgenic animals with overexpression of SIRT3 in the heart are protected against agonist-mediated cardiac hypertrophy (186). SIRT3 also deacetylates and activates LKB1, which in turn activates AMP-activated kinase, leading to the deactivation of Akt after its phosphorylation is suppressed (187).

SIRT6 deficient mice exhibit cardiac hypertrophy and heart failure, whereas transgenic overexpression of SIRT6 in mice heart blocks agonist-induced hypertrophy, suggesting its importance in protecting organisms from cardiovascular disease. More interestingly, enhanced NAD<sup>+</sup> biosynthesis via overexpression of nicotinamide mononucleotide adenylyltransferase (Nmnat2) blocks agonist-induced hypertrophy in neonatal rat cardiomyocytes, and the latter influence is due to the activation of SIRT6 (188). It has been demonstrated that SIRT6 blocks IGF-Akt signaling pathway and development of cardiac hypertrophy by targeting c-Jun (189). Very recent studies suggest that SIRT6 attenuate phenylephrine-induced cardiomyocytes hypertrophy in cultured neonatal rat cardiomyocytes at least partially via regulation of the p300 acetyltransferase and subsequent suppression of NF-κB (190).

#### ***1.5.4.3. Alzheimer's disease***

In the field of neurodegeneration, Resveratrol and SIRT1 have been proven to be beneficial in vitro and in vivo models of Alzheimer's disease by reducing amyloid-beta

protein accumulation. SIRT1 increases the level of  $\alpha$ -secretase through activation of the  $\alpha$ -secretase gene ADAM10. Because  $\alpha$ -secretase is the enzyme responsible for non-amyloidogenic cleavage of amyloid precursor protein (APP), up regulation of  $\alpha$ -secretase shifts APP processing to reduce the pathological accumulation of the presumptive toxic amyloid  $\beta$  (138).

#### ***1.5.4.4. Cancer***

All members of the sirtuin family have been involved in cancer. Since these enzymes are involved in a variety of different cellular functions, they have very complex and sometimes controversial roles in both promoting and/or suppressing tumorigenesis (191).

All members of the sirtuin family have been involved in cancer. Since these enzymes are involved in a variety of different cellular functions, they have very complex and sometimes controversial roles in both promoting and/or suppressing tumorigenesis(191).

The role of human SIRT1 in cancer is mostly debated. On one hand, SIRT1 plays an important role in DNA repair and genome integrity, thereby acting as a tumor suppressor to protect the cells from tumorigenesis. On the other hand, SIRT1 regulate DNA repair and promote cell survival with properties of oncogenes (192). It seems that the ability of SIRT1 to promote or suppress tumorigenesis is dependent on the specific tumor type, cellular context, and signaling pathway affected.

The roles of the other sirtuins in cancer development have just started to emerge. SIRT2 has been proposed to be a tumor suppressor protein due to its role in preventing chromosomal instability during mitosis. SIRT2-deficient mice develop gender-specific tumors. Females primarily develop mammary tumors, whereas males develop hepatocellular carcinomas (94). Mitochondrial sirtuins have been ascribed to play critical roles in cancer progression via metabolic reprogramming. Indeed, SIRT3 expression is down-regulated in human breast



cancers, and SIRT3 knock-out mice have a higher incidence of mammary tumors (193). SIRT6 has been recently demonstrated as a tumor suppressor that regulates cancer metabolism (194). SIRT6 expression is down-regulated in human pancreatic and colorectal cancers, and Sirt6 deletion promotes intestinal tumorigenesis in vivo. Finally, SIRT7 depletion has been reported to reduce tumorigenesis of cancer cells, suggesting that SIRT7 may have oncogenic properties in cancer development (98).

#### ***1.5.4.5. Calorie restriction, aging, and lifespan extension***

Calorie restriction (CR) is the most robust environmental intervention that attenuates aging and increases life span in many species. The correlation between calorie restriction (CR) and lifespan extension was first discovered by McCay et al. in 1935 on rodents (195). Subsequently, such lifespan extension effect has also been observed in other species, including yeast, fruit flies, fish, rats, mice and even primates (196-198). Extensive studies have led to the suggestion that lifespan extension and health benefits of caloric restriction are mediated by pathways involving sirtuins. Sir2, the first sirtuin enzyme identified in budding yeast, was found to increase the life span of yeast (23). Similar results found in fruit flies and mice provided evidence that the associated gene products (sirtuins) were responsible for promoting longevity, and these findings created enormous interest on anti-aging research. A number of independent studies provide evidences that CR dependent life extension requires the presence of sirtuins (199). First, a lot of protein substrates targeted by sirtuins (Table 1.2.) are involved in metabolism and pathways induced by CR. Second, the expression levels of several sirtuins could be elevated by CR. Third, knockout of sirtuins diminished CR effect on lifespan extension. Mostoslavsky et al observed genomic instability and aging-like phenotypes in the absence of mammalian SIRT6 (167). Fourth, elevation of sirtuins, either by overexpression of sirtuins or by

sirtuin activating compounds (STACs), protects organisms from non CR diet. Kanfi et al. reported that SIRT6 regulates lifespan in male mice (200). In recent past there has been a controversy whether lifespan expansion has been due to activation and/or overexpression of sirtuins (201). But such controversy has been fading way in the light of new experimental evidence (199, 202). However, the molecular basis of sirtuin and/or CR mediated enhancement in longevity and attenuation of age related diseases still remain to be fully elucidated.

## **1.6. Activators of Sirtuins**

As mentioned in the previous section, sirtuins play positive role in DNA repair, cell survival, inflammation, metabolism and ultimately, aging. Therefore, members of sirtuin family are considered as attractive therapeutical targets for treating age-related diseases, such as metabolic disorders, inflammatory disorders, and Alzheimer's disease. Circumstantial evidence that one of ingredients of red wine, resveratrol, activates sirtuins as well as elicits health benefits, the link between sirtuin activation, human health and longevity, and calorie restriction was anticipated, which initiated studies on designing sirtuin activators as anti-aging drugs.

### **1.6.1. Sirtuin activators and their physiological effects**

The first potent sirtuin activating compounds (STACs) were identified in a high-throughput screening using SIRT1(203). Among these native activators identified, resveratrol (3,5,4'-trihydroxy-trans-stilbene ) exhibited the maximum potency in enhancing the SIRT1-mediated deacetylation of AMC-conjugated fluorogenic substrate. Subsequently, several synthetic STACs were identified by tetramethylrhodamine-based (TAMRA-based) fluorescence polarization assay of SIRT1, and such results were verified by the mass spectrometric analysis (204, 205).

Resveratrol is a naturally occurring phytoalexin synthesized by certain plants in response to injury or fungal attack. Acting as an antioxidant, it has been linked to a variety of health benefits in humans and rodent, such as prevention of human cardiovascular diseases(206). Importantly, it has been demonstrated that resveratrol and other STACs extend the lifespan of numerous organisms including yeasts, worms, fish and bees (203, 207-209). Resveratrol also prevents the deleterious effects in mice fed with high-fat diet (HFD), including fatty liver, insulin resistance, and inflammation. STACs also increased the lifespan of HFD mice compared to controls. Many of the above preventative effects overlap those triggered by overexpression of SIRT1 or by CR diet and numerous reports have shown that the STACs effects are dependent on the presence of SIRT1. For example, SIRT1-null mice develop skin tumors at normal rate even in the presence of resveratrol (210). SIRT1 is also required for the beneficial effects of resveratrol on mitochondrial biogenesis and function (211). Similarly, the synthetic compound SRT1720 improves metabolism and extends both mean and maximum lifespan of mice fed with high-fat diet, but does not show the effects on SIRT1 knockout mice (212).

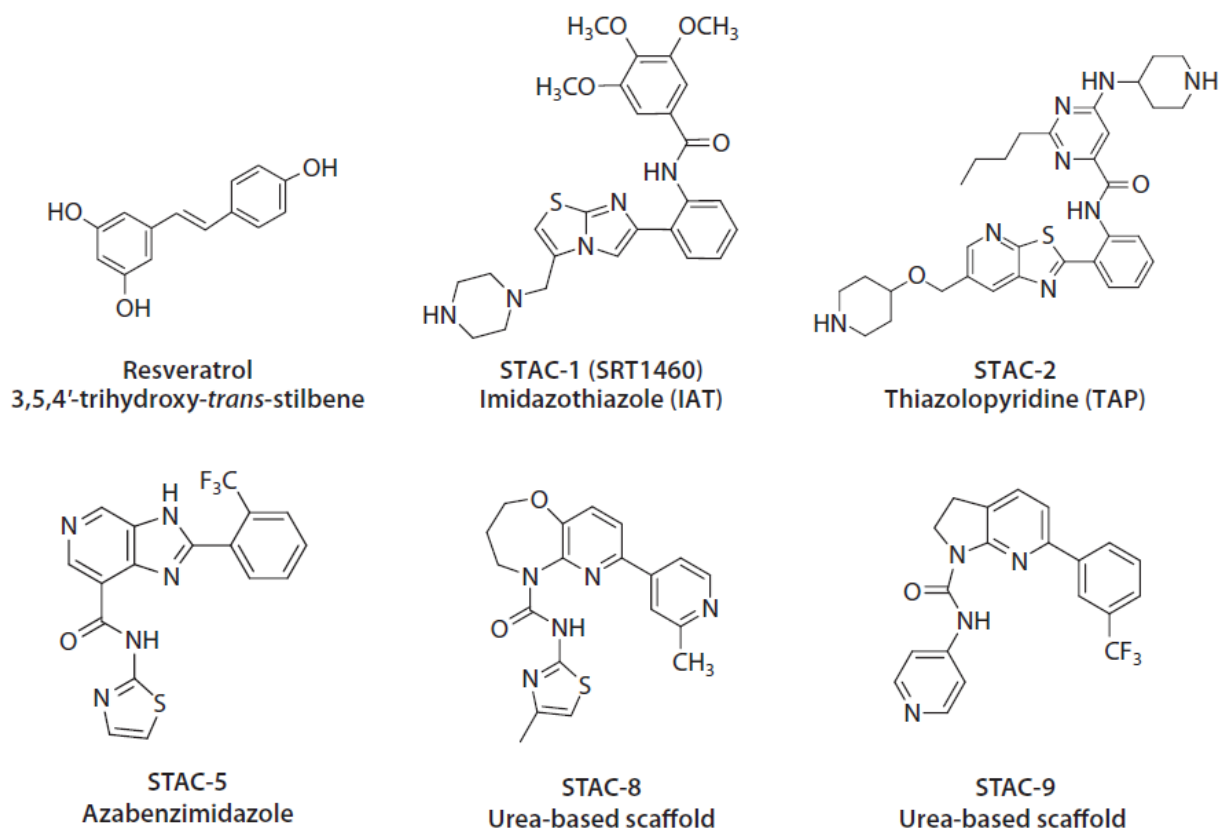


Figure 1.14. Structures of SIRT1-activating compounds (STACs). Figure is adapted from reference (213).

### 1.6.2. Controversy over the STACs

Although several biological effects of STACs have been studied and verified, the legitimacy of STACs as direct SIRT1 activators has been widely debated, mainly due to the nature of the fluorescent assays. It has been suggested that STACs increased SIRT1 activity in the presence of fluorophore-tagged substrates but not with untagged peptide substrates, leading to the suggestion that SIRT1 activation is an *in vitro* artifact of the assay system (214, 215). In the meantime, a series of studies have revealed that resveratrol directly targets other proteins instead of SIRT1 *in vivo*, but consequently indirectly upregulates SIRT1 to elicit its physiological effects. For example, Dasgupta et al. demonstrated that resveratrol activates

AMPK, which enhances the SIRT1 activity by activating the gene encoding the NAD<sup>+</sup> synthetic enzyme, nicotinamide phosphoribosyltransferase (NAMPT) (216).

Recently, the legitimacy of STACs as direct SIRT1 activators has received renewed support the fluorophoric moieties of the substrates mimic the requirement of aromatic amino acids which must present at the deacetylation site for efficient catalysis by the enzyme (217). The biochemical studies of Dai et al. suggest that the fluorescent moiety of the substrates is dispensable for activation if replaced by hydrophobic amino acids, such as Phe and Trp (205). The latter study further demonstrated that certain synthetic STACs interact directly with SIRT1 and activate the deacetylation reaction by an allosteric mechanism. Another study identified two native peptide substrates (PGC1- $\alpha$  and FOXO3a), containing hydrophobic residues at the +1 and +6 positions relative to the acetylated lysine, in the presence of which SIRT1 showed activation by resveratrol and other synthetic STACs (218). It was further demonstrated that the amino acid Glu230, located in the N-terminal domain of SIRT1, is critical for SIRT1 activation (55); SIRT1 E230K mutation blocks both STAC binding and activation of SIRT1. In SIRT1 knockout myoblasts with mouse SIRT1-E222K mutation (the murine equivalent of human SIRT1-E230K), the ability of STACs in increasing the mitochondrial mass, ATP concentration, and the mitochondrial DNA copy number has been found to be blocked. The mechanism for the role of E230 in the activation of SIRT1 has not been demonstrated. It has been proposed that E230K impairs the coupling between STAC and substrate due to electrostatic interaction between E230 and the positively charged residue (R446) in the catalytic domain of the substrate (55).

### **1.6.3. Other sirtuin activators**

Besides small molecule STACs, two endogenous protein activators of SIRT1 have been discovered in mammals, namely AROS (active regulator of SIRT1) and lamin A (219, 220). AROS was identified as a direct regulator of SIRT1 by yeast two-hybrid screening (219). It enhances the deacetylation of p53 by SIRT1, leading to the repression of p53-mediated transcriptional activity. Lamin A, a major component of the nuclear matrix, was also found to interact with recombinant SIRT1 and activate it under in vitro condition. More interestingly, resveratrol activates SIRT1 toward the native substrate p53 by enhancing the binding SIRT1 to lamin A (220). Ghosh et al. demonstrated that resveratrol activates SIRT1 by increasing its binding with lamin A, adding heat to the debate over the role of resveratrol in SIRT1 activation (221).

Isonicotinamide has been reported to serve as an activator of yeast sir2 both under in vitro and in vivo conditions, and the origin of its activating effect has been ascribed to the alleviation of the nicotinamide assisted reverse (base-exchange) reaction (222). However, the effective iNAM concentration needs to be at the millimolar range in the cell, limiting its pharmacological value.

In summary, STACs have anti-aging, anti-carcinogenic, anti-inflammatory properties that could be useful for treating or preventing age-related diseases. Currently, resveratrol and the other synthetic STACs are in clinical trials for evaluation of their pharmacokinetics, safety and toxicity (223-225). Although the previous progress seems promising, many questions regarding the mechanism of activation both in vitro and in vivo remain to be addressed.

## 1.7. Inhibitors of Sirtuins

While focus on activation of sirtuins has traditionally been dominating the drug discovery efforts in the field, the ability to inhibit these enzymes will still be important to clarify the roles of sirtuins as either antitumor targets or tumor suppressors. Concurrently, a number of small molecule sirtuin inhibitors have been developed either through the high throughput screening or via the mechanism-based design.

### 1.7.1. Mechanism-based sirtuin inhibitors

Sirtuins possess a unique catalytic mechanism which couples NAD<sup>+</sup> hydrolysis to deacetylation of the protein substrates. This unique mechanism has been utilized for the mechanism-based design and synthesis of sirtuin inhibitors. Several studies have employed acetyl-lysine analogs to probe the mechanistic differences among protein deacetylases (both sirtuins and HDACs). This work has led to the identification of thioacetyl lysine and trifluoroacetyl lysine containing peptides as potent sirtuin inhibitors.

#### 1.7.1.1. Nicotinamide

Nicotinamide is the product of sirtuin catalyzed reaction and also works as the physiological inhibitor of sirtuins. It has been proposed that the inhibition of several isoforms of sirtuins by nicotinamide is manifested via the “base-exchange” mechanism (i.e., the reversal of the step involved in the formation of nicotinamide during the enzyme catalysis; see Figure 1.15), and such event gives rise to the noncompetitive inhibition of sirtuins (68, 226, 227). It inhibits SIRT5’s desuccinylase activity ( $IC_{50} = 21 \pm 4 \mu\text{M}$ ), but is insensitive toward SIRT5’s deacetylase activity (228). Recently it has been proposed that with certain sirtuins (e.g., mouse SIRT2 and human SIRT3) the nicotinamide inhibition is mixed type with increasing component of the competitive inhibition (229).

### ***1.7.1.2. Carbanicotinamide adenine dinucleotide (carba-NAD<sup>+</sup>)***

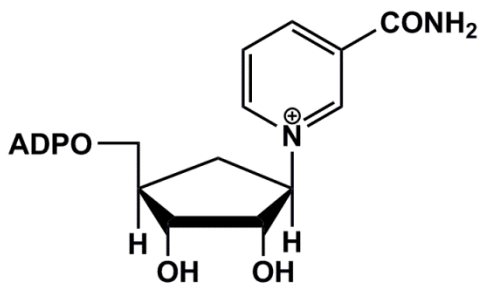
The NAD<sup>+</sup> analog carba-NAD<sup>+</sup> (**1** and **2** in Figure 1.16), in which a 2,3-dihydroxycyclopentane ring replaces the β-D-ribose ring of the nicotinamide riboside moiety of NAD<sup>+</sup>, and its diastereoisomer pseudocarba-NAD<sup>+</sup> were designed as inhibitors of enzymes that involved in ADP-ribosyl transfer, namely, NAD<sup>+</sup> glycohydrolases and ADP-ribosyl transferases (230). In these compounds, the structure of the dinucleotide is modified to prevent the cleavage of the glycosidic bond. Since sirtuin catalyzed deacylation reaction involves such cleavage, these NAD<sup>+</sup> analogs served the competitive inhibitors against NAD<sup>+</sup> (39). The X-ray crystal structures of several sirtuins bound with substrates and carba-NAD<sup>+</sup> have provided the structural basis of ligand binding and catalysis in sirtuins (39, 231).

### ***1.7.1.3. Thioacetyllysine peptides***

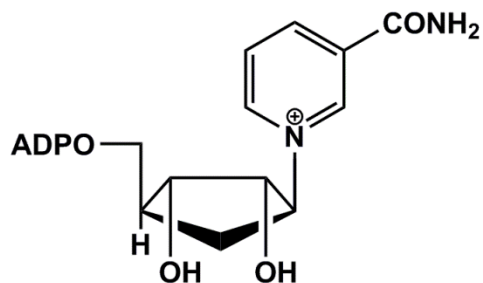
Several studies have employed acetyl-lysine analogs to probe the mechanistic differences among protein deacetylases (both sirtuins and HDACs). This work has led to the identification of thioacetyl lysine and trifluoro-acetyl lysine containing peptides as potent inhibitors. It has been proposed that the thioacetyl analogs follow the same reaction coordinate as their acetyl counterparts but the former analog is trapped at the thioimidate intermediate stage after the glycosidic bond cleavage and the acetyl group transfer step (Figure 1.9) (66). Thioacetyllysine derived from human acetyl-coenzyme A synthetase 2 inhibits SIRT1 with an IC<sub>50</sub> value of 0.9 μM (232). A thioacetyllysine peptide derived from H3 histone exhibits potent inhibition of SIRT1, SIRT2, SIRT3 and Hst2 with IC<sub>50</sub> values of 2.0, 5.6, 2.3, and 1.02 μM, respectively (66). The most potent compound derived from p53 (Figure 1.14) inhibits SIRT1 with an IC<sub>50</sub> of 180 nM and 20-fold selectivity over SIRT2 (233). Fluoroacetyllysine peptides also inhibit sirtuin activity by competing against acetyllysine peptide substrate, but less potently



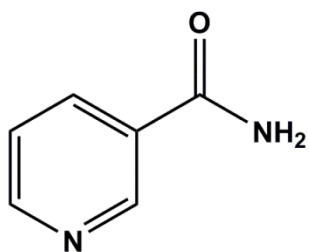
than thioacetyllysine peptide (66). Trifluoroacetyllysine peptide derived from H3 inhibits Hst2 with an IC<sub>50</sub> value of 61 μM. Similarly, since SIRT5 uses the same mechanism as the deacetylases to remove malonyl and succinyl groups, thiosuccinyl and thiomalonyl peptides could be mechanism-based, and isoform selective inhibitors for SIRT5. He et al. synthesized a H3K9 thiosuccinyl peptide, KGTAR(SuK)STGGKA, which competes against the peptide substrate and selectively inhibits SIRT5 with an IC<sub>50</sub> value of 5 μM (234). Such inhibitors are expected to serve as valuable tools for investigating the dsuccinylation/dmalonylation reactions of physiological substrates.



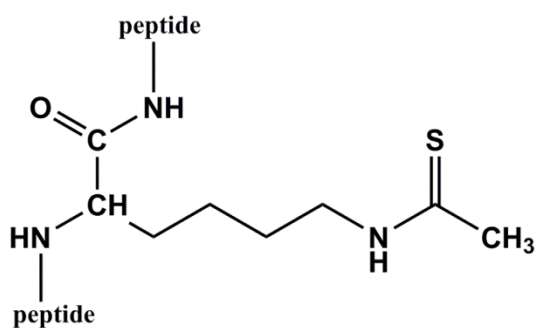
(1) Carba-NAD<sup>+</sup>



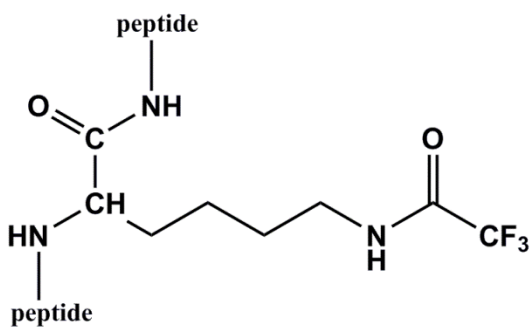
(2) Pseudocarba-NAD<sup>+</sup>



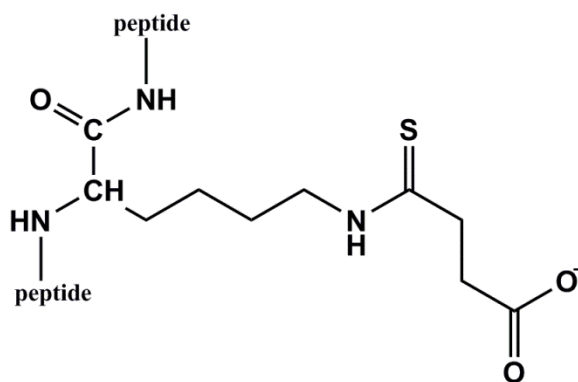
(3) Nicotinamide



(4) Thioacetyl peptide



(5) trifluoroacetyl peptide



(6) Thiosuccinyl peptide

Figure 1.15. Mechanism-based sirtuin inhibitors.

### 1.7.2. Sirtuins inhibitors discovered through high-throughput screening

High-throughput screening is a common and robust approach in drug discovery. A variety of sirtuins inhibitors have been discovered by high-throughput screening, including suramin derivatives (34), indole, sirtinol, cambinol, indoles, splitomicin and thiobarbiturates. Of these inhibitors identified, suramin and indole derivatives have been crystalized with selected sirtuins and their structures have been solved. The structural data have provided insights into the binding and inhibitory mechanisms of sirtuins.

#### 1.7.2.1. Suramin and analogs

Suramin, a polysulfonated naphylurea compound (8,8'-[carbonylbis [imino-3,1-phenylenecarbonylimino (4-methyl-3,1-phenylene) carbonylimino] bis-1,3,5-naphtalenetrisulfonic acid hexasodium salt), was one of the oldest synthetic therapeutics and has been used clinically for the treatment of African trypanosomiasis and onchocerciasis since 1920. Later on, it has also shown several other therapeutic potentials such as treatment of several cancers and the inhibition of HIV infection, presumable as result of its inhibition of growth factor/receptor interactions, inhibition of angiogenesis, and inhibition and activation of protein-tyrosine phosphatases (235-237). It was discovered as SIRT1/SIRT2 inhibitors via a large scale screening for sirtuin activators (203). The binding affinity ( $K_d$ ) determined from isothermal titration calorimetry is 5.5  $\mu\text{M}$ , whereas the  $\text{IC}_{50}$  value is 22  $\mu\text{M}$ . Crystallization data suggest that suramin binds to the  $\text{NAD}^+$  binding pocket B, C and the peptide-binding site of SIRT5, thereby has been assumed of competing with both the peptide substrates and the cosubstrate  $\text{NAD}^+$  (34). In the crystal structure of the SIRT5-suramin complex, the binding of the symmetric suramin bridges two SIRT5 molecules together to form a dimer (Figure 1.16). More interestingly, in the active pocket, Y102 and R105, which are responsible for SIRT5's unique

desuccinylase activity, formed hydrogen bonds with the trisulfonylnaphyl groups of suramin. But whether this unique binding pattern correlates to the inhibition mechanism has not been studied. Although suramin has been demonstrated as regulators in diverse pathways and exhibits side effect during clinical trials, a comprehensive understanding of its binding and inhibition mechanism on sirtuins will still provide important information for understanding the mechanism of sirtuin catalysis, and could be used as a lead chemical compound for designing more potent and selective inhibitors of sirtuins. Trapp et al. developed several suramin analogs and performed structure-activity studies and developed several suramin analogs as selective SIRT1 and SIRT2 inhibitors with nanomolar potency (238). The aminoanthranilic acid derivative NF675 (**7** in Figure 1.17) inhibits SIRT1 with an IC<sub>50</sub> of 93 nM and displays 24-fold higher selectivity for SIRT1 over SIRT2.

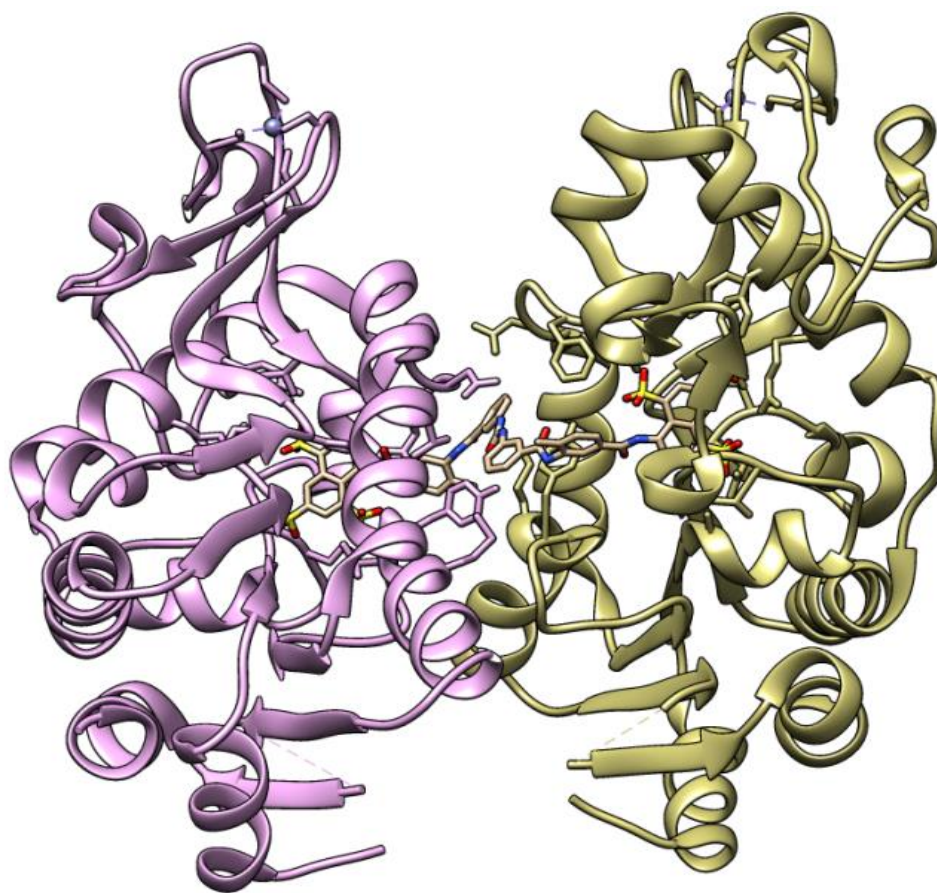


Figure 1.16. Overall structure of the SIRT5 suramin complex. Two monomers (pink and yellow) are linked by one molecule of suramin

### *1.7.2.2. Indole derivatives*

Indole-based SIRT1 inhibitors were also discovered by in vitro HST screening(239). EX527 (6-chloro-2,3,4,9-tetrahydro-1H-carbazole-1-carboxamide; **9** in Figure 1.17.) is one of few compounds for which both initial mechanistic and structural data are available and that combine high inhibitory potency with significant isoform selectivity (239). EX527 inhibits SIRT1 with an  $IC_{50}$  value of 120 nM and displays around 100-fold selectivity over SIRT2 and SIRT3, but shows no effect on either deacetylase or desuccinylase activities of SIRT5 (45). Kinetic analysis revealed noncompetitive inhibition against peptide substrate, and uncompetitive inhibition of deacetylation with respect to  $NAD^+$ , suggesting that EX527 binds to

the enzyme after the binding of NAD<sup>+</sup>(45). Crystal structure of SIRT1/NAD<sup>+</sup>/EX527 analog (**10**) complex suggests that binds deep in the catalytic cleft, displacing the NAD<sup>+</sup> nicotinamide and forcing the cofactor into an extended conformation which seems to sterically prevent substrate binding(44). However, a more recent structural study on several sirtuin inhibitor complexes suggests that EX527 could also bind to the enzyme-intermediate and enzyme-product complexes (45). These crystal structures show that EX527 occupies the nicotinamide binding site and a neighboring pocket and contacts the ribose of NAD<sup>+</sup> or of the coproduct 2'-O-AADPr. Kinetic data also suggest that sirtuin intermediate can exist for seconds, allowing the nicotinamide cleavage and EX527 binding. Complex structures with native alkylimidate and thio-analog suggest steric incompatibility between inhibitor and intermediate. Based on the above information, the authors conclude that EX527 stabilizes the closed enzyme conformation to prevent product release. A possible explanation about the discrepancy between these two studies could be that EX527 inhibits SIRT1 in multiple ways. It could bind to the active pocket with NAD<sup>+</sup> to stabilize the non-active conformation of the enzyme, preventing the binding of peptide substrate, while it could bind to the active Michaelis-Menten complex but prevent the release of product. Detailed mechanistic studies are crucial to resolve this controversy.

### ***1.7.2.3. Other inhibitors***

Other high-throughput screening assays have identified a number of compounds that display low  $\mu\text{M}$  to nM potency, including but not limited to sirtinol, cambinol, and triobarbiturates. Recently some analogues based on the structural frameworks of these inhibitors showed improved potency.

Sirtinol (**11**) was discovered through forward chemical genetics, cell-based phenotypic screening of 1600 unbiased compounds (240). It inhibits yeast Sir2p, SIRT1 and SIRT2 with

IC<sub>50</sub> values of 66, 131, and 38  $\mu\text{M}$ , respectively. Structure-activity relationship analysis suggests that the hydroxyl-naphthaldehyde moiety is necessary and sufficient for inhibitory activity (240). A series of sirtinol analogues were assayed against yeast Sir2, SIRT1 and SIRT2, among which para-sirtinol (11, Figure 1.17) showed 10-fold more potency than sirtinol against SIRT1 and SIRT2(241).

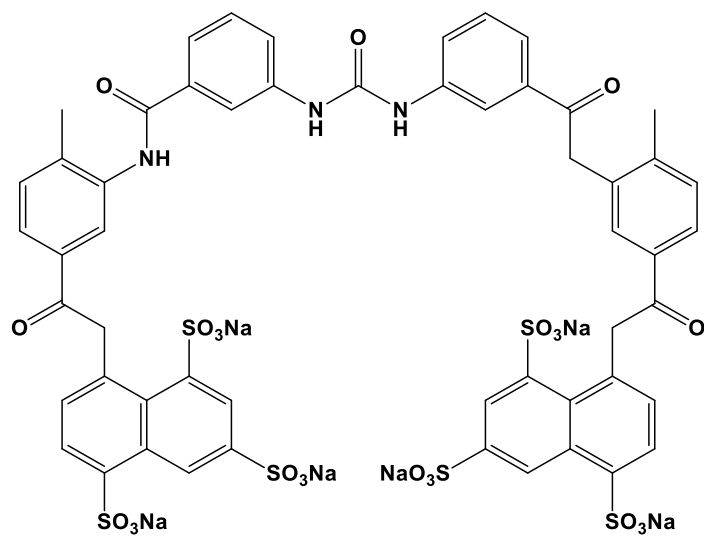
Cambinol (13 in Figure 1.18) exhibits micromolar potency against SIRT1 and SIRT2, but is insensitive against SIRT3 and SIRT5 (242, 243). Steady-state kinetic studies demonstrate that cambinol is competitive with histone H4 peptide substrate and noncompetitive with NAD<sup>+</sup>. Docking analysis using SIRT2 crystal structure suggests that the binding is stabilized by  $\pi$ - $\pi$  stacking interactions between the  $\beta$ -naphthol and two aromatic residues in the C pocket of the enzyme (244). The N1-substituents show increase in both activity and selectivity against SIRT2 with IC<sub>50</sub> values ranging from 1 (**14** in Figure 1.18) to 22  $\mu\text{M}$  (244). Antitumor activity of cambinol has been observed in lung cancer cells and Hela cells as a result of hyperacetylation of key stress response proteins (p53, Ku70, FOXO3a and  $\alpha$ -tubulin) and cell cycle arrest (242).

Thiobarbiturates were discovered as potential sirtuin inhibitors through a virtual screening of approximately 328,000 compounds (245). The most potent compound **15** inhibits SIRT1 and SIRT2 with IC<sub>50</sub> values of 13.2 and 9.1  $\mu\text{M}$ , respectively. Based on molecular dynamic simulation data, several novel thiobarbiturates with modified hydrophobic substituents were synthesized. For example, biphenyl derivative **16** shows selectivity on SIRT2 with an IC<sub>50</sub> value of 8.7  $\mu\text{M}$ , while indole derivative **17** has SIRT1 selectivity with an IC<sub>50</sub> of 5.9  $\mu\text{M}$  (245). Recently a series of thiobarbiturates were identified as SIRT5 inhibitors in the low micromolar range and are selective over SIRT3 (243). Compound **18** inhibits SIRT5 with an IC<sub>50</sub> value of 2.3  $\mu\text{M}$ .

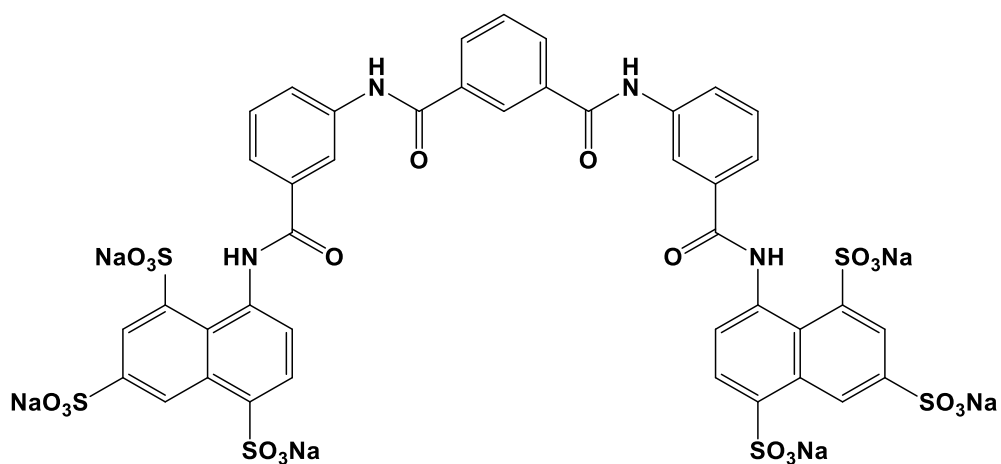
Splitomicin (**19**) was discovered as yeast Sir2 and Hst1 inhibitor through a yeast cell-based screening for inhibition of sirtuin-mediated telomeric silencing (246). Structure-activity studies on splitomicin derivatives suggest that the acetyllysine binding pocket is the site of interaction between splitomicin and Sir2, and structural differences in this hydrophobic cleft were accounted for inhibitor selectivity (247). Splitomicin derivative HR73 (**20**) has been identified as effective inhibitor of human SIRT1 with an IC50 value of 5  $\mu$ M. Elevated level of acetylation of p53 and suppression of HIV transcription were observed upon treatment of H473 in vivo (114).

In summary, a variety of small molecule inhibitors for sirtuins have been identified, some of which have been tested in physiological systems. However, identification of sirtuin isoform selective inhibitors still remains bottleneck for structural-functional studies of sirtuin enzymes. X-ray crystallographic studies with sirtuins and the above inhibitors will be beneficial for understanding the inhibition mechanism and designing of more potent inhibitors.

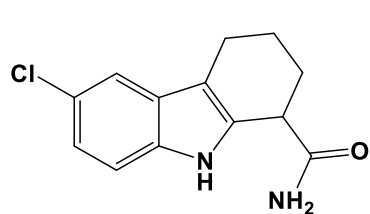




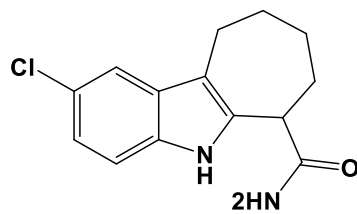
(7) Suramin



(8) NF675



(9) EX-527



(10)

Figure 1.17. Sirtuin inhibitors discovered through high-throughput screening (suramin and indole analogs).

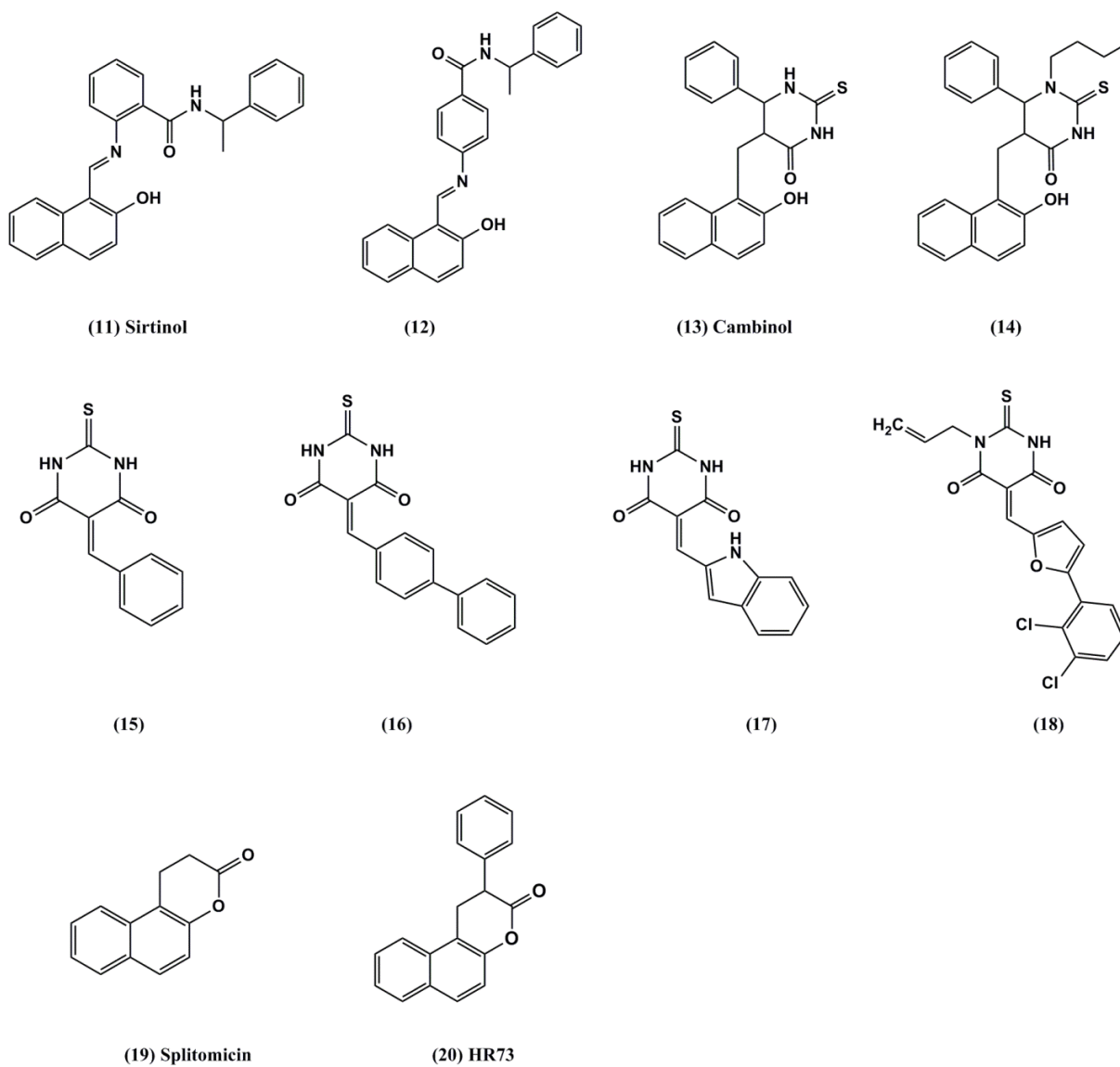


Figure 1.18. Sirtuin inhibitors discovered through high-throughput screening (continued, other inhibitors).

Table 1.3. Summary of representative sirtuin inhibitors<sup>a</sup>

Inhibitor	IC50 ( $\mu\text{M}$ )					Reference
	SIRT1	SIRT2	SIRT3	SIRT5	Others	
1 (carba-NAD <sup>+</sup> )	NA <sup>b</sup>	NA	NA	NA	300 (Hst2)	(39)
2 (pseudocarpa-NAD <sup>+</sup> )	NA	NA	NA	NA	NA	(39)
3 (nicotinamide)	25	100	30	21	130 (Hst2)	(228)
4 (thioacetyl peptides)	0.18-2.0	3.6-5.6	2	NA	1.02 (Hst2)	(66, 232, 233)
5 (trifluoroacetyl peptide)	NA	NA	NA	NA	61 (Hst2)	(66)
6 (thiosuccinyl peptides)	NA	NA	NA	5-100 <sup>c</sup>		(248)
7 (suramin)	0.297	1.15	NA	22	NA	(238, 249)
8 (NF675)	0.093	2.26	NA	NA	NA	(238)
9 (EX-527)	0.098	19.6	48.7	NA	NA	(239)
10 (EX-527 analogue)	0.124	277	>100 <sup>d</sup>	NA	NA	(239)
11 (sirtinol)	37-131	38-58	24% at 50 $\mu\text{M}$	48.9	NA	(249)
12	13	25.9	NA	NA	NA	(241)
13 (cambinol)	56	59	NA	42.5 <sup>c</sup>	NA	(249)
14	16.9	1	NA	NA	NA	(244)
15	13.2	9.1	NA	NA	NA	(245)
16	50.5	8.7	NA	NA	NA	(245)
17	5.9	20.3	NA	NA	NA	(245)
18	5.3	9.7	41% at 50 $\mu\text{M}$	2.3 <sup>c</sup>	NA	(243)
19 (splitomicin)	NA	NA	NA	NA	86 (sir2p)	(246)
20 (HR73)	5	NA	NA	NA	NA	(247)

<sup>a</sup> The schematic structures of the inhibitors in the table are presented in Figures 1.18 to 1.20.

<sup>b</sup> Data is not available

<sup>c</sup> Result was obtained by testing SIRT5 desuccinylase activity

<sup>d</sup> No inhibition at 100  $\mu\text{M}$

## 2. STATEMENT OF PROBLEM

Sirtuins are emerging as the key regulators of metabolism and aging, and their potential activators and inhibitors are being explored as therapeutics for improving health and treating diseases. However, there has been limited success in identifying highly potent sirtuin isoform selective activators and inhibitors. Despite the global structural-functional similarity among different isoforms of sirtuins, there are noticeable differences in their catalytic as well as modulatory features, which have not been elucidated at the molecular level. The goal of this dissertation is to contribute to the effort in comprehending mechanistic aspects of the SIRT1 and SIRT5 catalyzed reactions to facilitate designing isozyme selective activators and inhibitors as potential drugs. In particular, the investigation was carried out with the following four specific aims:

1. To discover novel inhibitors for sirtuins via high-throughput screening of the in-house library of small molecules
2. To determine the contributions of two critical amino acid residues, namely Y102 and R105 in SIRT5 (vis a vis the corresponding residues of SIRT1) on substrate selectivity and inhibition of the enzymes
3. To elucidate the ligand and mutation induced changes in the structural features of SIRT1 and SIRT5 variants.
4. To investigate the steady-state and transient kinetics as well as thermodynamics for the ligand binding to SIRT1 and SIRT5 isozymes.

### 3. MATERIALS

The plasmid containing the coding sequence of human SIRT1 (pCMV-SPORT6) and SIRT5 (pCMV-SPORT6) was obtained from Open Biosystems (Huntsville, AL). The ligation independent cloning (LIC) compatible *E. coli* expression vector pLIC-His was a kind gift from Dr. Stephen P. Bottomley (Monash University, Australia). The primers used for subcloning SIRT1, SIRT2, SIRT5 as well as site-directed mutagenesis of SIRT5 were synthesized by Integrated DNA Technologies (Coralville, IA). SacII restriction endonuclease and T4 DNA polymerase were obtained from New England Biolabs (Ipswich, MA). QuikChange II site-directed mutagenesis kit was purchased from Agilent Technologies (Santa Clara, CA). Polycarbonate membrane filters and syringe filtration devices were from Pall Life Sciences (Ann Arbor, MI). Dialysis membranes were from Spectrum Laboratories, Inc. (Rancho Dominguez, CA). 40% polyacrylamide solution, Bradford reagent and protein standards were purchased from BioRad (Hercules, CA). Suramin, Fluor-de-Lys® (KI-104), deacetylated lysine-coumarin adduct (BML-KI142) and Met-7-aminio-4-methylcoumarin, were purchased from Enzo Life Sciences Inc (Plymouth Meeting, PA). Trypsin from bovine pancreas, bovine serum albumin (BSA), ammonium per sulfate, 2-mecaptoethenol, imidazole, magnesium chloride, nicotinamide and isonicotinamide were purchased from Sigma (St. Louis, MO). EX527 was purchased from Cayman Chemical Company (Ann Arbor, MI). The succinylated substrate (Ac-SucLys-AMC) was synthesized following the protocol described by Andreas et al (250).

## 4. METHODS

### 4.1. Cloning, Expression and Purification of Recombinant Human Sirtuin Isoforms

#### 4.1.1. Sub-cloning of human SIRT1 and SIRT5

SIRT1 (193-747) and SIRT5 (51-301) were cloned into the pLIC-His expression vector provided by Dr. Stephen Bottomley and the overall process was accomplished via the ligation independent cloning methods as described by Cabrita et al.(251). The LIC vector has been designed to overexpress the recombinant protein under the control of the T7 promoter system. As shown in Figure 4.1, the vector encodes a hexa-histidine peptide followed by a TEV (Tobacco Etch Virus) protease recognition sequence and an LIC site. The clones containing the coding sequence of human SIRT1 (clone ID: 4518906; accession number: BC012449) and SIRT5 (clone ID: 3352592; accession number: BC000126) was obtained from Open Biosystems (Huntsville, AL) as live cultures. The plasmids DNA were extracted using QIAprep<sup>®</sup> miniprep DNA isolation kit and used as templates for the cloning. SIRT1 sequence (193-747) was amplified by PCR using the oligonucleotides 5'-CCAGGGAGCAGCCTCGATGATTGGCACAGATCCTCGA-3' and 5'-GCAAAGCACCGGCCTCGTTATGATTTGTTTGATGGATAGTTCATGTC-3' as the forward and reverse primers, respectively. The reagents used for 50 µL of PCR reaction were as follows: 5 µL of 10X cloned Pfu DNA polymerase buffer, 1.25 µL of dNTPs mixture (containing 10 mM of each dNTP), 1.0 µL of template (50-100 ng/µL), 2 µL of the primer mix (containing 250 ng/µL of each primer), 1.5 µL of cloned Pfu DNA polymerase and 5 µL glycerol. The PCR was performed on the MiniCycler<sup>™</sup> (MJ research) for 25 cycles under the following experimental conditions: initial denaturation at 94 °C for 50 sec, denaturation at 94 °C for 45 sec, annealing at 61 °C for 50 sec, extension at 72 °C for 90 sec. The PCR amplified DNA was gel purified using QIAquick gel extraction kit and treated with T4 DNA polymerase (1U/0.1 pmol)

and 2.5 mM dATP at 22 °C for 1 hour, followed by heat inactivation at 72 °C for 20 min. The pLIC vector was similarly treated but with 2.5 mM dTTP. To anneal the vector with the amplified DNA, 2 µL of the vector was mixed with 4 µL of the PCR product. The reaction mixture was incubated for one hour at 22 °C, and then stopped by the addition of 1 µL of 25 mM EDTA solution in water, pH 8.0 (adjusted with NaOH). The annealed vector was transformed into DH5α competent cells using standard molecular biology protocol. The cells were plated on LB (Luria Bertani) agar plates containing 0.1 mg/mL ampicillin and the plasmids DNA was extracted from the resulting colonies using QIAprep® miniprep DNA isolation kit.

SIRT5 (encoding 51-301) was amplified by PCR using the oligonucleotides 5'-CCAGGGAGCAGCCTCGGCTCGGCCAAGTTCAAGTATGGC-3' and 5'-GCAAAGCACCGGCCTCGTTAGGCAAGGGCTTCAGGAGTCG-3' as forward and reverse primers respectively. The cloning procedure was the same as that of SIRT1.

The clones containing SIRT1 and SIRT5 genes in the pLIC-His vectors were confirmed by sequencing of the resulting plasmid (Mclab, San Francisco, CA).

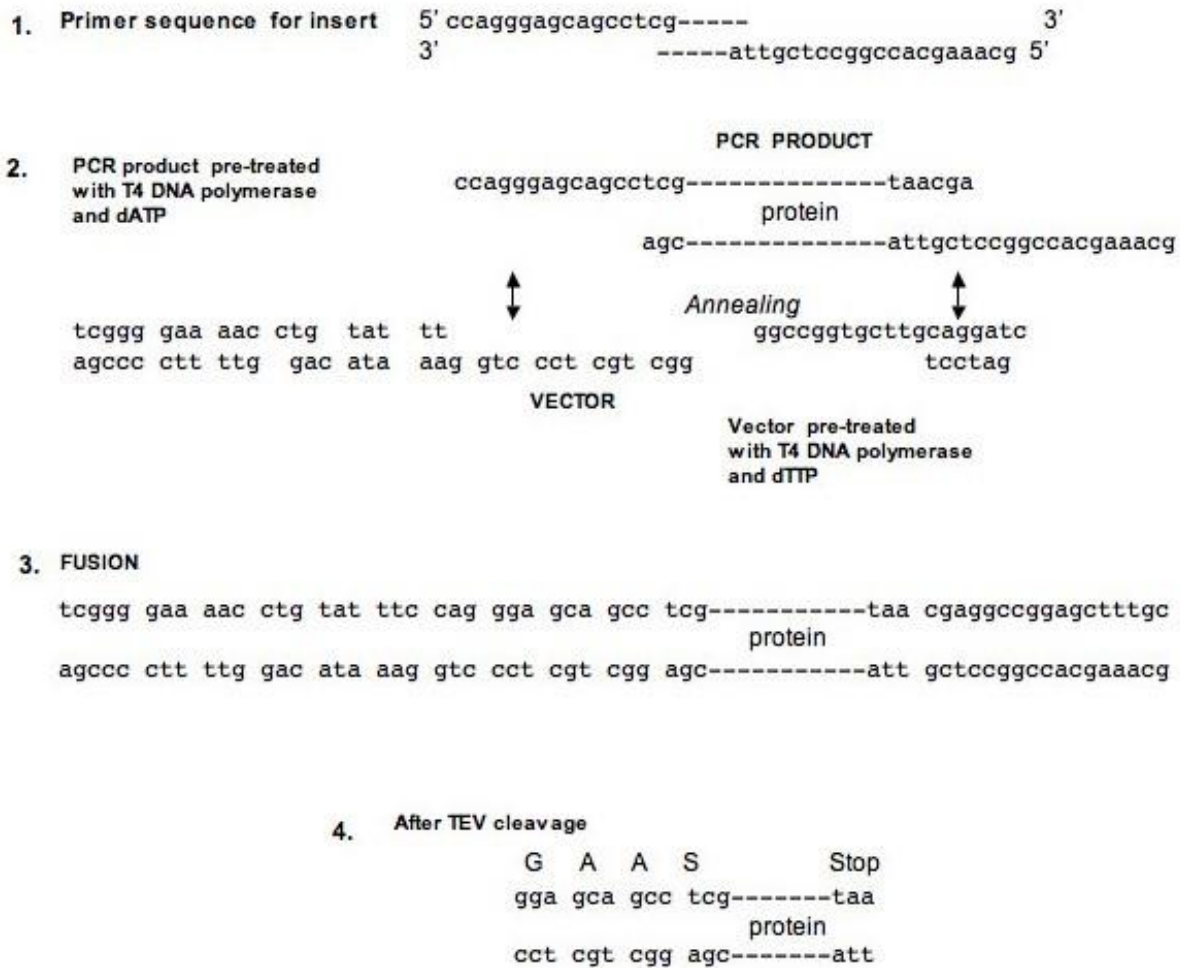


Figure 4.1. The ligation independent cloning strategy for the sub-cloning of the human SIRT1 and SIRT5 gene. The LIC compatible primers were used to amplify the SIRT1/SIRT5 gene. The PCR product was treated with the T4 DNA polymerase in the presence of dATP. The pLIC –His vector was digested with the SacII restriction enzyme prior to the T4 DNA polymerase treatment in the presence of dTTP. The T4 treatment of the PCR product, as well as the digested vector, in the presence of the respective dNTP generated the cohesive ends which could anneal with each other on mixing. The annealed product was transformed into DH5α *E. coli* cells. The nicks left in the recombinant plasmids were sealed by bacterial DNA ligase. TEV protease could be used to remove the His-tag from the fusion proteins, leaving the four extra amino acids (GAAS) at the N-terminal of the recombinant protein. Figure is adapted from reference (251).

#### 4.1.2. Site-directed mutagenesis of SIRT5

The wild type SIRT5 plasmid was used as a template for the site-directed mutagenesis, using the QuikChange II site-directed mutagenesis kit (Agilent Technologies) to create three SIRT5 mutants, Y102A, R105I and Y102A/R105I.



The forward and reverse primers for creating the three mutants are listed as follows:

#### SIRT5 Y102A

Forward: 5'-GGGTGTGGGAGTTCGCCCACTACCGGCGGG-3'

Reverse: 5'-CCCGCCGGTAGTGGGCGAACTCCCACACCC-3'

#### SIRT5 R105I

Forward: 5'-GGGAGTTCTACCACTACATTTCGGGAGGTCATGGGGAG-3'

Reverse: 5'-CTCCCCATGACCTCCCGAATGTAGTGGTAGAACTCCC-3'.

#### SIRT5 Y102A/R105I

Forward: 5'-CCGGGTGTGGGAGTTCGCCCACTACATTTCGGGAG-3'

Reverse 5'-CTCCCGAATGTAGTGGGCGAACTCCCACACCCGG-3'.

The PCR were set up with the following condition: initial denaturation for 30s at 95°C followed by 16 cycles of 30s at 95°C, 1 min at 55°C for annealing and 14 min at 68°C for extension. After PCR, the amplified DNA in the reaction mixtures were treated with 1 µl of DpnI restriction enzyme (10 U/ µl) and incubated at 37°C for 2 hours to digest the parental SIRT5 template DNA. The reaction was stopped by placing the reaction tubes on ice. The amplified products were then transformed into TOP10 chemically competent cells. Plasmids were extracted from the transformed cells and sent for sequencing to confirm the results.

#### **4.1.3. Expression and purification of SIRT1**

The plasmids containing SIRT1 were transformed into BL21(DE3) Star<sup>®</sup> (Invitrogen), expressed and purified as described by Milne et al with slight modification (204). Starter cultures were prepared by inoculating a single colony into 5 mL sterile LB medium containing 0.1 mg/mL of ampicillin. After incubation at 37 °C for 16 hours, the culture was used for inoculating 1 L of media containing ampicillin at 37 °C for 4 to 6 hours until the OD<sub>600</sub> reached 0.6 to 0.8.

The expression of the enzyme was induced by adding 0.5 mM IPTG and the cell continued to grow overnight at 18°C. The cells were then pelleted out by centrifugation at 6,000 g and 4 °C for 20 min. The pellets were resuspended in lysis buffer (50 mM Tris, pH 8, containing 250 mM NaCl, 2-mercaptoethanol 0.25% Triton X-100 and 0.1mg/ml PMSF) and lysed by sonication (power level 4, 50% duty cycle) in an ice-bath for 20 minute, in 30 sec steps. The lysate was centrifuged at 15,000 g and 4 °C for 30 min and resulting supernatant containing soluble proteins in the cell lysate were purified by immobilized metal affinity chromatography (IMAC) using a 5 mL HisTrap HP (GE Healthcare). The HisTrap column was made up of the highly cross-linked agrose containing IDA (Iminodiacetic Acid) as an immobilized chelating group. Due to the presence of the imidazole ring of the histidine, the His-tagged protein specifically bound to the metal chelating sites, facilitating the specific binding of the recombinant protein. The non-specific and weak binding of the contaminating proteins was prevented by the addition of 50 mM imidazole in the SIRT1 cell lysis buffer. A linear gradient of 50-375 mM imidazole in purification buffer was used to elute sirt1 from the HisTrap column in different fractions. The purified enzymes were dialyzed into storage buffer (50 mM HEPES, pH 7.5, containing 100 mM NaCl, 10 % glycerol and 1 mM TCEP) and stored at -70 °C.

#### **4.1.4. Expression and purification of SIRT5 wild type and mutants**

The plasmids containing SIRT5 or SIRT5 mutants were transformed into BL21(DE3) Star<sup>®</sup> (Invitrogen), expressed and purified as described by Milne et al. with slight modification (204). Starter cultures were prepared by inoculating a single colony into 5 mL sterile LB medium containing 0.1 mg/mL of ampicillin. After incubation at 37 °C for 16 hours, the culture was used for inoculating 1 L of media containing ampicillin at 37 °C for 4 to 6 hours until the OD<sub>600</sub> reached 0.6 to 0.8. The expression of the enzyme was induced by adding 0.5 mM IPTG and

continued overnight at room temperature. The cells were then pelleted out by centrifugation at 6,000 g and 4 °C for 30 min. The pellets were resuspended in lysis buffer (50 mM Tris, pH 8, containing 250 mM NaCl, 2-mercaptoethanol 0.25% Triton X-100 and 0.1mg/ml PMSF) and lysed by sonication (power level 4, 50% duty cycle) in an ice-bath for 20 minute, in 30 sec steps. The lysate was centrifuged at 15,000 g and 4 °C for 30 min and resulting supernatant containing soluble proteins in the cell lysate were purified by immobilized metal affinity chromatography (IMAC) using a 5 mL HisTrap HP column (GE Healthcare). The non-specific and weak binding of the contaminating proteins was prevented by the addition of 40 mM imidazole in the cell lysis buffer. A linear gradient of 40-375 mM imidazole in purification buffer was used to elute SIRT5 from the HisTrap column in different fractions. The purified enzymes were subjected to the SDS-PAGE analysis and stored in 50 mM HEPES (pH 7.5), 100 mM NaCl, 10 % glycerol and 1 mM TCEP at -70 °C.

#### **4.1.5. Purity of proteins**

During the course of purification, the expression level of each of the above proteins during each stage of purification was qualitatively determined by SDS-PAGE analysis as described in Current Protocols in Molecular Biology. A resolving gel of 12% acrylamide prepared in 1.5 M Tris, pH 8.8 and a stacking gel of 4% prepared in 0.5 M tris, pH 6.8 were utilized, both containing 0.1% SDS. Samples were dissolved in loading dye (300 mM Tris, pH 6.8, 10% SDS, 25% glycerol, 5 mM  $\beta$ -mercaptoethanol, and 0.015% bromophenol blue) and heated in a boiling water bath for 5 min before loading. The gels were run at 200 V in tris-glycine buffer (0.1% SDS, 25 mM tris, 190 mM glycine, pH 8.3), and then stained with 0.1% coomassie blue in 10% acetic acid and 10% methanol for 15 min followed by destaining with 10%

acetic acid and 40% methanol. Purity of the enzymes was qualitatively judged by the number and intensity of other protein bands relative to that of the protein of interest.

#### **4.1.6. Estimation of protein concentrations**

The concentration of enzyme was estimated by Bradford assay using BSA as a standard protein. The assay was performed using absorption micro plate reader (Spectra Max PLUS, Molecular Devices). A mixture of 1:1 diluted HDAC8 in storage buffer was mixed with 1:4 diluted Bradford reagent. The mixture was incubated for 5 minutes at room temperature and then the absorbance was measured at 595 nm. The molar concentration was calculated taking the molecular weight of SIRT1 as 62 kDa and SIRT5 as 31 kDa.

### **4.2. Electronic Spectroscopic Methods**

#### **4.2.1. Spectrophotometric studies**

All the absorption studies were performed on an absorption multi-mode microplate reader (Spectra Max PLUS, Molecular Devices). The absorbance spectra of 1  $\mu$ M enzymes were obtained at room temperature using a 1 cm path-length cuvette in 25 mM Tris-Cl, pH 7.5, containing 100 mM NaCl, 10 % glycerol and 1 mM TCEP. The spectrum MH5-75 was measured under the same condition. The Absorption change of MH5-75 in the presence of SIRT5 were measured by incubating 10  $\mu$ M MH5-75 with 70  $\mu$ M SIRT5 in a 1 cm path-length cuvette and taking the absorption spectra at different time intervals (immediately, after 2 hours, 3 hours and 5.5 hours, respectively).

#### **4.2.2. Measurements of protein emission spectra**

Steady state spectrofluorometric studies were performed on a Perkin Elmer lambda 50-B spectrofluorometer, equipped with a magnetic stirrer and thermostated water bath. The emission spectra of SIRT1 and SIRT5 were acquired by fixing the excitation wavelength at 280 nm while

maintaining both excitation and emission slits at 5 mm without any cut-off filter. All measurements were performed in a standard quartz cuvette at room temperature.

#### 4.2.3. Measurements of time-resolved fluorescence spectra

Fluorescence lifetime measurements were performed on a custom designed QuantaMaster 30™ (Photon Technology International, Birmingham, NJ). The Light Emitting Diode (LED) was used as the excitation source for measuring the time resolved fluorescence decay of proteins, with maximum power output at 280 nm. The start and end delays were set up at 70 ns and 120 ns, respectively. The data were collected in 200 channels. 30 repeated data were averaged to reduce the noise to signal ratio. To correct for the instrument response, a corresponding instrument response function (IRF) was generated by a coffee mate solution using the identical experimental instrumental parameters. The fluorescence decay curves was analyzed using the Felix32™ software (Photon Technology International, Birmingham, NJ), using the single or double exponential rate equations of the following format (Eq. 4.1)

$$I(t) = \sum_{i=1}^n a_i e^{-t/\tau_i} \quad \text{Eq. 4.1}$$

where  $\alpha_i$  and  $\tau_i$  are amplitude and fluorescence lifetime for the  $i^{\text{th}}$  component, respectively. The relative contribution of component  $i$  ( $f_i$ ) was calculated from the following equation (Eq. 4.2)

$$f_i = \left( \frac{\alpha_i \tau_i}{\sum_{i=1}^n \alpha_i \tau_i} \right) \times 100\% \quad \text{Eq. 4.2}$$

The goodness of the exponential fit of fluorescence curves was determined by the reduced chi-square, the Durbin Watson, and Z values.

#### 4.2.4. Measurements of circular dichroism (CD) spectra

Far-UV CD spectra (190-250 nm) were collected on a J-710 spectropolarimeter (Jasco, Tokyo, Japan) equipped with a Peltier temperature controller. The enzyme stocks were diluted to 10  $\mu$ M in 5 mM Tris-HCl buffer, pH 8.0, containing 0.5 % glycerol, 0.1 mM TCEP and 15 mM KCl, and transferred to a 1 mm path-length quartz cuvette for obtaining the CD spectra. The samples were subjected to the CD spectral acquisitions from 190 nm to 250 nm in triplicates and the spectra were averaged. The CD signals were converted to the mean residue ellipticity (MRE;  $\theta$ ) using Equation 4.3.

$$\theta = \frac{\text{signal}}{10 \cdot l \cdot c} \cdot \frac{1}{r} \quad \text{Eq. 4.3}$$

where “*signal*” is the amplitude of the raw CD signal; *l* is the path length (mm) of the cuvette; *c* is the protein concentration, and *r* is the number of amino acid residues in the protein.

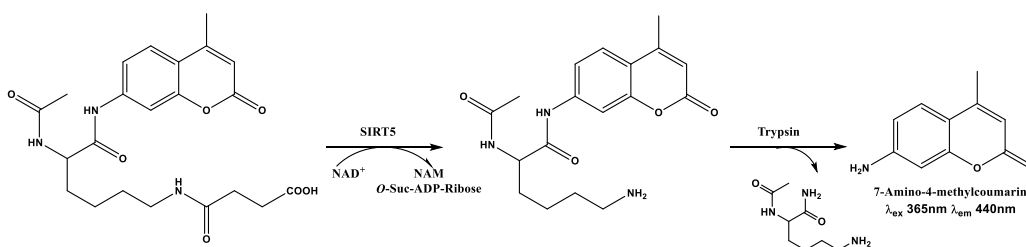
### 4.3. Steady-state Kinetic Methods

#### 4.3.1. Trypsin-coupled enzyme activity assay

The sirtuin catalyzed deacetylase and desuccinylase reactions were measured via the trypsin coupled assay system. Acetylated-Lys (*Fluor-de-lys*<sup>®</sup>) and succinylated-Lys (Ac-Suclys-AMC) were used as the substrates for the deacetylation and desuccinylation reactions. While the former substrate was obtained commercially, the succinylated substrate (Ac-Suclys-AMC) was synthesized according to the procedure described by Madsen et al. (250). As shown in Figure 4.2, the substrates contain the acetylated/succinylated lysine residue which is attached to an amino methyl coumarin moiety (AMC) via an amide linkage. Removal of the acetyl group from the substrates by sirtuin catalyzed reaction produces a deacetylated or desuccinylated product, which is hydrolyzed by trypsin liberating free AMC. The free AMC which is highly

fluorogenic ( $\lambda_{\text{ex}} = 365 \text{ nm}$  and  $\lambda_{\text{em}} = 500 \text{ nm}$ ) could be easily detected using spectrofluorometer. The enzymatic reactions were carried out at  $25 \text{ }^\circ\text{C}$  in  $50 \text{ mM}$  Tris-HCl assay buffer, pH 8.0, containing  $137 \text{ mM}$  NaCl,  $2.7 \text{ mM}$  KCl,  $1 \text{ mM}$   $\text{MgCl}_2$ , and  $1 \text{ mg/mL}$  bovine serum albumin. The initial velocity of the enzyme catalyzed reaction was determined by monitoring the time dependent increase in the fluorescence intensity at  $460 \text{ nm}$  ( $\lambda_{\text{ex}} = 365 \text{ nm}$ ) using a fluorescence microplate reader (SpectraMax Gemini, Molecular Devices). Since trypsin was used as a coupling enzyme, its concentration was optimized to ensure the emergence of minimal or negligible lag-phase prior to the onset of the steady state phase.

#### desuccinylase assay



#### deacetylase assay

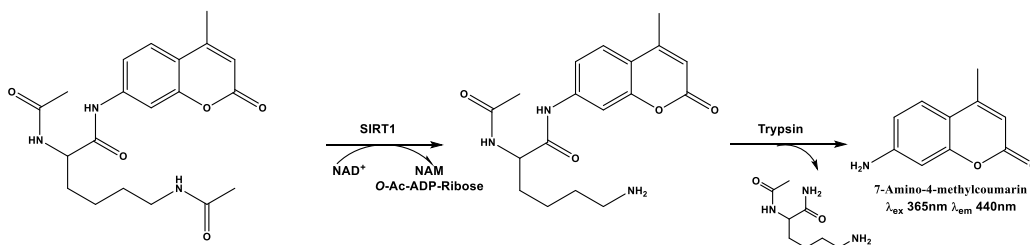


Figure 4.2. Schematic representation of the trypsin-coupled assay to measure the initial rate of the sirtuin catalyzed reaction.

#### 4.3.2. Bi-substrate kinetic analysis of the sirtuin catalyzed reactions

The bi-substrate kinetic experiments were performed by varying the concentrations of  $\text{NAD}^+$  (from  $100$  to  $500 \text{ } \mu\text{M}$ ) and Ac-SucLys-AMC or *Fluor-de-lys*<sup>®</sup> substrates (from  $100 \text{ } \mu\text{M}$

to 1200  $\mu\text{M}$ ) and 0.8  $\mu\text{M}$  trypsin. The steady state rates of the enzyme catalyzed reactions were derived from the time dependent changes in the fluorescence signal, and the data were analyzed by the sequential kinetic mechanism (Eq 4.4) via Grafit 4 software.

$$v = \left( \frac{V_{\max}[A][B]}{K_a K_{\text{mb}} + K_{\text{ma}}[B] + K_{\text{mb}}[A] + [A][B]} \right) \quad \text{Eq. 4.4}$$

Where  $V_{\max}$  is the maximum reaction velocity,  $K_a$  is the dissociation constant for the acylated substrates (A), and  $K_{\text{ma}}$  and  $K_{\text{mb}}$  are the Michaelis-Menten constants for acylated substrates and  $\text{NAD}^+$  (B), respectively.

#### 4.3.3. Screening of sirtuin effectors

In pursuit of developing novel inhibitors/activators (effectors) of sirtuins, a series of small molecules were synthesized in the laboratories of Dr. Greg Cook and Dr. Sanku Mallik from Department of Chemistry and Biochemistry and Department of Pharmaceutical Sciences at North Dakota State University, respectively. To evaluate their effectiveness on SIRT1/ SIRT5 catalyzed reaction, the initial screening was performed by measuring the change in SIRT1/SIRT5 activity in the presence of 10  $\mu\text{M}$  of the potential effectors using the coupled assay described in section §4.2.1. The assays were conducted in 96-well plates, and the reactions were initiated (simultaneously in each plate column) by addition of the enzyme using a multi-channel pipette. The small molecules inhibiting the SIRT1/SIRT5 activity > 30% were selected for further confirmation and characterization.

#### 4.3.4. $K_i$ measurement

The inhibition constants of half and fullsuramin on wild-type SIRT1 and SIRT5 catalyzed reactions and that of full-suramin on SIRT5 Y102A mutant enzyme were determined by performing the steady state kinetic studies using fixed concentrations of substrates and  $\text{NAD}^+$ .



For the inhibition studies of half suramin on SIRT1 catalysis, the experiment was performed in the presence of 100  $\mu\text{M}$  *Fluor-de-lys*<sup>®</sup> substrate, 500  $\mu\text{M}$   $\text{NAD}^+$ , and varying concentration (from 0  $\mu\text{M}$  to 100  $\mu\text{M}$ ) of half-sruamin. For the inhibition studies of SIRT5 catalyzed reactions by half suramin, the experiments were carried in the presence of 100  $\mu\text{M}$  *Ac-Suclys-AMC* substrate, 100  $\mu\text{M}$   $\text{NAD}^+$ , and varying concentrations (from 0  $\mu\text{M}$  to 7 mM) of half-suramin. Other reaction conditions were the same as described above. Since the enzyme concentration was much lower than the concentration of suramin, the data were analyzed using the quadratic equation describing the competitive steady state model for the inhibitors (Eq. 4.5) with Grafit 4.0.

$$v = \frac{v_0 \times K_i}{K_i + \left( [I]_t - 0.5 \left( [I]_t + [E]_t + K_i - \sqrt{([I]_t + [E]_t + K_i)^2 - 4 \times [I]_t \times [E]_t} \right) \right)} \quad \text{Eq. 4.5}$$

where  $v_0$  is the initial velocity of HDAC8 catalyzed reaction without any inhibitor,  $[I]_t$  is total concentrations of the inhibitor,  $[E]_t$  is the total concentration of enzyme used in the assay.

#### 4.3.5. IC<sub>50</sub> measurement

The IC<sub>50</sub> values of EX527 for the sirtuin catalyzed reactions were measured using the fixed concentrations of substrates and  $\text{NAD}^+$ . For the inhibition studies of SIRT1 catalysis, the experiment was performed in the presence of 100  $\mu\text{M}$  *Fluor-de-lys*<sup>®</sup> substrate, 500  $\mu\text{M}$   $\text{NAD}^+$ , and varying concentration (from 0  $\mu\text{M}$  to 40  $\mu\text{M}$ ) of EX527. For the inhibition studies of wild-type and SIRT5 mutants catalyzed reactions by EX527, the experiments were carried in the presence of 100  $\mu\text{M}$  *Ac-Suclys-AMC* substrate, 500  $\mu\text{M}$   $\text{NAD}^+$ , and varying concentrations (from 0  $\mu\text{M}$  to 200  $\mu\text{M}$ ) of EX527. Other reaction conditions were the same as described above.

The IC<sub>50</sub> values of MH5-75 for SIRT5 catalyzed reactions were measured in the presence of 50  $\mu\text{M}$  *Ac-Suclys-AMC*, 50  $\mu\text{M}$   $\text{NAD}^+$ , and increasing concentration of MH5-75 (from 0 to

400  $\mu\text{M}$ ). Other reaction conditions were the same as described above. All the data were fitted by equation (Eq. 4.6) by Grafit 4.0.

$$y = \frac{Range}{1 + \left(\frac{x}{IC_{50}}\right)^s} + Background \quad \text{Eq. 4.6}$$

Where the *Range* is the fitted uninhibited value minus the *Background*, and *s* is the slope factor. The parameters *x* and *y* are the concentrations of the inhibitor (EX527 or MH5-75) and initial rates of the enzyme catalysis.

#### 4.3.6. Inhibition mode

##### 4.3.6.1. Inhibition analysis of SIRT5 by suramin

The trypsin-coupled desuccinylase assay was performed as described previously (250). The reactions were carried out at 25 °C in an assay buffer (50 mM Tris, pH 8.0, 137 mM NaCl, 2.7 mM KCl, 1mM MgCl<sub>2</sub>, and 1 mg/mL bovine serum albumin). Trypsin was used as the coupled enzyme and its concentration was optimized to ensure the emergence of negligible lag-phase prior to the steady state phase. For determining the inhibition type with respect to the succinylated lysine-AMC substrate, the concentration of NAD<sup>+</sup> was kept constant (and 50  $\mu\text{M}$ , respectively), and the concentration of suramin was varied from 0  $\mu\text{M}$  to 100  $\mu\text{M}$ . For determining the inhibition type with respect to NAD<sup>+</sup>, the concentration of succinylated lysine-AMC was kept constant at 120  $\mu\text{M}$ . The initial velocities at different concentrations of succinylated lysine-AMC, NAD<sup>+</sup> and suramin were fitted to three possible inhibition mechanisms, competitive (Eq. 4.7), mixed inhibition (Eq. 4.8) and uncompetitive inhibition (Eq. 4.9) using Grafit 4.0 (Erithacus software).

$$v_0 = \frac{V_{\max} [S]}{K_m \left(1 + \frac{[I]}{K_i}\right) + [S]} \quad \text{Eq. 4.7}$$

$$v_o = \frac{V_{\max} [S]}{K_m \left(1 + \frac{[I]}{K_i}\right) + [S] \left(1 + \frac{[I]}{K_i}\right)} \quad \text{Eq. 4.8}$$

$$v_o = \frac{V_{\max} [S]}{K_m + [S] \left(1 + \frac{[I]}{K_i}\right)} \quad \text{Eq. 4.9}$$

#### 4.3.6.2. Inhibition analysis of SIRT1 and SIRT5 variants by nicotinamide

The nicotinamide inhibition of sirtuin catalyzed reactions was determined by performing the steady-state kinetic experiments in the absence and presence of nicotinamide as described above. The experiments were performed in the presence of either 100  $\mu\text{M}$  *Fluor-de-lys*<sup>®</sup> or Ac-SucLys-AMC substrate with varying concentration of  $\text{NAD}^+$  and nicotinamide. The steady-state kinetic data were fitted globally by the competitive, mixed, and noncompetitive inhibition models using the DYNAFIT software based on the rapid-equilibrium approximation (252). All the parameters were allowed to float except for the enzyme concentration. The software utilizes several model-discrimination criteria, including the second order Akaike Information Criterion (AIC) (253, 254), so that the best model out of the three different candidates could be identified.

#### 4.4. Transient Kinetic Methods

To determine the rate constants of binding of suramin to SIRT5, transient kinetic experiments were performed using an Applied Photophysics SX-18MV stopped-flow system. The stopped-flow system (dead time = 1.3 ms) was operated in the fluorescence mode with an emission path length of 2 mm. The time-dependent change in the tryptophan fluorescence was monitored by exciting the reaction at 280 nm. The change in protein fluorescence signal was detected using a cut-off filter of 320 nm. All the transient kinetic experiments were performed at least ten times in 25 mM Tris buffer, pH 7.5, containing 100 mM NaCl, 1 mM TCEP and the

resultant kinetic traces were averaged and analyzed by Origin 8.5.1 using either a single (Eq. 4.10) or double exponential rate equation (Eq. 4.11)

$$Flut = Amp \times e^{(-\frac{1}{\tau})} + offset \quad \text{Eq. 4.10}$$

where  $Flut$  is the fluorescence at a given time.  $Amp$  and  $1/\tau$  are the total amplitude and relaxation rate constant, respectively.

$$Flut = Amp1 \times e^{(-\frac{1}{\tau_1})} + Amp2 \times e^{(-\frac{1}{\tau_2})} + offset \quad \text{Eq. 4.11}$$

where  $Flut$  is the fluorescence at a given time.  $Amp1$  and  $Amp2$  are the respective amplitudes associated with relaxation rate constants ( $1/\tau_1$  and  $1/\tau_2$ ). Relaxation rate constants were measured as a function of the ligand concentration and data were analyzed using appropriate kinetic models as described in the results section.

## 4.5. Thermodynamic Studies

### 4.5.1. Binding isotherms of suramin to SIRT1 and SIRT5

All the steady-state spectrofluorometric studies were performed in sirtuin storage buffer on a Perkin-Elmer lambda 50-B spectrofluorometer, equipped with a magnetic stirrer and thermostated water bath using a  $4 \times 4 \text{ mm}^2$  square quartz cuvette. The change in intrinsic fluorescence signal of the enzyme upon of ligand was used for the titration of fixed concentration of SIRT1 or SIRT5 with increasing concentration of suramin to obtain the overall binding isotherms. The fluorescence emission spectrum of SIRT1 or SIRT5 was monitored in the range of 330–500 nm after excitation at 280 nm. The excitation and the emission slit width in these experiments were 10 and 8 respectively with PMT (photo multiplier tube) voltage of 800. The resulting binding isotherms for the enzyme-ligand complex were analyzed via the complete solution of the quadratic equation modified for the decreasing signal (Eq.4.12)

$$F = F_{\max} - C * (L_t + K_d + n * E_t) - \sqrt{(L_t + n * E_t + K_d)^2 - 4 * L_t * E_t} / 2 \quad \text{Eq. 4.12}$$

where F is fluorescence signal of protein/ligand after the addition of other interacting partner;  $F_{\max}$  is the fluorescence signal of protein in the absence of the interacting partner,  $E_t$ , and  $L_t$  are the total enzyme and total ligand concentration, respectively;  $K_d$  is the dissociation constant of the enzyme-ligand complex, n is stoichiometry of the enzyme-ligand complex and C is the change in amplitude of the signal.

#### **4.5.2. Isothermal titration calorimetry**

Isothermal titration calorimetric (ITC) experiments were performed on a VP-ITC microcalorimeter (GE Healthcare). All experiments were performed in duplicate or triplicate using the same stock solutions of the ligands and the enzyme. The mean values of the ITC-derived thermodynamic parameters and the associated standard deviations are reported in the Results section.

##### ***4.5.2.1. EX527***

The sample cell was filled with 1.8 mL (effective volume = 1.4 mL) of 20  $\mu$ M Y102A/R105I mutant SIRT5 and 0 or 10 mM  $\text{NAD}^+$  in 50 mM HEPES buffer, pH 7.5, containing 100 mM NaCl, 10 % glycerol and 1 mM TCEP. The content of the sample cell was titrated with 45 aliquots (4  $\mu$ l each) of EX527 containing either 0 or 10 mM  $\text{NAD}^+$ , prepared in the same buffer.

##### ***4.5.2.2. Nicotinamide***

The thermodynamic parameters for the binding of nicotinamide to SIRT5 was obtained by titration of 40  $\mu$ M SIRT5 by 45 injections (5  $\mu$ l each) of 2 mM nicotinamide in the presence of 1 mM Ac-Suclys-AMC substrate. The sample cell of VP-ITC was filled with 1.8 mL (effective volume = 1.4 mL) of 40  $\mu$ M SIRT5 premixed with 0 or 1 mM Ac-Suclys-AMC

substrate in 50 mM HEPES buffer, pH 7.5, containing 100 mM NaCl, 10 % glycerol, 2% DMSO and 1 mM TCEP. The content of the sample cell was titrated with 40 aliquots (5  $\mu$ l each) of 2 Mm nicotinamide prepared in the same buffer.

#### ***4.5.2.3. Suramin and half-suramin***

The thermodynamic parameters for the binding of suramin to low concentration of SIRT5 were obtained by titration of 10  $\mu$ M SIRT5 with 45 aliquots (4  $\mu$ L each) of 300  $\mu$ M suramin in 50 mM Tris-HCl, pH 7.5, containing 100 mM NaCl, 10 % glycerol and 1 mM TCEP at 25 °C. The thermodynamic parameters for the binding of suramin to high concentration of SIRT5 were obtained by titration of 80  $\mu$ M SIRT5 with 45 aliquots (3  $\mu$ L each for the first 10 titrations and 5  $\mu$ L for the remaining 35 titrations) of 700  $\mu$ M or 1 mM suramin in the above buffer. The thermodynamic parameters for the binding of half suramin to SIRT5 were obtained by titration of 80  $\mu$ M of SIRT5 with 45 aliquots (4  $\mu$ l each) of 5 mM half suramin in the above buffer without TCEP. The experimental data were analyzed by appropriate binding models using the Origin® software package, which yielded the association constant ( $K_a$ ) and enthalpic ( $\Delta H^\circ$ ) Changes.

#### **4.5.3. Size exclusion chromatographic studies**

The molecular weights of SIRT5 in the presence of different molar ratios of enzyme to Suramin were determined by size exclusion chromatography using a Superdex 200 column (16 mm  $\times$  600 mm) on an AKTA design purifier (GE Healthcare). The superdex 200 column was packed using a packing reservoir (XK16/70 column) on the AKTA design pump P-901 following the protocol provided by GE Healthcare. The void volume of the column was determined by running a sample of 2mg/mL blue dextran dissolved in equilibration buffer (50 M HEPES, pH 7.5 with 100 M NaCl) containing 5% glycerol. The column was calibrated by detetmining the

elution volumes ( $V_e$ ) of five molecular weight standards, namely cytochrome C (12.4 kDa), carbonic anhydrase (29 kDa), BSA (66 kDa), yeast ADH (150 kDa) and  $\beta$ -amylase (200 kDa) (Sigma-Aldrich). SIRT5 (60  $\mu$ M) was mixed with varying concentration of suramin (0, 0.5  $\mu$ M, 1  $\mu$ M, 1.5  $\mu$ M, 5  $\mu$ M, 10  $\mu$ M, and 20  $\mu$ M) on ice in 25 mM HEPES buffer, pH 7.5, containing 100 mM NaCl and 1 mM TCEP. The mixture was loaded on to the Superdex 200 column and washed it with the above buffer containing the corresponding concentration of suramin. 1 mL sample was loaded to a 2 mL sample loop that was also pre-filled with the same concentration of suramin. After loading, the protein concentration was approximately diluted to 30  $\mu$ M while the concentration of suramin remained unchanged. The elution profile was monitored at 280 nm and recorded for different chromatographic runs. The peak deconvolution was performed by the peak analysis module of Origin 8.5.1 (OriginLab) using the Guassion function. (Eq. 4.13)

$$y = y_0 + \frac{A}{w\sqrt{\pi/2}} e^{-2\frac{(x-x_c)^2}{w^2}} \quad \text{Eq. 4.13}$$

where  $y_0$ ,  $x_c$  and  $A$  are the offset, center, and the area of the peak,  $w$  is the width derived from the “Full Width at Half Maximum” (FWHM) using the equation

$$FWHM = \sqrt{2\ln 2} \times w \quad \text{Eq. 4.14}$$

The molar ratio of dimer versus monomer was calculated based on the peak areas ( $A$ ) derived from the fitting results.

#### 4.5.4. Thermal stabilities

The thermal unfolding of the enzymes was performed by monitoring the changes in the CD signal at 208 nm as a function of increasing temperature (maintained via the Peltier

controller) from 12 to 95 °C at a rate of 1° C min<sup>-1</sup>. The data were analyzed either by a single (Equation 4.14) or double (Equation 4.15) Boltzmann equations,

$$\theta = \frac{A_1 - A_2}{1 + e^{(x - x_0)/dx}} + A_2 \quad \text{Eq 4.15}$$

Where  $x$  is the temperature,  $A_1$  and  $A_2$  are the initial (base line) and final (upon completion of unfolding) ellipticities, respectively;  $x_0$  is the melting temperature ( $T_m$ ), and  $dx$  is the width of the thermal transition,

$$\theta = \frac{A_0 - A_1}{1 + e^{(x - x_{01})/dx_1}} + \frac{A_1 - A_2}{1 + e^{(x - x_{02})/dx_2}} + A_2 \quad \text{Eq 4.16}$$

Where  $x$  is the temperature,  $A_0$ ,  $A_1$  and  $A_2$  are the initial, intermediate, and final baseline ellipticities for the two sequential (independent) thermal transitions, respectively, with  $x_{01}$  and  $x_{02}$  being the melting temperatures ( $T_m$ ) and  $dx_1$  and  $dx_2$  being the widths of the first and second thermal transitions, respectively.

#### 4.6. Atomic Force Microscope Size Measurements

The size distributions of SIRT5 in the presence of various concentrations of suramin were measured by AFM in collaboration with Dr. Yongki Choi from Department of Physics at North Dakota State University. The SIRT5 sample was prepared by premixing 10 μM SIRT5 solutions with suramin at the following four different concentrations; SIRT5 in the absence of suramin, and the mixtures of SIRT5 and suramin at the molar ratios of 1:1, 4:1, and 1:10. The solution was dropped on top of a freshly cleaned mica surface and incubated for 10 minutes at room temperature. The mica surface was rinsed and dried prior to the AFM imaging. AFM was used to measure the height of individual SIRT5 proteins on a mica flat surface. AFM measurements were carried out in non-contact mode at a scanning rate of 1.3 Hz and a resonance frequency at



145 kHz using a NT-MDT NTEGRA (NT-MDT America, Tempe, AZ). The cantilever was made of silicon nitride and was 100  $\mu\text{m}$  long. The scanning area was  $5 \times 5 \mu\text{m}$  at the resolution of 1024 points per line. The images were flattened by a first-order line correction to remove a vertical offset between scan lines and a first-order plane subtraction to level a tip-sample tilt. To measure protein's height, the ImageJ software was used to locate the proteins using a peak pointing tool. The peak locations of proteins were retrieved as x and y coordinates in each image, and a height profile was individually generated for all proteins to determine their heights using a LabVIEW program. The height distribution of proteins was obtained from a histogram analysis by dividing the entire range of heights into small intervals of equal width, sorting the proteins into a series of height intervals, and counting their numbers fallen into each interval. A log-normal function was found to be useful to examine a skewed distribution especially if the logarithm of the heights,  $\log(x)$ , is Gaussian. The function to find the most peak in the distribution is given by Eq. 4.17

$$f(x) \propto \exp \left[ - \left( \frac{\ln(x/x_0)}{w_0} \right)^2 \right] \quad \text{Eq. 4.17}$$

where two parameters,  $x_0$  and  $w_0$ , are the peak position and its width, respectively.

#### 4.7. Molecular Modeling

Molecular Operating Environment (MOE-2014) by Chemical computing group (CCG) was used for the molecular modeling of SIRT5-suramin interaction (255). The protein preparation step involved 3D protonation, energy minimization and active site identification. The crystal structure of the protein was retrieved from protein data bank (PDB code: 2NRY). Protein was energy minimized and 3-D protonated by using the structure preparation module of MOE. Since the protein contains the co-crystallized ligand, the active site was identified around the co-

crystallized ligand by using the LigX module of the MOE. The pocket was found to be a deep cavity lined with the key residues including both hydrophobic and hydrophilic amino acids. The ligand for the molecular docking studies were prepared using MOE and were followed by energy optimization at a standard MMFF94 force field level, with a 0.0001 kcal/mol energy gradient convergence criterion (256). The optimized geometry was saved in a molecular data base file for further studies. The optimized ligand was docked with the protein (PDB code: 2NRY) using the MOE-Dock program. For docking, the default MOE docking parameters were utilized to generate 50 poses of compound in each docking run. As a result of docking computations mdb output files were generated enclosing all docking results with scoring and multiple conformations of ligand. All the docked conformations were analyzed and the best scored pose from each docking run was retained for further studies of interaction evaluation. The 2D ligand-protein interactions were visualized using the MOE's ligand interactions program.

## 5. RESULTS

### 5.1. Cloning, Expression, Purification, and Physiochemical Properties Characterization of Recombinant Human SIRT1 and SIRT5

#### 5.1.1. Cloning, expression, purification of SIRT1, SIRT2 and SIRT5

##### *5.1.1.1. Cloning, expression and purification of SIRT1*

As elaborated in the previous chapter (§4.1.1), the coding sequence of human sirtuin 1 (SIRT1) from its parent plasmid pOTB7 was amplified by the PCR method and cloned into the pLIC-His vector (251). Besides containing a ligand independent cloning (LIC) site, the pLIC-His vector encodes for an N-terminal hexa-histidine peptide followed by a TEV (Tobacco Etch Virus) protease recognition sequence (Figure 5.1). The SIRT1 gene was cloned within the LIC site, located downstream of the TEV recognition site. The hexa-histidine peptide (His-tag) serves as a purification tag for Immobilized Metal Affinity Chromatography. As shown in Figure 5.2, the size of the PCR product was approximately 1.7 kb (between 1.5 and 2 kb), as expected for a 1665 base pair coding sequence of SIRT1 (193-747) with an additional 36 base pairs derived from the primers. The resultant plasmid was sequenced with the forward and reverse primers to confirm the SIRT1 coding region of the catalytic domain of SIRT1 (amino acid sequence 193-747) in the plasmid. The analysis of the sequence data by nucleotide BLAST revealed 100% identity with SIRT1 (193-747).

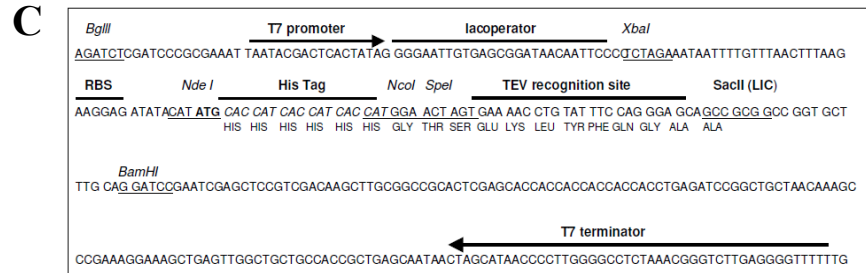
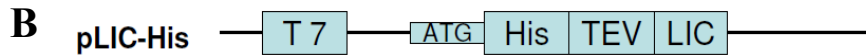
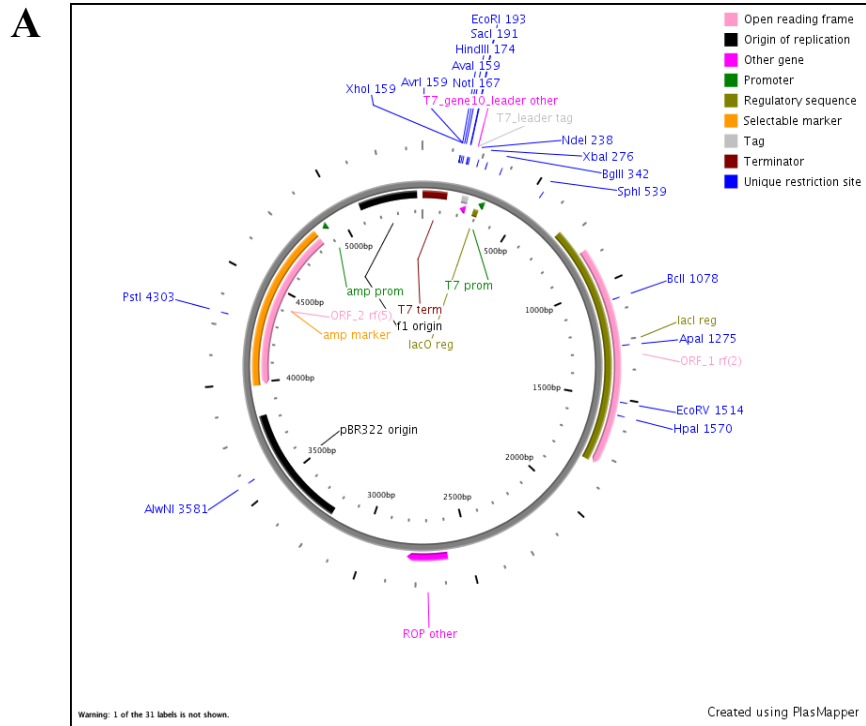


Figure 5.1. The vector map of the pLIC-His vector used for cloning human SIRT5 gene. The pLIC-His has a T7 promoter based system (Panel B) and has been derived from the pET921b (+) (Panel A). The SIRT1/SIRT5 gene was cloned at the LIC site.

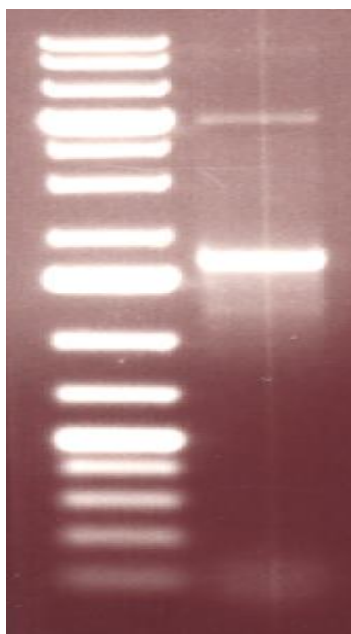


Figure 5.2. The agarose gel electrophoresis showing the PCR amplified SIRT1 gene using the pLIC compatible forward and reverse primers. The left lane shows the O'GeneRule™ 1 kb Plus DNA ladder.

The pLIC-His plasmid was transformed into the BL-21 Star (DE3) *E. coli* host cells. The expression of SIRT1 was induced by 0.5 M IPTG, serving as an inducer of the T7 promoter-lac operator system. After induction, the cells were further grown at 18 °C with constant shaking overnight to produce SIRT1 in the soluble (native) form. The cells were lysed by sonication, and the enzyme was purified from the soluble fraction of the crude lysate via the Immobilized Metal Affinity Chromatography (IMAC) using a HisTrap column as described in the Method section (§4.1.3). A linear gradient of 20-375 mM imidazole in purification buffer was applied to elute the enzyme from the column. The purity of the enzyme was confirmed by the SDS-PAGE analysis. Figure 5.3 shows the SDS-PAGE profile of SIRT1 (from 6 L culture) in different fractions of the eluants from Ni<sup>2+</sup>-IDA affinity chromatography. The major bands corresponded to the expected molecular mass of SIRT1 (62 kDa). When no imidazole was added to the lysis and the equilibration buffers, the fractions eluted from the column contained multiple bands

(Figure 5.3 A). On the other hand, when 50 mM imidazole was added to both the lysis and equilibration buffers, the fractions eluted from the column had lower contaminations of other proteins (Figure 5.3 B). Apparently, the presence of 50 mM imidazole efficiently reduced the non-specific binding of proteins to the column. The fractions containing pure SIRT1 were pooled and dialyzed against the storage buffer (25 mM HEPES, pH 7.5 containing 150 mM NaCl, 10% glycerol and 1 mM TECP). The protein concentration of the purified enzyme was estimated by the Bradford method using BSA as the standard (section §4.1.6). The yield of the purified SIRT1 obtained from six liters of the bacterial culture was approximately 15 mg.

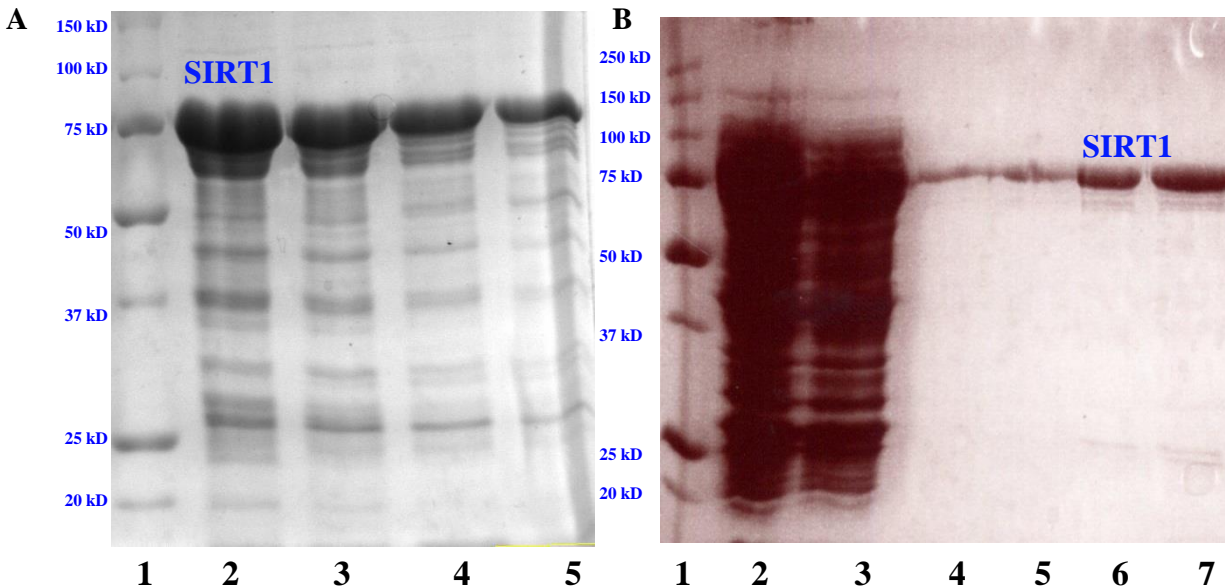


Figure 5.3. SDS-PAGE analysis of purified SIRT1 by  $\text{Ni}^{2+}$ -IDA affinity chromatography. (A) the HisTrap column was equilibrated in the absence of imidazole. The bands in lane 1 represent the protein standards with the molecular weights given in kDa. The bands from lane 2 to lane 8 represent SIRT1 eluted from the HisTrap column. (B) Elution profile of SIRT1 from the column equilibrated with 50 mM imidazole. The bands in lane 1 represent the protein standards with the molecular weights given in kDa. The bands in lane 2 and 3 represent the crude proteins before loading and after loading to the HisTrap column. The bands from lane 4 to lane 7 represent SIRT1 eluted from the HisTrap column.

### ***5.1.1.2. Cloning, expression and purification of SIRT5***

The coding sequence of human sirtuin 5 (SIRT5) from its parent plasmid pOTB7 was amplified by PCR and cloned into the pLIC-His vector using the ligation independent cloning (LIC) strategy. The resulting plasmid was sequenced using the forward and reverse primers (Mclab, San Francisco, CA) to confirm the presence of coding region of the catalytic domain of SIRT5 (amino acid sequence 51-301). Analysis of the sequencing data by nucleotide BLAST revealed 100% identity with SIRT5 (51-301). The pLIC-His-SIRT5 plasmid was transformed in the BL-21 Star (DE3) *E. coli* host cells and the expression was induced by 0.5 M IPTG. After induction, the cells were further grown at 18 °C with constant shaking overnight to enhance the expression of SIRT5 in soluble (native) form. The cells were then lysed by sonication, and the enzyme was purified from the soluble fraction of the crude lysate via the Immobilized Metal Affinity Chromatography (IMAC) using a HisTrap column as described in the Method section (§4.1.4). The non-specific and weak binding of the contaminating proteins was prevented by addition of 40 mM imidazole in the SIRT5 cell lysis buffer.

The purity of the enzyme was confirmed by the SDS-PAGE analysis (Figure 5.2). The band of SIRT5, which eluted between 200 to 300 M imidazole gradient, corresponding to the expected molecular mass of SIRT5 (31 kDa). The fractions containing pure SIRT5 were pooled and dialyzed against the storage buffer (25 mM HEPES, pH 7.5 containing 150 mM NaCl, 10% glycerol and 1 mM TECP). The protein concentration of the purified enzyme was estimated by the Bradford method using BSA as the standard. The yield of the purified SIRT5 obtained from one liter of the bacterial culture was proximately 34 mg.

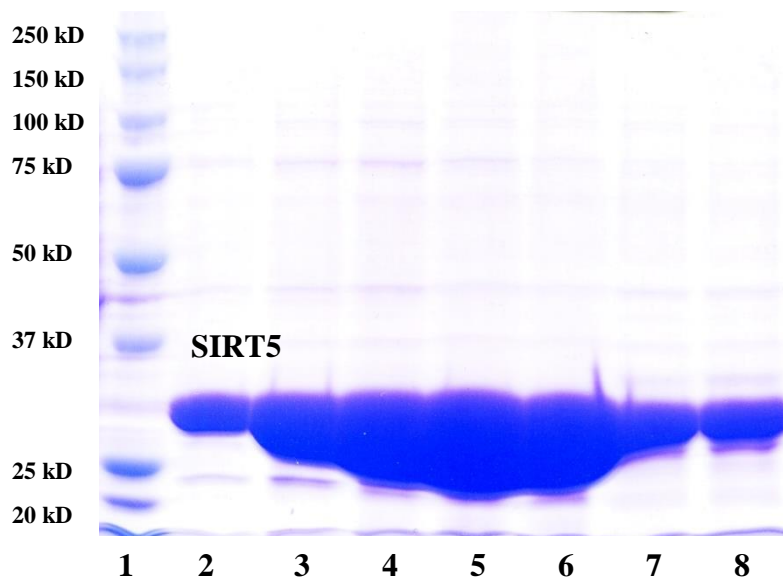


Figure 5.4. SDS-PAGE analysis of SIRT5 fractions eluted from the Ni<sup>2+</sup>-IDA affinity column. The bands in lane 1 represent the protein standards with the molecular weights given in kDa. The bands from lane 2 to lane 7 represent SIRT5 eluted from the Histrap column.

### 5.1.2. Cloning, expression and purification of SIRT5 mutants

Du et al. demonstrated that the presence of two amino acids, viz., Y102 and R105, at the active site pocket of SIRT5 changes the substrate specificity of the enzyme from carrying out normal deacetylation to desuccinylation/demalonylase reaction (257). The structural alignment between SIRT5 and SIRT1 (Figure 5.5) reveals that the above amino acids are substituted by Ala and Ile in SIRT1, respectively. To ascertain whether the above difference in the amino acid substitutions is exclusively responsible for the difference in the substrate specificity between SIRT1 and SIRT5, two single (Y102A and R105I) and one double mutation (Y102A/R105I) in SIRT5 were created by site-directed mutagenesis as described in section §4.1.2. After verification of the mutation sites in the coding sequence of SIRT5, the mutant plasmids were transformed into *E. coli* BL21 Star (DE3) cells, and the expression was induced by 0.5 M IPTG. After induction, the cells were further grown at 18 °C with constant shaking overnight to enhance



the expression of mutant SIRT5 in the soluble (native) form. The cells were lysed by sonication, and the mutant enzymes were purified from the soluble fractions of the crude lysates via the Immobilized Metal Affinity Chromatography (IMAC) using HisTrap columns as described in the Method section (§4.1.4). The purities of the enzymes were confirmed by the SDS-PAGE analysis (Figure 5.5 to 5.7). All of the SIRT5 mutant bands corresponded to the expected molecular mass of 31 kDa. . The protein concentration of the purified enzyme was estimated by the Bradford method using BSA as the standard. The expression levels of all three mutant enzymes were comparable to that of the wild type SIRT5. The yield of the purified SIRT5 Y102A, R105I, and Y102A/R105I obtained from the one liter of the bacterial culture was approximately 27 mg, 32 mg, and 37 mg, respectively.

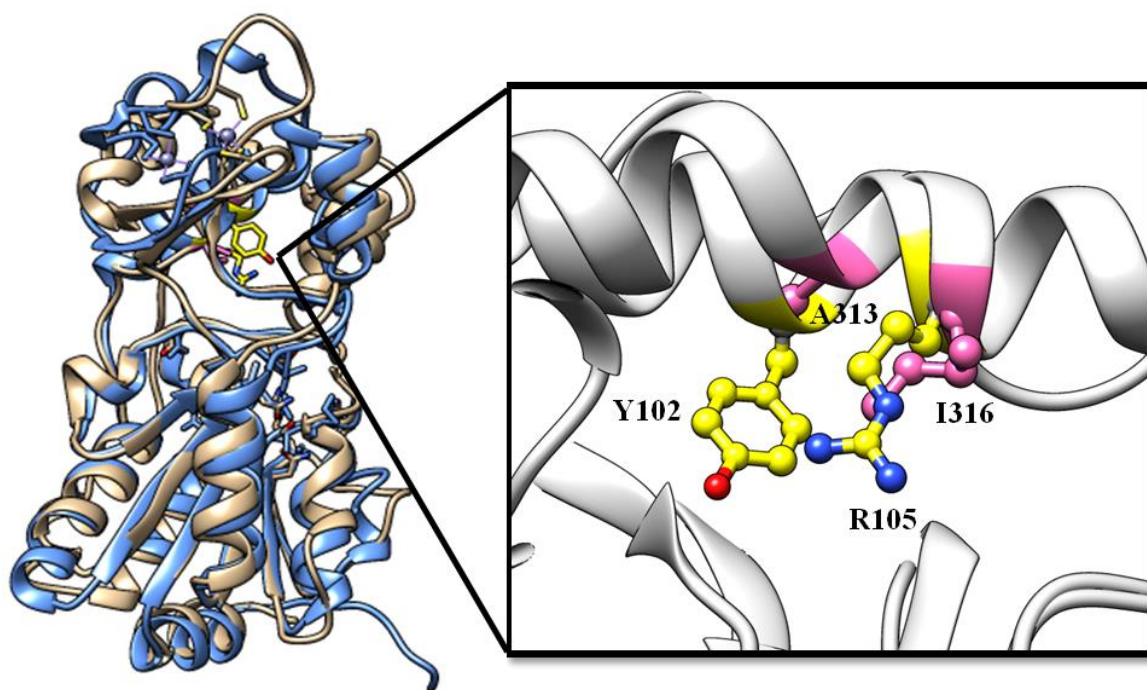


Figure 5.5. Comparative structural features in the catalytic domains of SIRT5 and SIRT1. (A) The superimposition (ribbon diagrams) of the catalytic domains of human SIRT5 (blue) and SIRT1 (tan). (B) A close view at the active site pockets of SIRT5 and SIRT1. The side chains of Y102 and R105I (yellow) in SIRT5 and of A313 and I316 (pink) in SIRT1 are presented as ball-and-stick models.

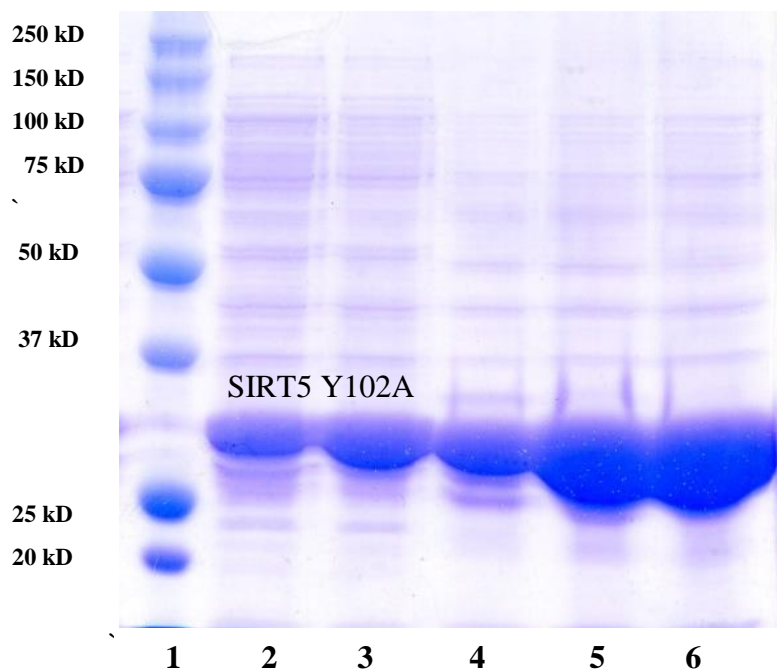


Figure 5.6. SDS-PAGE analysis of SIRT5 Y102A fractions eluted from the  $\text{Ni}^{2+}$ -IDA affinity column. The bands in lane 1 represent the protein standards with the molecular weights given in kDa. The bands from lane 2 to lane 6 represent SIRT5 Y102A eluted from the Histrap column.

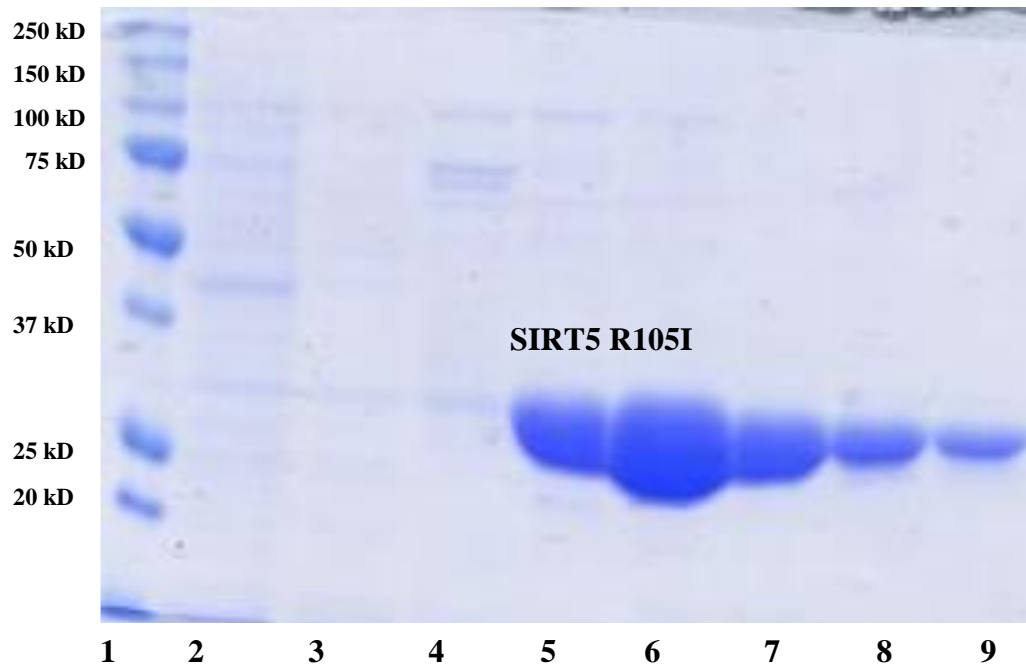


Figure 5.7. SDS-PAGE analysis of SIRT5 R105I fractions by  $\text{Ni}^{2+}$ -IDA affinity column. The bands in lane 1 represent the protein standards with the molecular weights given in kDa. The bands from lane 2 to 4 represent the unbound proteins washed from the Histrap column. The bands from lane 5 to 10 represent SIRT5 R105I eluted from the column.

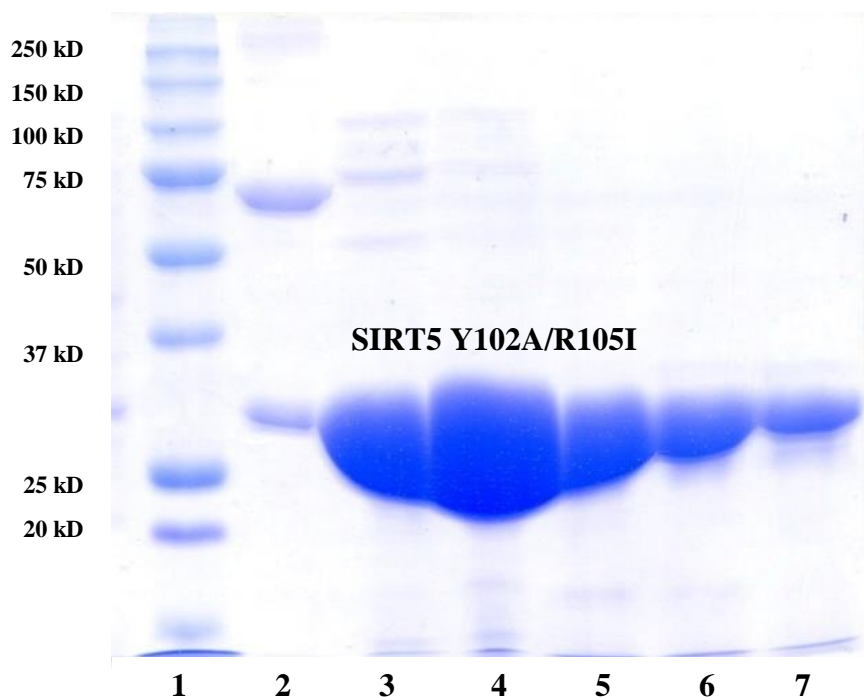


Figure 5.8. SDS-PAGE analysis of SIRT5 Y102A/R105I fractions by Ni<sup>2+</sup>-IDA affinity column. The bands in lane 1 represent the protein standards with the molecular weights given in kDa. The bands in lane 2 represent the unbound proteins washed from the Histrap column. The bands in lanes from 3 to lane 7 represent SIRT5 Y102A/R105I eluted from the Histrap column.

### 5.1.3. Physicochemical properties characterization of SIRT1, SIRT2 and SIRT5

#### 5.1.3.1. UV-Visible spectra of recombinant human SIRT1 and SIRT5

Proteins absorb in the UV range primarily because of the presence of peptide groups as well as the aromatic amino acids (Phe, Try, Trp). The molar extinction coefficients ( $\epsilon$ ) of proteins (expressed as  $M^{-1}cm^{-1}$ ) are dependent on the relative abundance of aromatic amino acids as well as their molecular microenvironment in protein structures. Hence, the molar concentrations of protein in aqueous solutions are often determined from their absorbance at 280 nm. Figure 5.8 and 5.9 show the UV-visible spectra of the recombinant form of the human SIRT1 and SIRT5 in 10 mM Tris-Cl, pH 7.5 containing 100 mM NaCl, 10 % glycerol and 1 mM TCEP. SIRT1 (193-747) contains 18 phenylalanine, 12 tyrosine and 2 tryptophan residues which

serve as the chromophores. As shown in the absorption spectrum of SIRT1 (Figure 5.8), the absorbance of 2  $\mu\text{M}$  SIRT1 at 280 nm measured in a 1 cm path length quartz cuvette was 0.069. On the other hand, SRIT5 (33-302) contains 13 phenylalanine, 5 tyrosine and 4 tryptophan residues. The absorbance of 1  $\mu\text{M}$  SIRT5 at 280 nm was 0.035 (Figure 5.9). Based on the absorbance values, the molar extinction coefficients of SIRT1 and SIRT5 were calculated as being equal to  $34500 \text{ M}^{-1} \text{ cm}^{-1}$  and  $34900 \text{ M}^{-1} \text{ cm}^{-1}$ , respectively. These values are in close agreement with values estimated by the method of Gill and von Hippel based on their amino acid sequences (258), which are  $28980 \text{ M}^{-1} \text{ cm}^{-1}$  and  $29640 \text{ M}^{-1} \text{ cm}^{-1}$  for SIRT1 and SIRT5, respectively.

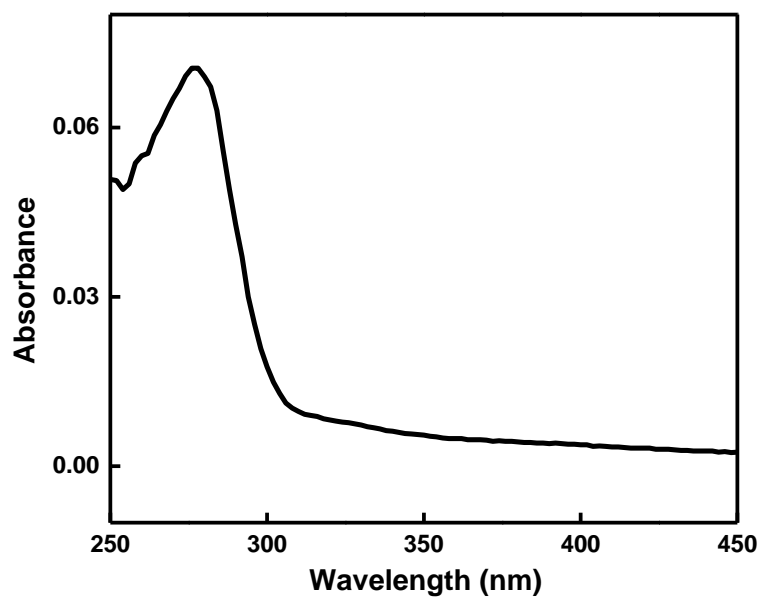


Figure 5.9. UV-visible spectrum of the recombinant human SIRT1. The spectrum of 2  $\mu\text{M}$  SIRT1 was obtained in the storage buffer (25 mM Tris-Cl, pH 7.5, 100 mM NaCl, 10 % glycerol and 1 mM TCEP) using a 1 cm path length quartz cuvette.

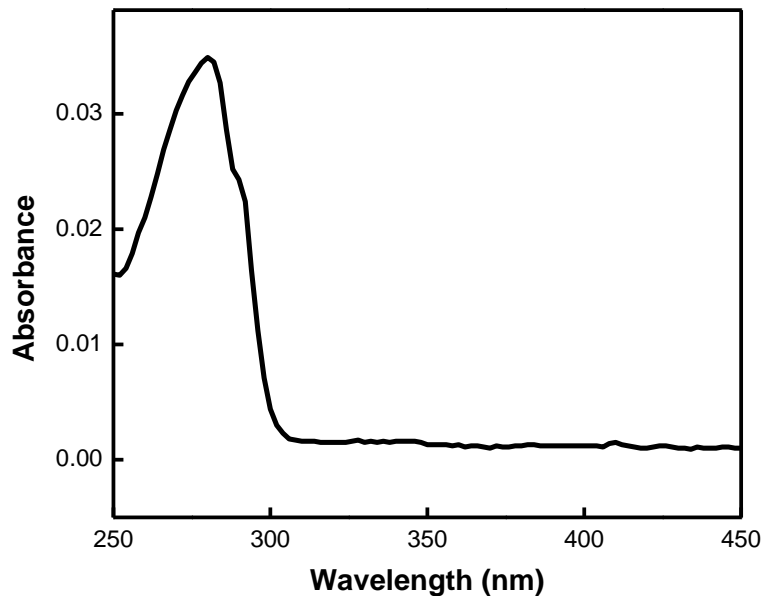


Figure 5.10. UV-visible spectrum of the recombinant human SIRT5. The spectrum was obtained using 1  $\mu$ M SIRT5 in the storage buffer (25 mM Tris-Cl, pH 7.5, 100 mM NaCl, 10 % glycerol and 1 mM TCEP).

### ***5.1.3.2. Circular dichroism (CD) spectral features in the far-UV region of recombinant human SIRT1 and SIRT5 variants***

In typical circular dichroism (CD) spectra of proteins, in the far-UV region are primarily contributed by their secondary structural features. In order to determine whether Y102A, R105I, and Y102A/R105I mutations in SIRT5 alter the secondary structural features of the wild-type SIRT5, the CD spectra of the native and mutant SIRT5 as well as SIRT1 were recorded. Figure 5.11 shows the changes in the mean residue ellipticities ( $\theta$ ) of the enzymes as a function of wavelength. Note that except for SIRT1, the wild-type and mutant SIRT5 enzymes exhibit double minima at 208 and 222 nm, which suggest the predominance of  $\alpha$  helices with minor (masked) contribution of  $\beta$  sheet structures. Although the elliptical features of both wild-type and mutant SIRT5 are qualitatively similar, there are noteworthy differences in the shapes as well as the amplitudes of the elliptical peaks among the above enzymes. Such differences are more

apparent with SIRT5 containing the R105 mutation. In contrast, the CD spectrum of SIRT1 is dominated by the random coil structural features, presumably due to its extended N-terminal and C-terminal segments which are not highly organized.

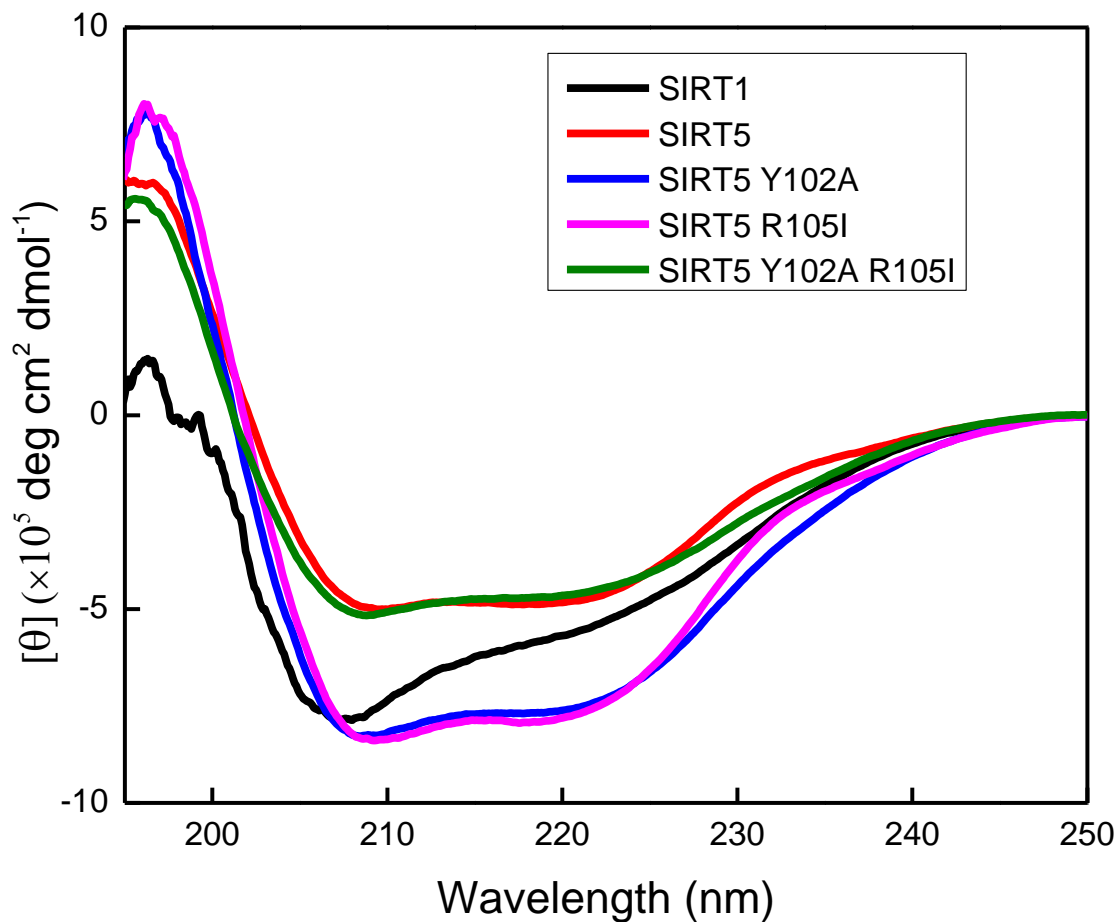


Figure 5.11. CD spectra of SIRT1 and SIRT5 variants. The mean residue ellipticities of 10  $\mu$ M enzymes as a function of wavelength are shown. The experiments were performed using a quartz cuvette of 1 mm path length in 5 mM Tris-HCl buffer, pH 7.5, containing 0.5 % glycerol, 5 mM TCEP and 15 mM KCl.

### 5.1.3.3. Steady state fluorescence spectra of recombinant human SIRT1 and SIRT5

In proteins, three aromatic amino acids, phenylalanine, tyrosine and tryptophan, contribute to the intrinsic fluorescence. Although both tryptophan and tyrosine residues could be



excited at 280 nm to obtain their fluorescence spectra, tryptophan exhibits marked selectivity when excited at 295-305 nm. Emission spectra, anisotropy, and quenching of tryptophan residues in proteins are frequently utilized to investigate their structural-functional features. For instance, changes in the protein fluorescence upon binding of ligands have been widely used to study ligand-protein interactions (259). Unfortunately, prior to this study, no fluorescence studies to discern the ligand-induced conformational changes in SIRT1 and SIRT5 had been performed. To determine signals that could be utilized for the characterization of recombinant sirtuins, the intrinsic fluorescence properties of the enzymes were investigated. The recombinant form of human SIRT1 (193-747) possesses two tryptophan (W232 and W624) and twelve tyrosine (Y280, Y301, Y317, Y343, Y376, Y428, Y497, Y523, Y650, Y642, Y658, Y699 and Y742) residues. However, of two available crystal structures of truncated SIRT1, none of the above tryptophan residues are present, and thus their precise locations as well as microenvironments are unclear. Figure 5.12 is the ribbon diagram of SIRT1 catalytic core (residues 241-516) showing seven tyrosine residues. The steady-state fluorescence emission spectrum of SIRT1 was obtained by setting the excitation monochromator at 280 nm, and scanning the emission profile from 320 to 500 nm (Figure 5.13). Note that the spectrum exhibits a maximum at 337 nm. SIRT5 harbors five tyrosine (Y76, Y102, Y104, Y176 and Y255) and four tryptophan residues (W77, W80, W99, and W222). In view of the structural data, all of the four tryptophan residues are present in the small domain and appear to be buried in the interior core of the enzyme. Figure 5.15 shows the steady-state fluorescence emission spectrum of SIRT5, obtained by setting the excitation monochromator at 295 nm, and scanning the emission profile from 320 to 500 nm. The fluorescence spectrum has the emission maximum at nearly 334 nm. Based on

these spectral features, it is apparent that the tryptophan residues of SIRT1 are present in more hydrophilic environment than those of SIRT5.

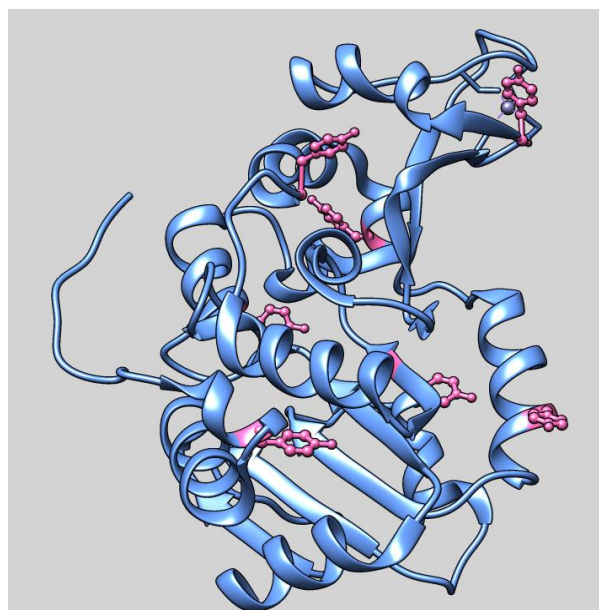


Figure 5.12. Ribbon Diagram of SIRT1 Catalytic Core Showing Seven Tyrosine Residues (Pink).

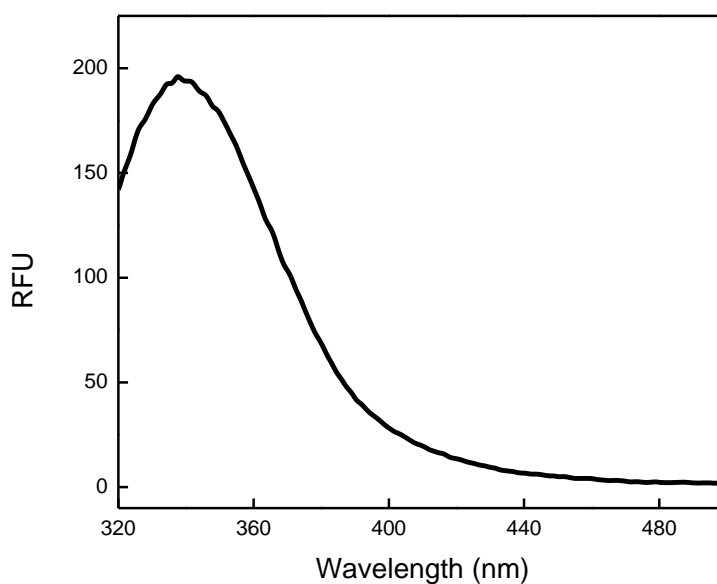


Figure 5.13. Steady-state fluorescence emission spectra (black color traces) of 1 μM SIRT1 in 25 mM Tris-Cl, pH 7.5, 100 mM NaCl, 10 % glycerol and 1 mM TCEP) upon excitation at 280 nm.

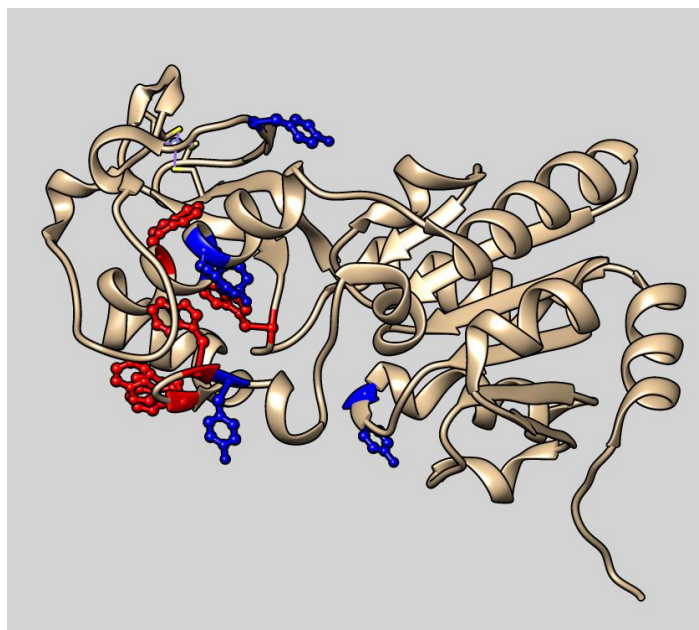


Figure 5.14. Ribbon diagram of SIRT5 showing the tryptophan (red) and tyrosine residues (blue).

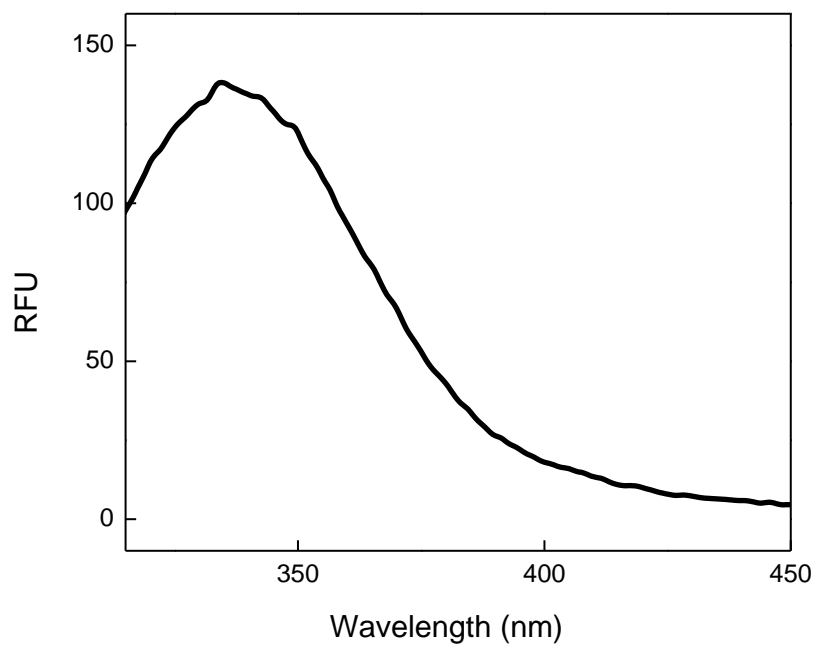


Figure 5.15. Steady-state fluorescence emission spectra of 1  $\mu$ M SIRT5 in 25 mM Tris-Cl, pH 7.5, 100 mM NaCl, 10 % glycerol and 1 mM TCEP) upon excitation at 280 nm.

#### 5.1.3.4. Fluorescence lifetimes of SIRT1 and SIRT5

In addition to the steady-state emission properties of SIRT1 and SIRT5, the fluorescence lifetime properties of the tryptophan residues in both SIRT1 and SIRT5 were investigated. The time-resolved fluorescence spectroscopy sheds light on the ligand induced conformation changes in the protein structures (260). Notably, the above measurement is free from any inner filter effect often encountered in the steady state fluorescence spectroscopic measurements.

To determine the lifetime of tryptophan residues in SIRT1 and SIRT5, the fluorescence lifetime decay curves of the enzymes were recorded ( $\lambda_{\text{ex}} = 280 \text{ nm}$ ,  $\lambda_{\text{em}} = 340 \text{ nm}$  for SIRT1, and  $\lambda_{\text{ex}} = 280 \text{ nm}$ ,  $\lambda_{\text{em}} = 336 \text{ nm}$  for SIRT5). Figure 5.15 shows the tryptophan fluorescence decay curve of SIRT1 in 25 mM Tris-Cl, pH 7.5, 100 mM NaCl, 10 % glycerol and 1 mM TCEP. The solid smooth lines are the best fit of the data for the double exponential rate equation with short ( $\tau_1$ ) and long ( $\tau_2$ ) lifetimes of 0.95 ns and 4.13 ns, respectively. The associated amplitudes of the two lifetimes are 11 and 89 fluorescence units, respectively. Figure 5.16 shows the tryptophan fluorescence decay curve of SIRT5 in the same buffer. The solid smooth lines are the best fit of the data for the double exponential rate equation with short ( $\tau_1$ ) and long ( $\tau_2$ ) lifetimes of 0.78 ns and 4.09 ns, and their associated amplitude of 34 and 66 fluorescence units, respectively. A comparative account of the above lifetimes of SIRT1 versus SIRT5 further reveals that the tryptophan residues of the enzyme are confined in different microenvironments.

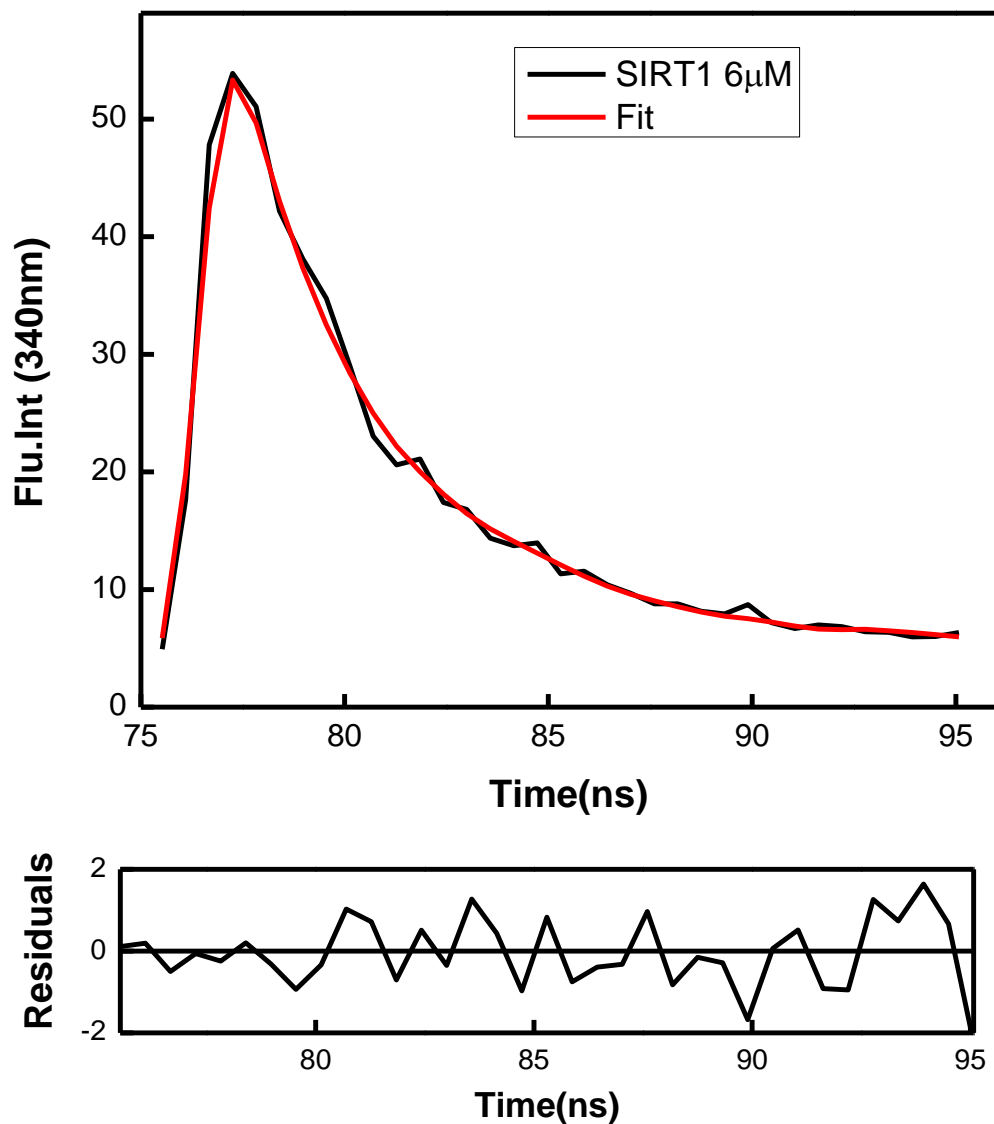


Figure 5.16. Fluorescence lifetime decay of SIRT1. The fluorescence lifetime decay profile of 6  $\mu\text{M}$  SIRT1 ( $\lambda_{\text{ex}} = 280 \text{ nm}$ ,  $\lambda_{\text{em}} = 340 \text{ nm}$ ) in 25 mM Tris-Cl, pH 7.5, 100 mM NaCl, 10 % glycerol and 1 mM TCEP. The solid smooth lines are the best fit of the data for the double exponential rate equation with short ( $\tau_1$ ) and long ( $\tau_2$ ) lifetimes of 0.95 ns (fixed) and  $4.13 \pm 0.23$  ns, respectively. The bottom panel shows the residuals of the fit of the lifetime trace.

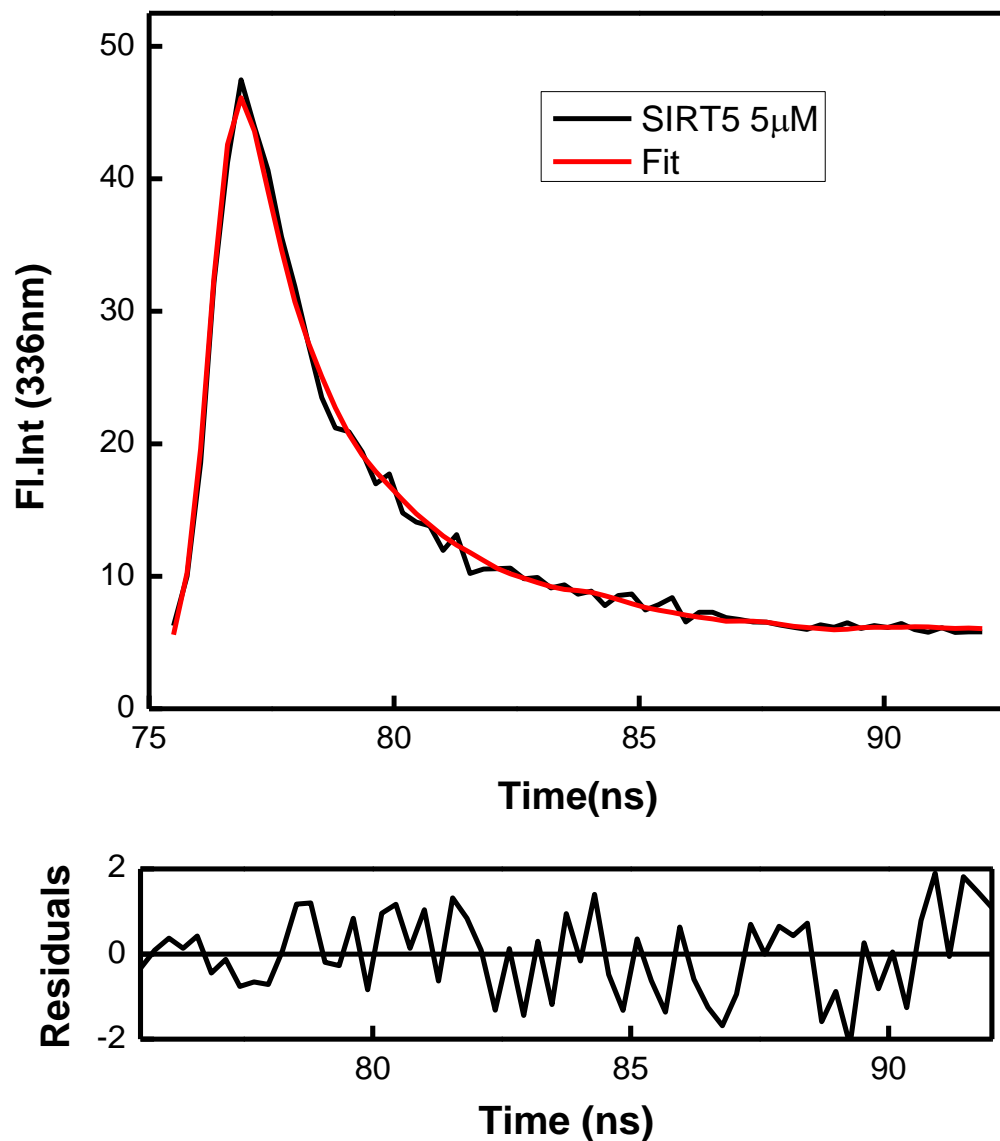


Figure 5.17. Fluorescence lifetime decay of SIRT5. The fluorescence lifetime decay profile of 5  $\mu\text{M}$  SIRT5 ( $\lambda_{\text{ex}} = 280 \text{ nm}$ ,  $\lambda_{\text{em}} = 336 \text{ nm}$ ) in 25 mM Tris-Cl, pH 7.5, 100 mM NaCl, 10 % glycerol and 1 mM TCEP. The solid smooth lines are the best fit of the data for the double exponential rate equation with short ( $\tau_1$ ) and long ( $\tau_2$ ) lifetimes of  $0.51 \pm 0.09 \text{ ns}$  and 3.05 ns (fixed value), respectively. The bottom panel shows the residuals of the fit of the lifetime trace.

## 5.2. Steady-state Kinetics of SIRT1 and SIRT5 Variants

It has been noted that except for SIRT6, most of the sirtuin catalyzed reactions follow a compulsory order mechanism, involving the binding of acylated substrates followed by the binding of NAD<sup>+</sup> (33, 261, 262). To ascertain the influence of mutations on the kinetic parameters of the enzyme catalyzed reaction, steady-state kinetic studies were performed on SIRT1 and SIRT5.

### 5.2.1. Trypsin coupled enzyme reaction of sirtuins

As elaborated in section § 1.8, several *in vitro* enzyme assays for sirtuins have been developed to determine the steady-state rates of the enzyme catalyzed reactions. Since the determination of the steady-state kinetic parameters of enzyme catalyzed reactions requires precise measurements of the initial rates of the enzyme catalysis, the trypsin coupled continuous assay system (250) was employed using acetylated-Lys (*Fluor-de-lys*<sup>®</sup>) and succinylated-Lys (Ac-Suclys)-AMC conjugates as the substrates for the deacetylation and descuccinylation reactions, respectively. While the former substrate was obtained commercially, we synthesized the succinylated substrate (Ac-Suclys-AMC) according to the procedure described by Madsen et al. (263).

In the sirtuin catalyzed assay system, trypsin cleaves the lysine-coumarin bond during the deacylation reaction, resulting in a time dependent increase in fluorescence. In order to optimize the signal to noise ratio of the overall reaction traces of the trypsin coupled sirtuin catalysis, the excitation and emission wavelengths were fine tuned. In that pursuit, the excitation and emission spectra of the substrate and the final product of the trypsin-coupled enzyme assay were obtained. As shown in Figure 5.18, these spectra have a significant overlapping region. In order to reduce the inner filter effect produced by high concentration of *Fluor-de-lys*<sup>®</sup> (150  $\mu$ M), used in sirtuin

activity measurement while obtaining reasonable signal of the product, the excitation and emission wavelengths were determined as being equal to 360 nm and 460 nm, respectively. The excitation and the emission spectra of Fluoro-de-Lys<sup>®</sup> substrate and the final product of the trypsin-coupled assay have minimal overlap at the above wavelengths (Figure 5.18), and thus eliminates any spectroscopic artifacts during the fluorescence based enzymatic assay.

The enzymatic assay conditions were optimized at different experimental settings on the microplate reader (SpectraMax Gemini, Molecular Devices). Figure 5.20 shows the representative time courses of the SIRT5 catalyzed reaction in the presence 100  $\mu$ M Ac-Suclys-AMC substrate, 50  $\mu$ M NAD<sup>+</sup>, 0.8  $\mu$ M enzyme, and increasing concentrations of trypsin. Since trypsin also degrades (albeit slowly) the enzyme protein, the assay condition was optimized (with respect to the trypsin concentration) such that the initial rate of the enzyme catalyzed reaction could be reliably determined (264). Note that at low concentration of trypsin (0.4  $\mu$ M; Figure 5.20.), the reaction proceeds with a finite lag phase. As the concentration of trypsin increases, the amplitude of the lag phase decreases and the initial steady-state rate reaches its maximum value at 0.8  $\mu$ M trypsin (Figure 5.20, trace 4). Further increase in trypsin concentration to 0.9  $\mu$ M did not affect the initial rate of the enzyme catalysis (Figure 5.20, trace 5) but slightly shortened the steady-state phase, suggesting that 0.8  $\mu$ M trypsin was adequate to satisfy the coupled reaction system. In the presence of latter concentration of trypsin, the steady-state rates could be reliably determined at time regimes significantly higher than those of the preceding lag phases as elaborated by Cleland (264). Since the objective had been to delineate the contributions of Y102 and R105 residues of SIRT5 in substrate selectivity, the acylated lysine-coumarin conjugates were chosen as the fluorogenic substrates instead of using physiologically relevant peptide substrates.



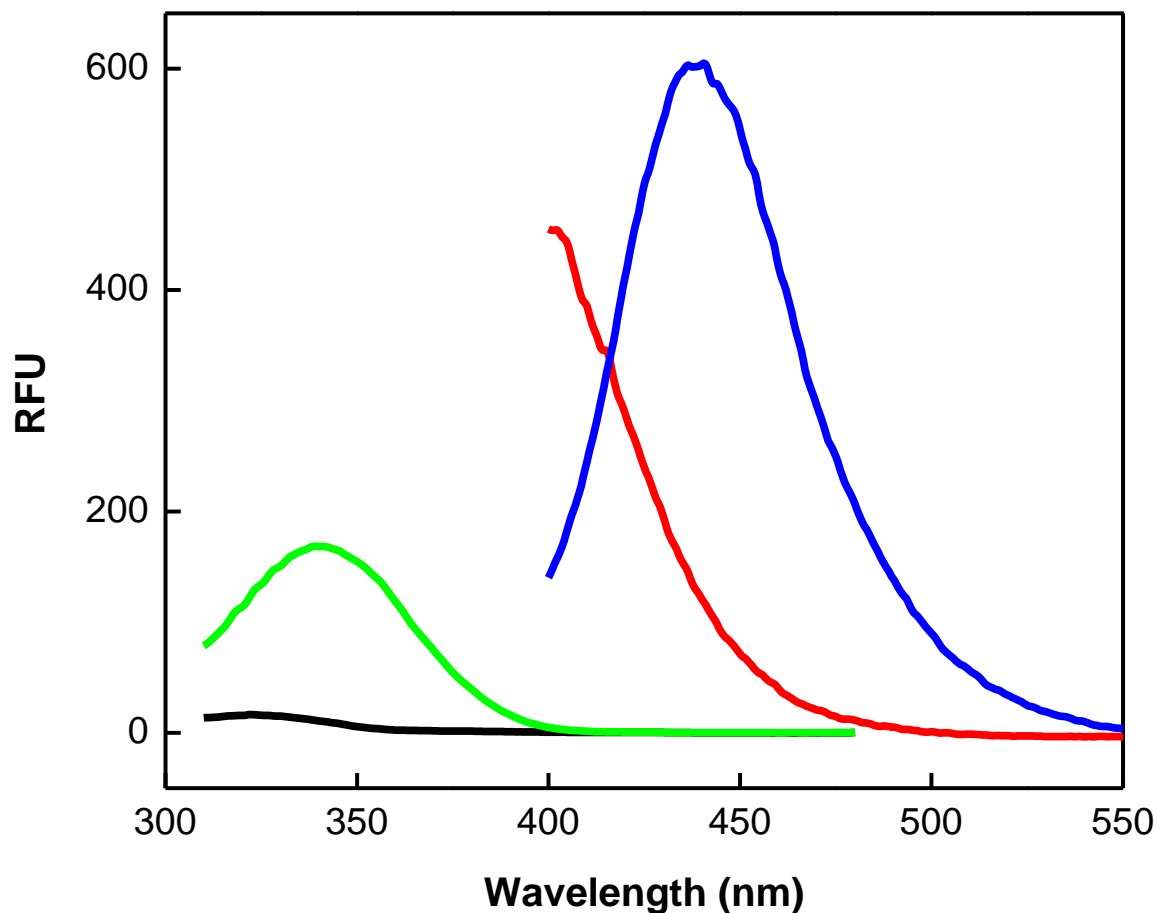


Figure 5.18. The excitation and the emission spectra of the fluorogenic substrate (Fluoro-de-Lys<sup>®</sup>) and the final product of the trypsin-coupled assay. The excitation spectra were obtained at the emission wavelength of 500 nm. To obtain the emission spectra, the fluorophores were excited at 365 nm. Due to significant overlap in the excitation and the emission spectra of the substrate and the product, the specific wavelengths i.e.,  $\lambda_{\text{ex}} = 360 \text{ nm}$ ,  $\lambda_{\text{em}} = 460 \text{ nm}$ , were chosen where the interference from the substrate was minimal, significantly reducing the inner filter effect.

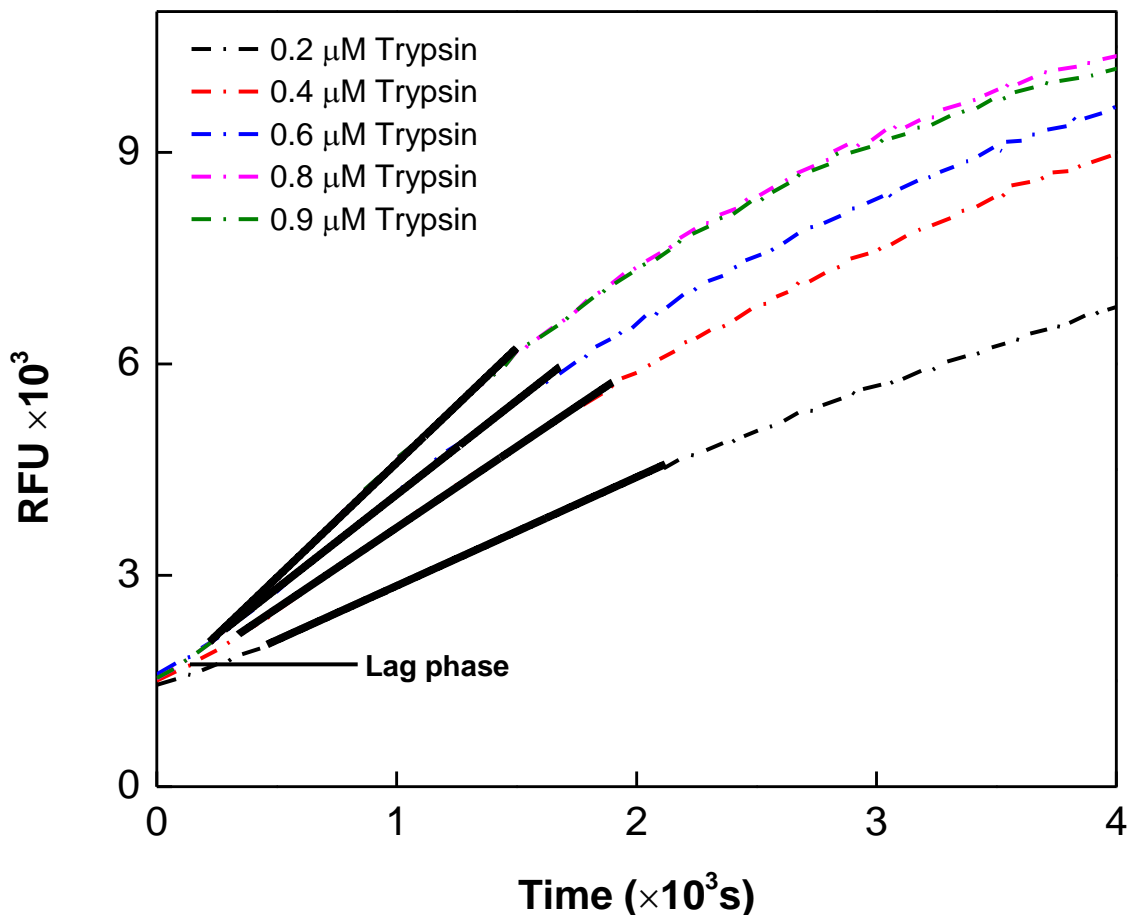


Figure 5.19. Real-time progress curve for SIRT5-catalyzed desuccinylation reaction. The time courses of the SIRT5 catalyzed reaction using the fixed concentrations of Ac-Suclys-AMC substrate and  $\text{NAD}^+$ , and varying concentrations of trypsin as the coupling enzyme are shown. The dashed curves represent the time dependent increase in fluorescence at 460 nm ( $\lambda_{\text{ex}} = 350$  nm) due to release of 7-hydroxyl-4-methylcoumarin (AMC) from the substrate after the cleavage of trypsin. The solid lines indicate the linear regression analysis of the data after the initial lag phases.

### 5.2.2. Bisubstrate kinetic studies of the wild-type and mutant sirtuin catalyzed reactions

It has been widely accepted that sirtuin catalyzed reactions follow a sequential mechanism in which the acetylated peptide binds first followed by the binding of  $\text{NAD}^+$  to generate the enzyme-substrate- $\text{NAD}^+$  ternary complex, which undergoes the chemical transformation reaction to produce the reaction products (261). In order to determine the kinetic

parameters for the deacetylation/desuccinylation reactions catalyzed by the wild-type and mutant enzymes (SIRT1, SIRT5, SIRT5 Y102A, SIRT5 R105I, SIRT5 Y102A/R105I), the initial velocities of the wild-type and mutant enzyme catalyzed reactions were determined with increasing concentrations of *Fluor-de-lys*<sup>®</sup> and Ac-Suclys-AMC substrates and changing fixed concentrations of NAD<sup>+</sup>. To determine the  $k_{\text{cat}}$  values of sirtuins, their corresponding  $V_{\text{max}}$  values (obtained as relative fluorescence unit, RFU, per second from the trypsin-coupled assays) were converted to the concentration units and divided by the enzyme concentrations. The raw initial rates (RFU/s) were converted to  $\mu\text{M/s}$  by measuring the increase in fluorescence of the reaction products (either AMC or the fluorophore of the *Fluor-de-lys*<sup>®</sup> substrate) of the sirtuin assays as function of the fluorophore concentration. Note that the fluorophore *Fluor-de-lys*<sup>®</sup> of was prepared by treatment of *Fluor-de-lys*<sup>®</sup> deacetylated standard (available from the Enzo Life Sciences) with 100  $\mu\text{M}$  of trypsin for 10 minutes. Figure 5.21 shows the kinetic data for the SIRT5 catalyzed reaction as a function of Ac-Suclys-AMC substrate and NAD<sup>+</sup> concentrations. Since all sirtuin (with exception of SIRT6) catalyzed reactions conform to the bi-substrate compulsory order mechanism (261), the product inhibition studies were not performed to substantiate the above mechanism. Instead, we analyzed the data of Figure 5.6 by the ternary complex kinetic mechanism (Eq 4.4 in section §4.3.2). The solid smooth lines are the best fit of the data for the  $K_{\text{m,sub}}$  and  $K_{\text{m,NAD}}$  values as being equal to  $290 \pm 29 \mu\text{M}$  and  $69 \pm 9 \mu\text{M}$ , respectively. The  $k_{\text{cat}}$  value of the enzyme was determined to be  $(3.83 \pm 0.38) \times 10^{-3} \text{ s}^{-1}$ . Similar studies were performed with Y102A, R105I, and Y102A/R105I double mutants of SIRT5 as well as with wild-type SIRT1 using both *Fluor-de-lys*<sup>®</sup> and Ac-Suclys-AMC substrates, and determined their  $K_{\text{m}}$  and  $k_{\text{cat}}$  values. It should be pointed out that although other groups (228, 257) have created mutations in the R105 residue of SIRT5 (to either Met or Leu) to assess its role in

modulating the substrate specificity and nicotinamide inhibition of the enzyme, no systematic studies on the influences of Y102 and R105 mutations in SIRT5 (to mimic the amino acid residues found in SIRT1) on the structural-functional features of the enzymes have been performed prior to our studies presented herein. These data are shown in Figures 5.22 to 5.25, and the derived parameters are summarized in Table 5.1. Consistent with the previous reports (106, 265), SIRT1 possesses strong deacetylase activity with  $K_{m,sub} = 356 \pm 56 \mu\text{M}$  and  $K_{m,NAD} = 388 \pm 73 \mu\text{M}$ , respectively, but no detectable desuccinylase activity. On the other hand, SIRT5 showed a strong desuccinylase activity but only weak deacetylase activity, which could not be further pursued to determine its  $K_m$  and  $k_{cat}$  values. The data of Table 5.1 unravels the fact that the  $K_{m,NAD}$  for SIRT5 of desuccinylase reaction ( $69 \mu\text{M}$ ) is about 5 fold lower than that obtained for the SIRT1 catalyzed deacetylation reaction. It should be pointed out that Madsen et al. reported the  $K_{m,NAD}$  for SIRT5 reaction using the same succinylated substrate as being equal to  $150 \pm 45 \mu\text{M}$  (250). But since the above authors used only a fixed substrate concentration, the  $K_{m,NAD}$  can, at the best, be taken as its apparent value. To our further interest, we noted that Y102A mutation exhibits both deacetylase and desuccinylase activity with comparable efficiency. On the other hand, both R105I and R015/Y102A mutant enzymes were devoid of the desuccinylase activity but both these enzymes exhibited the deacetylase activity. Upon quantitative comparison, the  $K_{m,NAD}$  for SIRT5 Y102A mutant was about 5 fold higher than that for the wild-type enzyme in case of the desuccinylation reaction, but the above discrepancy was about 20 fold in case of the deacetylase reaction. Clearly, the  $K_{m,NAD}$  is considerably higher when SIRT5 catalyzes the deacetylation versus the desuccinylation reaction. It is further noteworthy that R105I and Y102A/R105I double mutants of SIRT5 exhibit higher deacetylase activity, with  $k_{cat}$  values of  $(12.2 \pm 1.0) \times 10^{-5} \text{ s}^{-1}$ , and  $(2.6 \pm 0.1) \times 10^{-5} \text{ s}^{-1}$ , respectively, than that

determined for the Y102A mutant enzyme. Although Y102A/R105I double mutant of SIRT5 mimics the active site pocket of SIRT1, the  $K_{m,sub}$  for the double mutant ( $388 \pm 12 \mu\text{M}$ ) is comparable to that obtained for SIRT1 ( $356 \pm 56 \mu\text{M}$ ), but the  $k_{cat}$  value of the former enzyme ( $(2.6 \pm 0.1) \times 10^{-5} \text{ s}^{-1}$ ) was about 22 fold lower than that obtained for the latter enzyme ( $(5.8 \pm 0.9) \times 10^{-4} \text{ s}^{-1}$ ). Hence, the specificity constant ( $k_{cat}/K_m$ ) of Y102A/R105I double mutant SIRT5 is about 40 fold lower than that of SIRT5, suggesting that the Y102 and R105 are not exclusive determinant of the substrate specificity between SIRT1 and SIRT5. A cumulative account of these steady-state kinetic data leads to the conclusion that there is a mutual cooperation between Y102 and R105 residues in modulating the deacetylase versus desuccinylase activity of SIRT5.

Table 5.1. Steady-state kinetic parameters of SIRT5 variants and SIRT1 on acetyl and succinyl substrates

		$K_{m,sub}$ ( $\mu\text{M}$ )	$K_{m,NAD}$ ( $\mu\text{M}$ )	$k_{cat}$ ( $\times 10^{-5} \text{ s}^{-1}$ )	$k_{cat}/K_m$ ( $\text{M}^{-1} \text{ s}^{-1}$ )
SIRT5	deacetylation	ND <sup>a</sup>	ND <sup>a</sup>	ND <sup>a</sup>	0.006
	desuccinylation	$290 \pm 29$	$69 \pm 9$	$383.2 \pm 38.3$	13.207
SIRT5 Y102A	deacetylation	$720 \pm 144$	$1605 \pm 321$	$6.6 \pm 1.3$	0.091
	desuccinylation	$300 \pm 54$	$321 \pm 49$	$27.4 \pm 4.9$	0.409
SIRT5 R105I	deacetylation	$1658 \pm 140$	$609 \pm 120$	$12.2 \pm 1.0$	0.073
	desuccinylation	ND <sup>a</sup>	ND <sup>a</sup>	ND <sup>a</sup>	0.006
SIRT5 Y102A R105I	deacetylation	$388 \pm 12$	$1194 \pm 667$	$2.6 \pm 0.1$	0.065
	desuccinylation	N/A	N/A	N/A	0.002
SIRT1	deacetylation	$356 \pm 56$	$388 \pm 73$	$57.9 \pm 9.1$	1.626
	desuccinylation	NA <sup>b</sup>	NA <sup>b</sup>	NA <sup>b</sup>	NA <sup>b</sup>

<sup>a</sup>  $K_m$  and  $k_{cat}$  values could not be independently determined due to the experimental limitation of using high substrate concentration;  $k_{cat}/K_m$  was estimated from the linear first order region of the Michaelis-Menten plot at low concentrations of the substrates.

<sup>b</sup> N/A: no activity was observed.

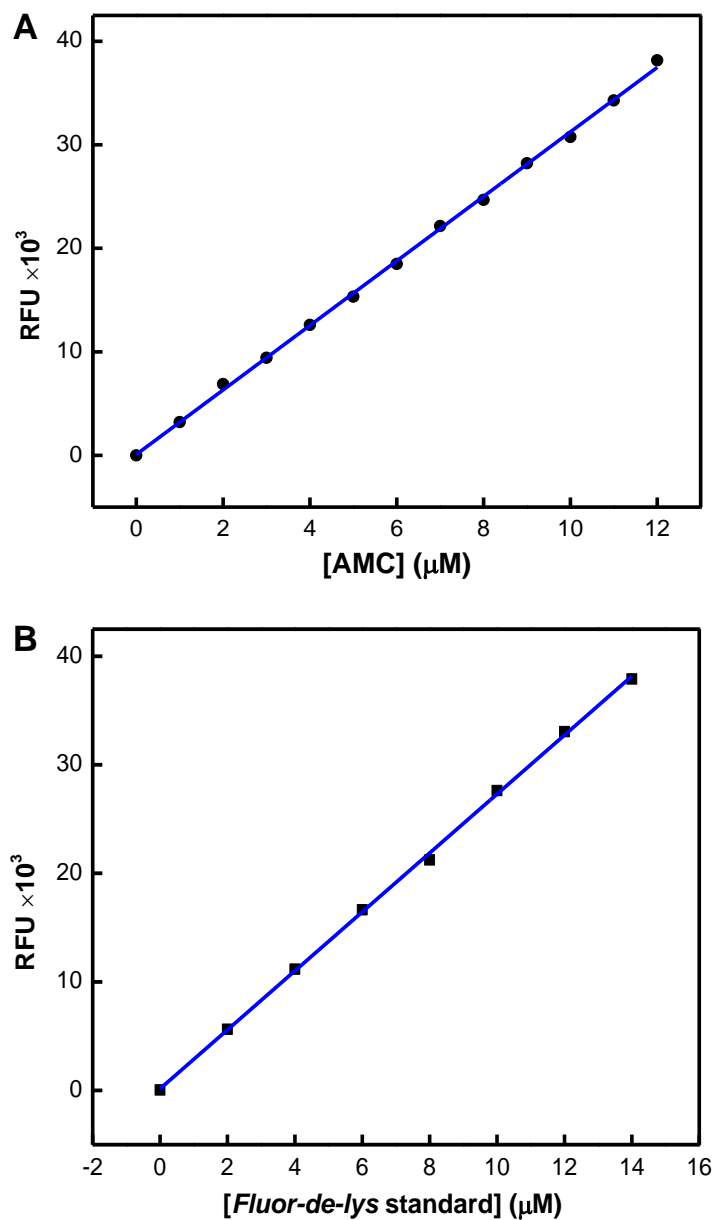


Figure 5.20. Standard plot the increase in fluorescence (RFU;  $\lambda_{\text{ex}} = 360 \text{ nm}$ ,  $\lambda_{\text{em}} = 460 \text{ nm}$ ) as a function of fluorophore concentration. (A) Standard plot for the assay using Ac-suclys-AMC as substrate. The fluorescence intensity was plotted against increasing concentration of AMC and the solid smooth line represents the linear fit of the data. (B) Standard plot for the assay using *Fluor-de-lys*<sup>®</sup> as substrate. The curve was prepared from the fluorescence end point reading of the known concentration of the fluorophore, which was generated upon the treatment of different concentrations of deacetylated standard with  $100 \mu\text{M}$  trypsin.

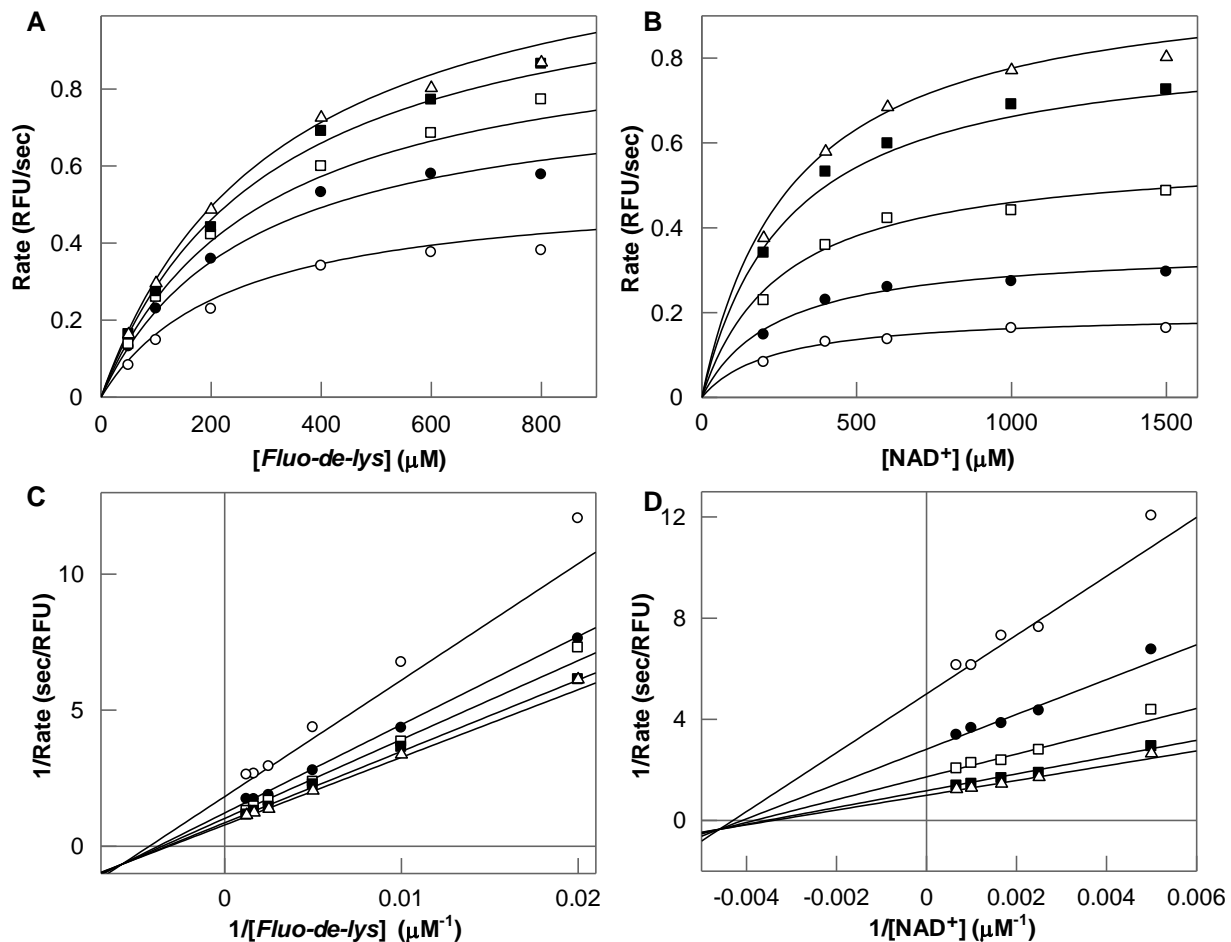


Figure 5.21. Two substrate reactions of SIRT1. The two substrate SIRT1 catalyzed reactions were performed under the steady-state conditions with varying concentrations of  $\text{NAD}^+$  (400, 600, 800, 1000, 1500 and 4000  $\mu\text{M}$ ) and *Fluo-de-lys*<sup>®</sup> substrate (100, 200, 400, 600, 800 and 1000  $\mu\text{M}$ ). The data were fitted to sequential mechanism using the Grafit software with varying concentration of *Fluo-de-lys*<sup>®</sup> substrate at various fixed concentration of  $\text{NAD}^+$  (A), and with varying concentration of  $\text{NAD}^+$  at various fixed concentration of *Fluo-de-lys*<sup>®</sup> substrate (B). The double-reciprocal plot of  $1/v$  vs  $1/[\text{NAD}^+]$  at increasing concentration of *Fluo-de-lys*<sup>®</sup> substrate (C), and the double-reciprocal plot of  $1/v$  vs  $1/[\text{Fluo-de-lys}]$  at increasing concentration of  $\text{NAD}^+$  (D) are also shown.

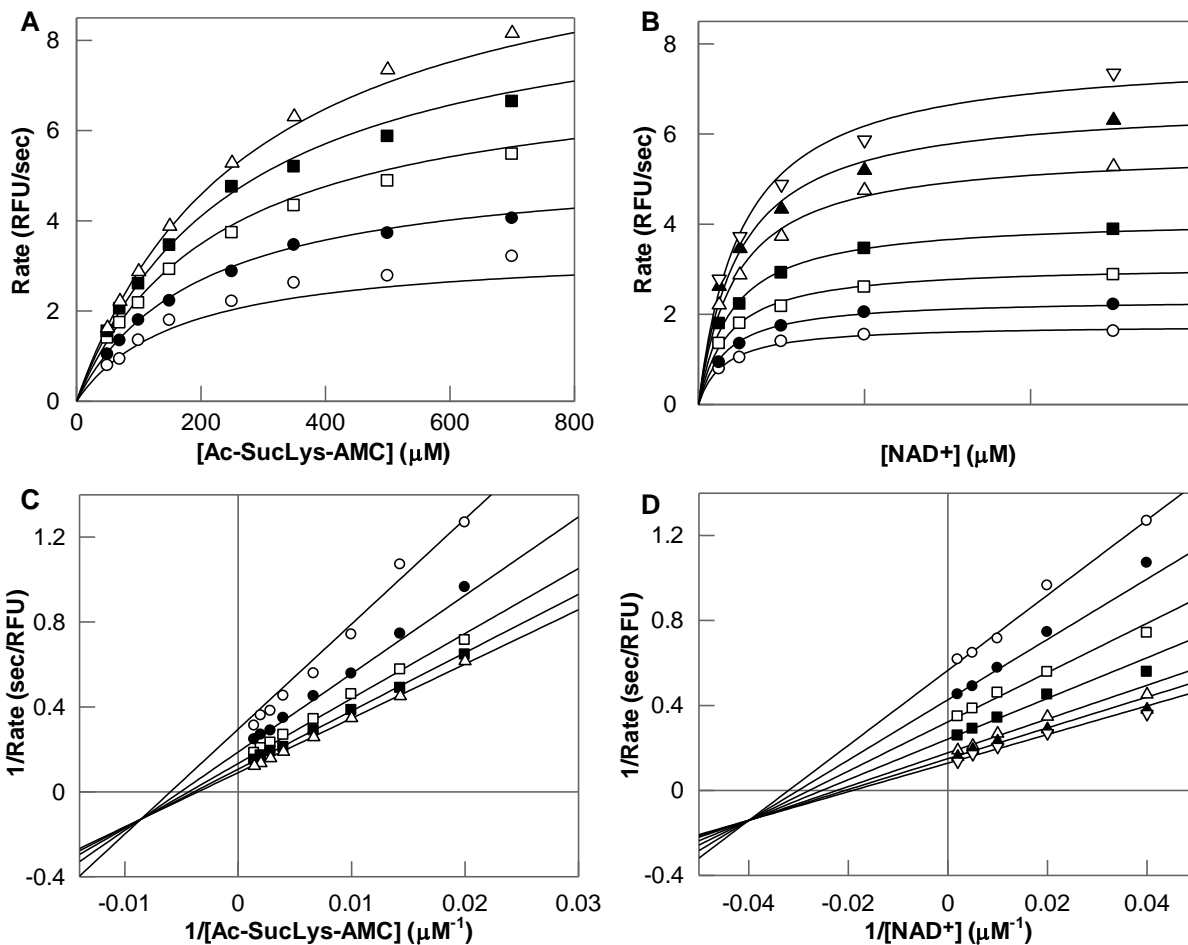


Figure 5.22. Two substrate reactions of SIRT5. The two substrate SIRT5 catalyzed reaction was performed under the steady-state condition with varying concentrations of Ac-SucLys-AMC substrate (25, 50, 100, 200, and 500 μM) and NAD<sup>+</sup> (50, 70, 100, 150, 250, 350, 500, and 700 μM). The data were fitted to the sequential kinetic mechanism for the binding of the substrate and NAD<sup>+</sup> using the Grafit software with varying concentration of Ac-SucLys-AMC substrate at various fixed concentration of NAD<sup>+</sup> (A), and with varying concentration of NAD<sup>+</sup> at various fixed concentration of Ac-SucLys-AMC substrate (B). The double-reciprocal plot of 1/v vs 1/[NAD<sup>+</sup>] at increasing concentration of Ac-SucLys-AMC substrate (C), and the double-reciprocal plot of 1/v vs 1/[Ac-SucLys-AMC] at increasing concentration of NAD<sup>+</sup> (D) are also shown.



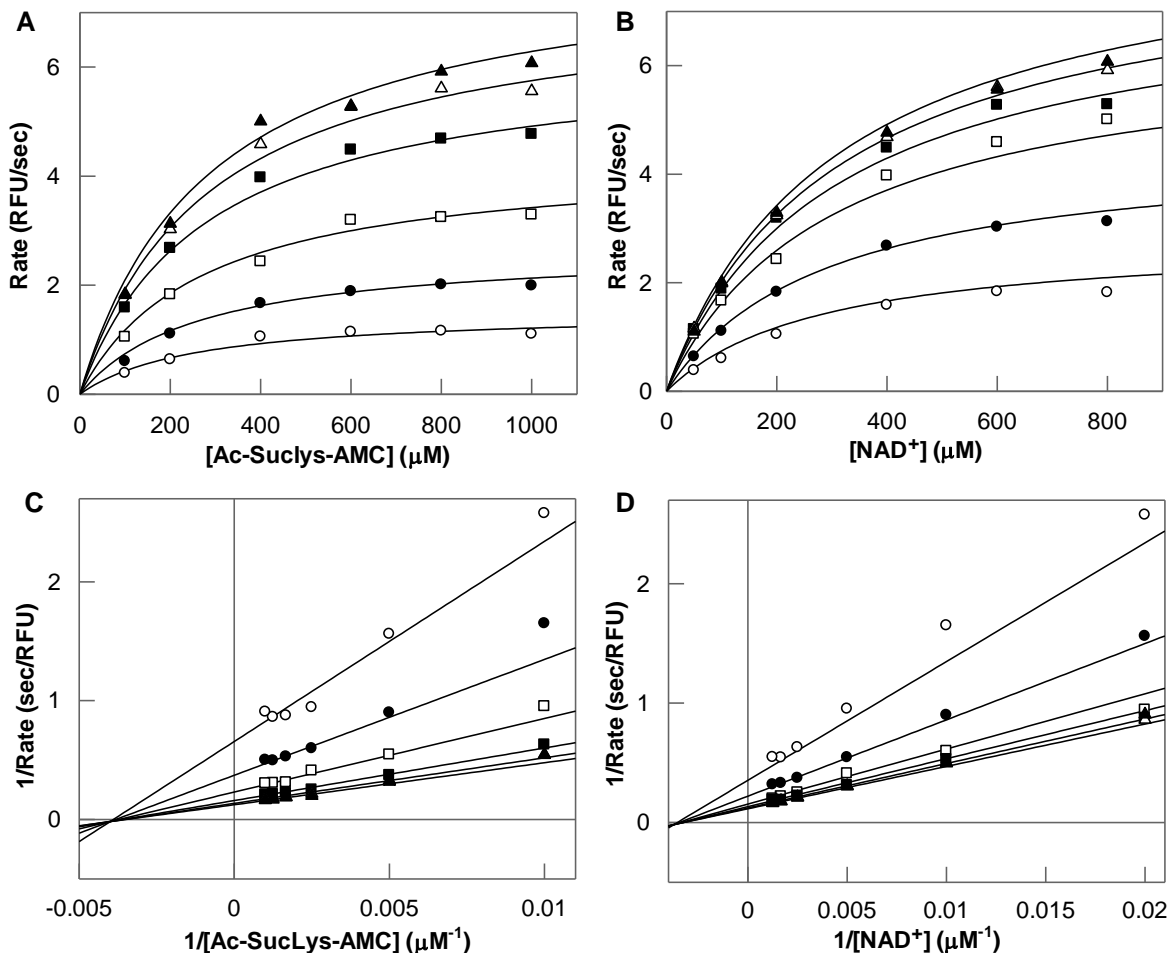


Figure 5.23. Two substrate sesuccinylation reactions of SIRT5 Y102A. The two substrate SIRT5 catalyzed reactions were performed under the steady-state conditions with varying concentrations of  $\text{NAD}^+$  (400, 600, 800, 1000, 1500 and 4000  $\mu\text{M}$ ) and Ac-SucLys-AMC substrate (100, 200, 400, 600, 800 and 1000  $\mu\text{M}$ ). The data were fitted to sequential mechanism using the Grafit software with varying concentration of Ac-SucLys-AMC substrate at various fixed concentration of  $\text{NAD}^+$  (A), and varying concentration of  $\text{NAD}^+$  at various fixed concentration of Ac-SucLys-AMC substrate (B). The double-reciprocal plot of  $1/v$  vs  $1/[\text{NAD}^+]$  at increasing concentration of Ac-SucLys-AMC substrate (C), and the double-reciprocal plot of  $1/v$  vs  $1/[\text{Ac-SucLys-AMC}]$  at increasing concentration of  $\text{NAD}^+$  (D) are also shown.

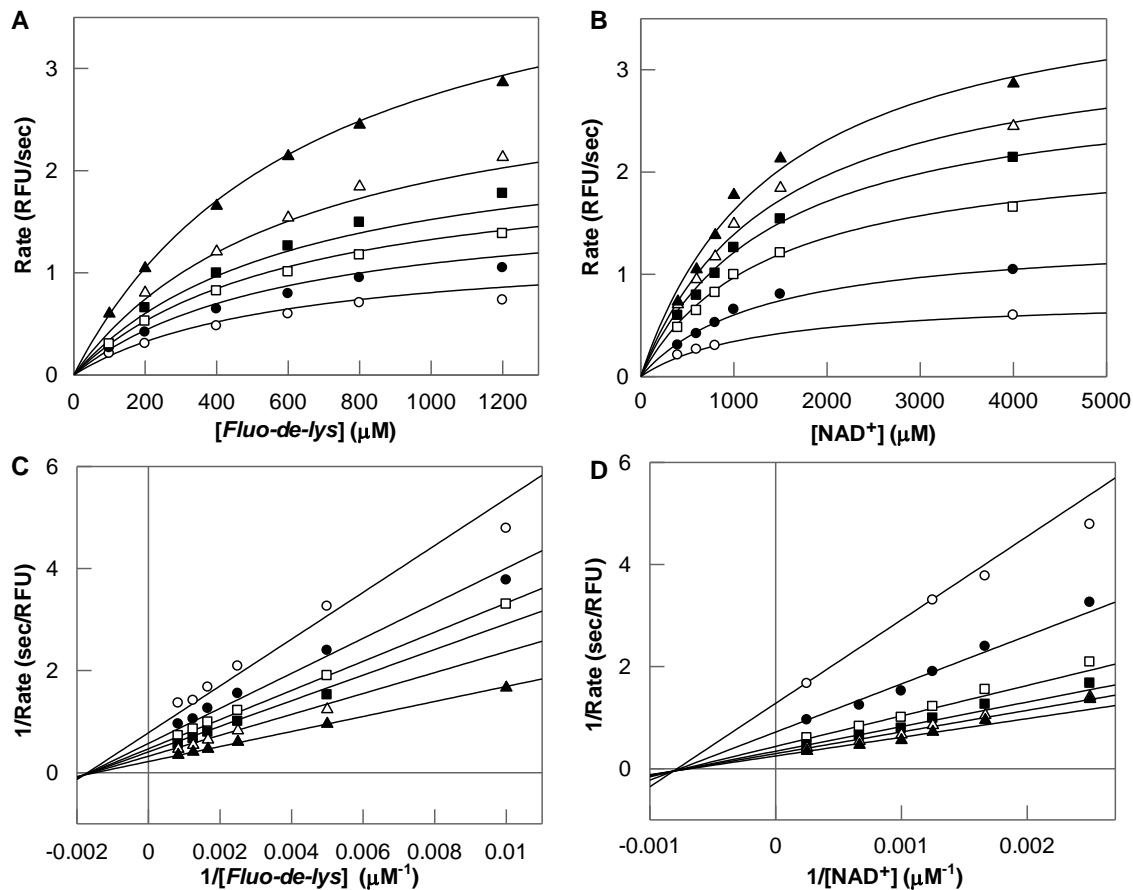


Figure 5.24. Two substrate deacetylation reactions of SIRT5 Y102A. The two substrate SIRT5 Y102A catalyzed reactions were performed under the steady-state conditions with varying concentrations of NAD<sup>+</sup> (400, 600, 800, 1000, 1500 and 4000 μM) and *Fluo-de-lys*<sup>®</sup> substrate (100, 200, 400, 600, 800 and 1200 μM). The data were fitted to sequential mechanism using the Grafit software with varying concentration of *Fluo-de-lys*<sup>®</sup> substrate at various fixed concentration of NAD<sup>+</sup> (A), and with varying concentration of NAD<sup>+</sup> at various fixed concentration of *Fluo-de-lys*<sup>®</sup> substrate (B). The double-reciprocal plot of 1/*v* vs 1/[NAD<sup>+</sup>] at increasing concentration of *Fluo-de-lys*<sup>®</sup> substrate (C), and the double-reciprocal plot of 1/*v* vs 1/[*Fluo-de-lys*] at increasing concentration of NAD<sup>+</sup> (D) are also shown.

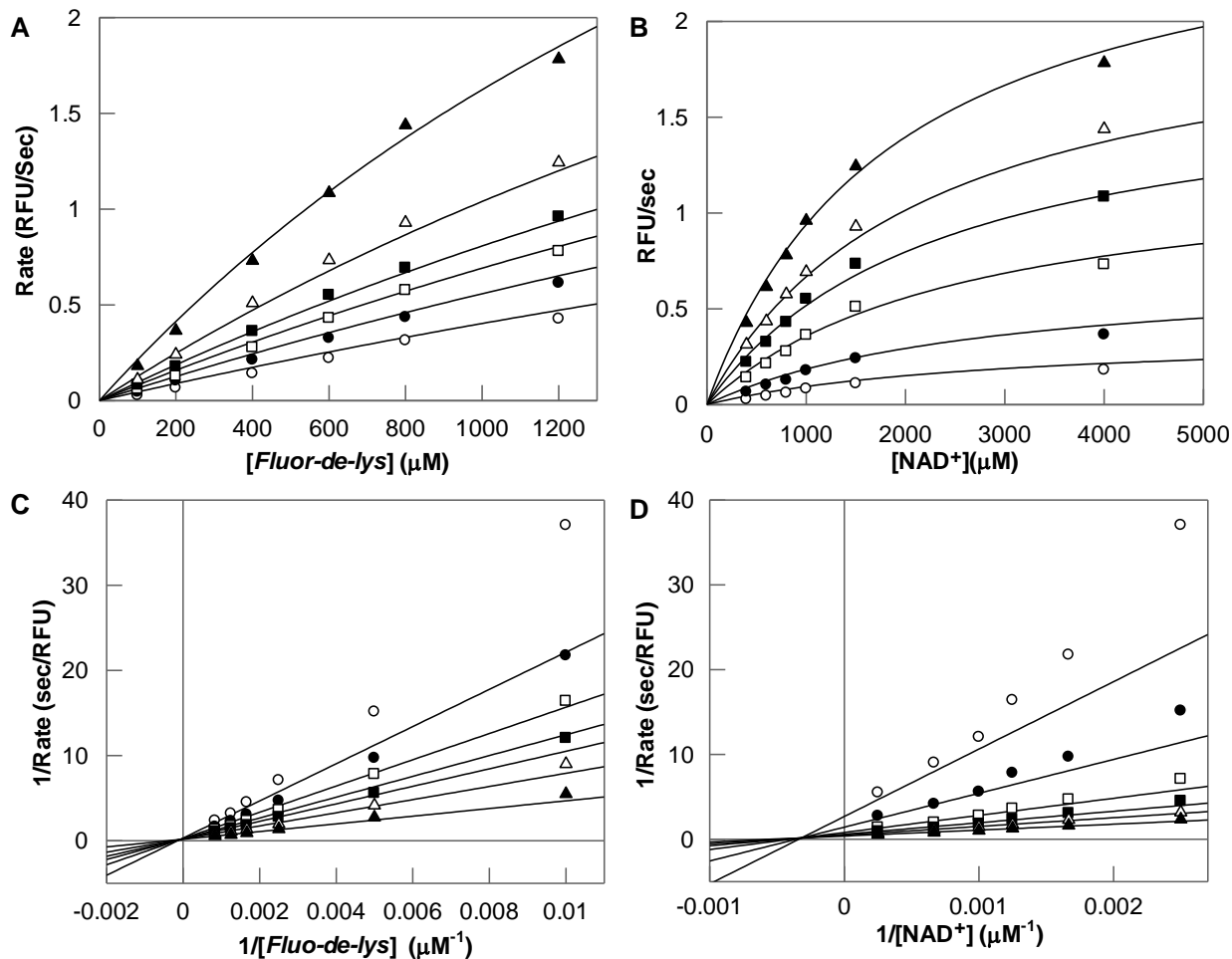


Figure 5.25. Two substrate reactions of SIRT5 R105I. The two substrate SIRT5 R105I catalyzed reactions were performed under the steady-state conditions with varying concentrations of  $\text{NAD}^+$  (400, 600, 800, 1000, 1500 and 4000  $\mu\text{M}$ ) and Fluor-de-lys® substrate (100, 200, 400, 600, 800 and 1200  $\mu\text{M}$ ). The data were fitted to sequential mechanism using the Grafit software with varying concentration of Fluor-de-lys® substrate at various fixed concentration of  $\text{NAD}^+$  (A), and with varying concentration of  $\text{NAD}^+$  at various fixed concentration of Fluor-de-lys® substrate (B). The double-reciprocal plot of  $1/v$  vs  $1/[\text{NAD}^+]$  at increasing concentration of Fluor-de-lys® substrate (C), and the double-reciprocal plot of  $1/v$  vs  $1/[\text{Fluor-de-lys}]$  at increasing concentration of  $\text{NAD}^+$  (D) are also shown.

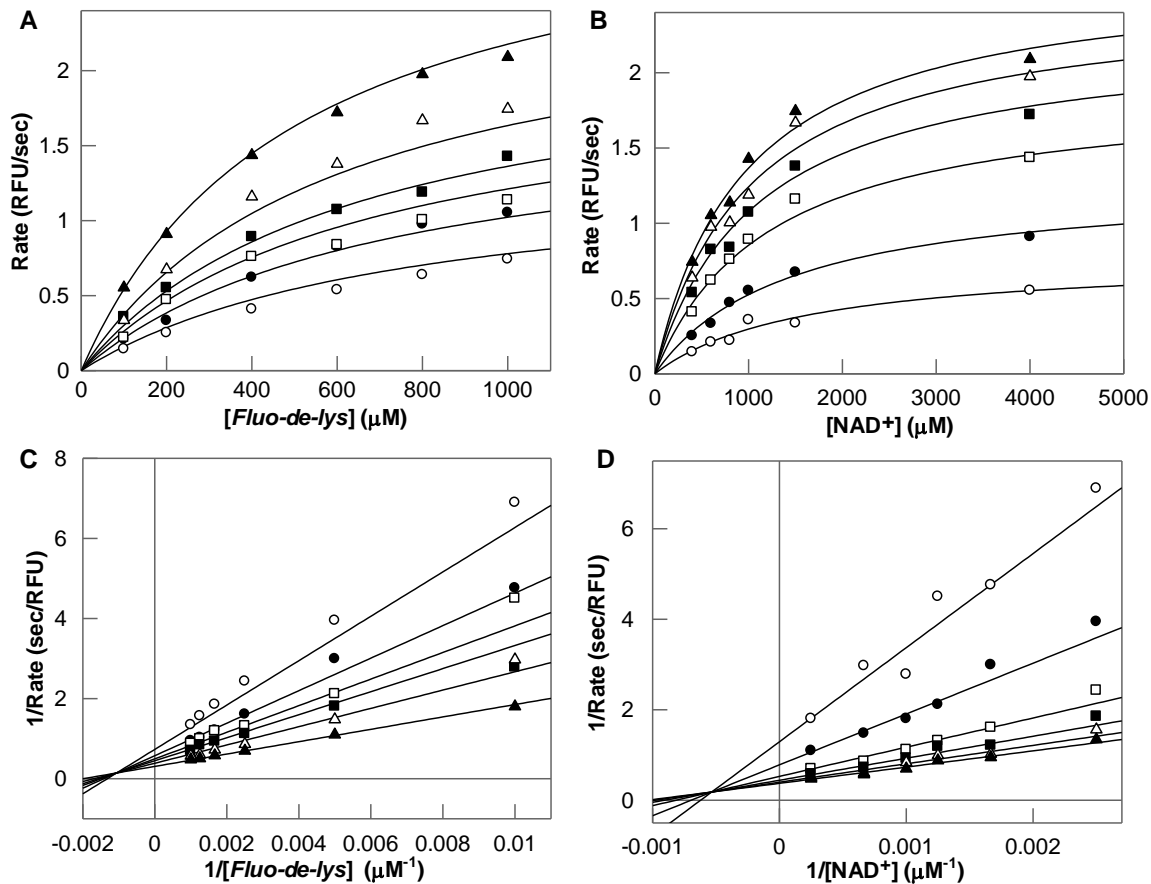


Figure 5.26. Two substrate reactions of SIRT5 Y102A/R105I. The two substrate SIRT5 Y102A/R105I catalyzed reactions were performed under the steady-state conditions with varying concentrations of NAD<sup>+</sup> (400, 600, 800, 1000, 1500 and 4000 μM) and *Fluo-de-lys*<sup>®</sup> substrate (100, 200, 400, 600, 800 and 1000 μM). The data were fitted to sequential mechanism using the Grafit software with varying concentration of *Fluo-de-lys*<sup>®</sup> substrate at various fixed concentration of NAD<sup>+</sup> (A), and with varying concentration of NAD<sup>+</sup> at various fixed concentration of *Fluo-de-lys*<sup>®</sup> substrate (B). The double-reciprocal plot of 1/v vs 1/[NAD<sup>+</sup>] at increasing concentration of *Fluo-de-lys*<sup>®</sup> substrate (C), and the double-reciprocal plot of 1/v vs 1/[*Fluo-de-lys*] at increasing concentration of NAD<sup>+</sup> (D) are also shown.

### 5.3. Inhibition Studies of SIRT1 and SIRT5 Variants

#### 5.3.1. Screening of inhibitors of SIRT1 and SIRT5

As elaborated in section §1.7, modulation of sirtuin activities have beneficial effects on several human diseases. For example, combined use of nicotinamide and pan type I/II HDAC (zinc-dependent histone deacetylases) inhibitors produced encouraging results in a recent B-cell

lymphoma phase I clinical trial, validating sirtuins as antilymphoma drug targets (266). However, most known sirtuin inhibitors are either poorly potent, or suffer from poor physiochemical properties. Hence, there is an urgent need to develop novel sirtuin inhibitors/activators as therapeutic agents. In a preliminary attempt to identify compounds with pharmaceutical potential, various small organic compounds were tested for their inhibition/activation potencies against SIRT1 and SIRT5. The screening of in house as well as commercially available compounds (10  $\mu$ M) was performed in a 96-well format via the trypsin-coupled assay using a microplate reader (SpectraMax Gemini, Molecular Devices) using 10  $\mu$ M of the effector. While SIRT1 catalyzed deacetylation reaction was monitored in the presence of 100  $\mu$ M *Fluor-de-lys*<sup>®</sup> substrate 500  $\mu$ M NAD<sup>+</sup>, SIRT5 catalyzed desuccinylation reaction was performed using 100  $\mu$ M Ac-Suclys-AMC and 50  $\mu$ M NAD<sup>+</sup>. Tables 5.2 to 5.7 show the summary of screening results, which were categorized into 5 groups based on the chemical structures of the compounds. The latter included thiolated compounds (Table 5.2), thiourea derivatives (Table 5.3), hydroxybezoic, hydroxypicolinic and nicotinic group containing compounds (Table 5.4), hydrazine/hydrazide derivatives (Table 5.5), barbiturate/thiobarbiturate derivatives (Table 5.6), and other miscellaneous compounds (Table 5.7). The compounds which inhibit the SIRT1 or SIRT5 catalyzed reaction >30 % at 10  $\mu$ M concentration were selected to determine their inhibition potency (IC<sub>50</sub>) as described in the Methods section (section §4.3.5).

Table 5.2. Summary of screening of thiolated compounds for SIRT1 and SIRT5

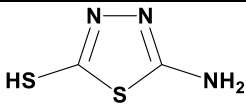
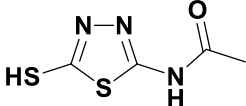
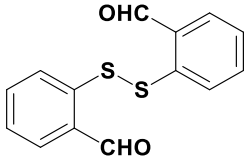
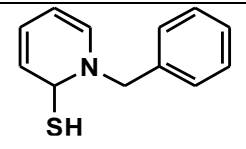
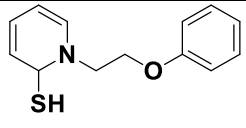
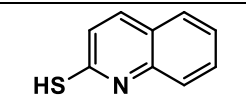
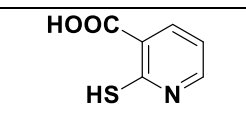
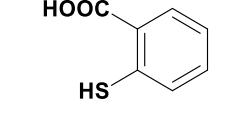
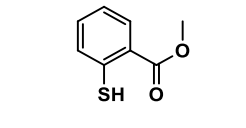
ID	Structure	% Inhibition or fold activation	
		SIRT1	SIRT5
BNG-2-74		NI/NA	NI/NA
BNG-2-73		NI/NA	NI/NA
TM-1-186		NI/NA	NI/NA
DP-180		NI/NA	NI/NA
DP-178		NI/NA	NI/NA
MT-105		23.5	23.5
VYU-2-15		NI/NA	NI/NA
VYU-2-59		NI/NA	NI/NA
VYU-2-14		NI/NA	NI/NA

Table 5.2. Summary of screening of thiolated compounds for SIRT1 and SIRT5 (continued)

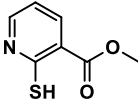
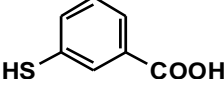
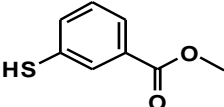
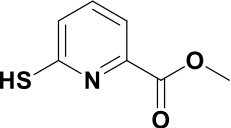
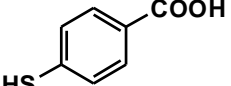
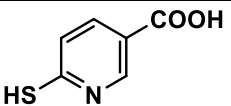
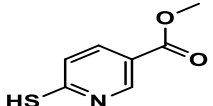
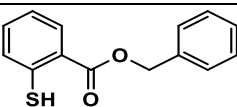
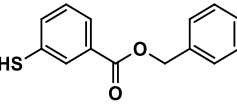
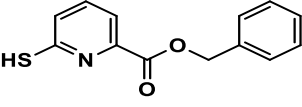
ID	Structure	% Inhibition or fold activation	
		SIRT1	SIRT5
VYU-2-58		NI/NA	NI/NA
VYU-2-17		NI/NA	NI/NA
VYU-2-16		NI/NA	NI/NA
JES-1-21		NI/NA	NI/NA
VYU-2-19		NI/NA	NI/NA
VYU-2-57		NI/NA	NI/NA
VYU-2-56		NI/NA	NI/NA
VYU-2-26		NI/NA	NI/NA
VYU-2-28		NI/NA	NI/NA
VYU-2-64		NI/NA	NI/NA

Table 5.2. Summary of screening of thiolated compounds for SIRT1 and SIRT5 (continued)

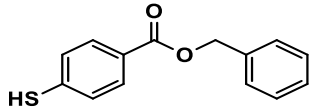
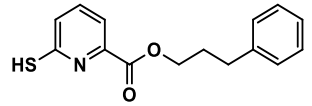
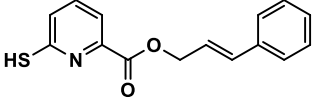
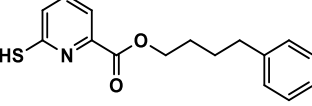
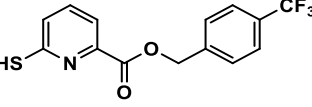
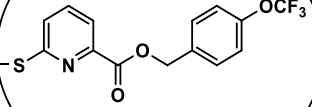
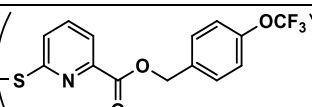
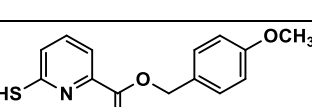
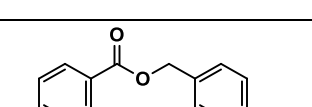
ID	Structure	% Inhibition or fold activation	
		SIRT1	SIRT5
VYU-2-30		NI/NA	NI/NA
VYU-2-136		NI/NA	NI/NA
VYU-2-204		NI/NA	NI/NA
VYU-2-152		NI/NA	NI/NA
MT-114		NI/NA	NI/NA
VYU-3-42		NI/NA	NI/NA
MT-106		NI/NA	NI/NA
VYU-2-246		NI/NA	NI/NA
VYU-2-72		NI/NA	NI/NA



Table 5.2. Summary of screening of thiolated compounds for SIRT1 and SIRT5 (continued)

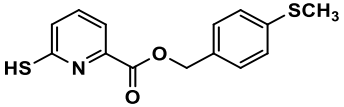
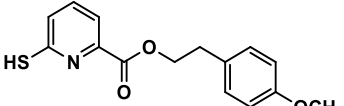
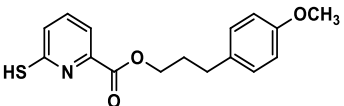
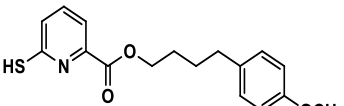
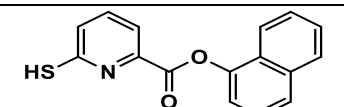
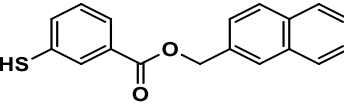
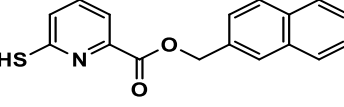
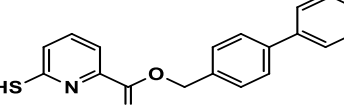
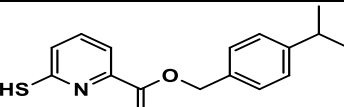
ID	Structure	% Inhibition or fold activation	
		SIRT1	SIRT5
TM-2-195		NI/NA	NI/NA
VYU-2-134		NI/NA	NI/NA
VYU-2-154		NI/NA	NI/NA
VYU-2-156		NI/NA	NI/NA
MT-109		NI/NA	NI/NA
MT-104		NI/NA	NI/NA
MT-111		NI/NA	NI/NA
VYU-2-166		NI/NA	NI/NA
BNG-2-148		NI/NA	NI/NA

Table 5.2. Summary of screening of thiolated compounds for SIRT1 and SIRT5 (continued)

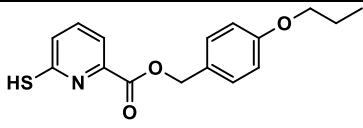
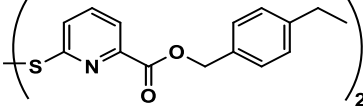
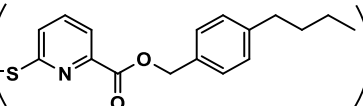
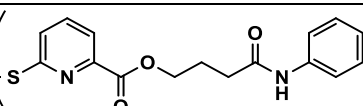
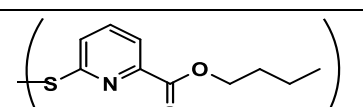
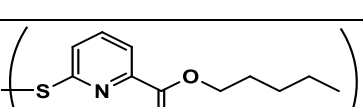
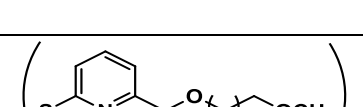

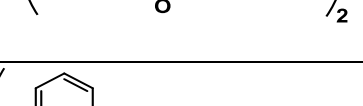
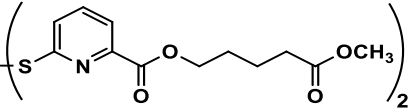
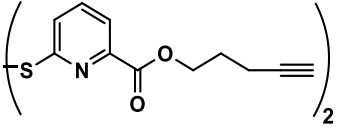
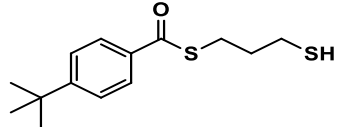
ID	Structure	% Inhibition or fold activation	
		SIRT1	SIRT5
BNG-167		NI/NA	NI/NA
VYU-2-270		NI/NA	NI/NA
VYU-2-272		NI/NA	NI/NA
VYU-2-296		NI/NA	NI/NA
VYU-2-219		NI/NA	NI/NA
VYU-2-221		NI/NA	NI/NA
VYU-2-264		NI/NA	NI/NA
VYU-2-266		NI/NA	NI/NA
VYU-3-54		NI/NA	NI/NA

Table 5.2. Summary of screening of thiolated compounds for SIRT1 and SIRT5 (continued)

ID	Structure	% Inhibition or fold activation	
		SIRT1	SIRT5
VYU-3-56		NI/NA	NI/NA
BNG-3-36		NI/NA	NI/NA
M-263		NI/NA	NI/NA

NI = No Inhibition

NA = No Activation

% = represents the % inhibition of SIRT1 enzyme activity at 10  $\mu$ M of the inhibitor

Table 5.3. Summary of screening of thiourea derivatives for SIRT1 and SIRT5

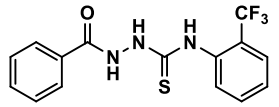
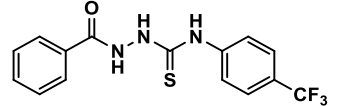
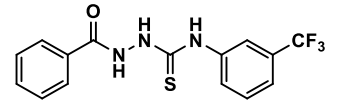
ID	Structure	% Inhibition or fold activation	
		SIRT1	SIRT5
TM-1-197		NI/NA	NI/NA
TM-1-202		NI/NA	NI/NA
TM-1-204		NI/NA	NI/NA

Table 5.3. Summary of screening of thiourea derivatives for SIRT1 and SIRT5 (continued)

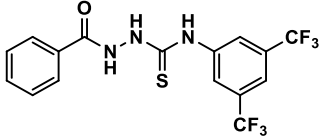
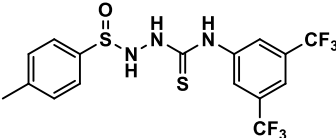
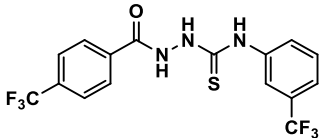
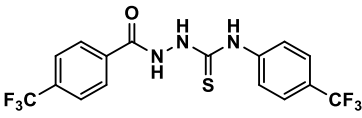
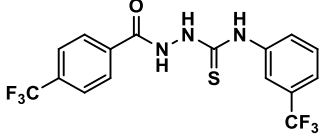
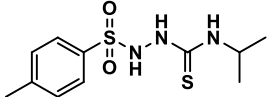
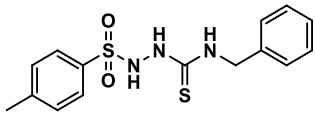
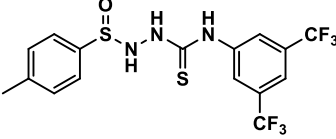
ID	Structure	% Inhibition or fold activation	
		SIRT1	SIRT5
TM-1-149		NI/NA	NI/NA
TM-1-155		NI/NA	NI/NA
TM-1-236		NI/NA	NI/NA
TM-1-235		NI/NA	NI/NA
TM-1-236		NI/NA	NI/NA
TM-1-185		NI/NA	NI/NA
TM-1-183		NI/NA	NI/NA
TM-1-155		NI/NA	NI/NA

Table 5.3. Summary of screening of thiourea derivatives for SIRT1 and SIRT5 (continued)

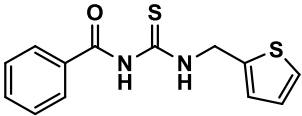
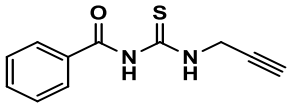
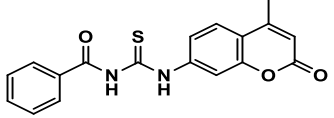
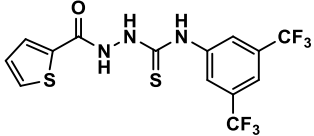
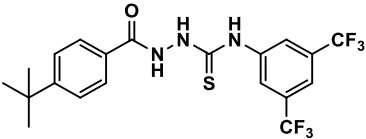
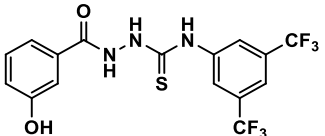
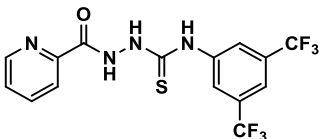
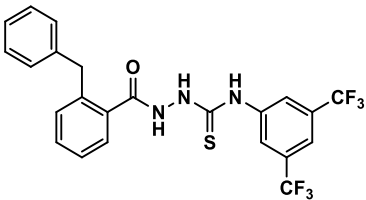
ID	Structure	% Inhibition or fold activation	
		SIRT1	SIRT5
TM-1-114		NI/NA	NI/NA
TM-1-113		NI/NA	NI/NA
TM-2-87		NI/NA	NI/NA
TM-1-261		NI/NA	NI/NA
TM-1-267		NI/NA	NI/NA
TM-1-274		NI/NA	NI/NA
TM-1-278		NI/NA	NI/NA
TM-1-288		NI/NA	NI/NA

Table 5.3. Summary of screening of thiourea derivatives for SIRT1 and SIRT5 (continued)

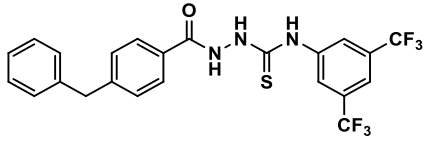
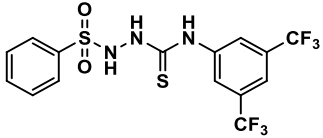
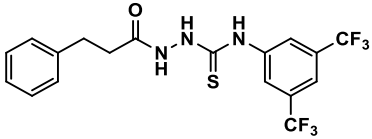
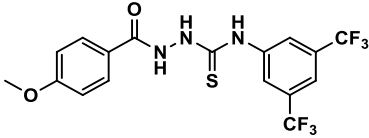
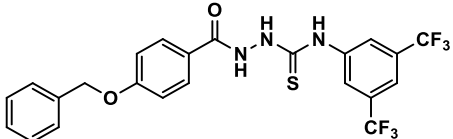
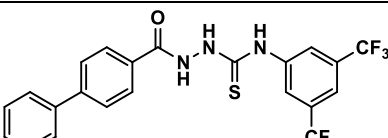
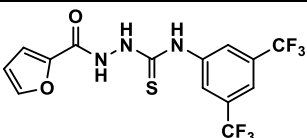
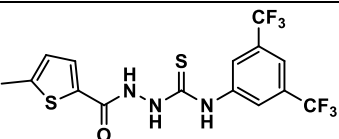
ID	Structure	% Inhibition or fold activation	
		SIRT1	SIRT5
TM-2-4		NI/NA	NI/NA
BNG-2-119		NI/NA	NI/NA
TM-2-7		NI/NA	NI/NA
TM-2-8		NI/NA	NI/NA
TM-2-16		NI/NA	NI/NA
TM-2-32		NI/NA	NI/NA
TM-II-48		NI/NA	NI/NA
TM-2-57		NI/NA	NI/NA

Table 5.3. Summary of screening of thiourea derivatives for SIRT1 and SIRT5 (continued)

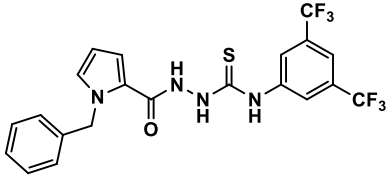
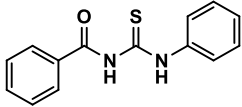
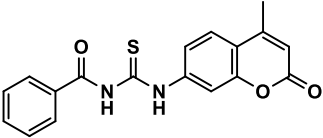
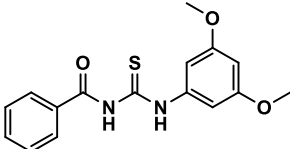
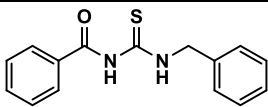
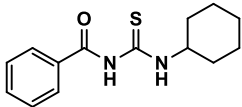
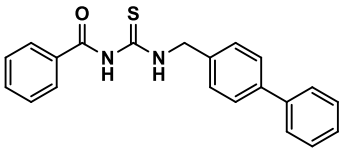
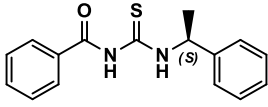
ID	Structure	% Inhibition or fold activation	
		SIRT1	SIRT5
TM-2-60		NI/NA	NI/NA
TM-2-51		NI/NA	NI/NA
TM-2-87		NI/NA	NI/NA
TM-2-88		NI/NA	NI/NA
TM-2-90		NI/NA	NI/NA
TM-2-97		NI/NA	NI/NA
TM-2-101		NI/NA	NI/NA
TM-2-104		NI/NA	NI/NA

Table 5.3. Summary of screening of thiourea derivatives for SIRT1 and SIRT5 (continued)

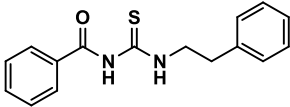
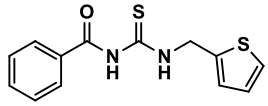
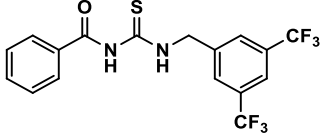
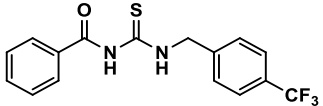
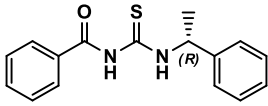
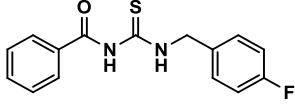
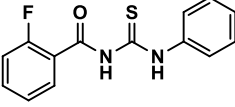
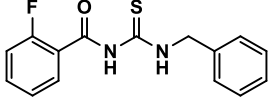
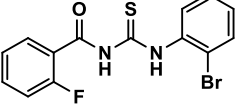
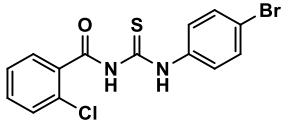
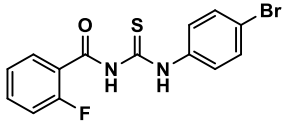
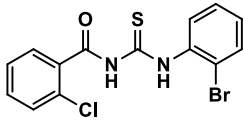
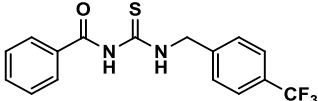
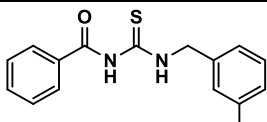
ID	Structure	% Inhibition or fold activation	
		SIRT1	SIRT5
TM-2-105		NI/NA	NI/NA
TM-2-107		NI/NA	NI/NA
TM-2-125		NI/NA	NI/NA
TM-2-126		NI/NA	NI/NA
TM-2-130		NI/NA	NI/NA
TM-2-131		NI/NA	NI/NA
TM-2-138		NI/NA	NI/NA
TM-2-139		NI/NA	NI/NA
TV-1-90		NI/NA	NI/NA



Table 5.3. Summary of screening of thiourea derivatives for SIRT1 and SIRT5 (continued)

ID	Structure	% Inhibition or fold activation	
		SIRT1	SIRT5
TV-1-91		NI/NA	NI/NA
TV-1-92		NI/NA	NI/NA
TV-1-93		NI/NA	NI/NA
TV-1-106		NI/NA	NI/NA
TV-1-114		NI/NA	NI/NA

NI = No Inhibition

NI = No Activation

% = represents the % inhibition of SIRT1 enzyme activity at 10  $\mu$ M of the inhibitor

Table 5.4. Summary of screening of hydroxybenzoic, hydroxypicolinic and nicotinic group containing compounds for SIRT1 and SIRT5

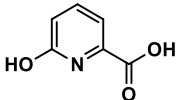
ID	Structure	% Inhibition or fold activation	
		SIRT1	SIRT5
VYU-2-11		NI/NA	NI/NA

Table 5.4. Summary of screening of hydroxybenzoic, hydroxypicolinic and nicotinic group containing compounds for SIRT1 and SIRT5 (continued)

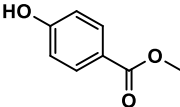
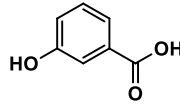
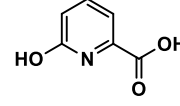
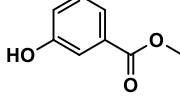
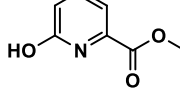
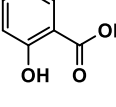
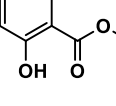
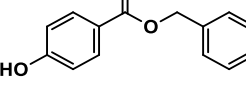
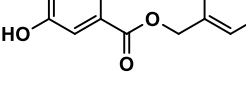
ID	Structure	% Inhibition or fold activation	
		SIRT1	SIRT5
VYU-2-10		NI/NA	NI/NA
VYU-2-23		NI/NA	NI/NA
VYU-2-13		NI/NA	NI/NA
VYU-2-20		NI/NA	NI/NA
VYU-2-22		NI/NA	NI/NA
VYU-2-62-1		NI/NA	NI/NA
VYU-2-62-2		NI/NA	NI/NA
VYU-2-48		NI/NA	NI/NA
VYU-2-46		NI/NA	NI/NA

Table 5.4. Summary of screening of hydroxybenzoic, hydroxypicolinic and nicotinic group containing compounds for SIRT1 and SIRT5 (continued)

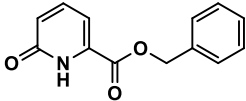
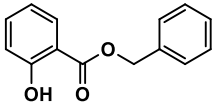
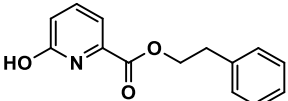
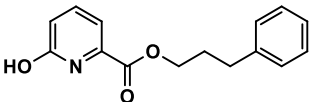
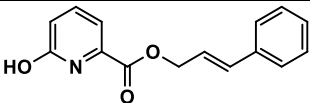
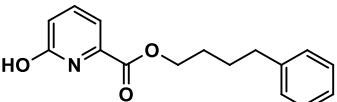
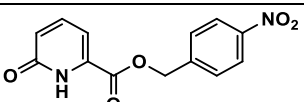
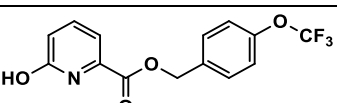
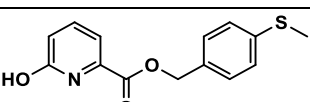
ID	Structure	% Inhibition or fold activation	
		SIRT1	SIRT5
BNG-2-39		NI/NA	NI/NA
VYU-2-44		NI/NA	NI/NA
VYU-2-98		NI/NA	NI/NA
VYU-2-114		NI/NA	NI/NA
VYU-2-181		NI/NA	NI/NA
VYU-2-122		NI/NA	NI/NA
TV-1-33		NI/NA	NI/NA
APB-177		NI/NA	NI/NA
TM-1-291		NI/NA	NI/NA

Table 5.4. Summary of screening of hydroxybenzoic, hydroxypicolinic and nicotinic group containing compounds for SIRT1 and SIRT5 (continued)

ID	Structure	% Inhibition or fold activation	
		SIRT1	SIRT5
APB-178		NI/NA	NI/NA
VYU-2-94		NI/NA	NI/NA
VYU-2-197		NI/NA	NI/NA
VYU-2-224		NI/NA	NI/NA
VYU-2-169		NI/NA	NI/NA
VYU-2-276		NI/NA	NI/NA
VYU-2-274		NI/NA	NI/NA
VYU-2-278		NI/NA	NI/NA

Table 5.4. Summary of screening of hydroxybenzoic, hydroxypicolinic and nicotinic group containing compounds for SIRT1 and SIRT5 (continued)

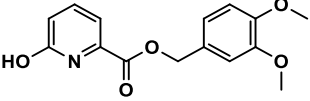
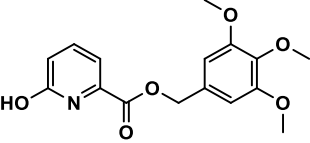
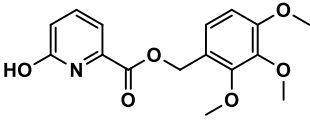
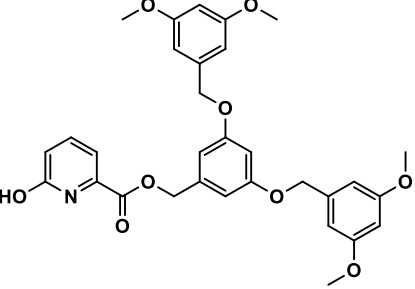
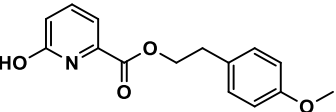
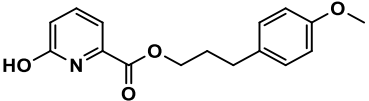
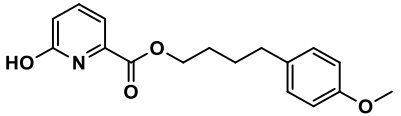
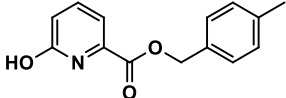
ID	Structure	% Inhibition or fold activation	
		SIRT1	SIRT5
VYU-2-234		NI/NA	NI/NA
VYU-2-195		NI/NA	NI/NA
VYU-2-212		NI/NA	NI/NA
VYU-2-280		NI/NA	NI/NA
VYU-2-110		NI/NA	NI/NA
VYU-2-124		NI/NA	NI/NA
VYU-2-126		NI/NA	NI/NA
OK-1-16		NI/NA	NI/NA

Table 5.4. Summary of screening of hydroxybenzoic, hydroxypicolinic and nicotinic group containing compounds for SIRT1 and SIRT5 (continued)

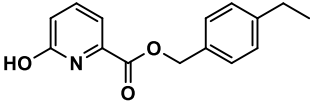
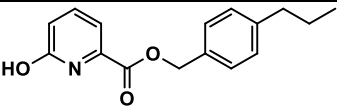
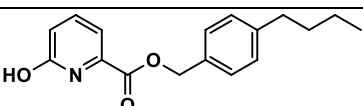
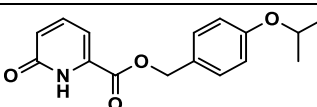
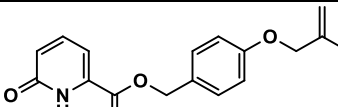
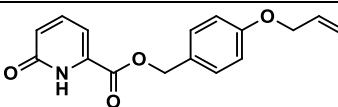
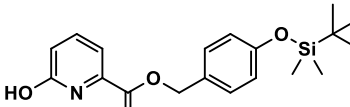
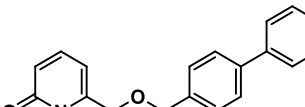
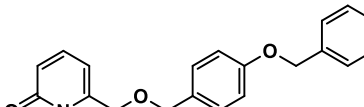
ID	Structure	% Inhibition or fold activation	
		SIRT1	SIRT5
VYU-2-208		NI/NA	NI/NA
OK-1-15		NI/NA	NI/NA
VYU-2-210		NI/NA	NI/NA
BNG-2-147		NI/NA	NI/NA
BNG-2-182		NI/NA	NI/NA
BNG-2-151		NI/NA	NI/NA
APB-1-181		NI/NA	NI/NA
BNG-2-117		NI/NA	NI/NA
BNG-2-152		NI/NA	NI/NA

Table 5.4. Summary of screening of hydroxybenzoic, hydroxypicolinic and nicotinic group containing compounds for SIRT1 and SIRT5 (continued)

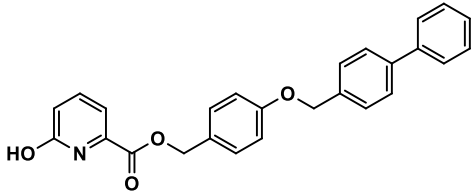
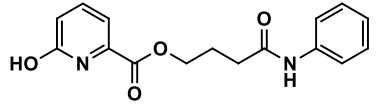
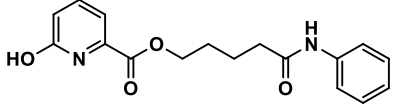
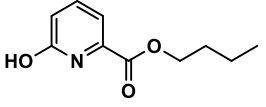
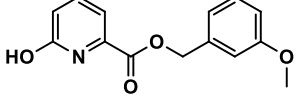
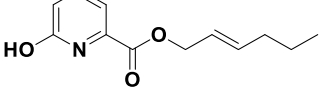
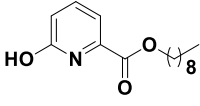
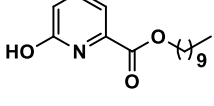
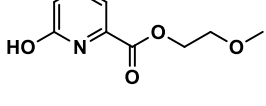
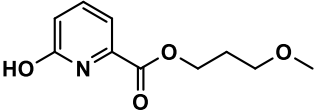
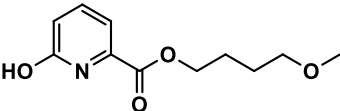
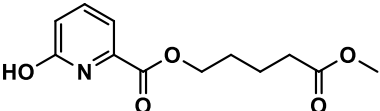
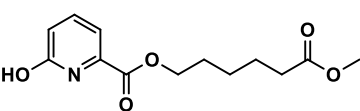
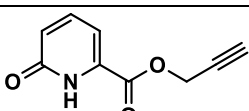
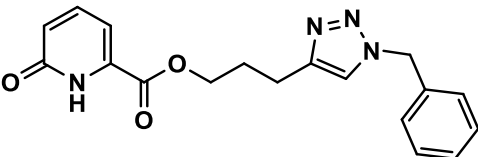
ID	Structure	% Inhibition or fold activation	
		SIRT1	SIRT5
VYU-3-45		NI/NA	NI/NA
JES-1-16		NI/NA	NI/NA
JES-1-45		NI/NA	NI/NA
VYU-2-189		NI/NA	NI/NA
VYU-2-191		NI/NA	NI/NA
APB-185		NI/NA	NI/NA
MJD-171		NI/NA	NI/NA
MJD-169		NI/NA	NI/NA
VYU-2-193		NI/NA	NI/NA

Table 5.4. Summary of screening of hydroxybenzoic, hydroxypicolinic and nicotinic group containing compounds for SIRT1 and SIRT5 (continued)

ID	Structure	% Inhibition or fold activation	
		SIRT1	SIRT5
VYU-2-226		NI/NA	NI/NA
VYU-2-228		NI/NA	NI/NA
VYU-3-40		NI/NA	NI/NA
VYU-3-38		NI/NA	NI/NA
BNG-2-175		NI/NA	NI/NA
BNG-3-33		NI/NA	NI/NA

NI = No Inhibition

NA = No Activation

% = represents the % inhibition of SIRT1 enzyme activity at 10  $\mu$ M of the inhibitor



Table 5.5. Summary of screening of hydrazine/hydrazide derivatives as potential inhibitors/activators for SIRT1

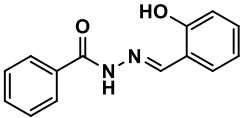
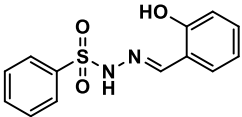
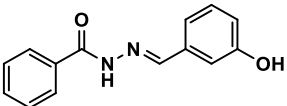
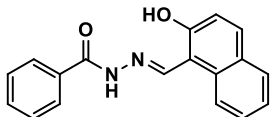
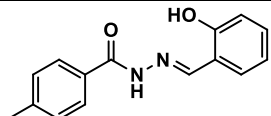
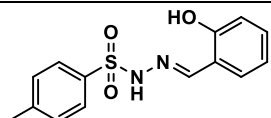
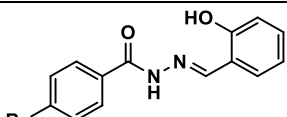
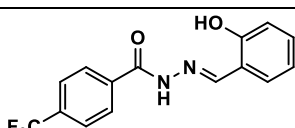
ID	Structure	% Inhibition	
		SIRT1	SIRT5
TM-1-121		NI/NA	NI/NA
TM-1-254		NI/NA	NI/NA
TM-1-243		NI/NA	NI/NA
TM-1-259		NI/NA	NI/NA
TM-1-144		NI/NA	NI/NA
TM-1-170		NI/NA	NI/NA
TM-1-182		NI/NA	NI/NA
TM-1-234		NI/NA	NI/NA

Table 5.5. Summary of screening of hydrazine/hydrazide derivatives as potential inhibitors/activators for SIRT1 (continued)

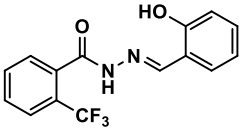
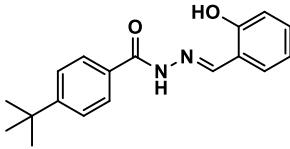
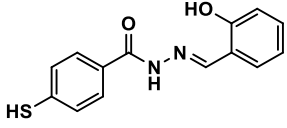
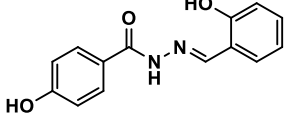
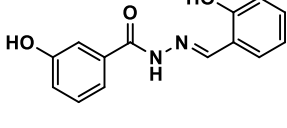
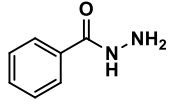
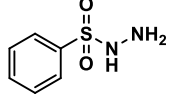
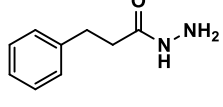
ID	Structure	% Inhibition	
		SIRT1	SIRT5
TM-1-272		NI/NA	NI/NA
TM-1-268		NI/NA	NI/NA
TM-1-246		NI/NA	NI/NA
TM-1-187		NI/NA	NI/NA
TM-1-248		NI/NA	NI/NA
TM-1-108		NI/NA	NI/NA
TM-1-255		NI/NA	NI/NA
TM-2-6		NI/NA	NI/NA

Table 5.5. Summary of screening of hydrazine/hydrazide derivatives as potential inhibitors/activators for SIRT1 (continued)

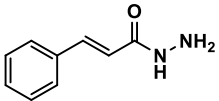
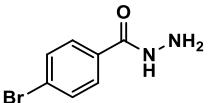
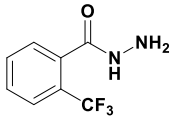
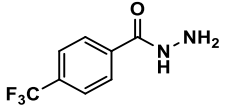
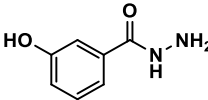
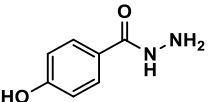
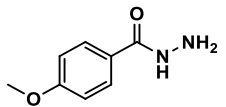
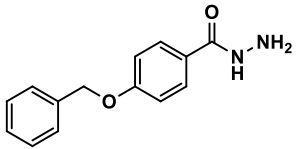
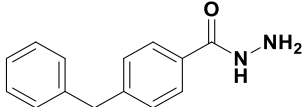
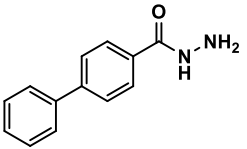
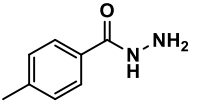
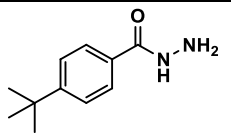
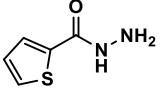
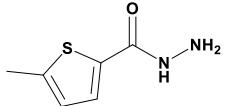
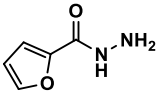
ID	Structure	% Inhibition	
		SIRT1	SIRT5
TM-2-19		NI/NA	NI/NA
TM-1-257		NI/NA	NI/NA
TM-1-288		NI/NA	NI/NA
TM-1-231		NI/NA	NI/NA
TM-1-245		NI/NA	NI/NA
TM-1-256		NI/NA	NI/NA
TM-2-21		NI/NA	NI/NA
TM-2-14		NI/NA	NI/NA
TM-1-293		NI/NA	NI/NA

Table 5.5. Summary of screening of hydrazine/hydrazide derivatives as potential inhibitors/activators for SIRT1 (continued)

ID	Structure	% Inhibition	
		SIRT1	SIRT5
TM-2-31		NI/NA	NI/NA
TM-1-258		NI/NA	NI/NA
TM-1-265		NI/NA	NI/NA
TM-1-253		NI/NA	NI/NA
TM-2-55		NI/NA	NI/NA
TM-II-46		NI/NA	NI/NA

NI = No Inhibition

NI = No Activation

% = represents the % inhibition of SIRT1 enzyme activity at 10  $\mu$ M of the inhibitor

Table 5.6. Summary of screening of barbiturate/thiobarbiturate derivatives as potential inhibitors/activators for SIRT1 and SIRT5

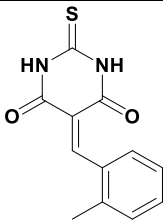
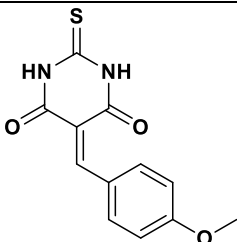
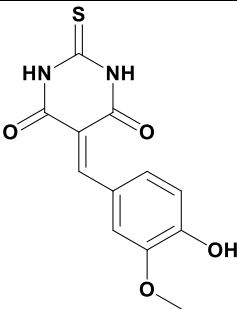
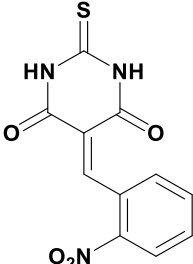
ID	Structure	% Inhibition	
		SIRT1	SIRT5
MDS-2-9		NI/NA	NI/NA
MDS-2-10		NI/NA	NI/NA
MDS-2-18		NI/NA	NI/NA
MDS-2-22		NI/NA	NI/NA

Table 5.6. Summary of screening of barbiturate/thiobarbiturate derivatives as potential inhibitors/activators for SIRT1 and SIRT5 (continued)

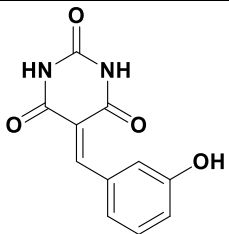
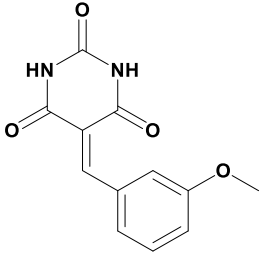
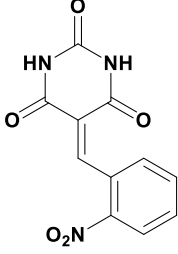
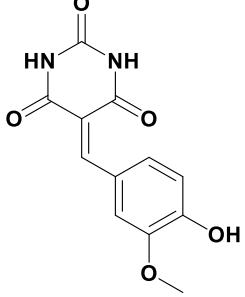
ID	Structure	% Inhibition	
		SIRT1	SIRT5
MDS-01-03		NI/NA	NI/NA
MDS-01-04		NI/NA	NI/NA
MDS-01-05		NI/NA	NI/NA
MDS-01-06		NI/NA	NI/NA

Table 5.6. Summary of screening of barbiturate/thiobarbiturate derivatives as potential Inhibitors/Activators for SIRT1 and SIRT5 (continued)

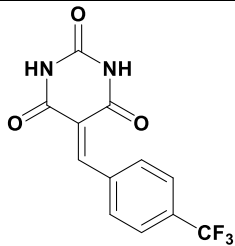
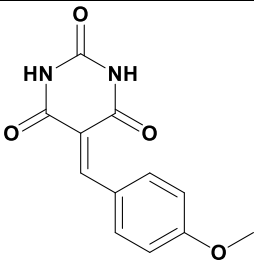
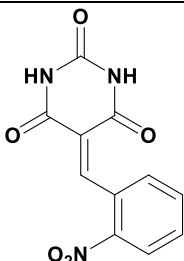
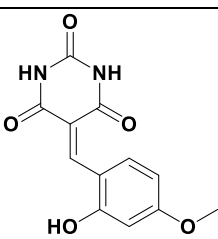
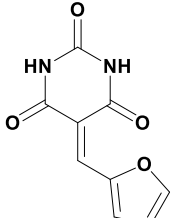
ID	Structure	% Inhibition	
		SIRT1	SIRT5
MDS-01-07		NI/NA	NI/NA
MDS-01-08		NI/NA	NI/NA
MDS-01-09		NI/NA	NI/NA
MDS-01-10		NI/NA	NI/NA
MDS-01-11		NI/NA	NI/NA

Table 5.6. Summary of screening of barbiturate/thiobarbiturate derivatives as potential Inhibitors/Activators for SIRT1 and SIRT5 (continued)

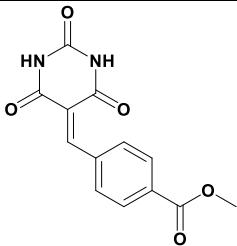
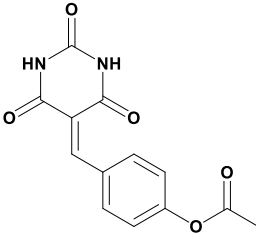
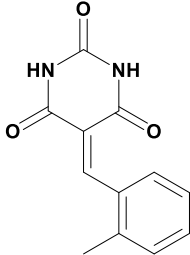
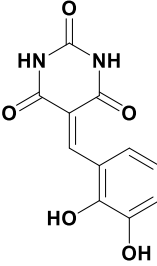
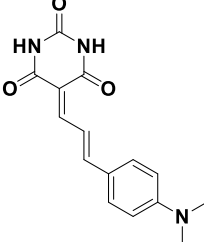
ID	Structure	% Inhibition	
		SIRT1	SIRT5
MDS-01-13		NI/NA	NI/NA
MDS-01-14		NI/NA	NI/NA
MDS-01-16		NI/NA	NI/NA
MDS-01-17		NI/NA	NI/NA
MDS-1-19		NI/NA	NI/NA



Table 5.6. Summary of screening of barbiturate/thiobarbiturate derivatives as potential inhibitors/activators for SIRT1 and SIRT5 (continued)

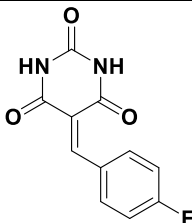
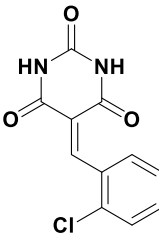
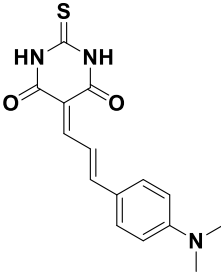
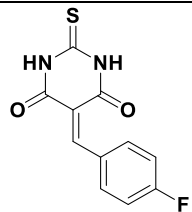
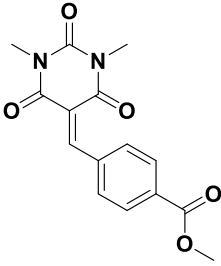
ID	Structure	% Inhibition	
		SIRT1	SIRT5
MDS-1-20		NI/NA	NI/NA
MDS-1-22		NI/NA	NI/NA
MDS-1-23		NI/NA	NI/NA
MDS-1-27		NI/NA	NI/NA
MDS-3-12		NI/NA	NI/NA

Table 5.6. Summary of screening of barbiturate/thiobarbiturate derivatives as potential inhibitors/activators for SIRT1 and SIRT5 (continued)

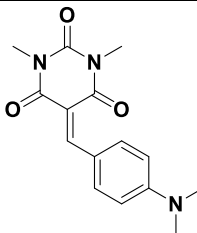
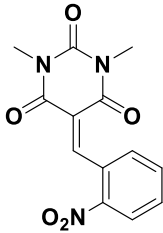
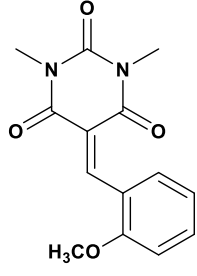
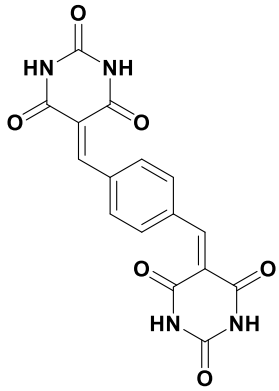
ID	Structure	% Inhibition	
		SIRT1	SIRT5
MDS-3-16		NI/NA	23
MDS-3-19		NI/NA	NI/NA
MDS-3-38		NI/NA	NI/NA
MDS-04-06		NI/NA	NI/NA

Table 5.6. Summary of screening of barbiturate/thiobarbiturate derivatives as potential inhibitors/activators for SIRT1 and SIRT5 (continued)

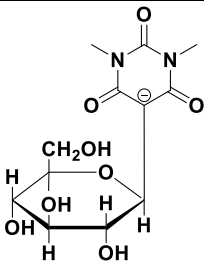
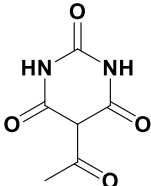
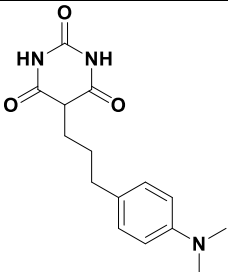
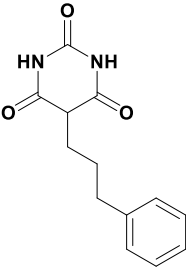
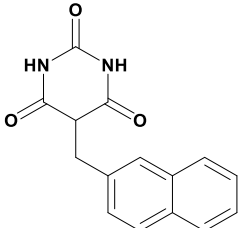
ID	Structure	% Inhibition	
		SIRT1	SIRT5
MDS-4-9		NI/NA	NI/NA
RS-IV-46		NI/NA	NI/NA
RS-V-46		NI/NA	NI/NA
RS-V-48		NI/NA	NI/NA
RS-V-50		NI/NA	NI/NA

Table 5.6. Summary of screening of barbiturate/thiobarbiturate derivatives as potential inhibitors/activators for SIRT1 and SIRT5 (continued)

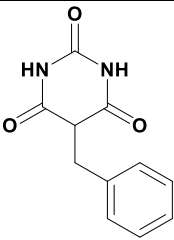
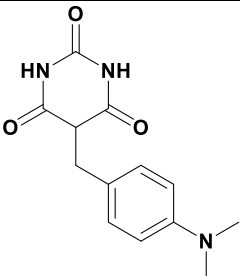
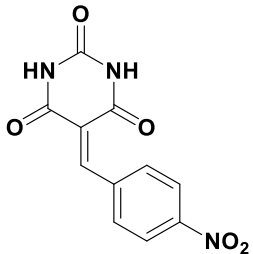
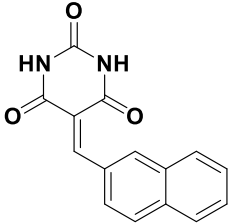
ID	Structure	% Inhibition	
		SIRT1	SIRT5
RS-V-53		NI/NA	NI/NA
RS-V-75		NI/NA	NI/NA
MH-5-51b		NI/NA	NI/NA
MH-5-52		NI/NA	NI/NA

Table 5.6. Summary of screening of barbiturate/thiobarbiturate derivatives as potential inhibitors/activators for SIRT1 and SIRT5 (continued)

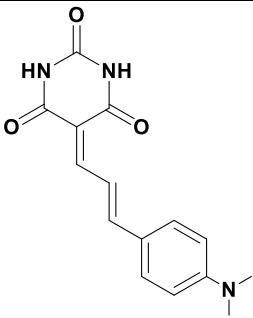
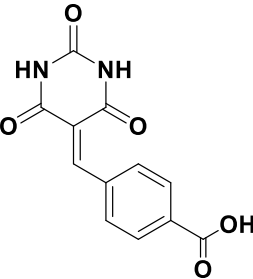
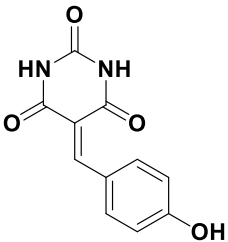
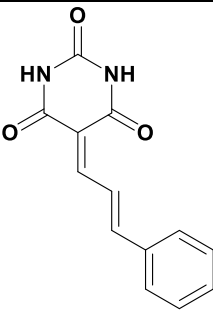
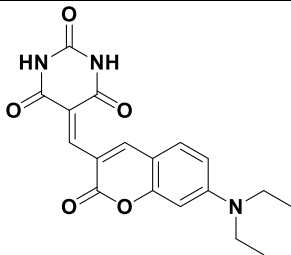
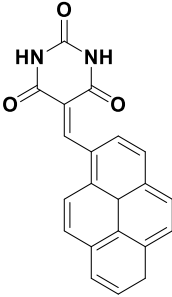
ID	Structure	% Inhibition	
		SIRT1	SIRT5
MH-5-53		NI/NA	NI/NA
MH-5-54		NI/NA	NI/NA
MH-5-68		NI/NA	NI/NA
MH-5-69		NI/NA	NI/NA

Table 5.6. Summary of screening of barbiturate/thiobarbiturate derivatives as potential inhibitors/activators for SIRT1 and SIRT5 (continued)

ID	Structure	% Inhibition	
		SIRT1	SIRT5
MH-5-75		20.1	40
MH-5-76		NI/NA	NI/NA

NI = No Inhibition

NA = No Activation

% = represents the % inhibition of SIRT1 enzyme activity at 10  $\mu$ M of the inhibitor

Table 5.7. Summary of screening of miscellaneous compounds as potential inhibitors/activators for SIRT1 and SIRT5

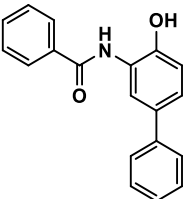
ID	Structure	% Inhibition	
		SIRT1	SIRT5
YT-2-212		NI/NA	NI/NA

Table 5.7. Summary of screening of miscellaneous compounds as potential inhibitors/activators for SIRT1 and SIRT5 (continued)

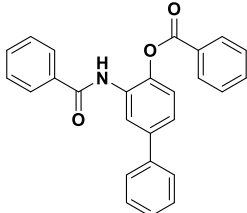
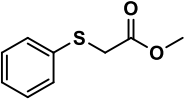
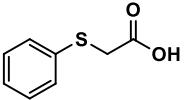
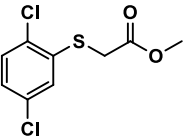
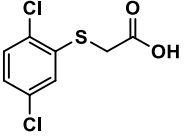
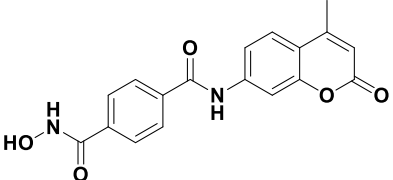
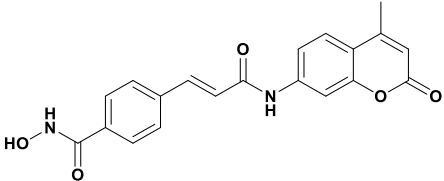
ID	Structure	% Inhibition	
		SIRT1	SIRT5
YT-2-201		NI/NA	NI/NA
VYU-2-86		NI/NA	NI/NA
VYU-2-87		NI/NA	NI/NA
VYU-2-88		NI/NA	NI/NA
VYU-2-89		NI/NA	NI/NA
TM-2-37		NI/NA	NI/NA
TM-2-103		NI/NA	NI/NA

Table 5.7. Summary of screening of miscellaneous compounds as potential inhibitors/activators for SIRT1 and SIRT5 (continued)

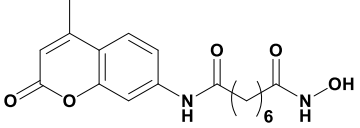
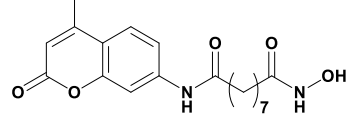
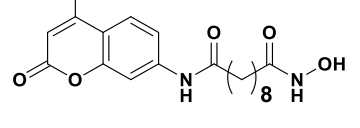
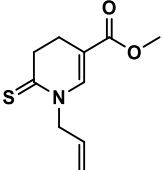
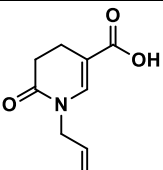
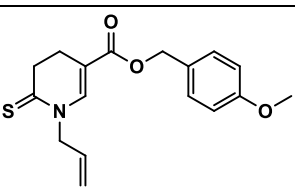
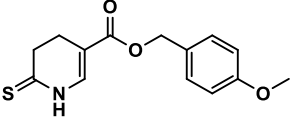
ID	Structure	% Inhibition	
		SIRT1	SIRT5
TM-2-3		NI/NA	NI/NA
BNG-3-93		NI/NA	NI/NA
BNG-3-90		NI/NA	NI/NA
MT-119		NI/NA	NI/NA
MT-122		NI/NA	NI/NA
MT-124		NI/NA	NI/NA
MT-128		NI/NA	NI/NA



Table 5.7. Summary of screening of miscellaneous compounds as potential inhibitors/activators for SIRT1 and SIRT5 (continued)

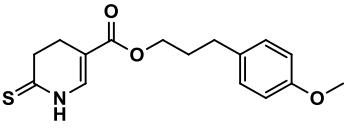
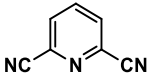
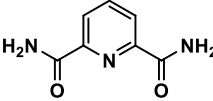
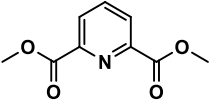
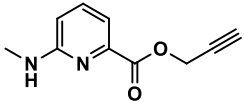
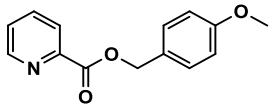
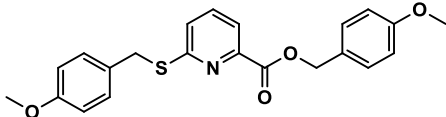
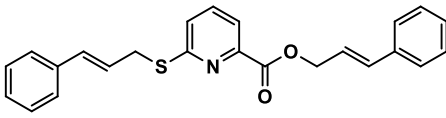
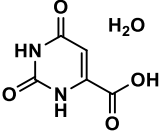
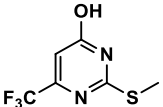
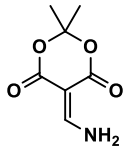
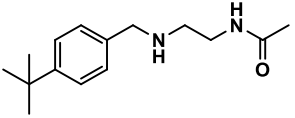
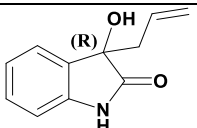
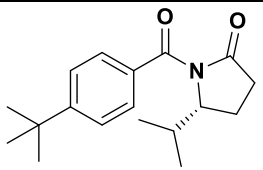
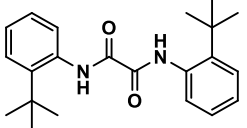
ID	Structure	% Inhibition	
		SIRT1	SIRT5
MT-129		NI/NA	NI/NA
VYU-2-62-4		NI/NA	NI/NA
VYU-2-250		NI/NA	NI/NA
VYU-2-248		NI/NA	NI/NA
TV-1-55		NI/NA	NI/NA
VYU-2-171		NI/NA	NI/NA
VYU-2-252		NI/NA	NI/NA
VYU-2-204-2		NI/NA	NI/NA
VYU-2-63-3		NI/NA	NI/NA

Table 5.7. Summary of screening of miscellaneous compounds as potential inhibitors/activators for SIRT1 and SIRT5 (continued)

ID	Structure	% Inhibition	
		SIRT1	SIRT5
BNG-3-60		NI/NA	NI/NA
TV-1-67		NI/NA	NI/NA
MK-249		NI/NA	NI/NA
BNG-2-23		NI/NA	NI/NA
M-264		NI/NA	NI/NA
BNG-4-87-1		NI/NA	NI/NA

NI = No Inhibition

NA = No Activation

% = represents the % inhibition of SIRT1 enzyme activity at 10  $\mu$ M of the inhibitor

Of all compounds screened, one thiolated compound (thio-quinoline, MT-105; Table 5-2) and two barbiturate derivatives (MDS-3-16 and MH5-75; Table 5-7) showed modest inhibitory potencies against SIRT1 or SIRT5. Of two barbiturate derivatives, MDS-3-16 was found to be

selective for SIRT5. It exhibited 30% inhibition (by 10  $\mu\text{M}$  compound) against SIRT5, but did not show any inhibition (by the same concentration of the compound) against SIRT1. On the other hand, 10  $\mu\text{M}$  concentration of MH5-75 exhibited 40% inhibition against SIRT5 but 20% inhibition against SRIT1. To test the efficacies of MDS-3-16 and MH5-75 on SIRT5, the  $\text{IC}_{50}$  values of the compounds were determined by measuring the initial rate of the SIRT5 desuccinylation reaction in the presence of increasing concentrations of the inhibitors. The data were analyzed using the equation described in section §4.3.5. As shown in Figures 5.28 and 5.29, the solid red lines represent the best fits of the experimental data, yielding the  $\text{IC}_{50}$  values of be  $76.0 \pm 7.5 \mu\text{M}$  and  $43.7 \pm 2.5 \mu\text{M}$  for MDS-3-16 and MH-5-75, respectively.

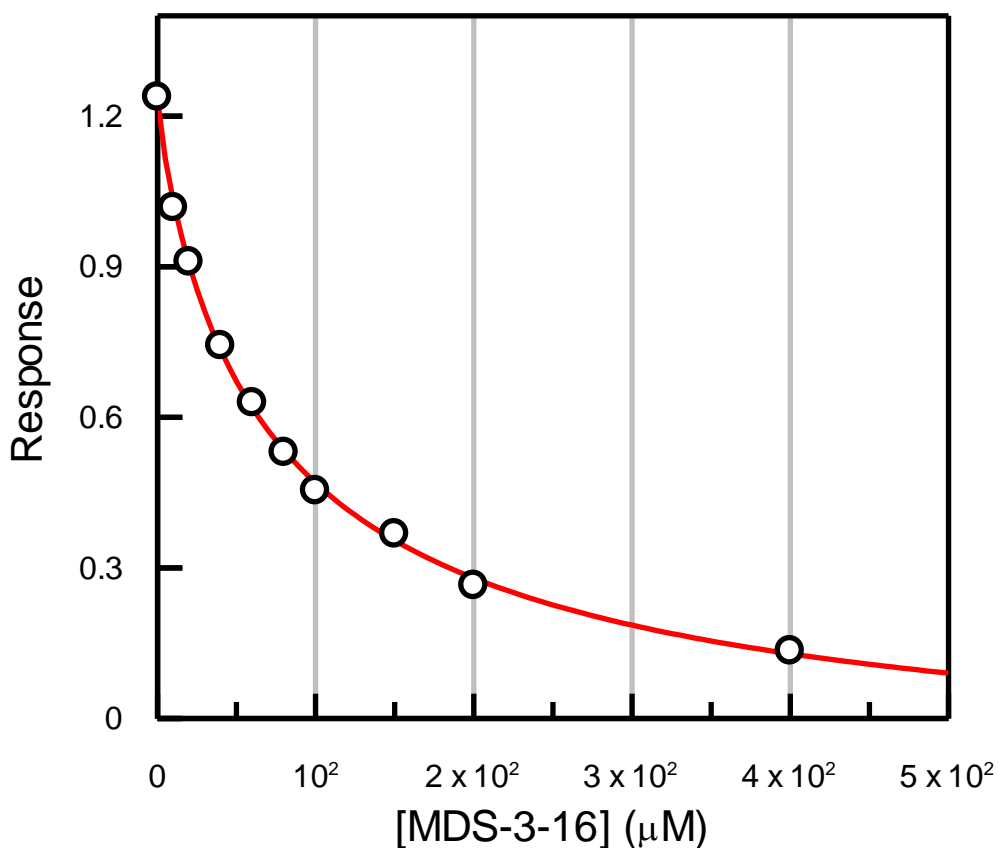


Figure 5.27. Dose-response of SIRT5 desuccinylase activity in the presence of 150  $\mu\text{M}$  Ac-Suclys-AMC, 50  $\mu\text{M}$   $\text{NAD}^+$ , and increasing concentration of MD-3-16 (from 0 to 100  $\mu\text{M}$ ). The solid smooth lines represent the best fit of the data for the  $\text{IC}_{50}$  value as  $76.0 \pm 7.5 \mu\text{M}$ .

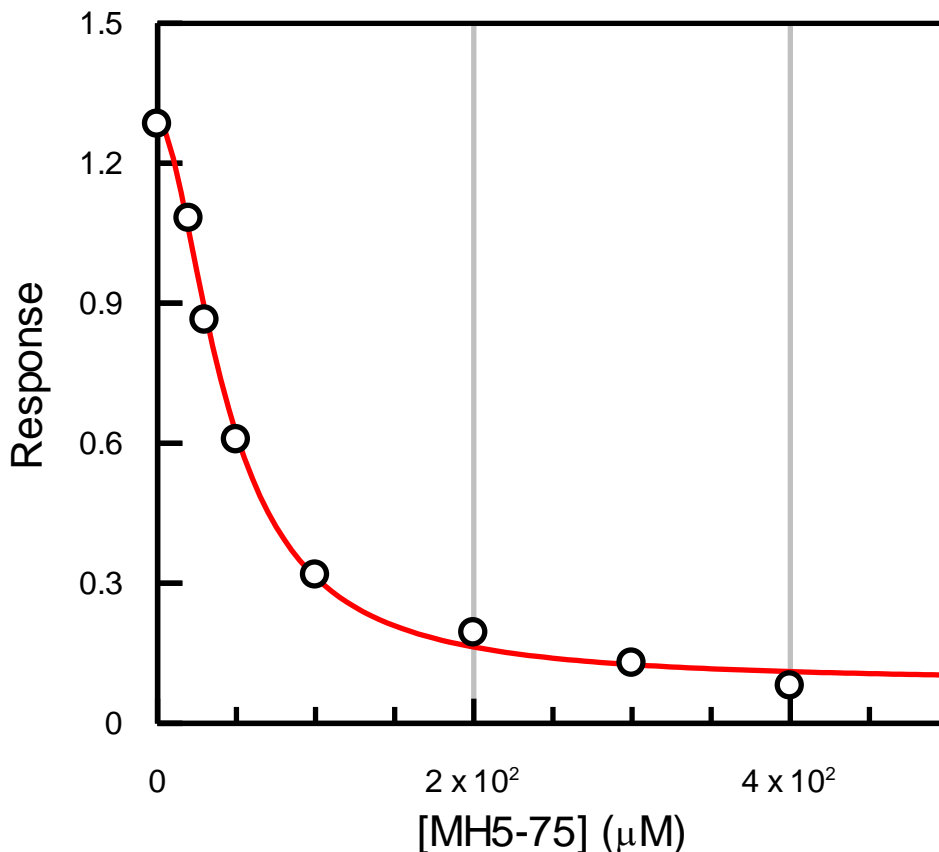


Figure 5.28. Dose-response of SIRT5 desuccinylase activity in the presence of 150  $\mu\text{M}$  Ac-Suclys-AMC, 50  $\mu\text{M}$   $\text{NAD}^+$ , and increasing concentration of MH5-75 (from 0 to 400  $\mu\text{M}$ ). The solid smooth lines represent the best fit of the data for the  $\text{IC}_{50}$  value as  $43.7 \pm 2.5 \mu\text{M}$ .

### 5.3.2. Steady-state kinetics for the inhibition of SIRT5 by MH5-75

Due to its highest inhibitory potency, detailed steady state kinetic studies for the inhibition of SIRT5 by MH-5-75 were performed. Such studies involved measuring the SIRT5 catalyzed reaction via the continuous (trypsin coupled) assay system in the absence and presence of MH-5-75. In this approach, the concentration of one substrate was varied while the other substrate was kept constant. The initial velocities of the reactions in the above conditions were measured and the mode of inhibition (viz., competitive, mixed, and uncompetitive) were

determined by the model discrimination module of DYNAFIT software. Figure 5.29 shows the double reciprocal plots ( $1/v$  versus  $1/[\text{substrate}]$ ) for the SIRT5 catalyzed reaction as a function of the succinylated substrate Ac-Suclys-AMC (Figure 5.29 A and B) and  $\text{NAD}^+$  (Figure 5.32 C and D) at various fixed concentration of MH5-75. As shown in Figure 5.29A, the double-reciprocal plots for the reactions in the presence of varying MH5-75 (0, 50, 100, 200 and 400  $\mu\text{M}$ ) and succinylated lysine concentration (50 to 600  $\mu\text{M}$ ) conform to the mixed inhibition model with the  $K_i$  and  $K_i'$  values of  $25.57 \pm 3.18 \mu\text{M}$  and  $48.92 \pm 5.35 \mu\text{M}$ , respectively, while the plots for the reactions with varying MH-5-75 (0, 50, 100, 200 and 400  $\mu\text{M}$ ) and  $\text{NAD}^+$  (40 to 300  $\mu\text{M}$ ) shows noncompetitive inhibition (Figure 5.29 D), with the  $K_i$  value of  $37.0 \pm 1.5 \mu\text{M}$ . Note that the three  $K_i$  values determined from the analysis are comparable, suggesting that the binding of MH5-75 is not apparently affected by the binding of the succinylated substrate and  $\text{NAD}^+$ . The mixed inhibition of MH-5-75 against the Ac-Suclys-AMC may indicate that the ligand partially competes against the succinylated substrate during SIRT5 catalysis.

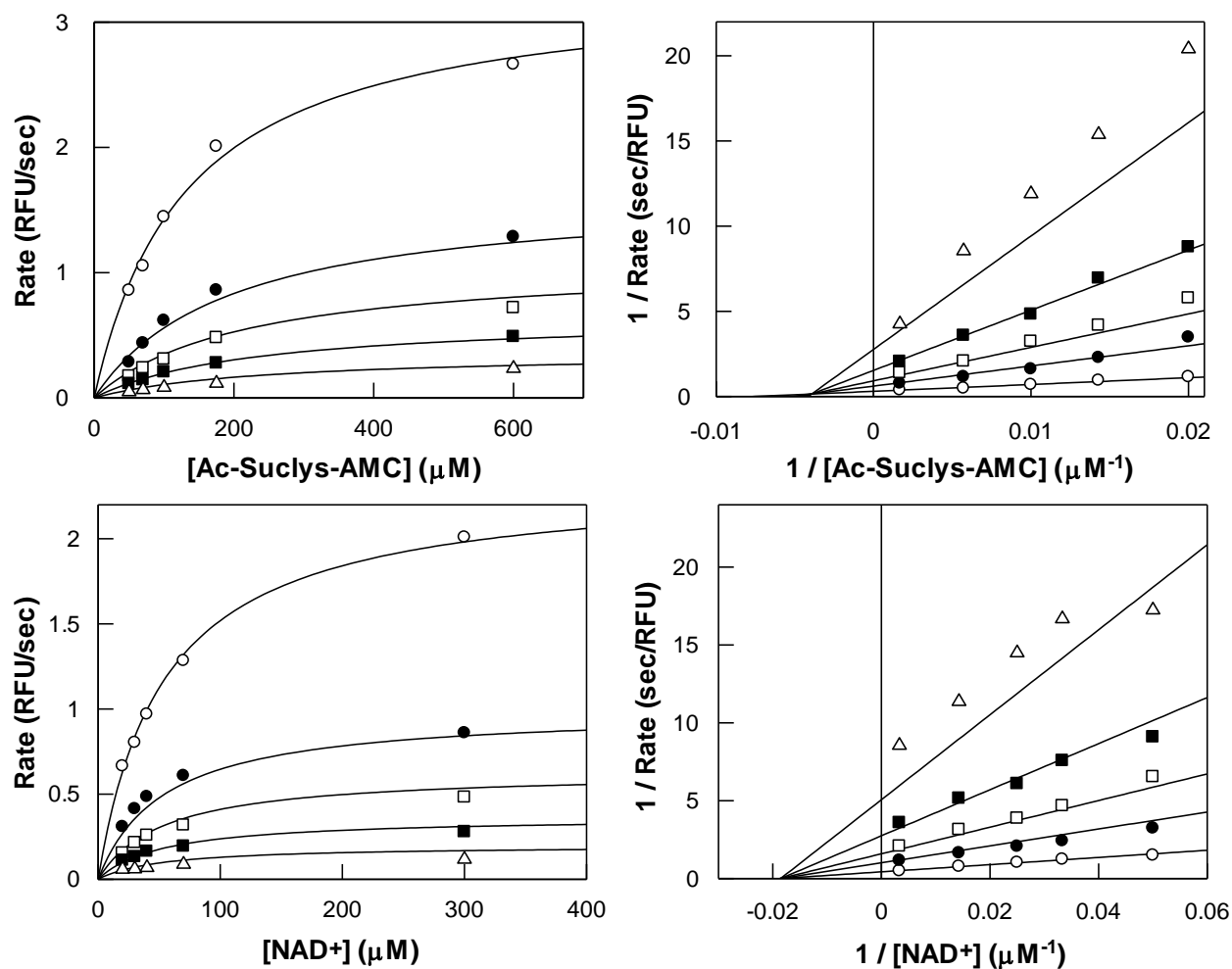


Figure 5.29. Steady-state kinetics for the inhibition of SIRT5 by compound MH5-75. (A) The SIRT5 catalyzed desuccinylation reactions were performed in the presence of 300  $\mu\text{M}$  NAD<sup>+</sup> and varying concentrations of Ac-SucLys-AMC (from 50 to 600  $\mu\text{M}$ ) in the presence of 0, 50, 100, 200 and 400  $\mu\text{M}$  concentrations of MH5-75. Data were fitted using DYNAFIT software yielding the  $K_i$  and  $K_i'$  values of  $(25.6 \pm 3.2)$   $\mu\text{M}$  and  $(48.9 \pm 5.3)$   $\mu\text{M}$ , respectively, under the mixed inhibition model. The double-reciprocal plot of  $1/v$  vs  $1/[\text{Ac-Suclys-AMC}]$  at increasing concentrations of MH5-75 are shown in (B). (C) The SIRT5 catalyzed reactions were performed in the presence of 100  $\mu\text{M}$  Ac-SucLys-AMC and varying concentrations of NAD<sup>+</sup> (from 40 to 300  $\mu\text{M}$ ) in the presence of 0, 50, 100, 200 and 400  $\mu\text{M}$  concentrations of MH5-75. Data were fitted using DYNAFIT software yielding the  $K_i$  value of  $(37.0 \pm 1.5)$   $\mu\text{M}$  under the non-competitive model. The double-reciprocal plot of  $1/v$  vs  $1/[\text{Ac-Suclys-AMC}]$  at increasing concentrations of MH5-75 are also shown in (D).

### 5.3.3. Inhibition of selected sirtuins by suramin

As elaborated in the Introduction section (section §1.7.2), suramin has been found to inhibit various isoforms of sirtuins. To compare the efficacy of suramin on SIRT1 and SIRT5, the initial velocities of SIRT1 catalyzed deacetylation reaction and SIRT5 catalyzed desuccinylation reaction were measured in the presence of increasing concentrations of suramin and the data were analyzed by competitive inhibition model (as detailed in the Methods section §4.3.4). The solid lines of the Figures 5.18 and 5.19 represent the best fit of the experimental data by Eq.4.5, yielding the  $K_i$  values of  $1.1 \pm 0.1 \mu\text{M}$  and  $189 \pm 14.9 \mu\text{M}$  for SIRT1 and SIRT5, respectively. Note that due to the low initial rate of SIRT5 catalyzed reaction with *Fluor-de-lys*<sup>®</sup> substrate, the  $K_i$  for SIRT5 with respect to deacetylation reaction could not be reliably determined.

The uniqueness of SIRT5 in catalyzing the desuccinylation (as opposed to the normal deacetylation reaction) has been ascribed to the presence of two amino acid residues (namely Y102 and R105) within the active site pocket of the enzyme (10). The crystal structure of SIRT5-suramin complex demonstrates that Y102 and R105 coordinate with the negatively charged sulfonyl moieties of suramin (34). In order to probe the contributions of these two amino acids for the inhibition of SIRT5 by suramin, the inhibition of three SIRT5 mutants (namely, Y102A, R105I, and Y102A/R105I) were also investigated. It should be pointed out that while the Y102A mutant enzyme maintained both detectable desuccinylase and deacetylase activities, R105I and Y102A/R105I lost the desuccinylase activity but retained the deacetylase activity (see section §5.2.2). Both the deacetylase and desuccinylase activities of Y102A mutant SIRT5 were evaluated in the presence of suramin (Figure 5.32). The Y102A catalyzed desuccinylation reaction was determined in the presence of  $100 \mu\text{M}$  Ac-SucLys-AMC,  $50 \mu\text{M}$   $\text{NAD}^+$ , and

increasing concentration of suramin (from 0 to 100  $\mu\text{M}$ ). Figure 5.32A shows the best fit of the data, yielding the  $K_i$  values determined to be  $3.69 \pm 1.4 \mu\text{M}$ . The SIRT5 Y02A catalyzed deacetylation reactions were performed in the presence of 100  $\mu\text{M}$  *Fluor-de-lys*<sup>®</sup> substrate, 500  $\mu\text{M}$   $\text{NAD}^+$ , and increasing concentration of suramin (from 0 to 100  $\mu\text{M}$ ), with the  $K_i$  value determined to be  $6.8 \pm 1.7 \mu\text{M}$ .

The SIRT5 Y102A/R105I catalyzed deacetylation reactions were performed in the presence of 100  $\mu\text{M}$  Ac-SucLys-AMC, 500  $\mu\text{M}$   $\text{NAD}^+$ , and increasing concentration of suramin (from 0 to 50  $\mu\text{M}$ ). Figure 5.33 shows the best fit of the data for the  $K_i$  values as  $25.7 \pm 3.0 \mu\text{M}$ . On the contrary, only 10% of R105I mutant enzyme was inhibited by 250  $\mu\text{M}$  suramin. Clearly, despite of the fact that Y102 and R105 coordinate with suramin in the active site, the roles these two residues play are opposite. Y102 prevents the inhibition of the enzyme by suramin, while R105 assist the inhibition by suramin.



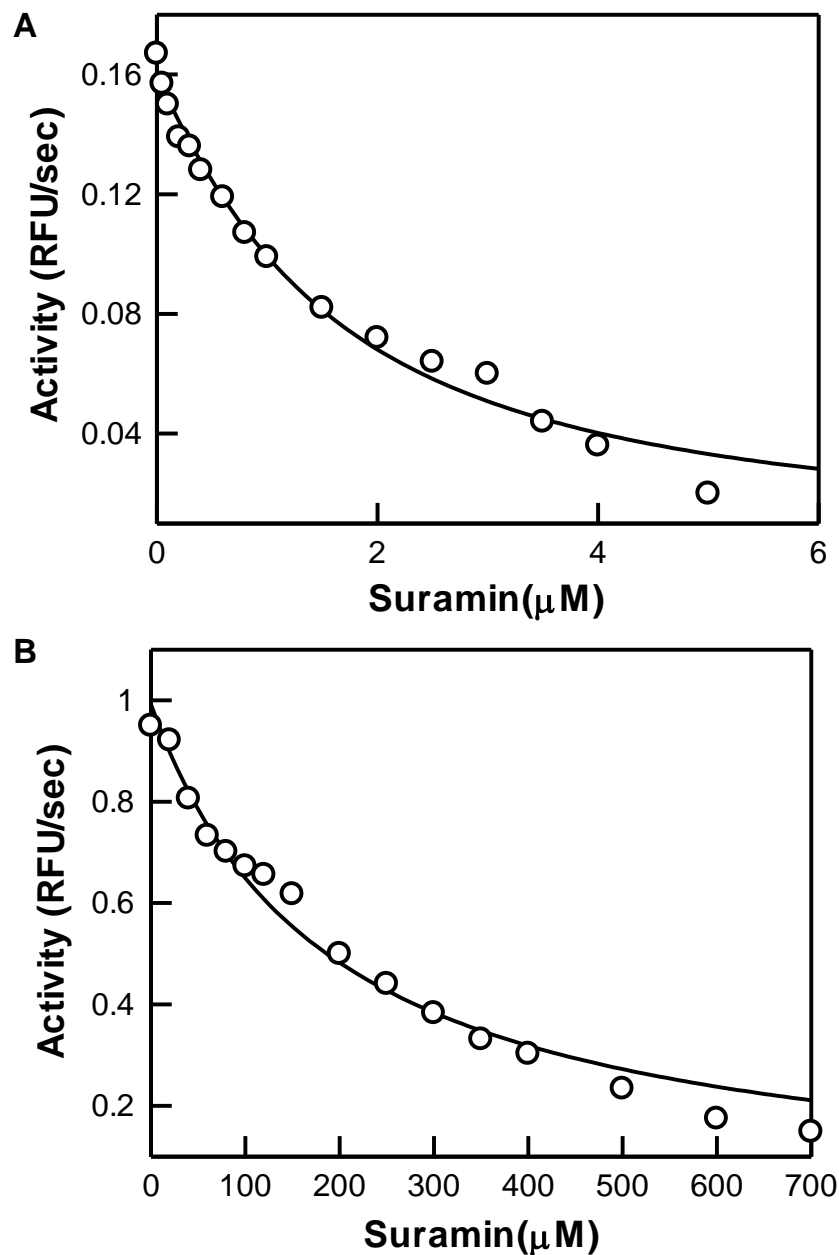


Figure 5.30.  $K_i$  determination of SIRT1 and SIRT5 by suramin. (A) SIRT1 deacetylase activity was measured in the presence of 100  $\mu\text{M}$  *Fluor-de-lys*<sup>®</sup> substrate, 500  $\mu\text{M}$   $\text{NAD}^+$ , and increasing concentration of suramin (from 0 to 5  $\mu\text{M}$ ). The solid smooth line represents the best fit of the data for the  $K_i$  values as  $1.1 \pm 0.1 \mu\text{M}$ . (B)  $K_i$  determination of SIRT5 by suramin. The SIRT5 catalyzed reactions were performed in the presence of 100  $\mu\text{M}$  Ac-SucLys-AMC, 50  $\mu\text{M}$   $\text{NAD}^+$ , and increasing concentration of suramin (from 0 to 700  $\mu\text{M}$ ). The solid smooth line represents the best fit of the data for the  $K_i$  values as  $189.1 \pm 14.9 \mu\text{M}$ .

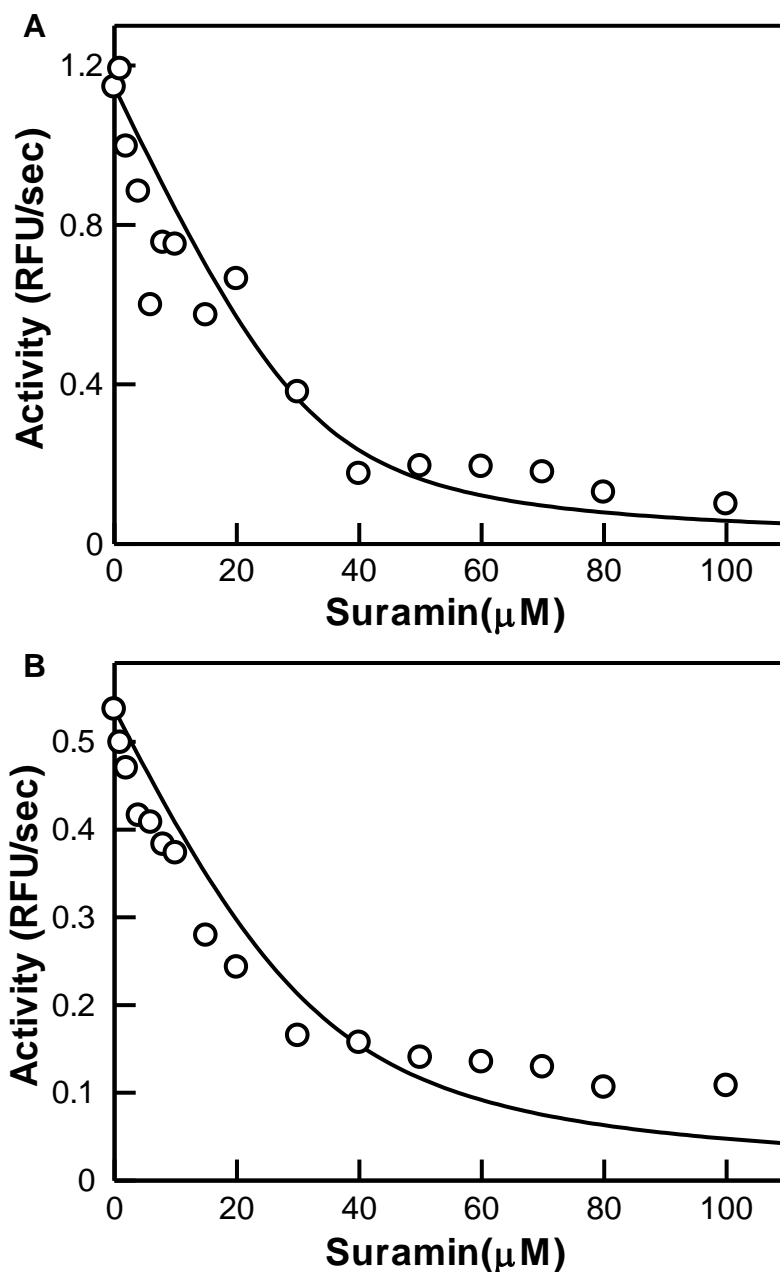


Figure 5.31.  $K_i$  determination of SIRT5 Y102A by suramin. (A) The SIRT5 Y102A catalyzed desuccinylation reactions were performed in the presence of 100  $\mu\text{M}$  Ac-SucLys-AMC, 50  $\mu\text{M}$   $\text{NAD}^+$ , and increasing concentration of suramin (from 0 to 100  $\mu\text{M}$ ). The solid smooth lines represent the best fit of the data for the  $K_i$  values as  $3.7 \pm 1.4 \mu\text{M}$ . (B) The SIRT5 Y02A catalyzed deacetylation reactions were performed in the presence of 100  $\mu\text{M}$  *Fluor-de-lys*<sup>®</sup> substrate, 500  $\mu\text{M}$   $\text{NAD}^+$ , and increasing concentration of suramin (from 0 to 100  $\mu\text{M}$ ). The solid smooth lines represent the best fit of the data for the  $K_i$  values as  $6.8 \pm 1.7 \mu\text{M}$ .

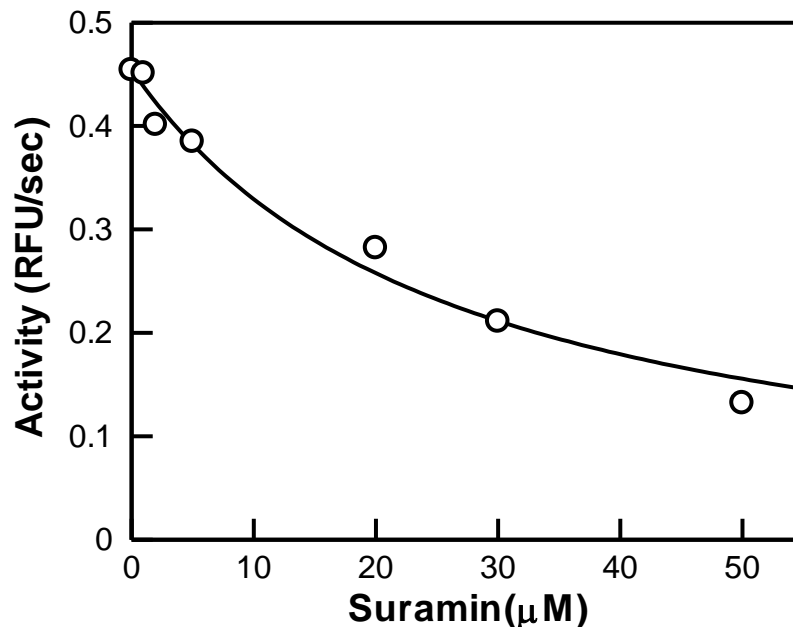


Figure 5.32.  $K_i$  determination of SIRT5 Y102A/R105I by suramin. The SIRT5 Y102A/R105I catalyzed deacetylation reactions were performed in the presence of 100  $\mu\text{M}$  Ac-SucLys-AMC, 500  $\mu\text{M}$   $\text{NAD}^+$ , and increasing concentration of suramin (from 0 to 50  $\mu\text{M}$ ). The solid smooth lines represent the best fit of the data for the  $K_i$  values as  $25.7 \pm 3.0 \mu\text{M}$ .

Table 5.8 Inhibition potency of suramin against SIRT1 and SIRT5 variants

Enzyme	Activity	$K_i$ or % inhibition
SIRT1	deacetylase	$1.14 \pm 0.1 \mu\text{M}$
SIRT5	desuccinylase	$189.1 \pm 14.9 \mu\text{M}$
SIRT5 Y102A	deacetylase	$6.8 \pm 1.7 \mu\text{M}$
	desuccinylase	$3.7 \pm 1.4 \mu\text{M}$
SIRT5 R105I	deacetylase	10% by 250 $\mu\text{M}$ suramin
SIRT5 Y102A/R105I	deacetylase	$25.7 \pm 3.0 \mu\text{M}$

#### 5.3.4. Inhibition mode of SIRT5 desuccinylase activity by suramin

The X-ray crystallographic data of SIRT5-suramin complex revealed that the inhibitor binds at the  $\text{NAD}^+$  binding pockets B and C, as well as the peptide-binding pocket of the enzyme, suggesting that it has the potential to compete against both  $\text{NAD}^+$  and the peptide substrates (34). To investigate the inhibition mode of SIRT5 desuccinylase activity by suramin,

steady-state kinetic studies of SIRT5 catalyzed desuccinylation reaction were performed in the presence of suramin, using the continuous assay as described in section §4.3.1. The concentrations of one substrate and suramin were varied while the other substrate was kept constant. The initial velocities of the reactions in the above conditions were measured, and the double reciprocal plots of  $1/v$  versus  $1/[\text{substrate}]$  were fitted to the competitive, mixed, and uncompetitive inhibition models to distinguish the mode of inhibition. Figure 5.34 shows the steady-state rates and the corresponding double-reciprocal plots for the SIRT5 catalyzed reaction as a function of  $\text{NAD}^+$  (Figure 5.34A and B) or succinylated substrate (Figure 5.34C and D) at various fixed concentration of suramin. As shown in Figure 5.34B, the double-reciprocal plots for the reactions in the presence of varying suramin (0, 100  $\mu\text{M}$ , 200  $\mu\text{M}$ ) and succinylated lysine concentrations (90 to 700  $\mu\text{M}$ ) conform to the competitive inhibition model with the  $K_i$  determined to be  $46.9 \pm 3.2 \mu\text{M}$ , while the plots for the reactions with varying suramin (0, 100  $\mu\text{M}$ , 200  $\mu\text{M}$ ) and  $\text{NAD}^+$  (40 to 300  $\mu\text{M}$ ) show mixed inhibition (Figure 5.34 C and D), with the  $K_i$  and  $K_{i'}$  values determined to be  $90.5 \pm 13.4 \mu\text{M}$  and  $270.7 \pm 36.2 \mu\text{M}$ , respectively. The above results indicate that besides being fully competitive against succinylated substrate, suramin also partially competes against  $\text{NAD}^+$  during SIRT5 catalyzed reaction. Such inhibition modes are consistent with the model of binding of suramin in the crystal structure of SIRT5-suramin complex (34).

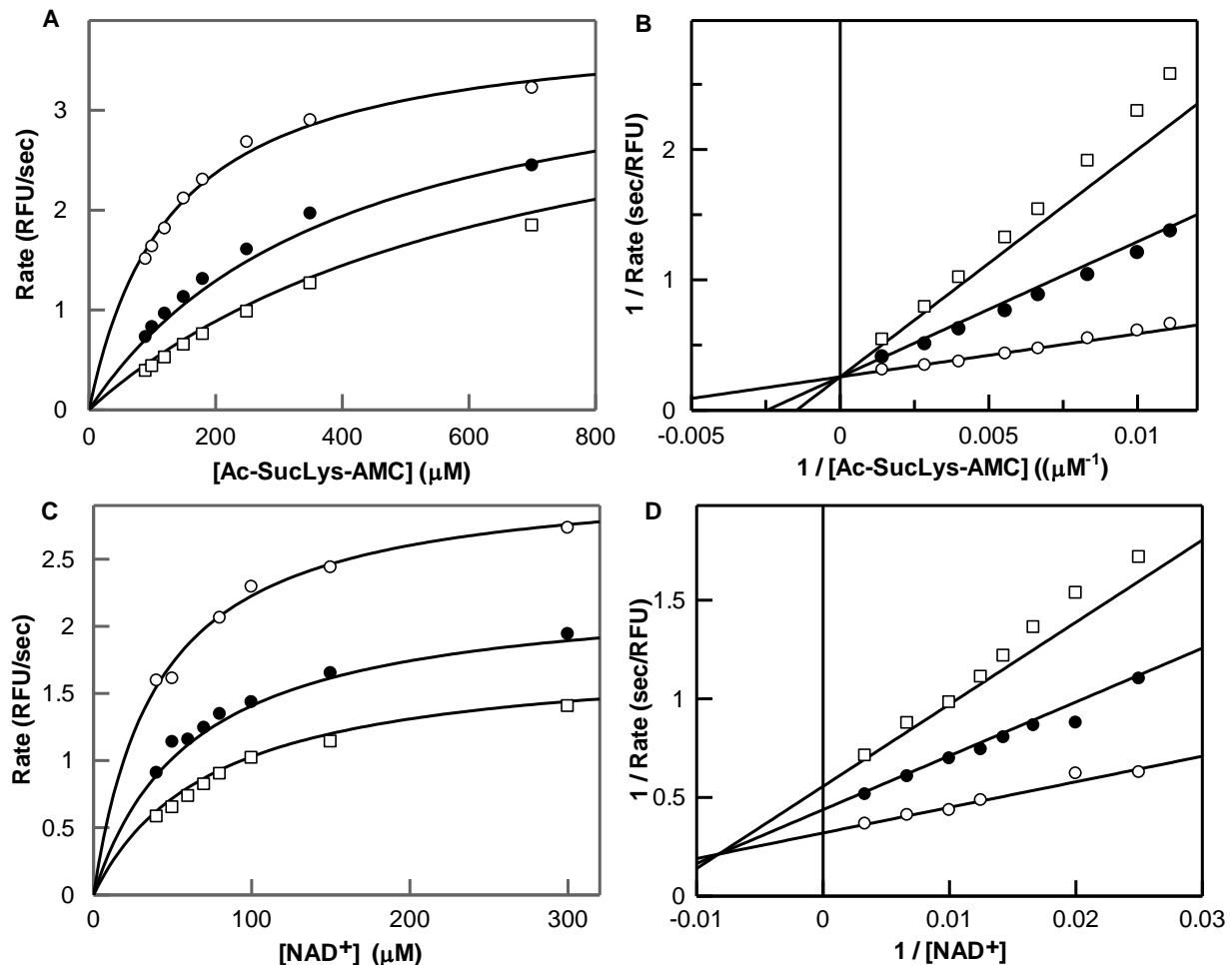


Figure 5.33. Steady-state kinetics for the inhibition of SIRT5 desuccinylase activity by suramin. (A) The wild-type SIRT5 catalyzed reactions were performed in the presence of 50  $\mu\text{M}$   $\text{NAD}^+$  and varying concentrations of Ac-SucLys-AMC (from 50 to 700  $\mu\text{M}$ ) in the presence of 0, 50 and 100  $\mu\text{M}$  suramin. The double-reciprocal plot of  $1/v$  vs  $1/[\text{Ac-SucLys-AMC}]$  at increasing concentration of suramin (B) are also shown. Data were fitted using Grafit software with the mixed inhibition model. (C) The wild-type SIRT5 catalyzed reactions were performed in the presence of 100  $\mu\text{M}$  Ac-SucLys-AMC and varying concentrations of  $\text{NAD}^+$  (from 40 to 300  $\mu\text{M}$ ) in the presence of 0, 50 and 100  $\mu\text{M}$  concentrations of suramin. The double-reciprocal plot of  $1/v$  vs  $1/[\text{NAD}^+]$  at increasing concentration of suramin (D) are also shown. Data were fitted using Grafit software with the mixed inhibition model.

### 5.3.5. Inhibition of sirtuins by nicotinamide

It has been proposed that the inhibition of several isoforms of sirtuins by nicotinamide is manifested via the “base-exchange” mechanism (i.e., the reversal of the step involved in the

formation of nicotinamide during the enzyme catalysis as elaborated in section §1.3.2; see Figure 5.34), and such event gives rise to the noncompetitive inhibition of the enzyme (68, 226, 227). Recently it has been proposed that with certain sirtuins (e.g., mouse SIRT2 and human SIRT3) the nicotinamide inhibition is mixed type with increasing component of the competitive inhibition (229). To ascertain the effect of nicotinamide on human SIRT1 and SIRT5 as well as its mutants in the presence of different substrates, detailed steady-state kinetic studies were performed via the same continuous (trypsin coupled) assay system as described in the previous sections. Figure 5.35 shows the steady-state rates and the corresponding double reciprocal plot for the SIRT5 catalyzed desuccinylation reaction as a function of succinylated substrate concentration (in the presence of 50  $\mu\text{M}$   $\text{NAD}^+$ ) at various fixed concentrations of nicotinamide. The double-reciprocal plots for the reactions in the presence of varying suramin (0, 100  $\mu\text{M}$ , 200  $\mu\text{M}$ ) and succinylated lysine concentration (90 to 700  $\mu\text{M}$ ) conform to the mixed inhibition model, with the  $K_i$  and  $K_i'$  values determined to be  $15.8 \pm 0.7 \mu\text{M}$  and  $71.2 \pm 7.7 \mu\text{M}$ , respectively. The higher  $K_i'$  value suggests that the inhibition potency of nicotinamide is reduced by approximately 5 folds after the binding of the succinylated substrate. The double-reciprocal plots for the reactions in the presence of varying suramin (0, 100  $\mu\text{M}$ , 200  $\mu\text{M}$ ) and succinylated lysine concentration (90 to 700  $\mu\text{M}$ ) conform to the mixed inhibition model, with the  $K_i$  and  $K_i'$  values determined to be  $15.8 \pm 0.7 \mu\text{M}$  and  $71.2 \pm 7.7 \mu\text{M}$ , respectively. The higher  $K_i'$  value suggests that the inhibition potency of nicotinamide is reduced by approximately 5 folds after the binding of the succinylated substrate. Figure 5.36 shows the steady-state rates and the corresponding double reciprocal plot for the SIRT5 catalyzed desuccinylation reaction as a function of  $\text{NAD}^+$  concentration (in the presence of 100  $\mu\text{M}$  succinylated substrate) at various fixed concentrations of nicotinamide. Although the double reciprocal plot of Fig 5.36B appeared

to be competitive in nature, to ensure its validity, the data were analyzed by the model discrimination analysis protocol of the DYNAFIT software (252-254). The above analysis confirmed that the nicotinamide inhibition data of Figure 5.36 adheres to the “pure” competitive inhibition model; the data could not be reliably fitted either by non-competitive, uncompetitive, or mixed inhibition model. As will be discussed in the later section (§5.3.6), the competitive inhibition of nicotinamide (against NAD<sup>+</sup>) is unlikely to be contributed by the base-exchange mechanism. When similar studies were performed for the inhibition of nicotinamide (against NAD<sup>+</sup>) with other mutant enzymes, it is notable that Y102A also showed the competitive inhibition (Figure 5.38). However, SIRT1 and SIRT5 Y102A/R105I double mutant showed the mixed type of inhibition (Figure 5.37 and 5.39), and such inhibition could either be partly or entirely contributed by the base-exchange mechanism.

Based on their findings on different sirtuins, Sauve and Shramm concluded that while the base-exchange inhibition of nicotinamide for bacterial and yeast enzymes partially impaired their catalytic activities, it resulted in nearly 95% inhibition of the mouse enzyme (68). The origin of such inhibitory potency of nicotinamide has been ascribed to the relative magnitude of the forward and reverse rates of formation and decay of the intermediate formed during the catalytic cycles of different sirtuins (Figure 5.34). It should be mentioned that partial inhibition of nicotinamide was not observed with either SIRT1 or SIRT5 or its mutants. Fisher et al. reported that while SIRT5 deacetylase activity is insensitive to the inhibition of the enzyme by nicotinamide, the enzyme’s desuccinylase activity is highly sensitive (i.e., strongly inhibited) to nicotinamide (228). They concluded that Arg105/succinate interaction accounted for the differential nicotinamide sensitivities of SIRT5 activities. The above conclusion appears to be corroborated by our finding of the nicotinamide inhibition with the mutant enzymes (see Table

5.9). For example, as shown in Figure 5.39 and table 5.9, Y102A is competitively inhibited by nicotinamide with a  $K_i$  value of  $49.1 \pm 4.1 \mu\text{M}$  in the presence of the succinylated substrate, but the above enzyme was only weakly inhibited (about 36% inhibition at  $800 \mu\text{M}$ ) in the presence of the acetylated substrate. Interestingly, the nicotinamide inhibition in terms of the deacetylase activity becomes more potent and conforms to the mixed mode in the case Y102A/R105I double mutant enzyme ( $K_i = 169.3 \pm 16.8 \mu\text{M}$ ,  $K_i' = 267.2 \pm 52.4 \mu\text{M}$ ). A similar mixed mode of inhibition was also observed with SIRT1 ( $K_i = 76.7 \pm 12.2 \mu\text{M}$ ,  $K_i' = 340.5 \pm 102.4 \mu\text{M}$ ) in the presence of the acetylated substrate. Apparently, both Y102 and R105 residues of SIRT5 coordinate with each other in modulating the sensitivity of nicotinamide inhibition during catalysis. Combining the aforementioned results of SIRT5 catalysis and inhibition, it is apparent evident that the binding of succinylated substrate to SIRT5 favorably promotes the binding of  $\text{NAD}^+$  which is competitively displaced by nicotinamide. Whether the origin of the above phenomenon is kinetically or thermodynamically controlled must await further studies.

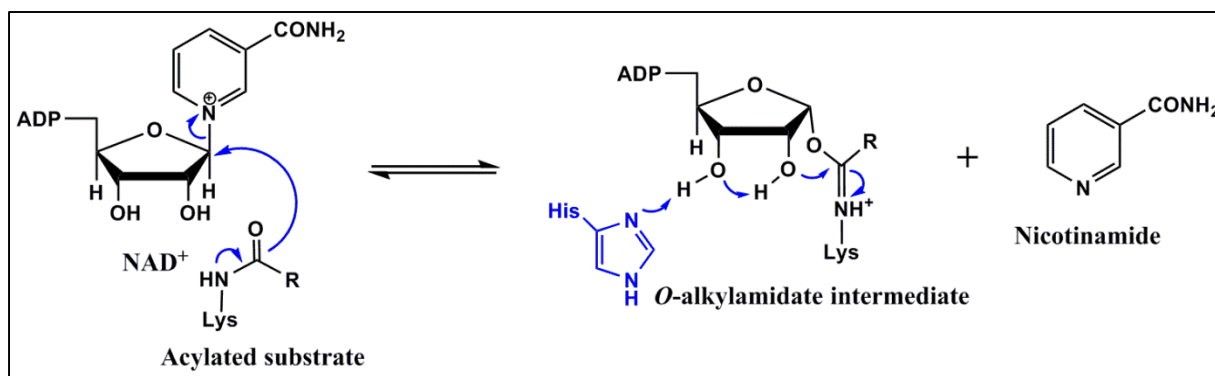


Figure 5.34. Proposed nicotinamide inhibition as a result of reversible cleavage of glycosidic bond of  $\text{NAD}^+$ . The chemical mechanism that unites base-exchange and deacetylation reactions arises from a covalent *O*-alkylamidate intermediate that releases nicotinamide from the active site. This intermediate is sufficiently stable to permit regeneration of  $\text{NAD}^+$  in the presence of elevated nicotinamide concentrations.



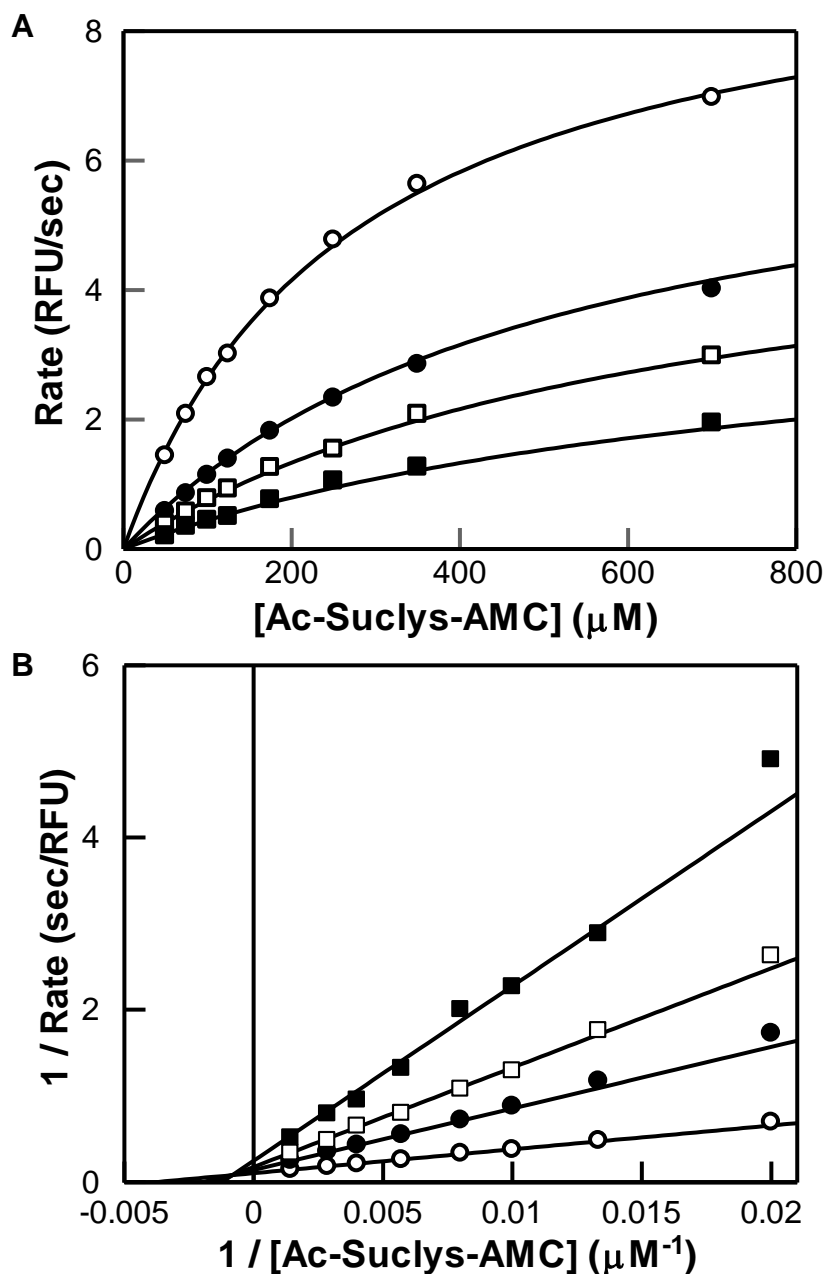


Figure 5.35. Inhibition of nicotinamide on SIRT5 with varying concentrations of Ac-Suclys-AMC. The wild-type SIRT5 catalyzed reactions (A) were performed in the presence of 50  $\mu\text{M}$   $\text{NAD}^+$  and varying concentrations of Ac-SucLys-AMC (from 50 to 700  $\mu\text{M}$ ) in the presence of 0, 25, 50 and 100  $\mu\text{M}$  concentrations of nicotinamide. The double-reciprocal plot of  $1/v$  vs  $1/[\text{Ac-SucLys-AMC}]$  at increasing concentration of nicotinamide (B) are also shown. Data were fitted using DYNAFIT software with the mixed inhibition model.

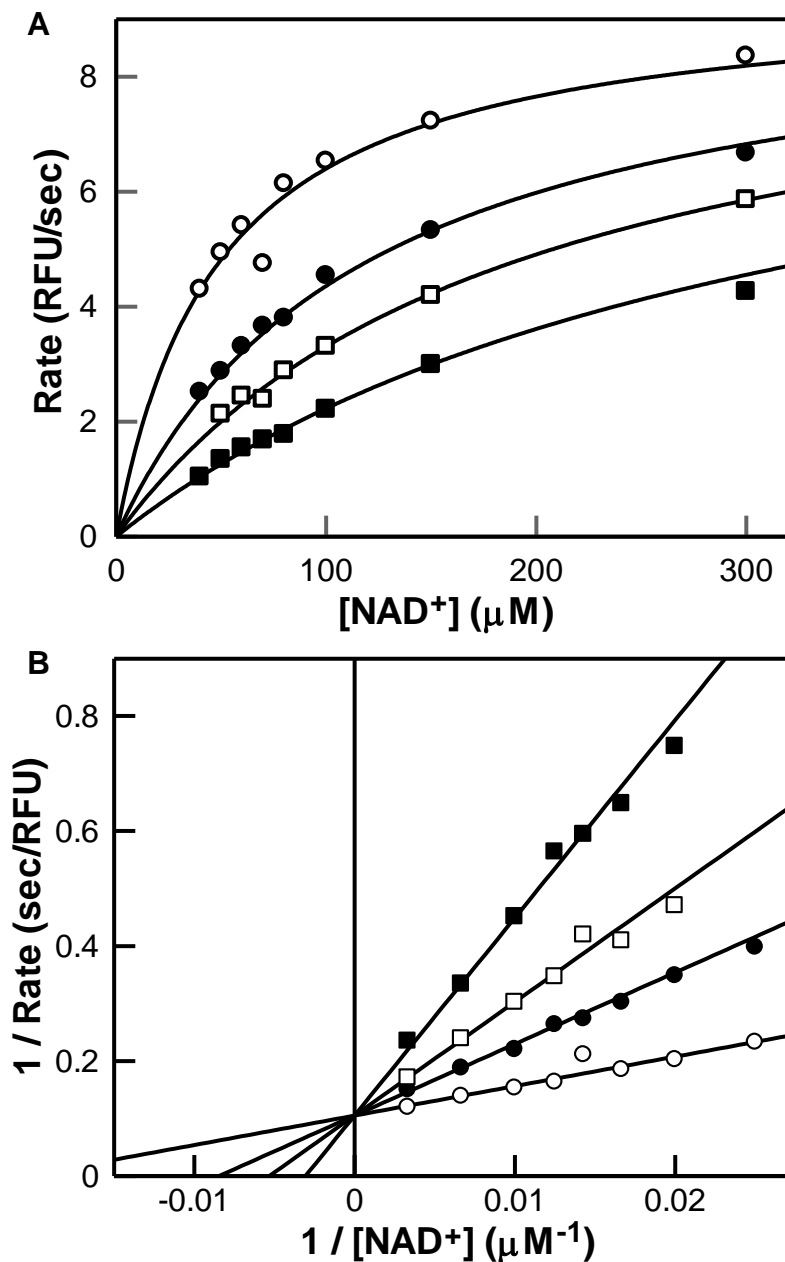


Figure 5.36. Inhibition of nicotinamide on SIRT5 with varying NAD<sup>+</sup>. The wild-type SIRT5 catalyzed reactions (A) were performed in the presence of 100 μM Ac-SucLys-AMC and varying concentrations of NAD<sup>+</sup> (from 40 to 300 μM) in the presence of 0, 25, 50 and 100 μM concentrations of nicotinamide. The double-reciprocal plot of 1/v vs 1/[NAD<sup>+</sup>] at increasing concentration of nicotinamide (B) are also shown. Data were fitted using DYNAFIT software with the competitive inhibition model and the derived K<sub>i</sub> values are summarized in Table 5.9.

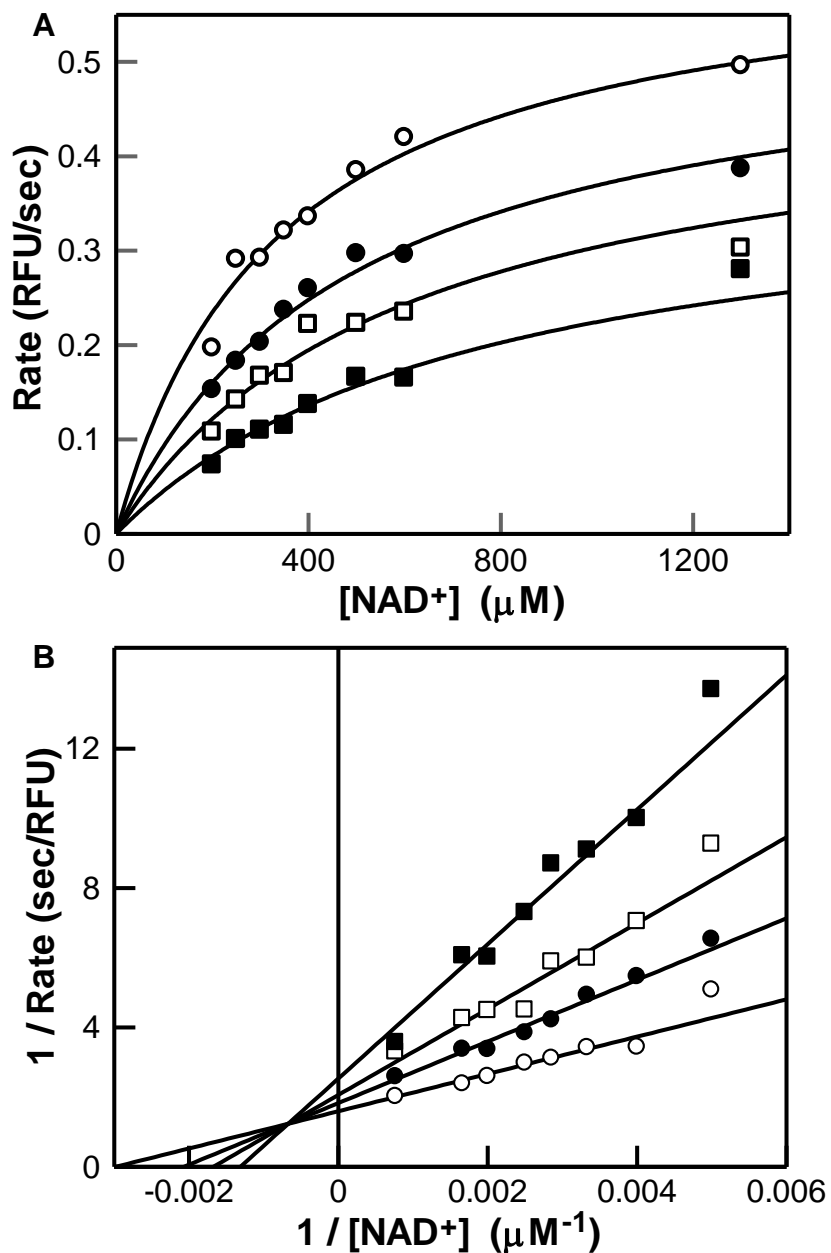


Figure 5.37. Inhibition of nicotinamide on SIRT1 with varying NAD<sup>+</sup>. SIRT1 reactions (A) were performed in the presence of 100 μM *Fluo-de-lys*<sup>®</sup> acetylated substrate, and varying concentrations of NAD<sup>+</sup> (from 40 to 300 μM) in the presence of 0, 50, 100, and 200 μM nicotinamide. The double-reciprocal plot of 1/v vs 1/[NAD<sup>+</sup>] at increasing concentration of nicotinamide (B) are also shown. Data were fitted using DYNAFIT software with the mixed inhibition model and the derived K<sub>i</sub> values are summarized in Table 5.9.

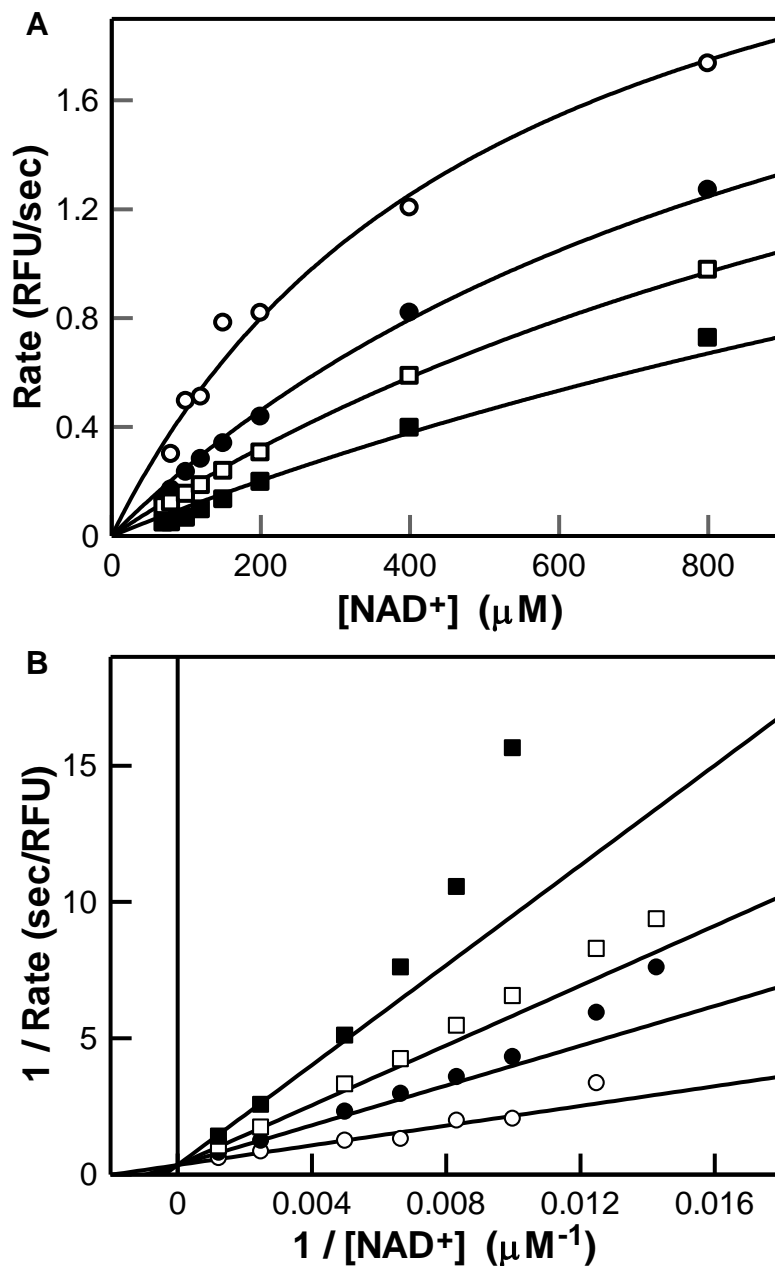


Figure 5.38. Inhibition of nicotinamide on SIRT5 Y102A with varying NAD<sup>+</sup>. The Y102A mutant catalyzed reactions (A) were performed in the presence of 500 μM Ac-SucLys-AMC and varying concentrations of NAD<sup>+</sup> (from 70 to 800 μM) in the presence of 0, 50, 100 and 200 μM nicotinamide. The double-reciprocal plot of 1/v vs 1/[NAD<sup>+</sup>] at increasing concentration of nicotinamide (B) are also shown. Data were fitted using DYNAFIT software with the competitive inhibition model and the derived K<sub>i</sub> values are summarized in Table 5.9.

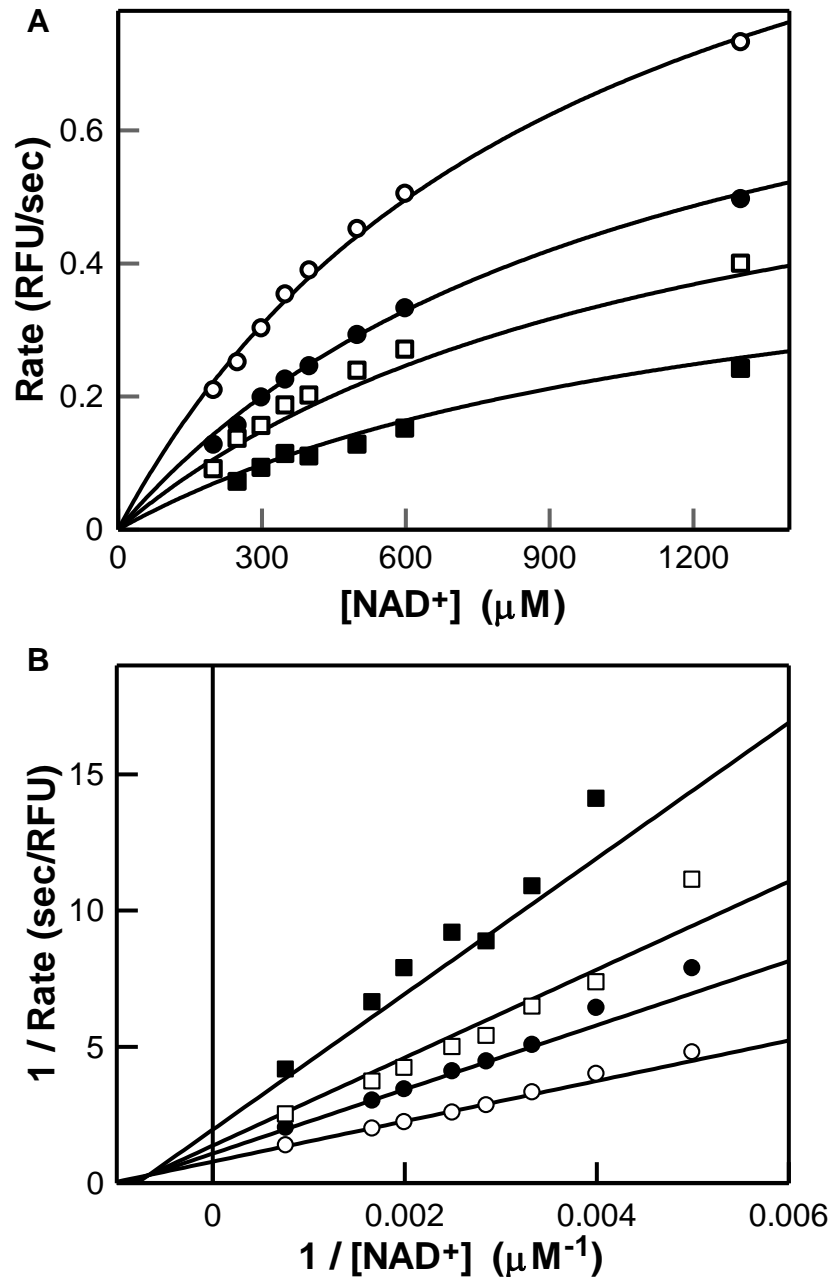


Figure 5.39. Inhibition of nicotinamide on SIRT5 Y102A/R102A with varying NAD<sup>+</sup>. The Y102A/R105I mutant catalyzed reactions (A) were performed in the presence of 500 μM *Fluo-de-lys*<sup>®</sup> acetylated substrate, and varying concentrations of NAD<sup>+</sup> concentration (from 200 to 1300 μM), in the presence of 0, 100, 200 and 400 μM nicotinamide. The double-reciprocal plot of 1/v vs 1/[NAD<sup>+</sup>] at increasing concentration of nicotinamide (B) are also shown. Data were fitted using DYNAFIT software with the mixed inhibition model and the derived K<sub>i</sub> values are summarized in Table 5.9.

Table 5.9. Nicotinamide inhibition against SIRT1 and SIRT1 variants

		Inhibition Mode	Inhibition Constant(s)
SIRT5	deacetylation	ND	ND
	desuccinylation	Competitive	$(17.5 \pm 1.1) \mu\text{M}$
SIRT5 Y102A	deacetylation	ND	N/A, 36% inhibition at $800\mu\text{M}$
	desuccinylation	Competitive	$(49.1 \pm 4.1) \mu\text{M}$
SIRT5 R105I	deacetylation	ND	N/A, 40% inhibition at $800\mu\text{M}$
	desuccinylation	ND	ND
SIRT5 Y102A R105I	deacetylation	Mixed	$K_i = (169.3 \pm 16.8) \mu\text{M}$ $K_r = (267.2 \pm 52.4) \mu\text{M}$
	desuccinylation	ND	ND
SIRT1	deacetylation	Mixed	$K_i = (76.7 \pm 12.2) \mu\text{M}$ $K_r = (340.5 \pm 102.4) \mu\text{M}$
	desuccinylation	ND	ND

### 5.3.6. Effects of isonicotinamide on sirtuin catalysis and inhibition

Isonicotinamide has been reported to serve as an activator of yeast sir2 both under in vitro and in vivo conditions, and the origin of its (activating) effect has been ascribed to the alleviation of the nicotinamide assisted reverse (base-exchange) reaction (222). To ascertain whether isonicotinamide activates SIRT1 or SIRT5, the initial rates of the enzyme catalyzed reactions were determined as a function of increasing concentrations of isonicotinamide. Figure 5.39 shows the normalized rates (represented as the relative rates) of SIRT1 catalyzed deacetylation reactions and SIRT5 catalyzed desuccinylation reactions as a function of increasing concentration of isonicotinamide in the presence of low ( $50 \mu\text{M}$ ) and high ( $5 \text{ mM}$ ) concentrations of  $\text{NAD}^+$ . The data of Figure 5.39 clearly shows that under neither of the above reaction conditions, the rates of the enzyme catalyzed reactions decrease upon increase in

isonicotinamide concentration. This observation is contrary to that observed for the other sir2 catalyzed reactions (222). The data of Figure 5.39A was analyzed by Eq. 4.6 as described in section §4.3.5, and obtained the magnitudes of  $IC_{50}$  values as being equal to  $7.0 \pm 2.9$  mM and  $8.9 \pm 3.3$  mM in the presence of 50  $\mu$ M and 5 mM  $NAD^+$ , respectively, for SIRT1. The corresponding  $IC_{50}$  values for SIRT5 under above condition were found to be  $11.1 \pm 2.2$  mM and  $17.1 \pm 4.0$  mM, respectively (Figure 5.39B). Note that although the  $IC_{50}$  values are slightly higher in the presence of higher concentration of  $NAD^+$ , they are not significant. To further confirm that isonicotinamide does not alleviate the nicotinamide inhibition, the  $IC_{50}$  values of nicotinamide for both SIRT1 (deacetylation) and SIRT5 (desuccinylation) were determined both in the absence and presence of 10 mM isonicotinamide (Table 5.9). The data of Table 5.9 suggests that there is only miniscule effect of isonicotinamide on the  $IC_{50}$  value of nicotinamide inhibition in case of both SIRT1 and SIRT5. However, since the inhibitory effect of isonicotinamide was found to be alleviated in the presence of high concentration of  $NAD^+$  in case of both SIRT1 and SIRT5 catalyzed reaction (Figure 5.39), it is reasonable to surmise that like nicotinamide, isonicotinamide also competes (directly) against the binding of  $NAD^+$  to the enzyme sites. The above results are consistent with the reports of Guan et al. revealing that isonicotinamide weakly inhibits human SIRT3 and does not alleviate the inhibition of nicotinamide (267).

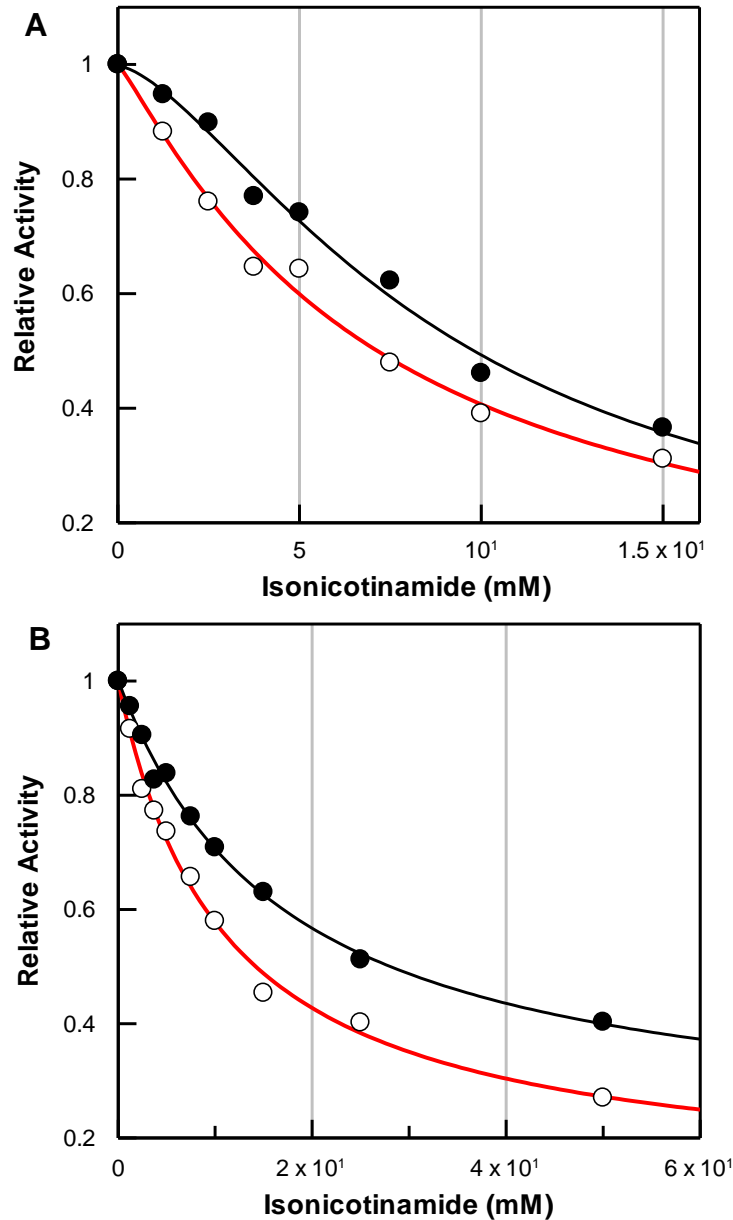


Figure 5.40. Effects of isonicotinamide on SIRT1 and SIRT5 catalyzed reactions. (A) Dose-response of SIRT1 deacetylation activity in the presence of varying concentrations of isonicotinamide (from 0 to 15 mM) and NAD<sup>+</sup> (50  $\mu$ M and 5 mM). The solid smooth lines represent the best fit of the data for the IC<sub>50</sub> values as  $7.0 \pm 2.9$  mM (in the presence of 50  $\mu$ M NAD<sup>+</sup>) and  $8.9 \pm 3.3$  mM (in the presence of 5 mM NAD<sup>+</sup>), respectively. (B) Dose-response of SIRT5 desuccinylation activity in the presence of varying concentrations of isonicotinamide (from 0 to 15 mM) and NAD<sup>+</sup> (50  $\mu$ M and 5 mM). The solid smooth lines represent the best fit of the data for the IC<sub>50</sub> values as  $11.1 \pm 2.2$  mM (in the presence of 50  $\mu$ M NAD<sup>+</sup>) and  $17.1 \pm 4.0$  mM (in the presence of 5 mM NAD<sup>+</sup>), respectively.



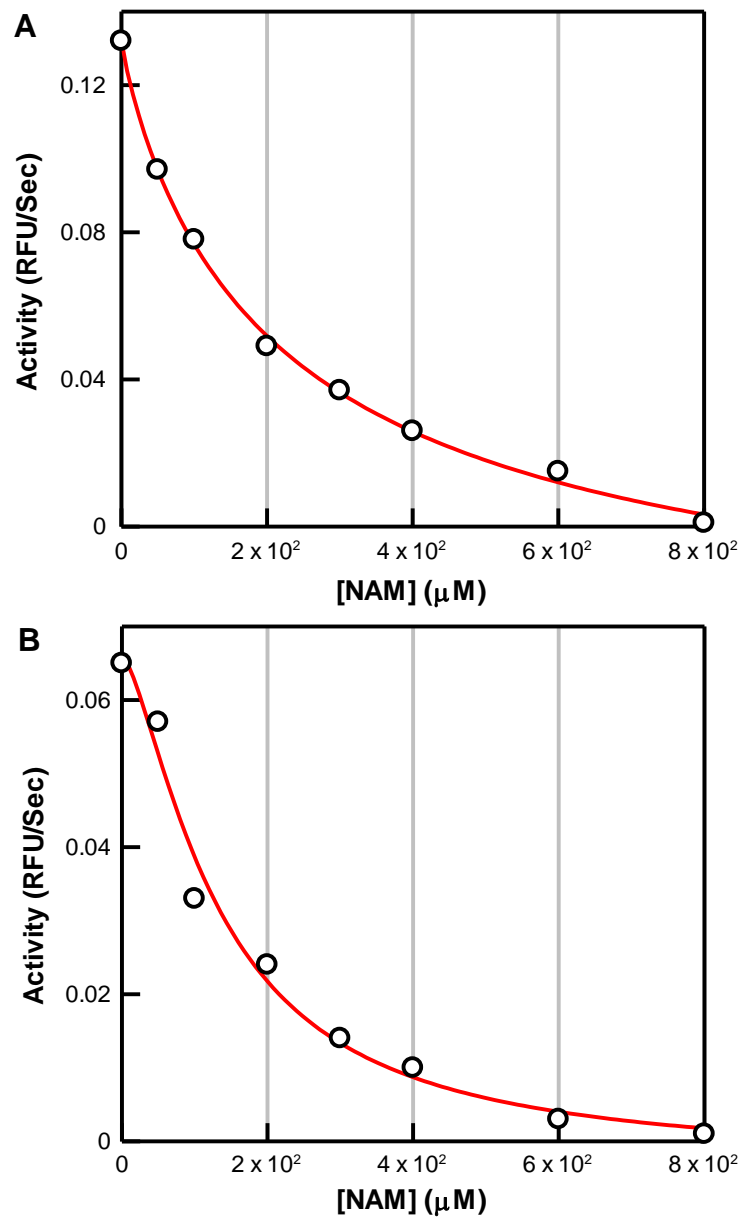


Figure 5.41. Effects of nicotinamide on SIRT1 catalyzed reaction in the absence (A) and presence (B) of isonicotinamide. The solid smooth lines represent the best fit of the data for the  $IC_{50}$  values as  $7.0 \pm 2.9$  mM (in the absence of isonicotinamide) and  $8.9 \pm 3.3$  mM (in the presence of 10 mM isonicotinamide), respectively.

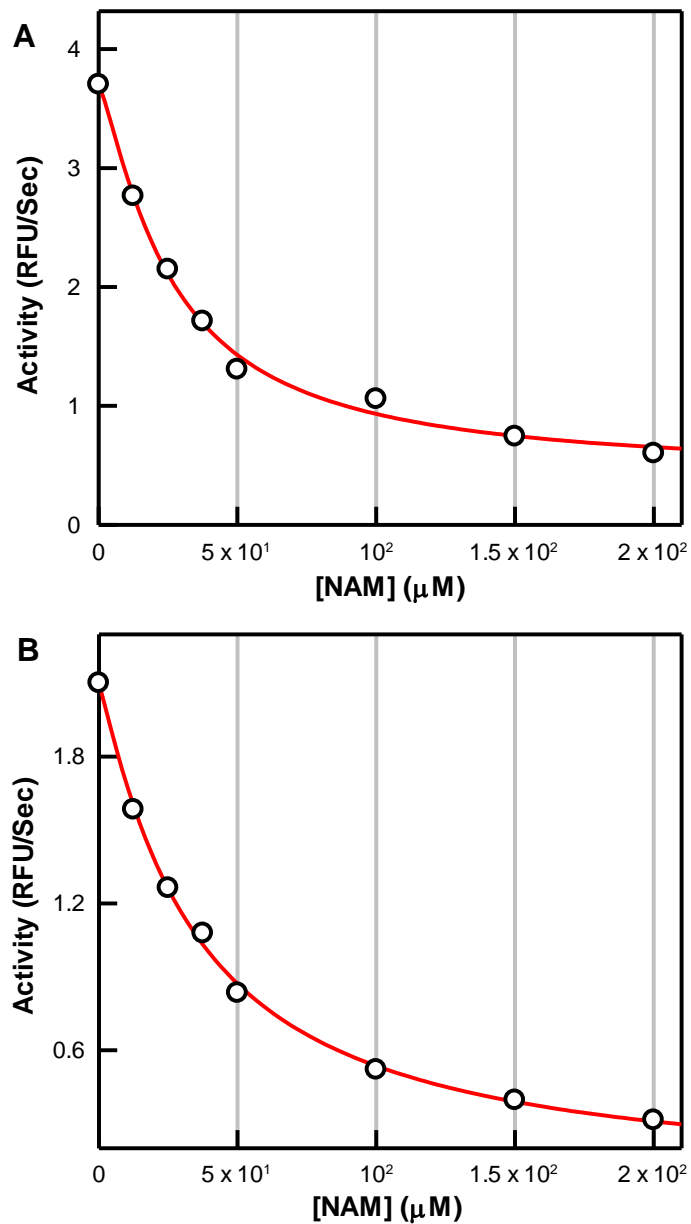


Figure 5.42. Effects of nicotinamide on SIRT5 catalyzed reaction in the absence (A) and presence (B) of isonicotinamide. The solid smooth lines represent the best fit of the data for the  $IC_{50}$  values as  $7.0 \pm 2.9$  mM (in the absence of isonicotinamide) and  $8.9 \pm 3.3$  mM (in the presence of 10 mM isonicotinamide), respectively.

Table 5.10. Isonicotinamide (iNAM) effect on the nicotinamide inhibition of SIRT1 and SIRT5

	IC <sub>50</sub> of Nicotinamide	
	In the absence of iNAM	In the presence of 10 mM iNAM
SIRT1	232.5 ± 52.7 μM	133.8 ± 27.2 μM
SIRT5	26.2 ± 2.9 μM	34.7 ± 3.4 μM

### 5.3.7. Inhibition of sirtuins by EX527

EX527 (6-chloro-2,3,4,9-tetrahydro-1H-carbazole-1-carboxamide; Figure 9A) is one of few compounds that possess both high inhibitory potency as well as isoform selectivity against sirtuins (239). This compound is also among the most studied of the published inhibitors and has been used as a standard inhibitor in biological studies (45, 268-270). EX527 inhibits SIRT1 but shows no effect on either deacetylase or desuccinylase activities of SIRT5. It has been suggested that the insensitivity of SIRT5 against EX527 is due to the unique Arg105 residue within the active site pocket of the enzyme. To date, however, there has been no experimental data to support or refute the above hypothesis. To probe the contributions of R105 and/or Y102 of SIRT5 in modulating the inhibitory potency of EX527, the initial rates of Y012A, R105I, and Y102A/R105I mutant catalyzed reactions were measured as a function of increasing concentrations of EX527. Figure 5.42 shows the relative activities of SIRT5 variants in the absence and presence of 50 μM EX527. The same as reported previously, neither the deacetylase nor the desuccinylase activity of wild-type SIRT5 was not inhibited by EX527 (45). On the other hand, EX527 showed about 14% inhibition against Y102A mutant SIRT5 with the *fluoride-lys*<sup>®</sup> substrate, but showed no inhibition with succinylated substrate. R105I mutant was found to be inhibited by about 22% by 50 μM EX527 in terms of both deacetylase and desuccinylase activities. The double mutant, Y102A/R105I, was inhibited by 36% and 69% by 50 μM EX527 in terms of deacetylase activity and desuccinylase activity, respectively. More interestingly, the

SIRT5 double mutant Y102A/R105I exhibited EX527 sensitivity comparable to that of human SIRT3. As shown in Figure 5.44, the  $IC_{50}$  value for the inhibition of the double mutant enzyme ( $21.7 \pm 1.0 \mu\text{M}$ ) was found to be similar to that reported ( $22.4 \pm 2.7 \mu\text{M}$ ) for the inhibition of SIRT3. However, the inhibitory potency of EX527 for SIRT1 ( $IC_{50} = 0.9 \pm 0.1 \mu\text{M}$ ; Figure 5.44) is still significantly higher than that accountable for the exclusive contributions of Y102 and/or R105 in SIRT5 (Figure 5.45). These data suggest that both Tyr102 and Arg105 mutually contribute to the sensitivity of inhibition by EX527 in SIRT1 versus SIRT5 enzymes during deacetylase reaction.

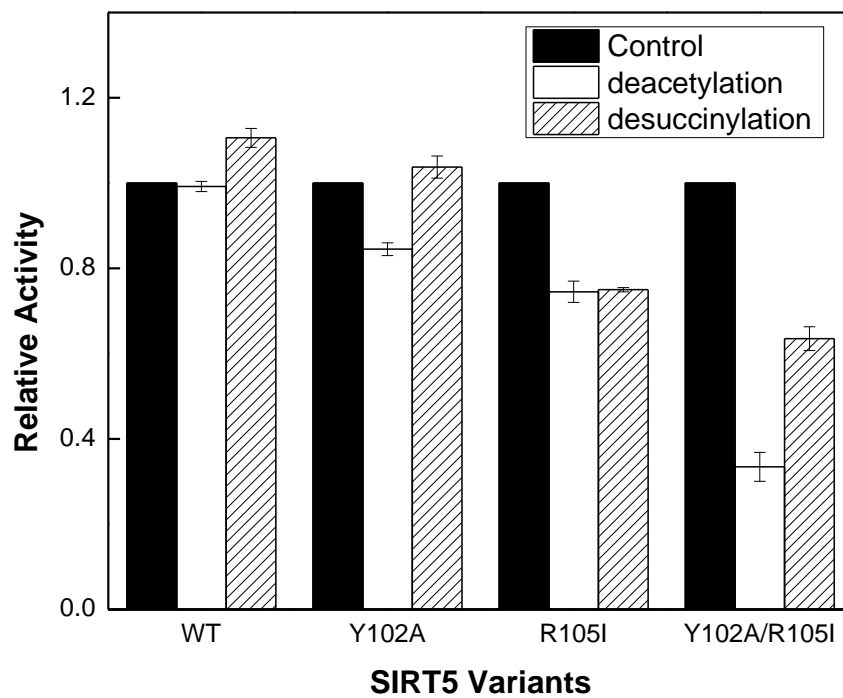


Figure 5.43. Effects of EX527 on SIRT5 variants catalyzed reactions. Relative activities of SIRT5 variants in the absence and presence of 50  $\mu\text{M}$  EX527 using 100  $\mu\text{M}$  *Fluor-de-lys*<sup>®</sup> substrate and  $\mu\text{M}$   $\text{NAD}^+$ .

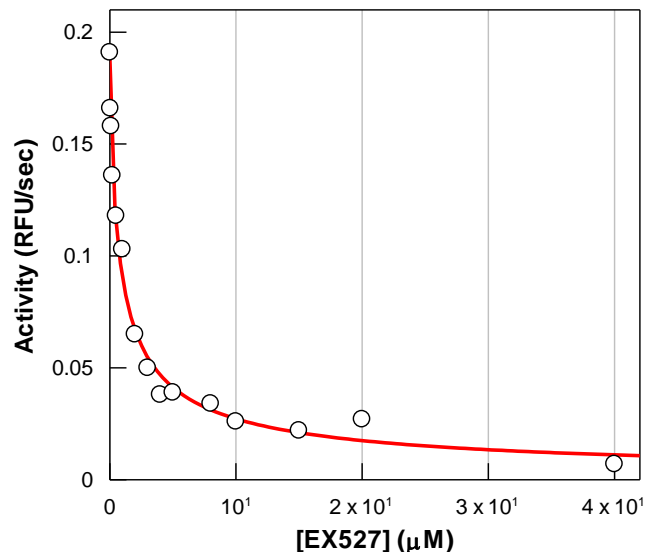


Figure 5.44. Steady-state kinetics for the inhibition of SIRT1 activity by EX527. Dose-response of SIRT1 deacetylase activity in the presence of 50 μM *Fluor-de-lys*<sup>®</sup> substrate, 50 μM NAD<sup>+</sup>, and increasing concentration EX527 (from 0 to 40 μM). The solid smooth lines represent the best fit of the data for the IC<sub>50</sub> of EX527 against SIRT1 as being equal to 0.9 ± 0.2 μM.

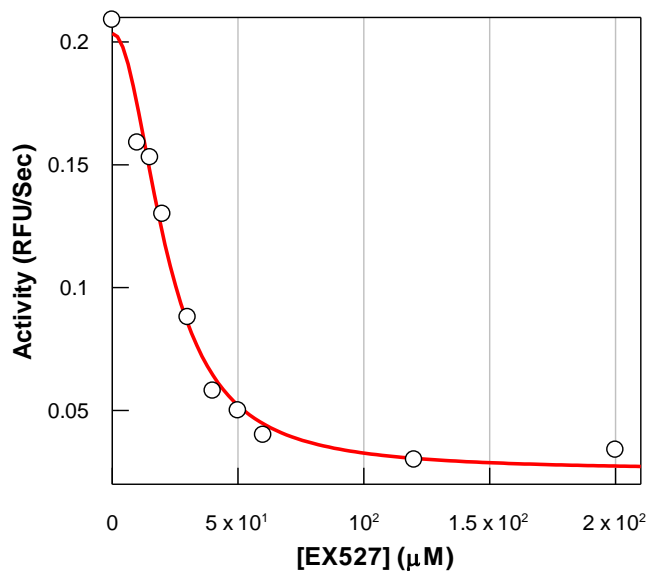


Figure 5.45. Steady-state kinetics for the inhibition of SIRT5 Y102A/R105I activity by EX527. Dose-response of SIRT5 Y102A/R105I deacetylase activity were tested in the presence of 50 μM *Fluor-de-lys*<sup>®</sup> substrate, 50 μM NAD<sup>+</sup>, and increasing concentration of EX527 (from 0 to 200 μM). The solid smooth lines represent the best fit of the data for the IC<sub>50</sub> of EX527 against SIRT5 Y102A/R105I as being equal to 21.7 ± 1.0 μM.

## 5.4. Spectroscopic, Kinetic, and Thermodynamic Basis for the Binding of Selected Inhibitors to Sirtuins

### 5.4.1. Binding of MH5-75 to SIRT5

As demonstrated in section §5.3.2, MH5-75 serves as a non-competitive inhibitor against SIRT5 with micromolar inhibition potency. Since the compound contains a coumarin group, it is expected to possess specific spectroscopic properties. Figure 5.46 A shows the absorbance spectrum of MH5-75 in 10 mM HEPES, pH 7.5, 100 mM NaCl, 10 % glycerol and 1 mM TCEP. The absorbance spectrum of MH5-75 has two peaks at 264 and 410 nm. In order to determine the influence of SIRT5 on the absorbance of MH5-75, the absorption spectrum of MH5-75 in the presence of SIRT5 was recorded at different time intervals (Figure 5.46 B). Note that SIRT5 enzyme itself possesses strong absorbance between 260 to 300 nm (see section §5.1.3.1). In order to assess the kinetics of SIRT5 induced changes in the electronic structure of MH5-75, the absorption contributions of the individual species were subtracted from their mixture (Figure 5.46B). The data of Figure 5.46B clearly shows that while the peak at 410 nm decreased, a new peak at 445 nm started to emerge as a function of time, suggesting that the 410 nm peak was slowly red shifted to 445 nm upon binding of MH5-75 to the enzyme. Such time-dependent spectral changes are suggestive of the slow conformational changes in the SIRT5 structure in concomitance with red shift in the electronic spectra of the ligand.

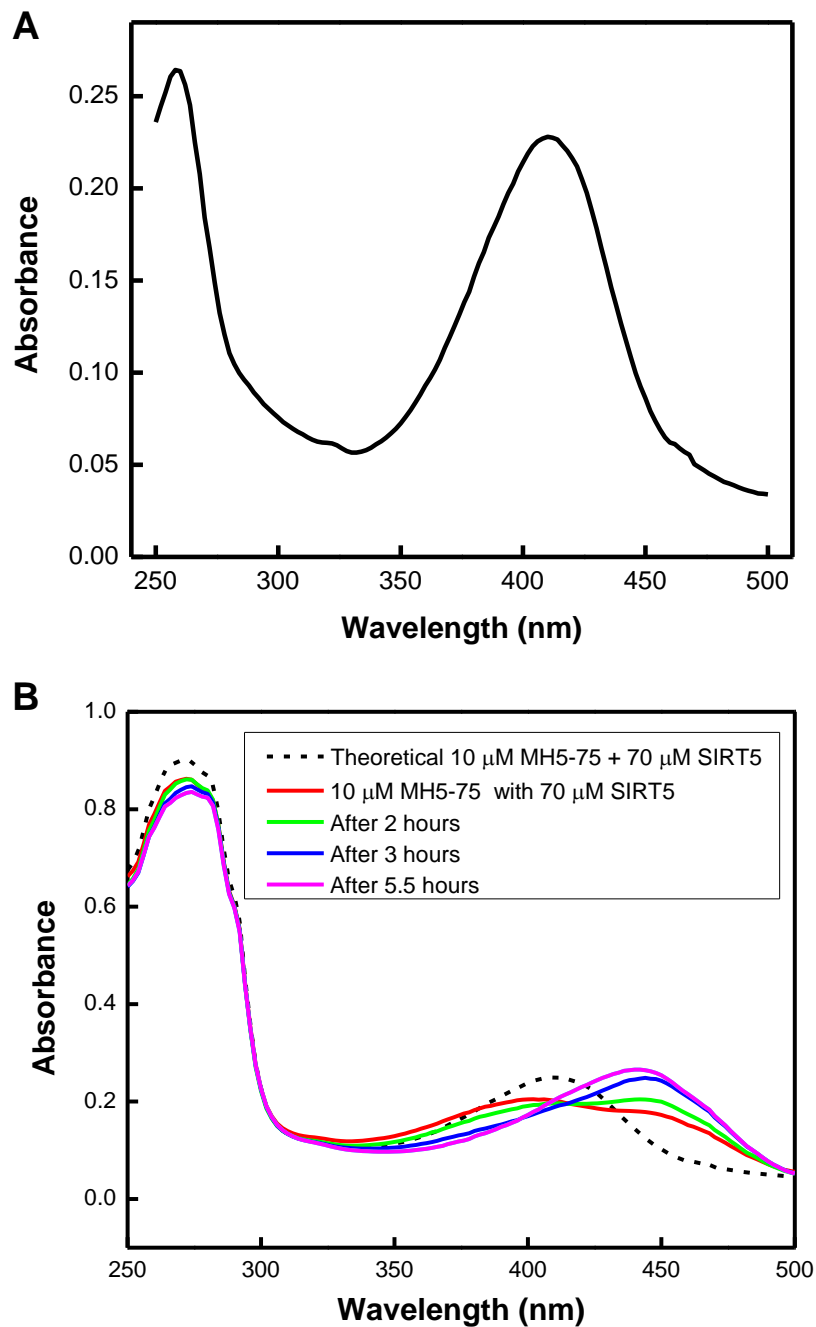


Figure 5.46. Time-dependent changes in the UV/Vis absorption spectra of MH5-75 in the presence of SIRT5. (A) 10  $\mu\text{M}$  MH5-75 was prepared in 10 mM HEPES, pH 7.5, 100 mM NaCl, 10 % glycerol and 1 mM TCEP and the absorption spectrum was measured in a quartz cuvette. (B) 10  $\mu\text{M}$  MH5-75 was incubated with 70  $\mu\text{M}$  SIRT5, and the absorption spectra was measured immediately (red), after 2 hours (green), 3 hours (blue) and 5.5 hours (pink) in a cuvette. The dash line represents the theoretical add-up of the spectra of 70  $\mu\text{M}$  SIRT5 and 10  $\mu\text{M}$  MH5-75.



## 5.4.2. Binding studies of SIRT1 and suramin

### 5.4.2.1. Binding isotherms of suramin to SIRT5

As mentioned in section §5.1.3, changes in intrinsic fluorescence of proteins upon binding of their cognate ligands are widely utilized to study protein-ligand interactions. In order to investigate the intrinsic fluorescence change of SIRT5 in the presence of suramin, the steady state fluorescence emission spectra of SIRT5 ( $\lambda_{\text{ex}} = 280 \text{ nm}$ ) in the absence and presence of suramin were determined on a Perkin Elmer lambda 50-B spectrofluorometer in the enzyme storage buffer (50 mM Tris-HCl, pH 7.5, containing 100 mM NaCl, 10 % glycerol and 1 mM TCEP) as described in section §4.5.1, and the result is shown in Figure 5.47 A. Note that upon binding of 1  $\mu\text{M}$  suramin, approximately 80% of the intrinsic protein fluorescence of 1  $\mu\text{M}$  SIRT5 was quenched without any shift in the fluorescence emission peak. The binding isotherm of the SIRT5-suramin complex was determined by monitoring the change in the protein fluorescence at 334 nm ( $\lambda_{\text{ex}} = 280 \text{ nm}$ ) as a function of the ligand concentration as described in the Methods section (section §4.5.1). Figure 5.64 B shows the fluorescence intensity of 1  $\mu\text{M}$  SIRT5 as a function of increasing concentration of suramin. As the concentration of SIRT5 was comparable to that of the ligand during the course of the titration, the binding isotherm was analyzed by a complete solution of the quadratic equation (Eq. 4.12 in section §4.5.1). The solid line is the best fit of the titration data, yielding the equilibrium dissociation constant ( $K_d$ ) of SIRT5-suramin complex as being equal to  $0.13 \pm 0.01 \mu\text{M}$ . Note that that the  $K_d$  value obtained by the above titration is about two orders of magnitude lower than the inhibition constant (50  $\mu\text{M}$ ) of suramin determined via the steady state enzyme kinetic assay. The origin of the above discrepancy is believed to lie in more than one binding site of suramin in SIRT5; while binding

of suramin with SIRT5 at one of the sites was responsible the spectral changes, that to the other site caused the enzyme inhibition.

The above studies were performed for the binding of suramin to SIRT1 as well. Figure 5.65 shows the quenching of the intrinsic fluorescence of SIRT1 in the presence of suramin (Figure 5.65 A), giving rise to the binding isotherm of SIRT1-suramin complex (Figure 5.65 B). The solid line is the best fit of the data for the  $K_d$  value of SIRT1-suramin complex as being equal to  $0.6 \pm 0.1 \mu\text{M}$ . It is noteworthy that the latter  $K_d$  value of SIRT1-suramin complex is comparable to the apparent inhibition constant ( $1.1 \mu\text{M}$ ) of suramin during SIRT1 catalyzed reaction, suggesting that the suramin binding site which quenches the intrinsic fluorescence of SIRT1 is also responsible for inhibition of the enzyme.

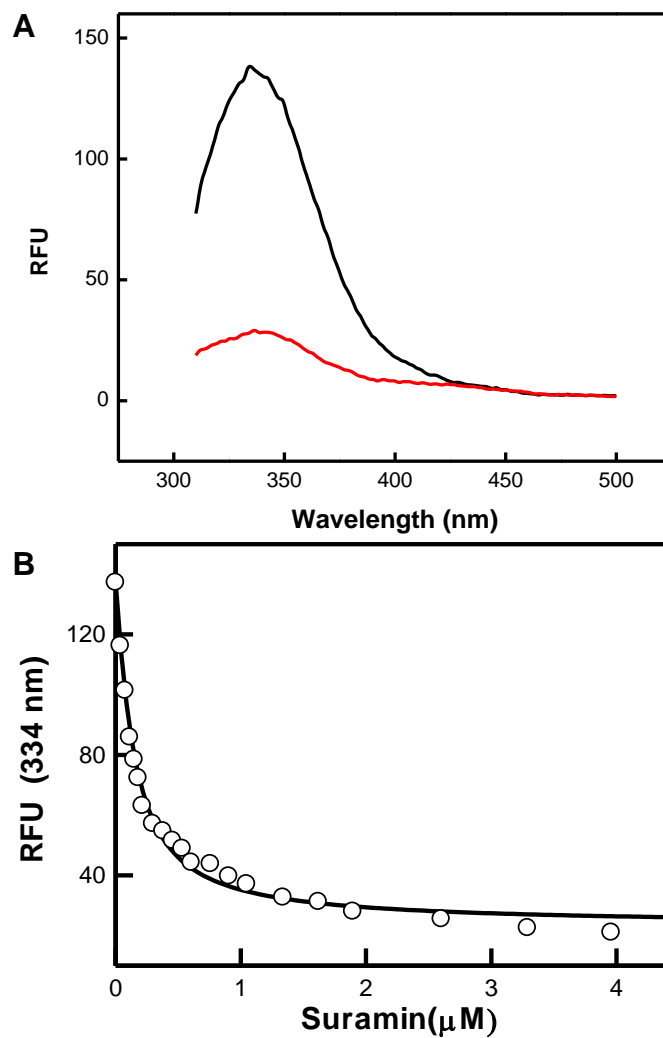


Figure 5.47. Binding isotherm for the interaction of suramin with SIRT5. (A) Fluorescence spectra of 1  $\mu\text{M}$  SIRT5 ( $\lambda_{\text{ex}} = 280 \text{ nm}$ ) in the absence of suramin and presence of 1  $\mu\text{M}$  suramin. (B) Binding affinity of the SIRT5-suramin complex. The decrease in intensity at 334 nm on titration of suramin into 1  $\mu\text{M}$  SIRT5 is plotted as a function of suramin concentration. The smooth line is the best fit of the data for the  $K_d$  value of the SIRT5-suramin complex being equal to  $0.13 \pm 0.01 \mu\text{M}$ .

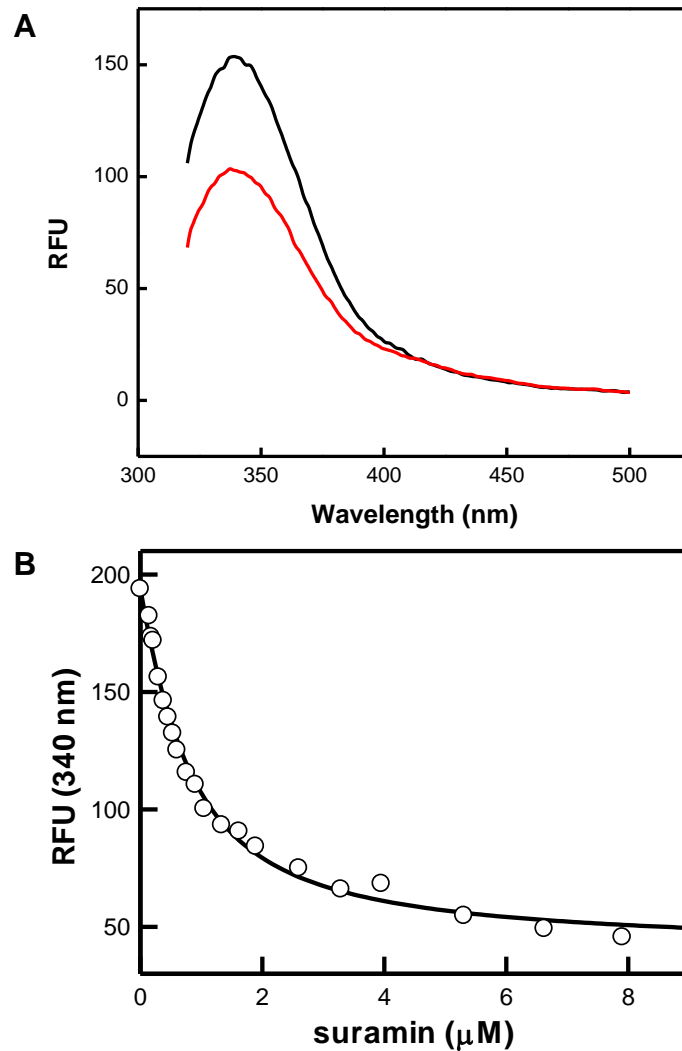


Figure 5.48. Binding isotherm for the interaction of suramin with SIRT1. (A) Fluorescence spectra of 1  $\mu\text{M}$  SIRT1 ( $\lambda_{\text{ex}} = 280 \text{ nm}$ ) in the absence of suramin and presence of 1  $\mu\text{M}$  suramin. (B) Binding affinity of the SIRT1-suramin complex. The decrease in intensity at 340 nm on titration of suramin into 1  $\mu\text{M}$  SIRT1 is plotted as a function of suramin concentration. The smooth line is the best fit of the data for the  $K_d$  value of the SIRT1-suramin complex being equal to  $0.6 \pm 0.1 \mu\text{M}$ .

#### ***5.4.2.2. Time-resolved fluorescence spectroscopic studies for the ligand-induced conformational changes in SIRT5***

To determine the mechanism of quenching of intrinsic fluorescence of SIRT5 by suramin, the fluorescence lifetime studies were performed. The time course of the decay of excited state population of 5  $\mu\text{M}$  SIRT5 in the absence and presence of 1  $\mu\text{M}$  suramin were recorded ( $\lambda_{\text{ex}} = 280 \text{ nm}$ ,  $\lambda_{\text{em}} = 336 \text{ nm}$ ) via a custom designed fluorescence-lifetime instrument as described in section §4.2.3. Figure 5.66 shows the tryptophan fluorescence decay curves of free and the ligand (suramin)-bound form of SIRT5 (the black and blue traces, respectively) in 25 mM Tris-Cl, pH 7.5, 100 mM NaCl, 10 % glycerol and 1 mM TCEP. The experimental data were fitted using the double exponential rate equation (Eq. 4.1). The red smooth lines are the best fit of the data for the free form of SIRT5 using the double exponential rate equation, yielding the short ( $\tau_1$ ) and long ( $\tau_2$ ) life times as being equal to  $0.78 \pm 0.01 \text{ ns}$  and  $4.09 \pm 0.03 \text{ ns}$ , respectively, with their respective amplitude of 34% and 66% as calculated by Eq. 4.2. The corresponding lifetime values for the suramin-bound form of SIRT5 were as follows:  $\tau_1 = 0.38 \pm 0.10 \text{ ns}$  and  $\tau_2 = 2.26 \pm 0.16 \text{ ns}$  with their associated amplitudes being equal to 45% and 55 %, respectively. Evidently, both the short and long lifetimes of SIRT5 were reduced by approximately two fold upon the binding of suramin, which could be attributed to the change in the microenvironment of the enzyme as a result of conformational modulation in the protein structure upon binding of the ligand. However, the precise deduction of the microenvironment of individual tryptophan moieties in SIRT5 could not be achieved due to the inherent complexity of the fluorescence decay curves.

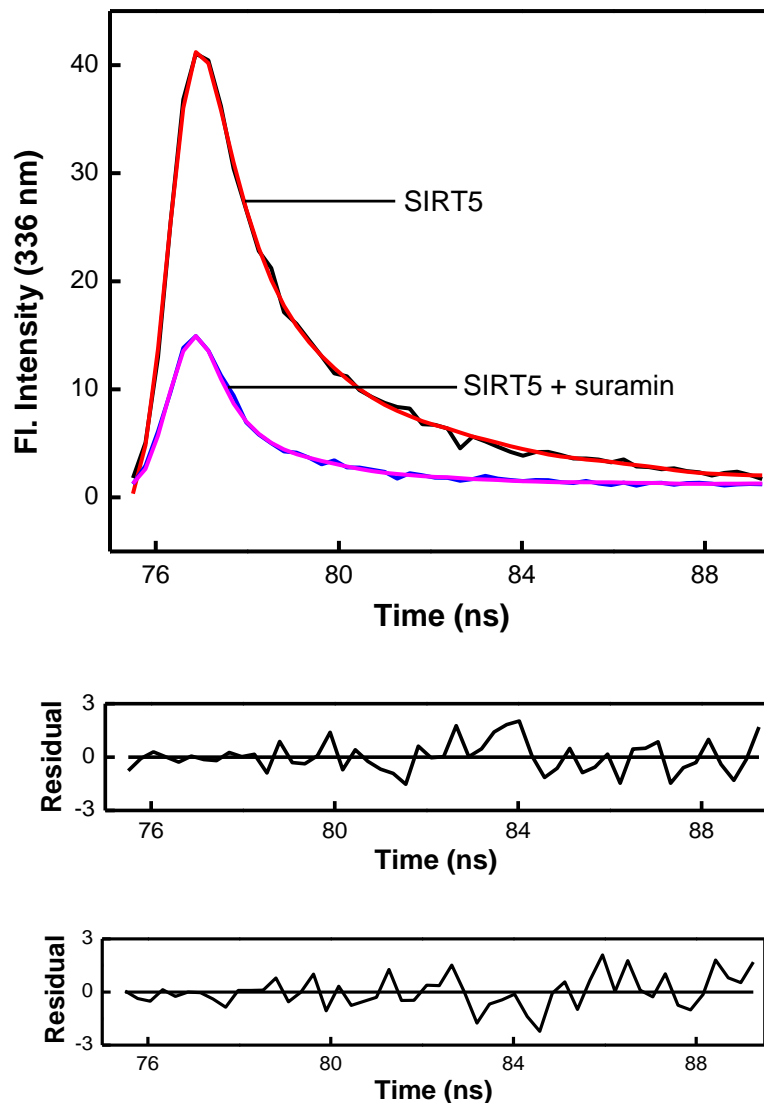


Figure 5.49. The time resolved fluorescence decay curve of the tryptophan residues of 5  $\mu\text{M}$  SIRT5 in the absence and presence of 1  $\mu\text{M}$  suramin. The red solid smooth line is the best fit of the data in the absence of suramin for the double exponential rate equation with short ( $\tau_1$ ) and long ( $\tau_2$ ) lifetimes of  $0.50 \pm 0.09$  ns and 3.05 ns (fixed), respectively. The pink solid smooth line is the best fit of the data in the presence of 1  $\mu\text{M}$  suramin for the double exponential rate equation for the double exponential rate equation with short ( $\tau_1$ ) and long ( $\tau_2$ ) lifetimes of  $0.38 \pm 0.10$  ns and  $2.26 \pm 0.16$  ns, respectively. The bottom panel shows the residuals of the fit of the lifetime trace.

### 5.4.2.3. *Transient kinetic studies for the binding of suramin to SIRT5*

The quenching of the intrinsic protein fluorescence of SIRT5 upon binding of suramin served as the signal for pursuing the transient kinetic studies for their interactions via the stopped-flow system as described in Methods section (section §4.4). The transient kinetic studies for the association of suramin with SIRT5 were conducted by mixing varying concentrations of the inhibitor and 1  $\mu\text{M}$  enzyme via the stopped-flow syringes and monitoring the change in the fluorescence signal using the excitation wavelength of the Xenon lamp of 280 nm and the emission cutoff filter of 320 nm. A representative kinetic trace for the association of suramin with SIRT5 is shown in Figure 5.50. The data were analyzed by the double exponential rate equation (Eq. 4.10 in section §4.4), yielding the relaxation rate constants for the fast and the slow phases as being equal to  $5.6 \pm 0.09 \text{ s}^{-1}$  and  $0.21 \pm 0.01 \text{ s}^{-1}$ , respectively. While the fast phase was attributed to the initial binding/encounter of the inhibitor to the active site of the enzyme, the slow phase was due to the isomerization of the initial encounter complex.

The above kinetic studies were extended at increasing concentrations of suramin (from 4 to 12  $\mu\text{M}$ ) while maintaining a fixed concentration of the enzyme (the pseudo first-order condition). The resulting data conformed to the double exponential rate, and the observed rates increased or remained constants as a function of suramin concentration (Figure 5.68). The data of Figure 5.68 reveals that the fast phase showed the linear (first order) dependence on the suramin concentration, yielding the gradient and intercept as being equal to  $7.5 \pm 7.0 \mu\text{M}^{-1}\text{s}^{-1}$  and  $468.0 \pm 59.9 \text{ s}^{-1}$ , respectively. The data for the slow phase showed the zero order dependence on suramin concentration with the Y-Axis intercept as being equal to  $53 \pm 8.2$ . However due to technical difficulties in performing the transient kinetic experiments at lower concentrations of suramin

while maintaining the pseudo-first condition, the individual microscopic rate constants for SIRT5-sruamin interactions could not be reliably determined.

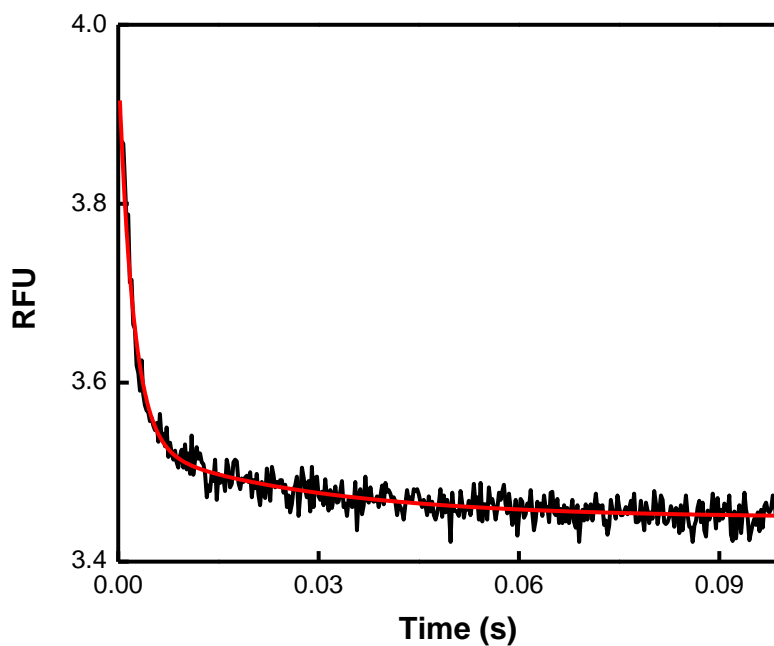


Figure 5.50. The representative stopped flow trace for the association of SIRT5 and suramin. The association of the enzyme with the ligand was triggered by mixing 2  $\mu\text{M}$  SIRT5 with 10  $\mu\text{M}$  suramin in 10 mM Tris-Cl, pH 7.5, 100 mM NaCl, 10 % glycerol and 1 mM TCEP. The reaction was monitored at 280 nm. The solid smooth line is the best fit of the data with double exponential rate equation, yielding the relaxation rate constants for the fast and the slow phase as  $5.58 \pm 0.09 \text{ s}^{-1}$  and  $0.21 \pm 0.01 \text{ s}^{-1}$ , respectively.



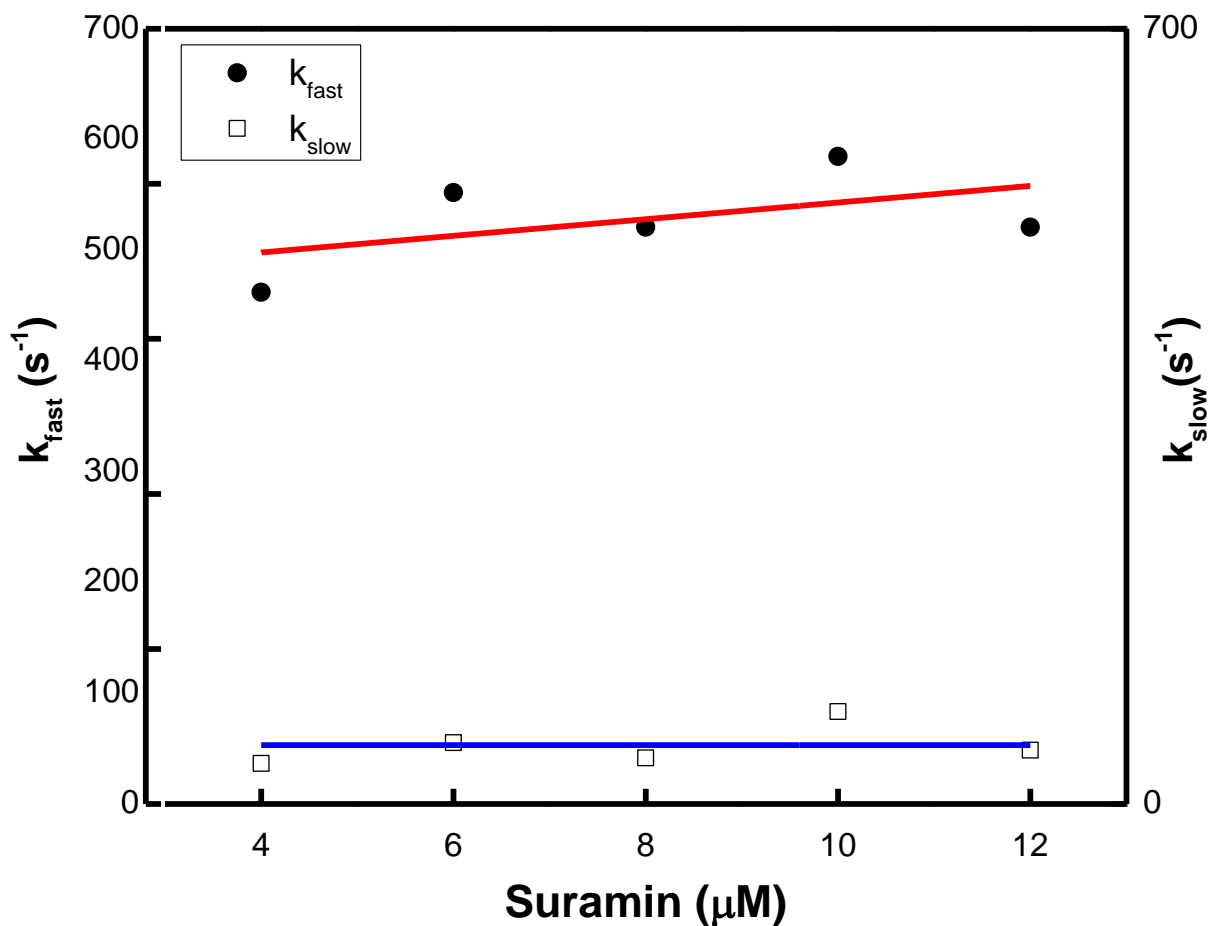


Figure 5.51. Dependence of the observed rate constants on suramin concentrations for the association of suramin to SIRT5.  $k_{\text{fast}}$  and  $k_{\text{slow}}$  depict the fast and slow observed rate constants as a function of suramin concentration, respectively. The data for the fast phase were fitted with linear regression, yielding the gradient and intercept as  $7.5 \pm 7.0 \text{ s}^{-1} \mu\text{M}^{-1}$  and  $468.0 \pm 59.9 \text{ s}^{-1}$ , respectively. The data for the slow phase were fitted with horizontal line with the intercept determined to be  $53.1 \pm 8.2 \text{ s}^{-1}$ .

#### 5.4.2.4. ITC profiles for the binding of suramin to SIRT5

The X-ray crystallographic as well as the isothermal titration calorimetric (ITC) data of Schuetz et al. demonstrated that two molecules of SIRT5 were bridged by one (symmetrical) suramin molecule to form a dimer, and the overall ITC binding profile confirmed to the single site binding model with  $K_d$  as being equal to  $5.5 \mu\text{M}$  (34). besides the hydrogen bonds formed

between the trisulfonylnaphthyl groups of suramin and amino acid residues in the active site pocket, the structural data of SIRT5-suramin complex also showed hydrogen bonds between the urea (NH-CO-NH) group (the symmetric point) and Y255 on the surface of one SIRT5 molecule (Figure 5.52) which seems to stabilize the dimerization. However, the above binding affinity was not significantly different from that observed for the binding of suramin to SIRT1, which does not appear form the dimeric structure (see below). To probe the origin of the above anomaly, a series of ITC experiments were performed using different concentrations of SIRT5 and suramin in the enzyme storage buffer (50 mM Tris-HCl, pH 7.5, containing 100 mM NaCl, 10 % glycerol and 1 mM TCEP at 25 °C). Figure 5.53 shows the ITC profile for the titration of 50  $\mu$ M SIRT5 with 45 aliquots (3  $\mu$ L each of first 10 titrants and 5  $\mu$ L each of the remaining 35 titrants) of 700  $\mu$ M suramin. However, in a marked contrast to the ITC binding profile of Sheutz et al. (conforming to the single site binding model of surmain to SIRT5), the above ITC data revealed that, under the above experimental condition, suramin binds to SIRT5 at least in two distinct modes. As apparent both from the raw (top panel of Figure 5.53) as well as the calculated ITC signals (bottom panel of Figure 5.53), the binding isotherm of SIRT5-suramin complex could not be fitted by the single site binding model. The ITC data, however, could be fitted by a minimal two independent binding site model (solid smooth line in the bottom panel of Figure 5.53), and the analytical outcome yielded the stoichiometry ( $n$ ), equilibrium association constants ( $K_a$ ) and the enthalpy changes ( $\Delta H^\circ$ ) for the binding of suramin to the first site as being equal to  $0.2 \pm 0.0$ ,  $(6.2 \pm 2.1) \times 10^6 \text{ M}^{-1}$ , and  $-2.6 \pm 0.3 \text{ kcal/mol}$ , respectively. The corresponding parameters for the binding of suramin to SIRT5 at the second binding site were derived to be  $0.64 \pm 0.01$ ,  $(2.3 \pm 0.1) \times 10^5 \text{ M}^{-1}$ , and  $-12.5 \text{ kcal/mol}$ , respectively. Based on these parameters, the entropic changes ( $T\Delta S^\circ$ ) for the binding of suramin to first and second binding sites of SIRT5 were found

to be 4.9 and -5.1 kcal/mol, respectively. Clearly, while the binding of suramin to the first site of SIRT5 is entropically driven, that to the second site is enthalpically driven.

To ascertain whether the binding isotherm for the SIRT5-suramin complex invariably conformed to the two site binding model (Figure 5.53), the above ITC studies were performed under two different experimental conditions: (1) titration of 50  $\mu\text{M}$  SIRT5 with 45 aliquots (5  $\mu\text{L}$  each) of 1 mM suramin (Figure 5.54A), and (2) titration of 5  $\mu\text{M}$  of SIRT5 with 45 aliquots (3  $\mu\text{L}$  each for the first 10 titrants followed by 5  $\mu\text{L}$  each of the remaining 35 titrants) of 200  $\mu\text{M}$  suramin (Figure 5.54B). Note that under both these experimental conditions, the first binding site peaks remain unresolved. In ITC titration of Figure 5.54A, it appears that the first site of SIRT5 becomes nearly saturated by the first 5  $\mu\text{L}$  aliquot of 1 mM suramin, and thus it is not detected. On the other hand, in Figure 5.54B, due to low stoichiometry and enthalpic values for the binding of suramin to the first binding site of SIRT5, it remains masked by the higher magnitudes of the stoichiometry and pronounced enthalpic contributions for the binding of suramin to the second binding site of SIRT5. Hence, the binding isotherms of both Figures 2B and 2C are devoid of the first binding site and they only show one binding site. The data of above figures conform to the single binding site models, yielding the magnitudes of  $n$ ,  $K_a$ , and  $\Delta H^\circ$  being equal to  $0.78 \pm 0.01$ ,  $(4.0 \pm 0.4) \times 10^5 \text{ M}^{-1}$  and  $-14.4 \pm 0.3 \text{ kcal/mol}$  (Figure 5.54A), and  $0.84 \pm 0.05$ ,  $(4.5 \pm 0.4) \times 10^5 \text{ M}^{-1}$  and  $-15.3 \pm 1.1$  (Figure 5.54B), respectively. Note that these thermodynamic parameters are similar to those obtained for the binding of suramin to the second binding site in Figure 5.53. It is reasonable to surmise that due to lower stoichiometry and enthalpic changes for the binding of suramin to the first binding site of SIRT5, Sheutz et al. might have missed the initial data points in their ITC profiles, and thus ended up only analyzing the data corresponding to the second binding site

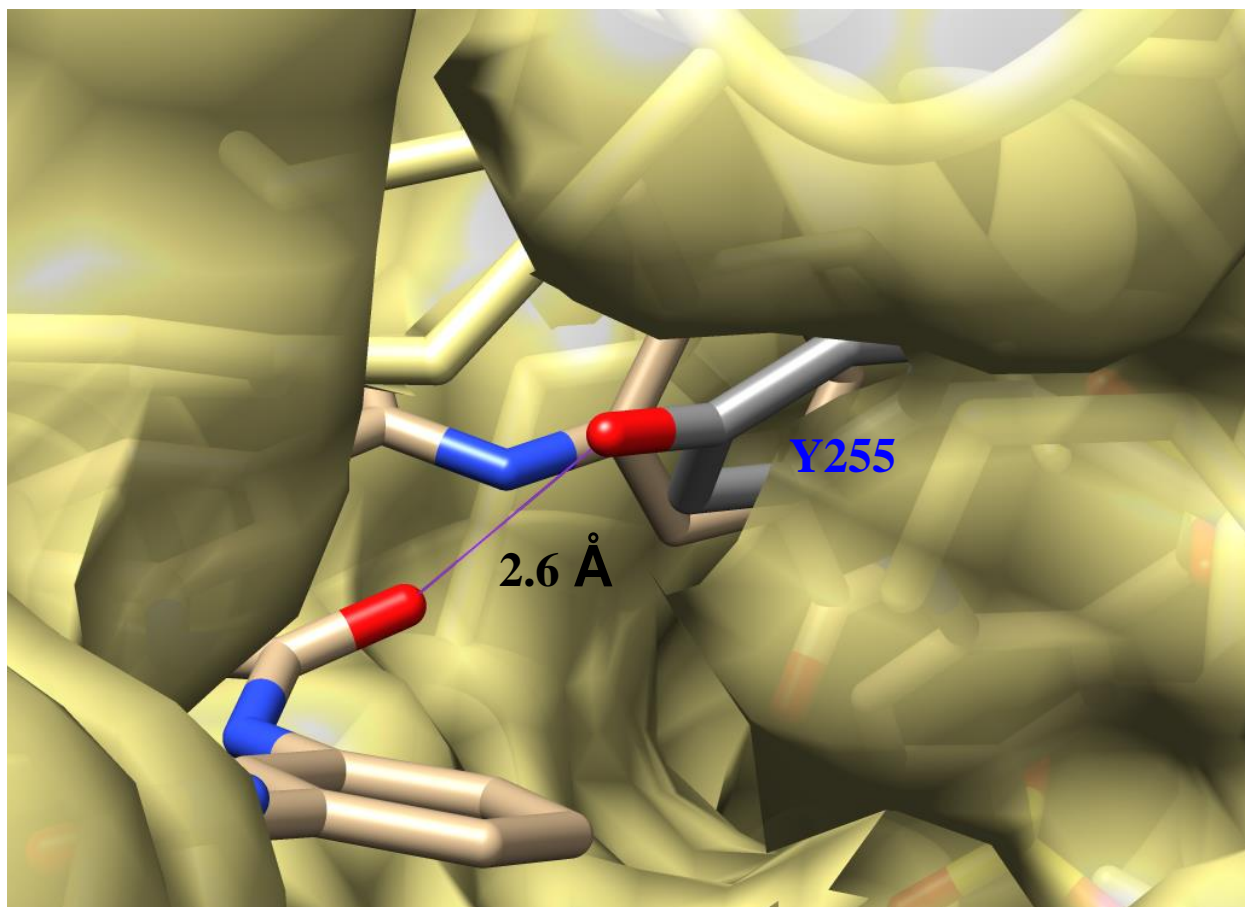


Figure 5.52. Crystal structure of SIRT5-suramin complex showing hydrogen bond between the urea (NH-CO-NH) group and Y255.

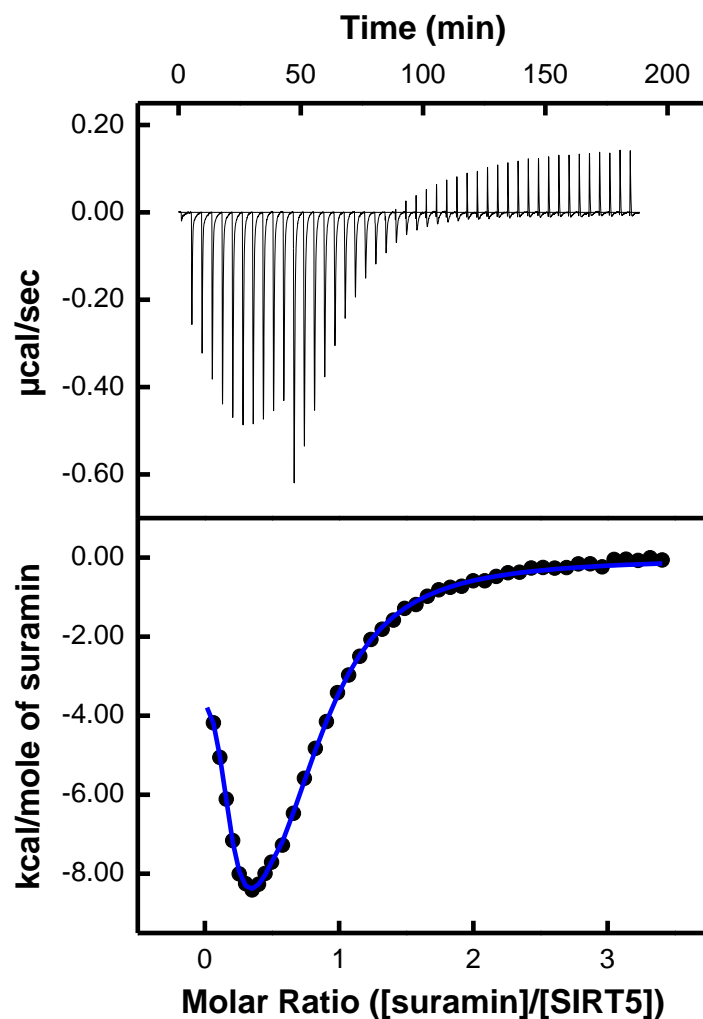


Figure 5.53. ITC profiles of SIRT5 titrated with suramin showing two binding sites. ITC profile of 35  $\mu\text{M}$  SIRT5 titrated with 700  $\mu\text{M}$  suramin in 50 mM HEPES, pH 7.5 containing 100 mM NaCl, 10 % glycerol and 1 mM TCEP at 25  $^{\circ}\text{C}$ . Fitted line corresponds to two-independent binding sites model (reference subtracted). The thermodynamic parameters determined from the fitting are listed in Table 5.10.

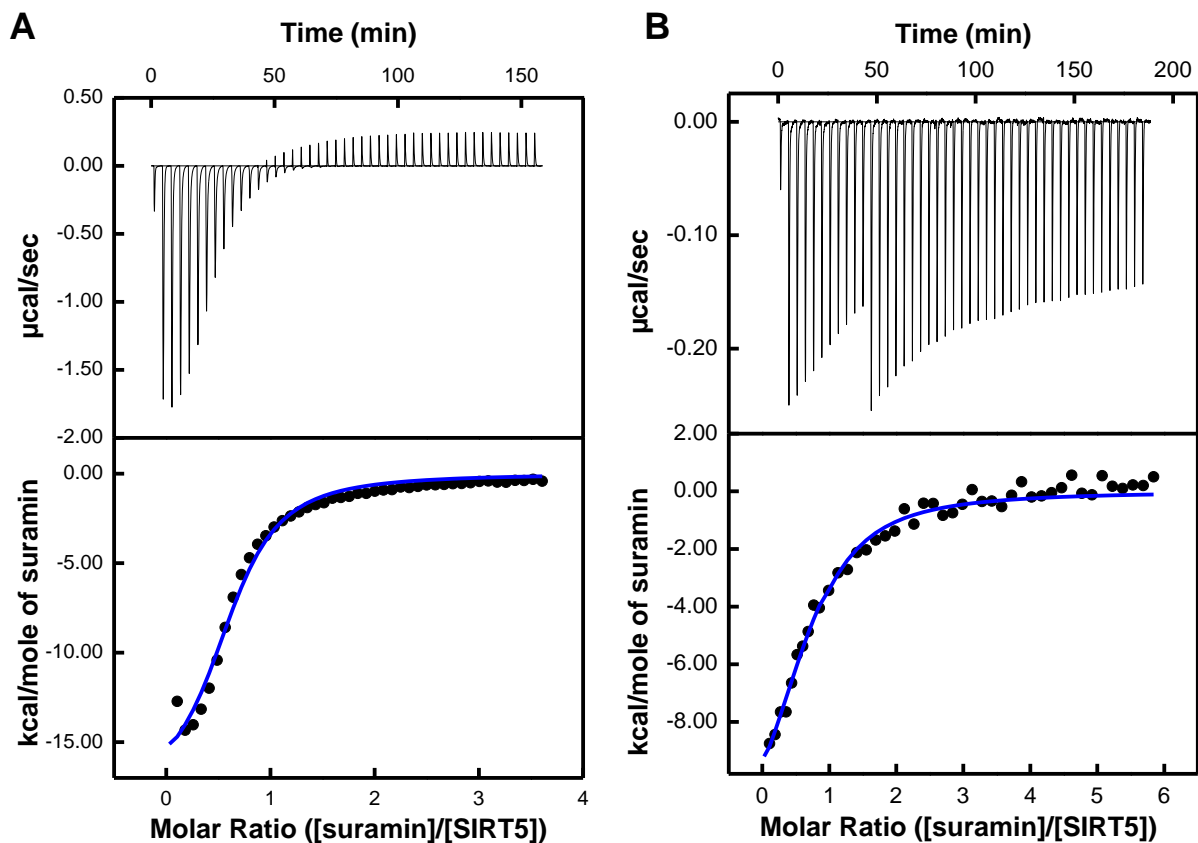


Figure 5.54. ITC profiles of SIRT5 titrated with suramin showing one binding sites. (A) ITC profile of 35  $\mu\text{M}$  SIRT5 titrated with 700  $\mu\text{M}$  suramin in 50 mM HEPES, pH 7.5 containing 100 mM NaCl, 10 % glycerol and 1 mM TCEP at 25  $^{\circ}\text{C}$ . Fitted line corresponds to single binding site model (reference subtracted). (B) ITC profile of 10  $\mu\text{M}$  SIRT5 titrated with 150  $\mu\text{M}$  suramin at 25 $^{\circ}\text{C}$ . Fitted line corresponds to single binding site model (reference subtracted). The thermodynamic parameters determined from the fitting are listed in Table 5.10.

#### 5.4.2.5. ITC profiles for the binding of suramin to SIRT1

In pursuit of delineating whether the binding of suramin to SIRT5 and its inhibition was unique, we realized that suramin also inhibits another isoform of sirtuin, namely SIRT1 (238). Assuming that the latter feature will reflect in the binding affinity of suramin to SIRT1, the ITC studies for the binding of suramin to SIRT1 were performed under identical experimental condition. Figure 5.53 shows the titration of 10  $\mu\text{M}$  SIRT1 by 45 aliquots (5  $\mu\text{L}$  each) of 150  $\mu\text{M}$  suramin. Both raw calorimetric and calculated ITC derived heat signals showed a saturating

profile, and they could be easily fitted (solid smooth line in the bottom panel of Figure 5.55) by the single site binding model of SIRT1-suramin complex with stoichiometry ( $n$ ), association constant ( $K_a$ ), and the enthalpy changes ( $\Delta H^\circ$ ) as being equal to  $1.12 \pm 0.01$ ,  $(3.3 \pm 0.2 \times 10^5 \text{ M}^{-1})$ , and  $-(16.6 \pm 0.3) \text{ kcal/mol}$  respectively (Table 5.11). The latter value translates to the  $\Delta G^\circ$  of binding as being equal to  $-7.5 \text{ kcal/mol}$ . Given the  $\Delta H^\circ$  and  $\Delta G^\circ$  values, the  $T\Delta S^\circ$  was calculated to be  $-9.1 \text{ kcal/mol}$ . Note the above thermodynamic parameters are comparable to those obtained from the binding of suramin to the second binding site of SIRT5. However, due to slow aggregation of the enzyme at high concentration, the ITC studies for the binding of suramin at high concentration of SIRT5 could not be performed. Considering that SIRT1 possesses extended N-terminal and C-terminal regions, which might preclude the bridging of suramin between two protein molecules, it is reasonable to conjecture that SIRT1 would be unlikely to undergo the dimerization process in the presence of suramin.

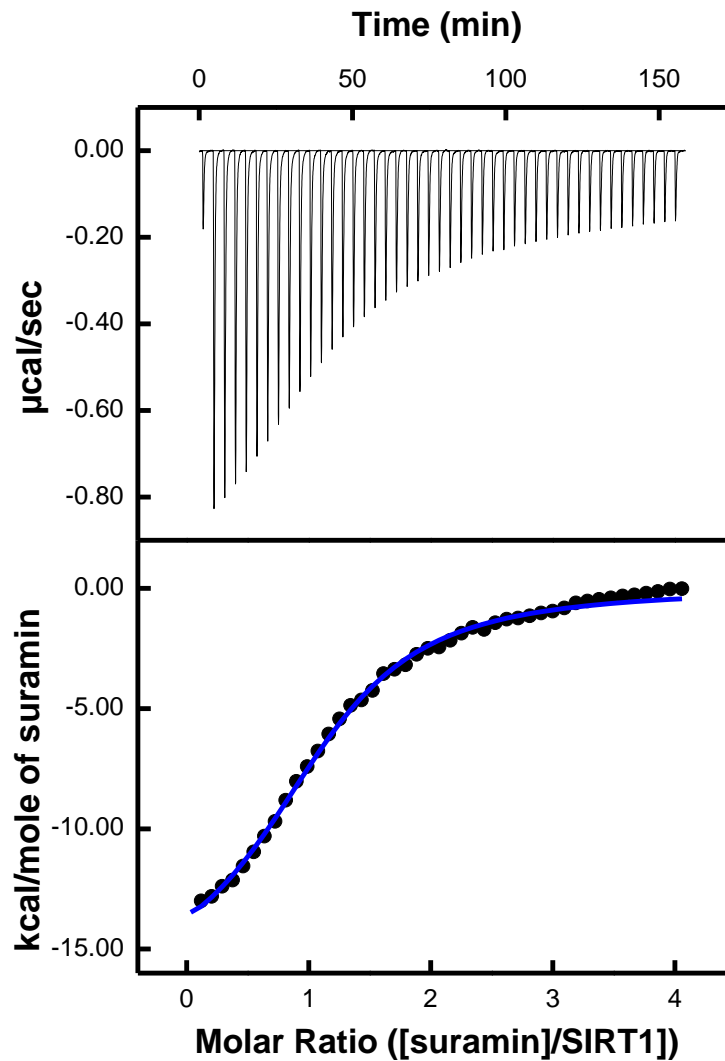


Figure 5.55. ITC profiles of SIRT1 titrated with suramin in 50 mM HEPES, pH 7.5 containing 100 mM NaCl, 10 % glycerol and 1 mM TCEP at 25 °C. The top panels show the raw data generated by titration of 10  $\mu\text{M}$  SIRT1 by 45 injections (5  $\mu\text{l}$  each) of 150  $\mu\text{M}$  suramin. The area under each peak was integrated and plotted against the molar ratio of suramin to SIRT1.



Table 5.11. Thermodynamic parameters for binding of suramin/half suramin to SIRT5

	Stoichiometry		$K_a$ ( $M^{-1}$ )	$\Delta G^\circ$ (kcal/mol)	$\Delta H^\circ$ (kcal/mol)	$T\Delta S^\circ$ (kcal/mol)
5 $\mu$ M SIRT5 with 200 $\mu$ M suramin	0.84 $\pm$ 0.05		$(4.5 \pm 0.4) \times 10^5$	-7.7	-15.3 $\pm$ 1.2	-7.6
50 $\mu$ M SIRT5 with 700 $\mu$ M suramin	Site 1	0.17 $\pm$ 0.01	$(6.2 \pm 1.1) \times 10^6$	-9.0	-4.1 $\pm$ 0.1	4.9
	Site 2	0.63 $\pm$ 0.01	$(2.3 \pm 0.1) \times 10^5$	-7.4	-12.5 $\pm$ 0.3	-5.1
50 $\mu$ M SIRT5 with 1 mM suramin	0.78 $\pm$ 0.02		$(4.0 \pm 0.4) \times 10^5$	-7.7	-14.4 $\pm$ 0.3	-6.7
10 $\mu$ M SIRT1 with 150 $\mu$ M suramin	1.12 $\pm$ 0.01		$(3.3 \pm 0.2) \times 10^5$	-7.5	-16.6 $\pm$ 0.3	-9.1
50 $\mu$ M SIRT5 with 5 mM half-suramin	1.09 $\pm$ 0.10		$(5.6 \pm 0.3) \times 10^3$	-4.8	-3.8 $\pm$ 0.5	2.7

#### 5.4.2.6. ITC profiles for the binding of suramin to SIRT5 mutants

The crystal structure of SIRT5-suramin complex demonstrates that Y102 and R105 coordinate with the negatively charged sulfonyl moieties of suramin. To determine the direct binding affinities of suramin to Y102A and R105I mutant SIRT5, the isothermal titration microcalorimetric (ITC) studies for the binding of suramin to SIRT5 mutants were performed as described above as well as in section §4.5.2. Figure 5.56 shows the raw calorimetric data and the ITC-derived binding isotherms for the interaction of suramin to R105I mutant SIRT5 under the experimental condition used for the binding of suramin to wild-type SIRT5 (see Figure 5.53). Note that unlike the two-phase binding of suramin to wild-type SIRT5, the data of Figure 5.56 clearly shows that suramin binds to R105I mutant only in one phase with binding stoichiometry ( $n$ ) of  $0.91 \pm 0.01$ . Evidently, the binding of suramin to R105I mutant enzyme does not trigger

the dimerization of the protein. The magnitudes of  $K_a$  and  $\Delta H^\circ$  values derived from the data of Figure 5.56 were found to be  $(9.1 \pm 0.3) \times 10^4 \text{ M}^{-1}$  and  $-11.3 \pm 0.1 \text{ kcal/mol}$ , respectively. Clearly, the binding of suramin to R105I mutant enzyme is impaired both enthalpically as well as from the free energy point of view vis a vis the binding of suramin to the wild-type SIRT5 (see Table 5.11). Hence, R105 residue is not only responsible for the enhanced binding of suramin to the enzyme but it also induces the dimeric state of the enzyme when  $[\text{SIRT5}] > [\text{suramin}]$ . Moreover, only 10% of R105I mutant enzyme was inhibited by 250  $\mu\text{M}$  suramin, suggesting that the above inhibitory feature is further impaired by the presence of  $\text{NAD}^+$ , utilized during the steady-state kinetic studies but not during the direct binding studies.

The ITC experiment of suramin to Y102A was performed by titrating 12  $\mu\text{M}$  Y102A with 45 aliquots of 300  $\mu\text{M}$  suramin in the same buffer at 25  $^\circ\text{C}$  and the result is shown in Figure 5.57. The thermodynamic parameters  $n$ ,  $\Delta H^\circ$  and  $K_a$  were determined to be as  $0.8 \pm 0.1$ ,  $-(6.7 \pm 0.8) \text{ kcal/mol}$  and  $(2.5 \pm 0.5) \times 10^5 \text{ M}^{-1}$ , respectively. A comparative account of the ITC data suggests that although the binding of suramin to Y102A mutant SIRT5 (vis a vis the wild-type enzyme) is minimally affected from the free energy point of view, it is significantly impaired from the enthalpic point of view. Hence, there is a marked enthalpy-entropy compensation in binding of suramin to Y102A mutant enzyme as compared to the wild type enzyme. Also, it is noteworthy that the binding affinity of suramin to Y102A mutant enzyme derived from the above ITC data ( $K_d = 4.03 \mu\text{M}$ ) is comparable to the inhibition constants ( $K_i$ ) determined for the inhibition of suramin on both the deacetylase and desuccinylase activities of Y102A ( $6.8 \pm 1.7 \mu\text{M}$  for the deacetylase activity and  $3.7 \pm 1.4 \mu\text{M}$  for the desuccinylase activity; see Table 5.8 in section §5.3.3).

The ITC binding studies of suramin to Y102A/R105I double mutant of SIRT5 were performed by titrating 20  $\mu\text{M}$  enzyme with 45 aliquots of 500  $\mu\text{M}$  suramin in the above buffer at 25  $^{\circ}\text{C}$  (Figure 5.56). The solid lines represent the best fit of the experimental data for the one site binding model, yielding the thermodynamic parameters  $n$ ,  $K_a$  and  $\Delta H^{\circ}$  as being equal to  $0.71 \pm 0.05$ ,  $-(10.7 \pm 0.8)$  kcal/mol and  $(1.4 \pm 0.1) \times 10^5 \text{ M}^{-1}$ , respectively. The binding affinity derived from the  $K_a$  is 7.3  $\mu\text{M}$ , which is about 3 fold lower than the inhibition constant determined by steady-state kinetic studies ( $25.7 \pm 3.0 \mu\text{M}$ ; see Table 5.8 in section §5.3.3)

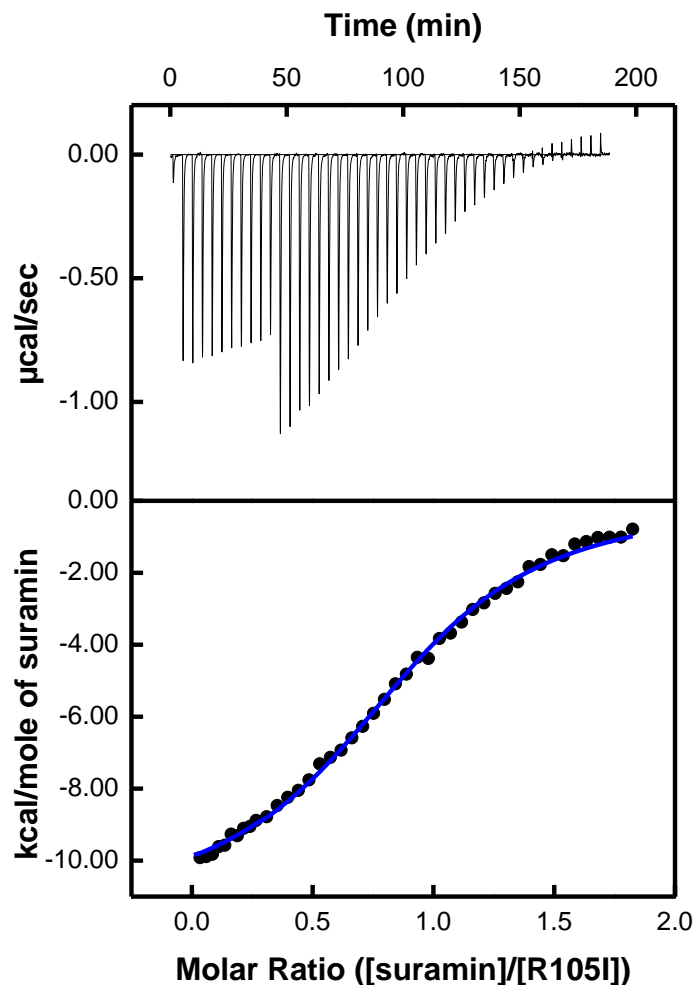


Figure 5.56. ITC profile of SIRT5 R105I titrated with suramin in 50 mM HEPES, pH 7.5 containing 100 mM NaCl, 10 % glycerol and 1 mM TCEP at 25 °C. The top panels show the raw data generated by titration of 12  $\mu\text{M}$  SIRT5 R105I by 45 injections (5  $\mu\text{l}$  each) of 400  $\mu\text{M}$  suramin. The area under each peak was integrated and plotted against the molar ratio of suramin to SIRT5 R105I. The solid lines represent the best fit of the experimental data for the one binding site model, yielding the thermodynamic parameters of  $n$ ,  $\Delta H^\circ$  and  $K_a$  as  $0.91 \pm 0.01$ ,  $-(11.3 \pm 0.80)$  kcal/mol and  $(9.1 \pm 0.4) \times 10^4 \text{ M}^{-1}$ , respectively.

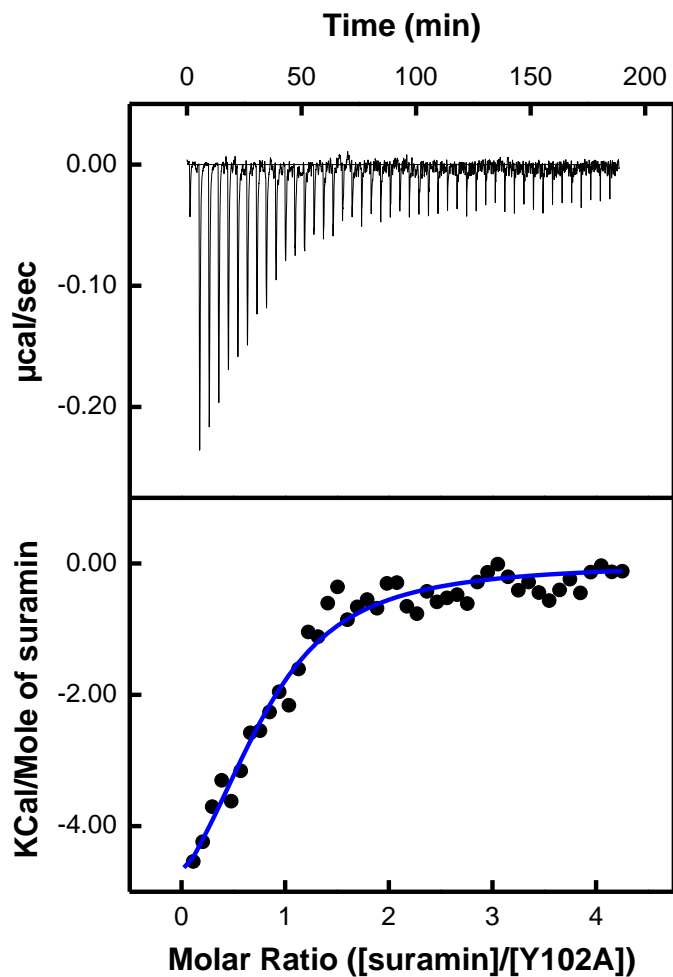


Figure 5.57. ITC profile of SIRT5 Y102A titrated with suramin in 50 mM HEPES, pH 7.5 containing 100 mM NaCl, 10 % glycerol and 1 mM TCEP at 25 °C. The top panels show the raw data generated by titration of 12  $\mu$ M SIRT5 Y102A by 45 injections (5  $\mu$ l each) of 400  $\mu$ M suramin. The area under each peak was integrated and plotted against the molar ratio of suramin to SIRT5 Y102A. The solid lines represent the best fit of the experimental data for the one binding site model, yielding the thermodynamic parameters of  $n$ ,  $\Delta H^\circ$  and  $K_a$  as  $0.8 \pm 0.1$ ,  $-(6.7 \pm 0.8)$  kcal/mol and  $(2.5 \pm 0.5) \times 10^5 \text{ M}^{-1}$ , respectively.

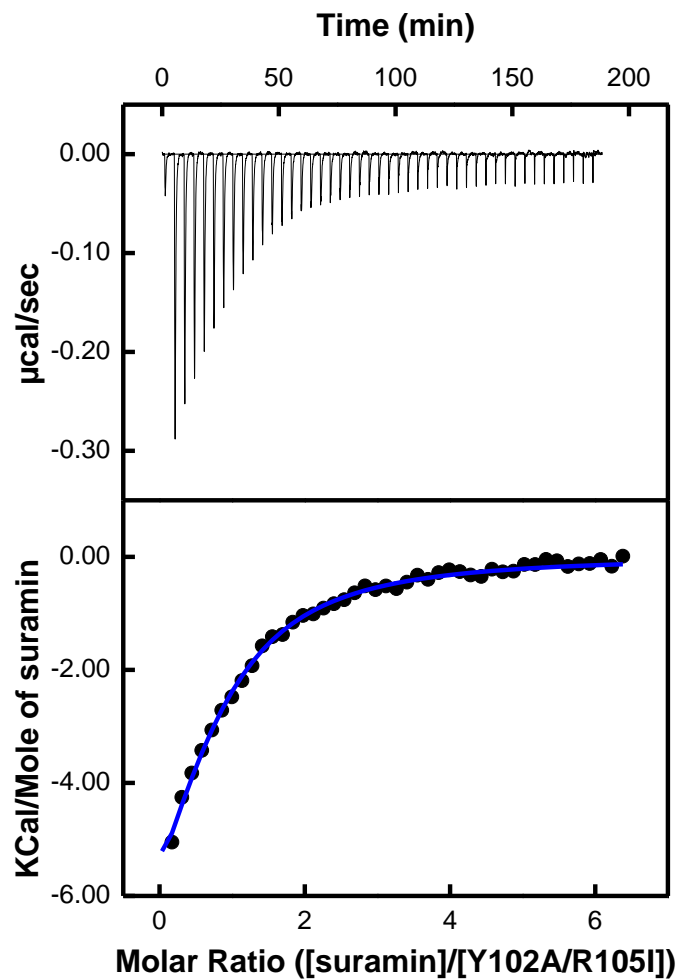


Figure 5.58. ITC profile of SIRT5 Y102A/R105I titrated with suramin in 25 mM HEPES, pH 7.5 containing 100 mM NaCl, 10 % glycerol and 1 mM TCEP at 25 °C. The top panels show the raw data generated by titration of 20  $\mu\text{M}$  SIRT5 Y102A/R105I by 45 injections (5  $\mu\text{l}$  each) of 500  $\mu\text{M}$  suramin. The area under each peak was integrated and plotted against the molar ratio of suramin to SIRT5 Y102A/R105I. The solid lines represent the best fit of the experimental data for the one binding site model, yielding the thermodynamic parameters of  $n$ ,  $\Delta H^\circ$  and  $K_a$  as  $0.7 \pm 0.1$ ,  $-(10.7 \pm 0.8)$  kcal/mol and  $(1.4 \pm 0.1) \times 10^5 \text{ M}^{-1}$ , respectively.

#### 5.4.2.7. *Binding and inhibition studies of half suramin to SIRT5*

The symmetrical “bis” form of suramin has been known to undergo hydrolytic cleavage to generate nearly two identical fragments of the naphthylsulfonate derivatives (Figure 5.42), referred herein as “half suramin”, which was generated by hydrolysis of suramin following the procedures described by Kettenes-van den Bosch et al (271). Briefly, native suramin was dissolved in deionized water and heated in a water bath at 80 °C. The heated solution was removed from the water bath after six hours followed by cooling in an ice bath. The above treated produced half-suramin, which was further purified via a C18 HPLC column. Although the “half-suramin” was unlikely to bridge between the two SIRT5 molecules (Figure 5.59), its binding thermodynamic profile was conceived to shed light on the mechanistic feature of SIRT5-suramin interaction. The ITC studies for the binding of half-suramin to SIRT5 were performed as described above as well as in section §4.5.2. Figure 5.61 shows a representative ITC profile for the titration of SIRT5 (60 μM) by 45 aliquots (5 μL each) of 5 mM half-suramin in the standard buffer. The experimental data conformed to the single-site binding model with stoichiometry (n), enthalpy change ( $\Delta H^\circ$ ) and the equilibrium association constant ( $K_a$ ) as being equal to  $0.83 \pm 0.10$ ,  $-3.82 \pm 0.45$  kcal/mol and  $(5.6 \pm 0.3) \times 10^3 \text{ M}^{-1}$ , respectively. Note that as compared to the binding of full suramin to SIRT5 (Table 5.11), the  $\Delta H^\circ$  and  $K_a$  values for the binding of half suramin to SIRT5 are about 4 and 30 fold less favorable, respectively. The ITC derived thermodynamic parameters for the binding of half suramin to SIRT5 are summarized in Table 5.10. To ascertain whether the binding isotherm for the SIRT5-suramin complex invariably conformed to the one site binding model (Figure 5.53), the above ITC studies were also performed at different concentration of suramin. Under no condition did the second binding site emerge in ITC titration profiles involving different concentrations of SIRT5. In addition, the

stoichiometry of SIRT5-half-suramin complex is invariably close to unity, suggesting that half-suramin does not bridge between two SIRT5 molecules.

To compare the inhibition effect of half-suramin on SIRT1 and SIRT5, the steady-state kinetic rates of SIRT1 catalyzed deacetylation reaction and SIRT5 catalyzed desuccinylation reaction were measured as a function of increasing concentration of half suramin. The  $K_i$  determined by fitting the data in Figure 5.62 using the competitive equation (Eq.4.5 in section 4.3.4) are  $13.1 \pm 0.7 \mu\text{M}$  and  $1.3 \pm 0.2 \text{ mM}$ , respectively, indicating that the inhibitory potencies of half suramin for both SIRT1 and SIRT5 are significantly lower than those observed with full suramin molecule.

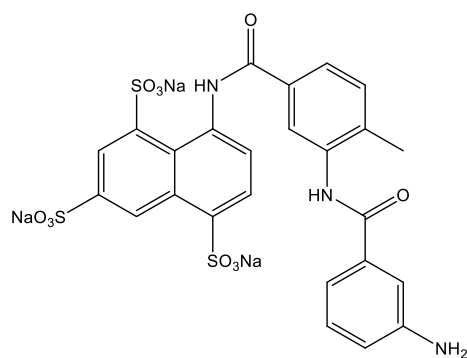


Figure 5.59. Structure of half-suramin



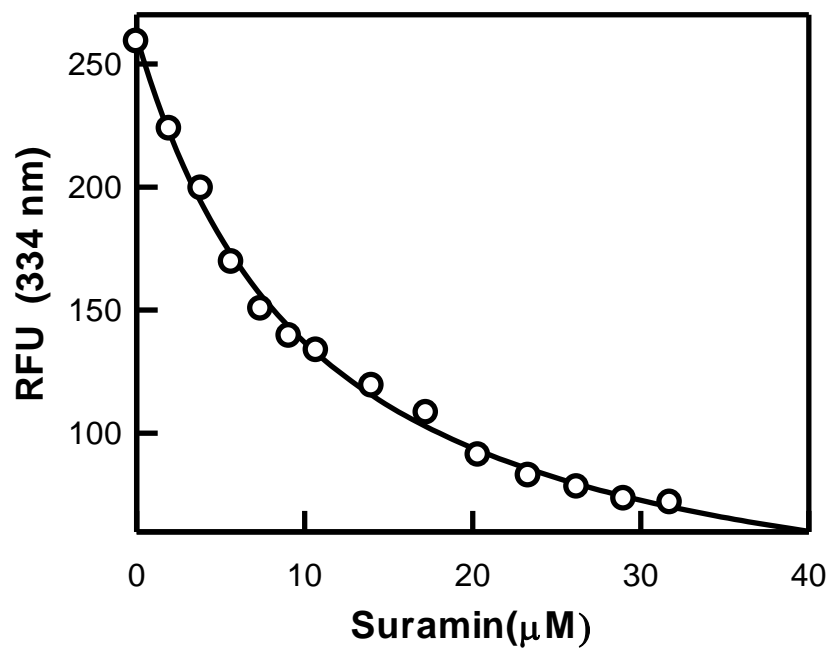


Figure 5.60. Binding isotherm for the interaction of half-suramin with SIRT5. Binding affinity of the SIRT5-suramin complex. The decrease in fluorescence intensity of 1  $\mu\text{M}$  SIRT5 ( $\lambda_{\text{ex}} = 280$  nm) at 334 nm upon titration of suramin is plotted as a function of suramin concentration. The smooth line is the best fit of the data for the  $K_d$  value of the SIRT5-suramin complex being equal to  $9.4 \pm 0.8 \mu\text{M}$ .

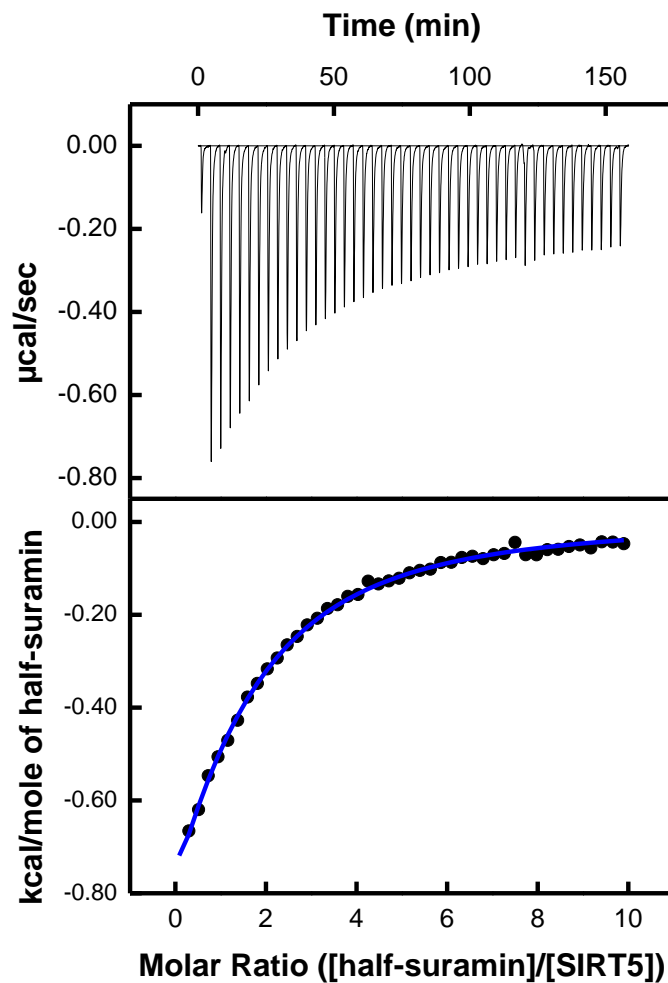


Figure 5.61. ITC profile of SIRT5 titrated with half-suramin. 25 mM HEPES, pH 7.5 containing 100 mM NaCl, 10 % glycerol and 1 mM TCEP at 25 °C. The top panels show the raw data generated by titration of 80  $\mu$ M SIRT5 by 45 injections (5  $\mu$ l each) of 1 mM half-suramin. The area under each peak was integrated and plotted against the molar ratio of half-suramin to SIRT5. The thermodynamic parameters determined from the fitting are listed in Table 5.10.

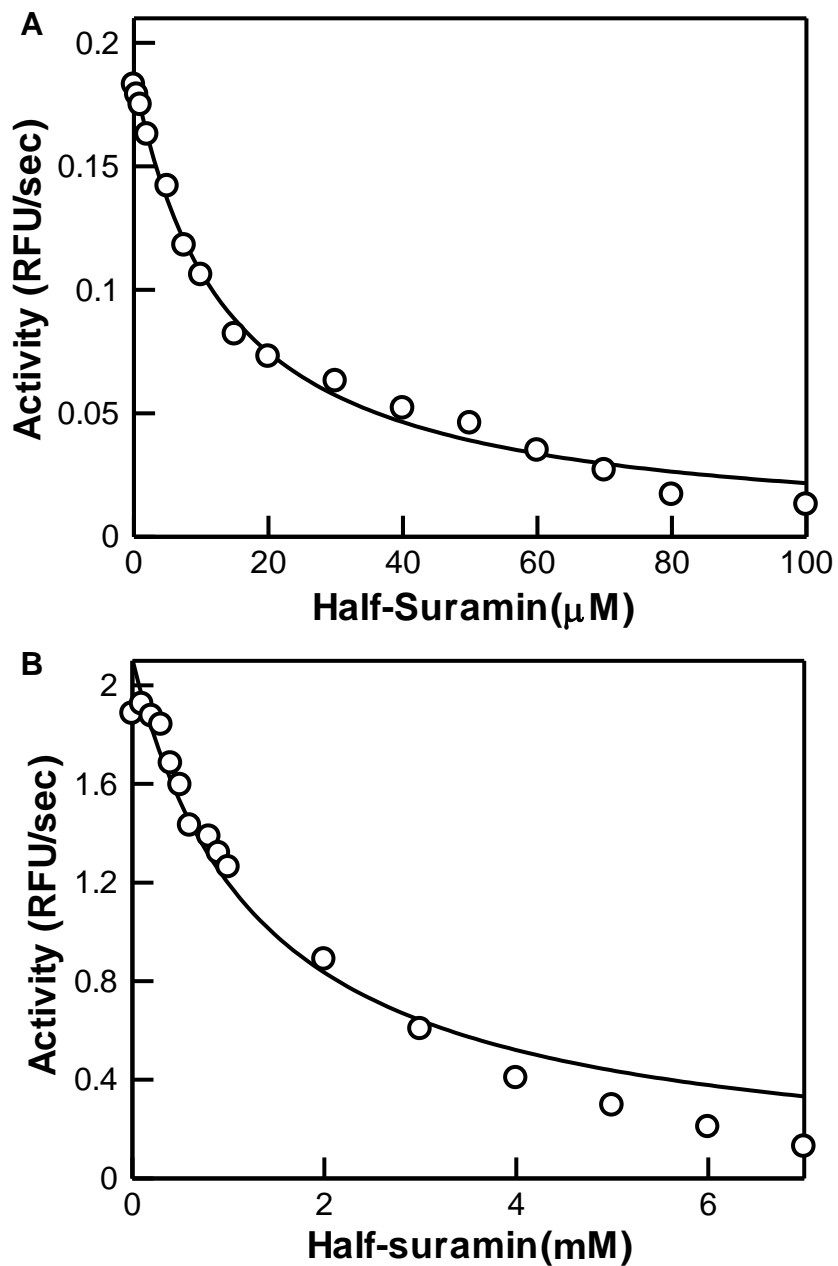


Figure 5.62. Effects of half-suramin on SIRT1 and SIRT5 catalyzed reactions. (A) Activity of SIRT1 in the presence of 150  $\mu\text{M}$  *Fluor-de-lys*<sup>®</sup> substrate, 500  $\mu\text{M}$   $\text{NAD}^+$ , and increasing concentration of half-suramin. The solid smooth lines represent the best fit of the data for the  $K_i$  value as  $13.1 \pm 0.7 \mu\text{M}$  (B) Activity of SIRT5 in the presence of 150  $\mu\text{M}$  Ac-SucLys-AMC substrate, 50  $\mu\text{M}$   $\text{NAD}^+$ , and increasing concentration of half-suramin. The solid smooth lines represent the best fit of the data for the  $K_i$  value as  $1.3 \pm 0.2 \text{ mM}$ .

#### ***5.4.2.8. Oligomeric States of SIRT5 in the presence of suramin***

To ascertain whether or not the crystallographically derived dimeric state of SIRT5 in the presence of suramin really exists in the aqueous solution (or the above feature emerged merely due to an artifact of the crystallization condition (238)), size exclusion chromatographic studies were performed (via a Superdex 200 column) in the presence of varying concentrations of suramin. Such studies were intended to decipher the relationship between the alternative modes of binding of suramin to SIRT5, discerned from the ITC titration profiles (Figures 5.53 and 5.54).

To perform size exclusion chromatographic studies, a superdex 200 column was assembled using a packing reservoir (XK16/70 column) on the AKTA design pump P-901 as described in the Methods section §4.5.3. The total volume of the resin ( $V_t$ ) after packing calculated based on the height of the resin was approximately 124.055. To determine the void volume ( $V_o$ ) of the column, 2 mL of 2 mg/ml blue dextran was loaded and eluted from the column pre-equilibrated with 25 mM HEPES, pH 7.5, containing 100 mM NaCl as described in the Methods section. The  $V_o$  determined based on the elution volume of blue dextran was 45.372. The calibration curve for the column was generated with five molecular weight standards, namely cytochrome C (12.4 kDa), carbonic anhydrase (29 kDa), BSA (66 kDa), yeast ADH (150 kDa) and  $\beta$ -amylase (200 kDa) (Sigma-Aldrich). Figure 5.63 shows the  $K_{av}$  of the five protein standards plotted as a function of the corresponding log molecular weight. The solid smooth line represents the linear fitting of the data, yielding the slope and intercept to be  $-0.3686 \pm 0.0178$  and  $1.0829 \pm 0.0325$ , respectively.

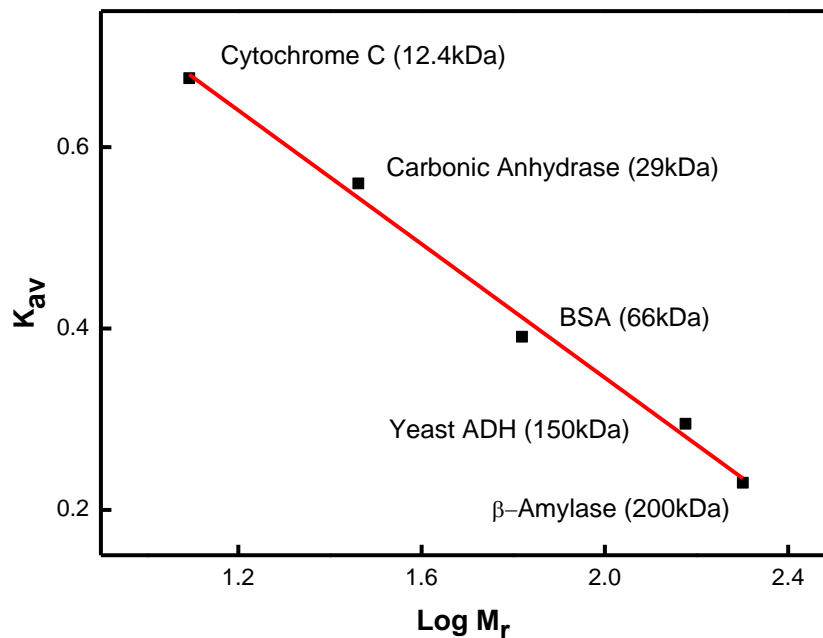


Figure 5.63. Calibration curve for the column superdex 200 using five known proteins as standards. The  $K_{av}$  of 5 known protein standards (cytochrome C, carbonic anhydrase, BSA, Yeast ADH and  $\beta$ -amylase) is plotted as a function of the corresponding log molecular weight. The solid smooth line represents the linear fitting of the data, yielding the slope and intercept to be  $-0.3686 \pm 0.0178$  and  $1.0829 \pm 0.0325$ , respectively.

After the calibration of the column, the experiments were performed by loading SIRT5 with different concentrations of suramin and recording the elution profile by monitoring the absorption of the effluents at 280 nm (see Methods section §4.5.3). Figure 5.64 shows the elution profiles of SIRT5 in the presence of increasing concentrations of suramin in 25 mM HEPES, pH 7.5, containing 100 mM NaCl, and 1 mM TCEP. To ensure that the suramin concentration remains unchanged while the enzyme migrates through the column, enzyme was mixed with appropriate concentration of suramin prior to loading the column, and the column was equilibrated with the same concentration of suramin. First, a control experiment was performed in the absence of suramin. Figure 5.64A shows the elution profile (A<sub>280</sub> vs. elution volume) of 30  $\mu$ M SIRT5 alone (without suramin) from the above column. Note that although most of

SIRT5 elutes as a major symmetrical peak at 91 mL, there is a small (albeit discernible) shoulder band around 86 mL. To deconvolute the individual peaks of Figure 5.64A, we fitted the elution profile was fitted by Eq. 4.13 using the peak analysis module of Origin 8.5, and extracted the peak elution volumes of the minor and major peaks as being equal to 86 ml and 91 ml respectively. From the standard plot derived from the elution profiles of known molecular weight protein standards under an identical experimental condition (Figure 5.63), the above peak elution volumes of SIRT5 could be translated to 33 kDa and 24 kDa molecular weights, respectively. Of these values, 24 kDa molecular weight of SIRT5 (eluting as a major peak) is somewhat smaller than the predicted molecular weight of monomeric SIRT5 (31 kDa). The origin of the above discrepancy presumably lies in the shape of SIRT5 eluting from the column. However, it was somewhat surprising to observe that the 33 kDa molecular weight peak of SIRT5 eluted as a shoulder band. The latter peak was unlikely to be due to the contamination of other protein in our SIRT5 preparation since it was absent in the presence of 1, 5 and 10  $\mu\text{M}$  suramin, This coupled with the fact that the above peak re-emerged when the eluants of the major peak were re-chromatographed on the same column, led to the suggestion that the shoulder peak was indeed the dimeric form of SIRT5 but it was eluting at a much lower molecular weight (33 kDa) fraction (data not shown) presumably due to a dynamic equilibrium between the monomeric and dimeric forms of SIRT5. The above size exclusion chromatographic studies of SIRT5 were then performed in the presence of increasing concentrations of suramin. Figure 5.64B, 5.64C, 5.64D, and 5.64E show the elution profiles of 30  $\mu\text{M}$  SIRT5 in the presence of 1, 5, 10, and 20  $\mu\text{M}$  concentrations of suramin, respectively. Note that in the presence of 1  $\mu\text{M}$  suramin (Figure 5.64B), SIRT5 elutes as two equally predominant peaks corresponding to the molecular weights of 24 kDa (monomer) and 49 kDa (dimer), respectively. When the

concentration of suramin was increased to 5  $\mu\text{M}$  (Figure 5.64C), the dimeric peak (49 kDa) of SIRT5 became the most pronounced, while the monomeric peak (24 kDa) significantly decreased in magnitude. Surprisingly, upon further increase in suramin concentration to 10  $\mu\text{M}$  (Figure 5.64D), both monomeric and dimeric peaks of SIRT5 became nearly equally pronounced, similar to the situation observed in case of 1  $\mu\text{M}$  suramin (Figure 5.64B). Upon further increase in suramin concentration to 20  $\mu\text{M}$  (Figure 5.64E), the monomeric peak of SIRT5 became most pronounced while the dimeric peak decreased in magnitude. A cumulative account of these data lead to the suggestion that at lower concentration of suramin (Figure 5.64B and 5.64C), SIRT5 exists as a dimer presumably due to bridging of two monomeric units of SIRT5 by suramin, On the other hand, in the absence of suramin (Figure 5.64A) as well as in the presence of high concentration suramin (Figure 5.64E) SIRT5 predominantly exists in the monomeric form. To quantitate the distribution between the monomeric and dimeric forms of SIRT5 as a function of suramin, the areas of the resolved peaks were determined using the Guassian Function (Eq.4.13). Based on the determined areas, the molar ratios of the dimers versus monomers of SIRT5 were calculated and plotted against the corresponding concentrations of suramin (Figure 5.65). The latter plot clearly shows that the percent of SIRT5 dimer increase from 6% to 77% with suramin concentration varying from 0 to 10  $\mu\text{M}$ , and decrease back to 5% when suramin concentration further increases to 20  $\mu\text{M}$ .

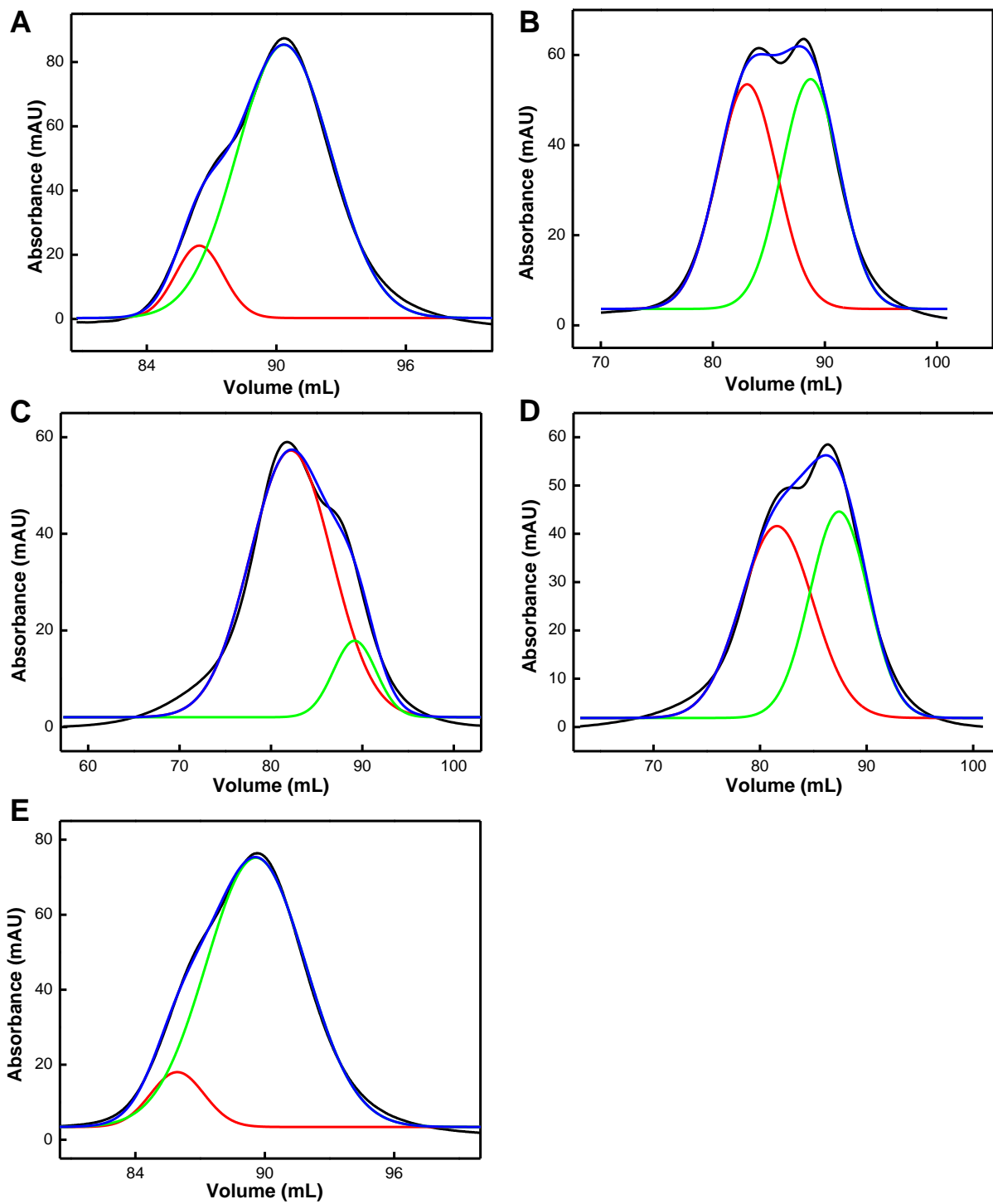


Figure 5.64. Size exclusion chromatography profile and multiple peaks analysis for 26  $\mu\text{M}$  SIRT5 the absence and presence of suramin. Size exclusion chromatography profile and multiple peaks analysis for 26  $\mu\text{M}$  SIRT5 in the, in the absence (A), presence of 1  $\mu\text{M}$  (B), 5  $\mu\text{M}$  (C), 10  $\mu\text{M}$  (D) and 20  $\mu\text{M}$  (E) suramin.



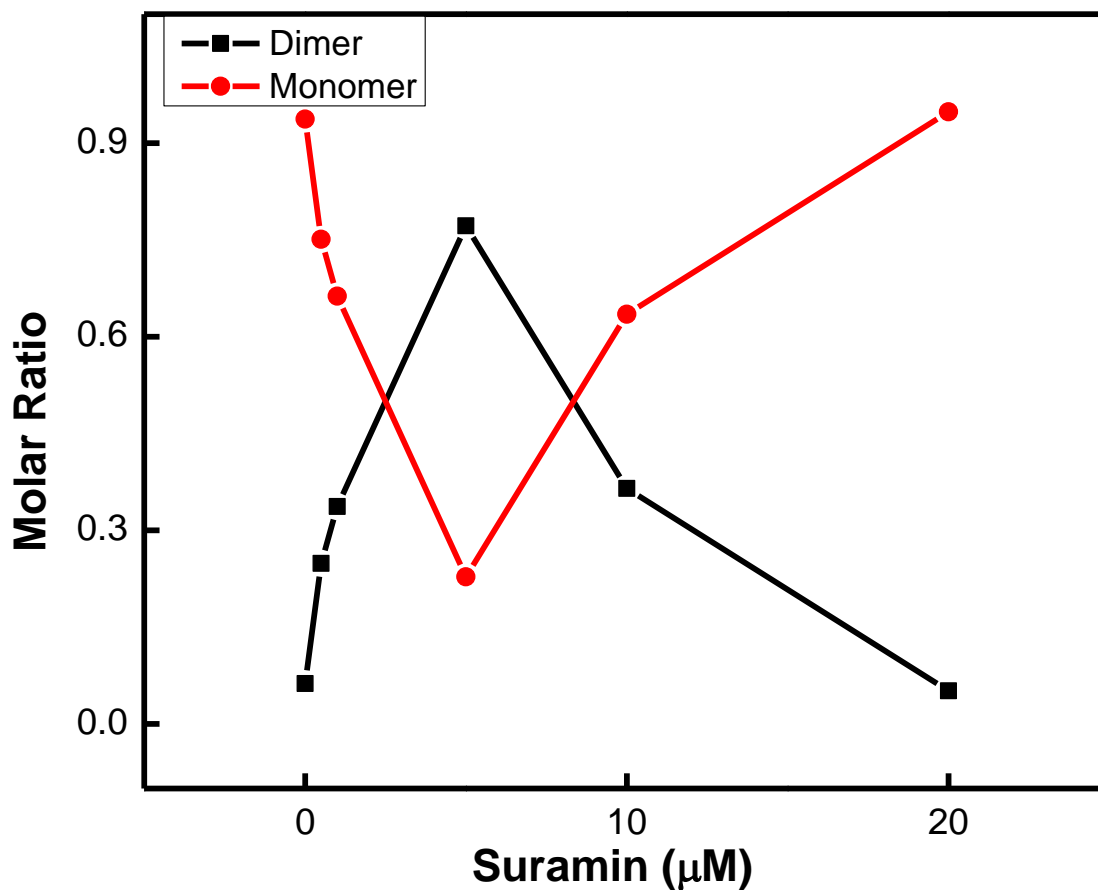


Figure 5.65. Molar ratios of monomer/total and dimer/total are plotted against different concentrations of suramin from size exclusion chromatography profiles.

#### 5.4.2.9. AFM images of SIRT5 as a function of suramin concentration

To determine the size distribution as well as topology of SIRT5 as a function of suramin concentration, atomic force microscopic (AFM) studies were performed on a mica surface in collaboration with Dr. Yongki Choi from Department of Physics at North Dakota State University. The samples were prepared by premixing 10  $\mu\text{M}$  SIRT5 with suramin at the following four conditions: SIRT5 in the absence of suramin, and SIRT5 and suramin at the molar ratios of 1:1, 4:1, and 1:10, respectively. The above mixtures were dropped on top of a freshly cleaved mica surface and incubated them for 10 minutes at the room temperature. The mica

surface was rinsed and dried prior to subjecting the samples to AFM assisted height measurement. The AFM measurements were carried out in a non-contact mode at a scanning rate of 1.3 Hz and the resonance frequency of 145 kHz (see Methods section §4.6). The AFM images of SIRT5-suramin complexes are shown in Figure 5.66 (panels A-D). Note the prevalence of both dim (representing the monomeric form of SIRT5) and bright (representing the dimeric form of SIRT5) in different panels of Figure 5.66. In the absence of suramin (Figure 5.66A), the dim spots are most predominant, suggesting that in the absence of suramin, a major fraction of SIRT5 exists in the monomeric form. This is further evident by zooming and measuring the heights of two neighboring dim spots of Figure 5.64A as shown in Figure 5.66 panel E, The graphic analysis of the zoomed images reveal their heights being equal to 2.3 nm, corresponding to the crystallographically determined width of SIRT5. As the concentration of suramin increased (Figure 5.66, panels B and C), whereas the number of dimmer spots decreased, the number of brighter spots increased, suggesting an increase in the number of SIRT5 dimers upon increase in suramin concentration. Figure 5.66F shows the height measurements of zoomed brighter spots from the AFM image of panel C, yielding the height of SIRT5 molecules being equal to 4.3 nm, representing the dimeric form of SIRT5. When the suramin concentration was further increased (molar ratio of SIRT5 to suramin being equal to 1:10 (Figure 5.66, panel D), the dim spots became more predominant as compared to the bright spots, suggesting that at the above molar ratio of SIRT5 to suramin, the enzyme reverts back to the monomeric form as noted with size exclusion chromatographic analysis of SIRT5 in the presence of increasing concentrations of suramin (section §5.4.2.8). To determine the size distribution of all SIRT5 molecules (in the presence of varying concentrations of suramin), the number of SIRT5 molecules in the presence of varying concentrations of suramin were plotted as a function of their heights as shown in the

corresponding panels of Figure 5.66. The solid smooth lines of Figure 5.67 are the best fit of the data for the log normal distribution function of the protein molecules and their heights using eq. 4.17 as described in the Methods section (§4.6). Although the peak heights of different panels were found to range between 2.2 and 2.4 nm, the arithmetic average of the plots of A, B, C, and D were found to be 2.9, 4.9, 3.6, and 3.3 nm, respectively. Clearly, the dimeric form of SIRT5 becomes more abundant at lower molar ratios of SIRT5 to suramin, but as the above ratio increases, the dimeric SIRT5 reverts back to the monomeric form. These data are consistent with size exclusion chromatographic analysis of SIRT5 in the presence of increasing concentrations of suramin.

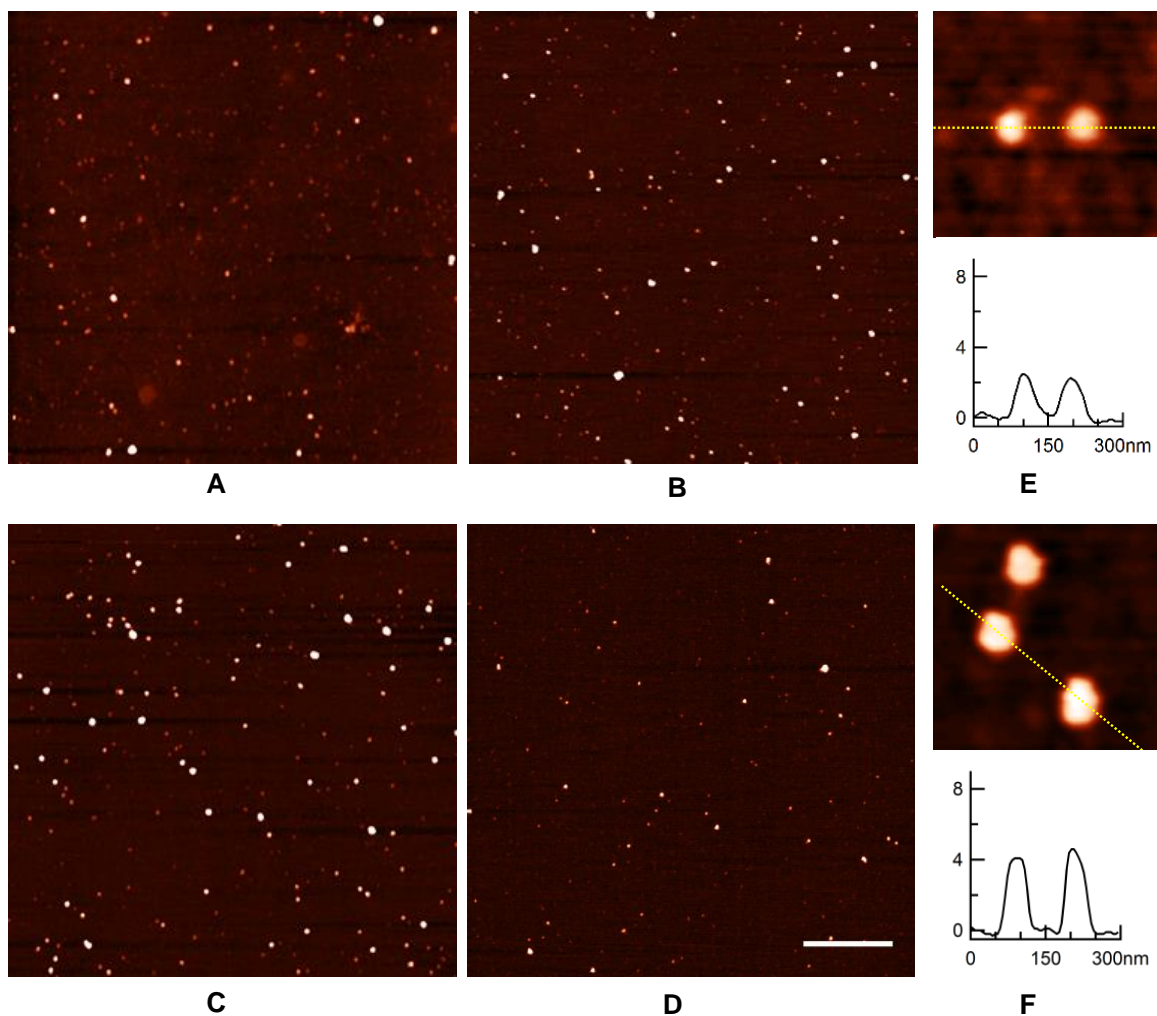


Figure 5.66. AFM images of SIRT5 on a mica surface at various concentrations of Sumarin. (A) SIRT5 in the absence of suramin, (B) SIRT5 and sumarin at the molar ratio of 1:1, (C) SIRT5 and sumarin at the molar ratio of 4:1, and (D) SIRT5 and sumarin at the molar ratio of 1:10; (E) two monomeric SIRT5 circled in (A) are zoomed in and their height profile is shown as below. The heights are about 2.3nm; (F) two multimeric SIRT5 circled in (C) are zoomed in and their height profile is shown as below. The heights are about 4.3 nm. The scale bars are 1  $\mu\text{m}$  for (A)-(D) and 50  $\mu\text{m}$  for (E) and (F).

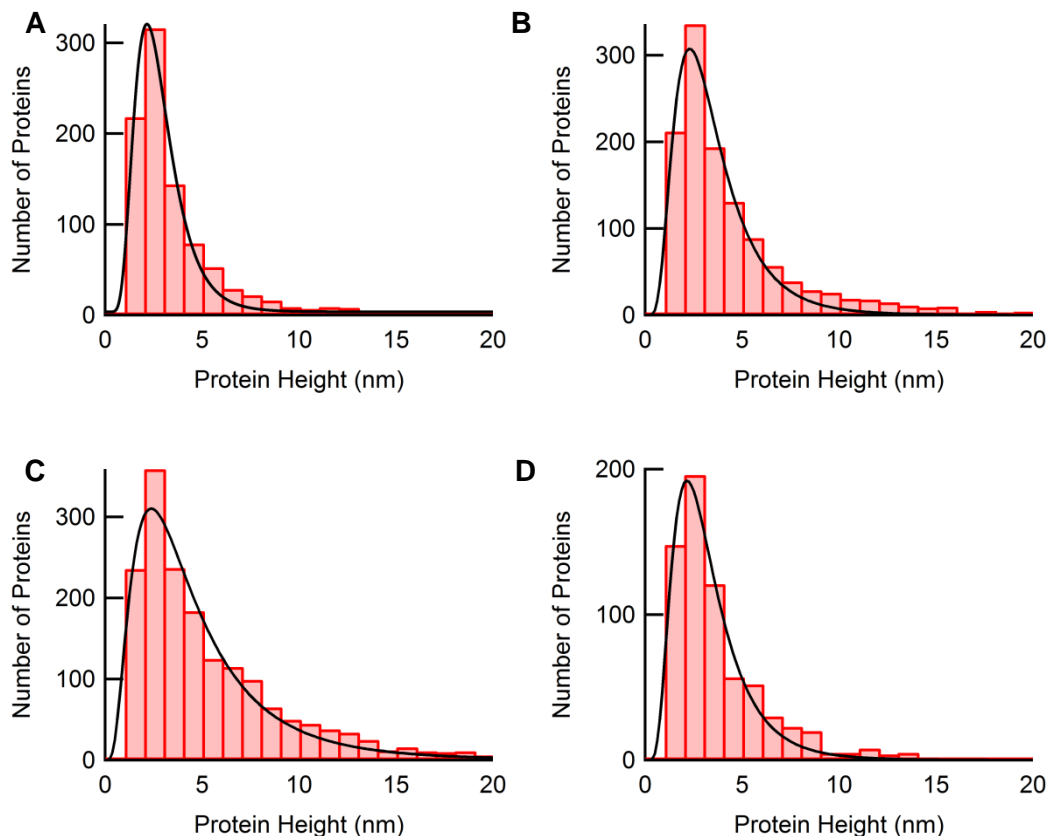


Figure 5.67. Size distributions of SIRT5 at various concentrations of suramin. (A) SIRT5 in the absence of suramin, (B) SIRT5 and suramin at the ratio of 1:1, (C) SIRT5 and suramin at the ratio of 4:1, (D) SIRT5 and suramin at 1:10. The solid lines represent the fit of log-normal distribution function. The peak heights are 2.2, 2.3, 2.4, and 2.2 nm for (A), (B), (C), and (D), respectively. The average height is about 2.3 nm.

#### 5.4.2.10. Molecular modeling

To gain insight into the structural basis of alternative modes of binding of suramin to SIRT5, we performed the molecular modeling studies were performed by collaborating with Dr. Farukh Jabeen from Center for Computationally Assisted Science and Technology at North Dakota State University using the Molecular Operating Environment (MOE) software. The crystal structure of SIRT5-suramin complex was retrieved from protein data bank (PDB code: 2NYR), and following separation of the ligand (suramin) from the protein structure, they were

individually subjected to the energy minimizations via the structure preparation module of MOE. The optimized structure of suramin was docked to the energy minimized SIRT5 (dimeric form) via the MOE-Dock program. As shown in Figure 5.68A, the best docked structure (revealed by the score function) showed a similar binding mode of suramin as observed in the crystal structure of SIRT5-suramin complex. On the other hand, when suramin was docked to the monomeric form of SIRT5, it was observed that while half of the suramin molecule bound at the active site pocket of SIRT5 had similar orientation as observed crystallographically, the remaining half of the suramin structure protruded away from the protein mass (Figure 5.68B). The above modeling conclusions are similar to those obtained by Trapp et al. However, to probe whether or not the protruded structure of suramin had the potential to bend and interact on the surface of monomeric SIRT5, the structure of suramin was drawn in a cyclic form and subjected it to energy minimization (Figure 5.69A). When the optimized suramin structure was docked to SIRT5, it exhibited an entirely different binding mode both within the active site pocket of the enzyme as well as of outside. As shown in Figure 5.69B and C, half of the suramin molecule, protruding from the enzyme's active pocket, formed hydrogen bonds with bonding with Gln83 and Gly224 (2.44 Å) present on the surface of the protein. The latter binding mode justifies our experimental data that when  $[\text{suramin}] \gg [\text{SIRT5}]$ , only the monomeric form of the enzyme-ligand complex becomes predominant. The binding of half suramin structure on the surface of the SIRT5 monomer supports our experimental data that both binding affinity and inhibitory potency of full suramin is higher than that of the half suramin.

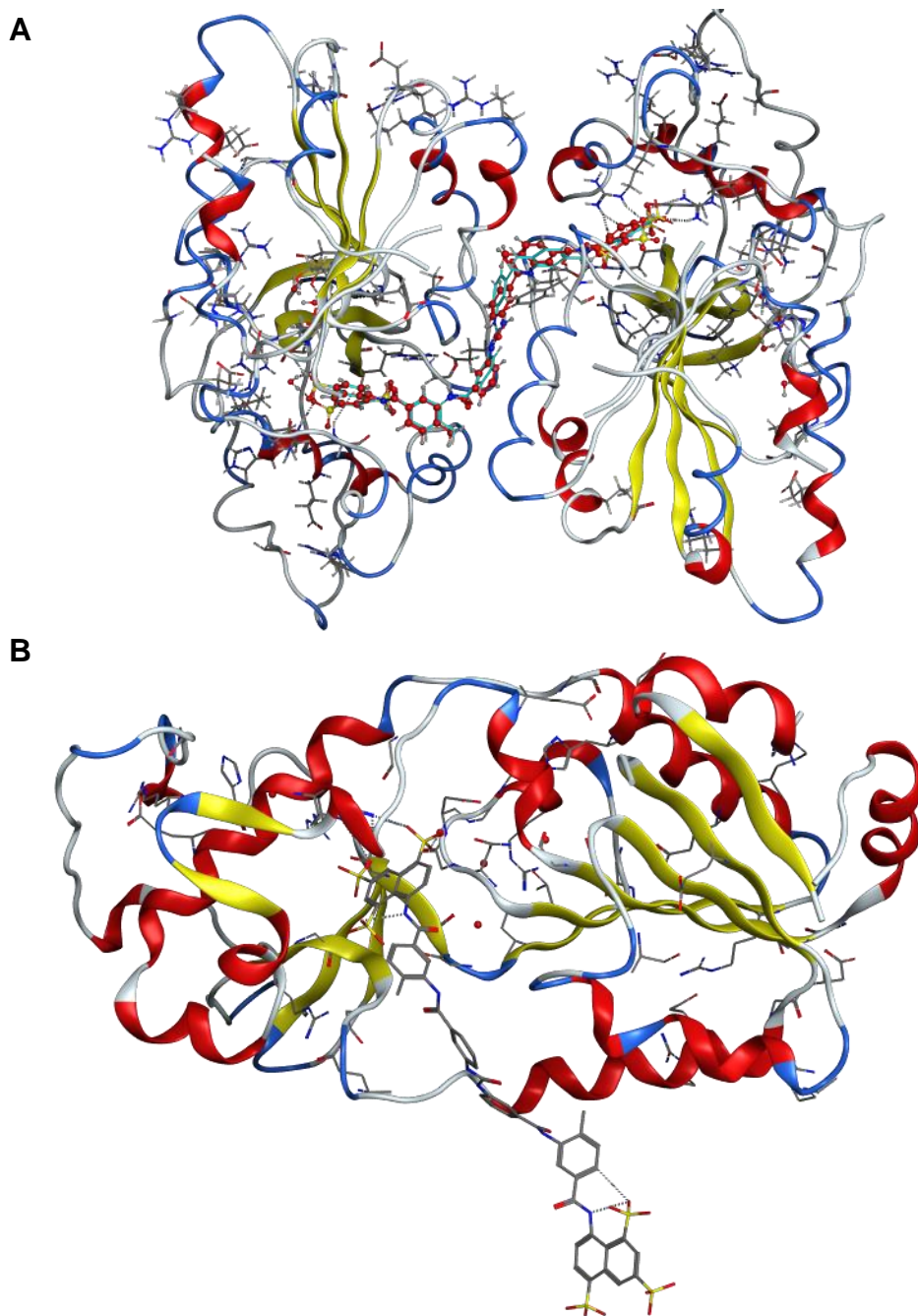


Figure 5.68. Molecular modeling of SIRT5 with suramin. (A) Docking of suramin to dimeric form of SIRT5. (B) Docking of suramin to monomeric form of SIRT5. The crystal structure of SIRT5-suramin complex used for the docking was retrieved from protein data bank (PDB code: 2NYR).

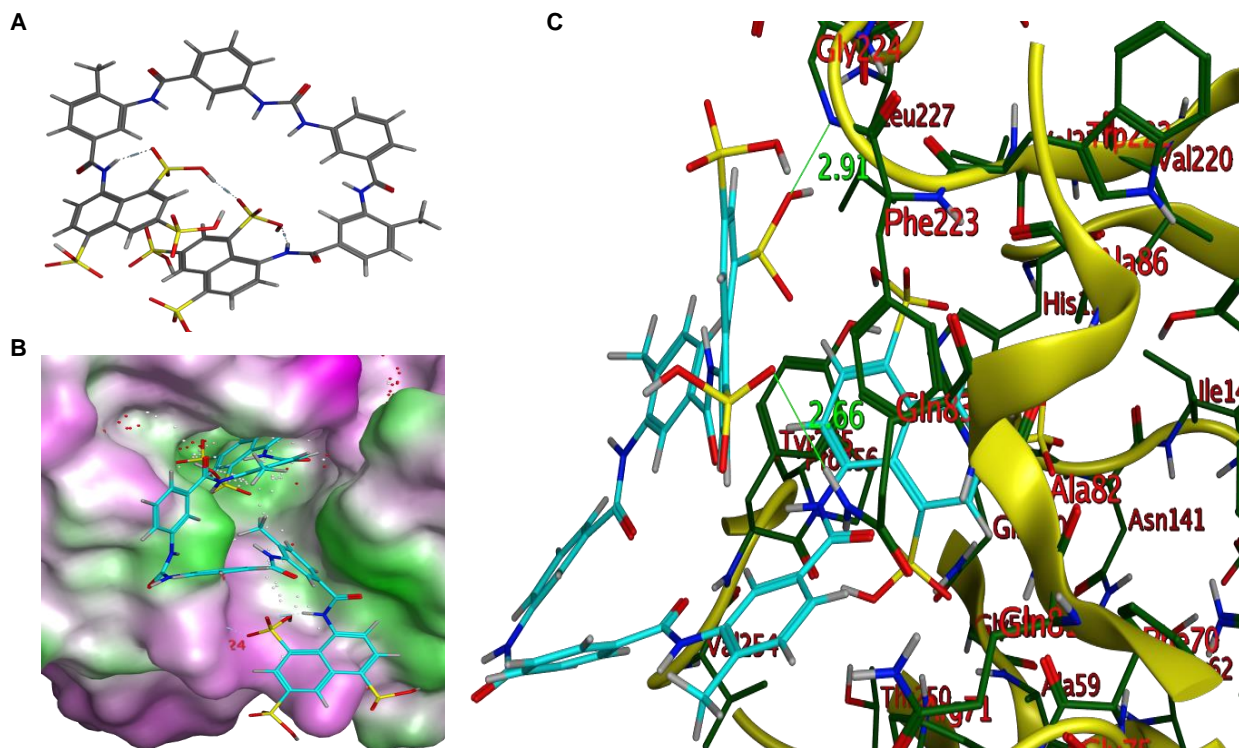


Figure 5.69. Molecular modeling of SIRT5 with energy minimized suramin. (A) Structure of energy minimized suramin. (B) Docking pose of suramin in 3D space (ligand is shown in stick mode in cyan color, heavy atoms are shown in elemental color, and receptor is shown in solid surface mode) (C) Hydrogen bond of sulfonate groups of suramin with Gln224, and Gln83 (shown in solid green line marked with distances).

### 5.4.3. Binding of nicotinamide to SIRT5

Steady-state kinetic studies for the inhibition of nicotinamide on SIRT1 and SIRT5 variants (section §5.3.5) show that the desuccinylation reaction (catalyzed by wild-type SIRT5 and its SIRT5 Y102A mutant) unequivocally exhibits the competitive inhibition of nicotinamide against  $\text{NAD}^+$ , suggesting that the “base-exchange” mechanism is either nonexistent or negligible in the latter cases. An alternative explanation for the inhibition mechanism could be that nicotinamide competitively displaces  $\text{NAD}^+$  from the enzyme-substrate- $\text{NAD}^+$  complex. In order to investigate the binding of nicotinamide to SIRT5, isothermal titration calorimetric (ITC)



studies were performed to determine the thermodynamic parameters for the binding of nicotinamide to SIRT5 and SIRT5-substrate complex in 50 mM HEPES buffer, pH 7.5, containing 100 mM NaCl, 10 % glycerol and 1 mM TCEP at 25 °C. Figure 5.68 shows the ITC profile of nicotinamide to SIRT5 (Figure 5.68A) and HEPES buffer (Figure 5.68B), suggesting that only miniscule heat signals were generated as a result of heat dilution for the titration of nicotinamide to SIRT5 in the absence of Ac-Suclys-AMC substrate. On the other hand, in the presence of 10 mM NAD<sup>+</sup> (Figure 5.69), nicotinamide produces higher magnitude of the heat signal, suggesting tighter binding affinity of the inhibitor to the enzyme. The data of Figure 5.69 was analyzed by using the single site binding model, yielding the magnitudes of  $n$ ,  $\Delta H^\circ$  and  $K_a$  as being equal to  $2.1 \pm 0.1$ ,  $-(1.3 \pm 0.1)$  kcal/mol and  $(2.7 \pm 0.2) \times 10^4 \text{ M}^{-1}$ , respectively. The latter value translates to the  $\Delta G^\circ$  of binding as being equal to  $-4.2 \pm 0.1$  kcal/mol. Given the  $\Delta H^\circ$  and  $\Delta G^\circ$  values, the  $T\Delta S^\circ$  was calculated to be 2.9 kcal/mol. Note that ITC data shows that the  $K_d$  value (41  $\mu\text{M}$ ) for the binding of nicotinamide to the enzyme-substrate complex is comparable to the  $K_m$  value of NAD<sup>+</sup> (69  $\mu\text{M}$ ) during the wild-type SIRT5 catalyzed desuccinylation reaction. Thus, the possibility of nicotinamide competitively displacing NAD<sup>+</sup> from the enzyme-substrate-NAD<sup>+</sup> complex is further supported.

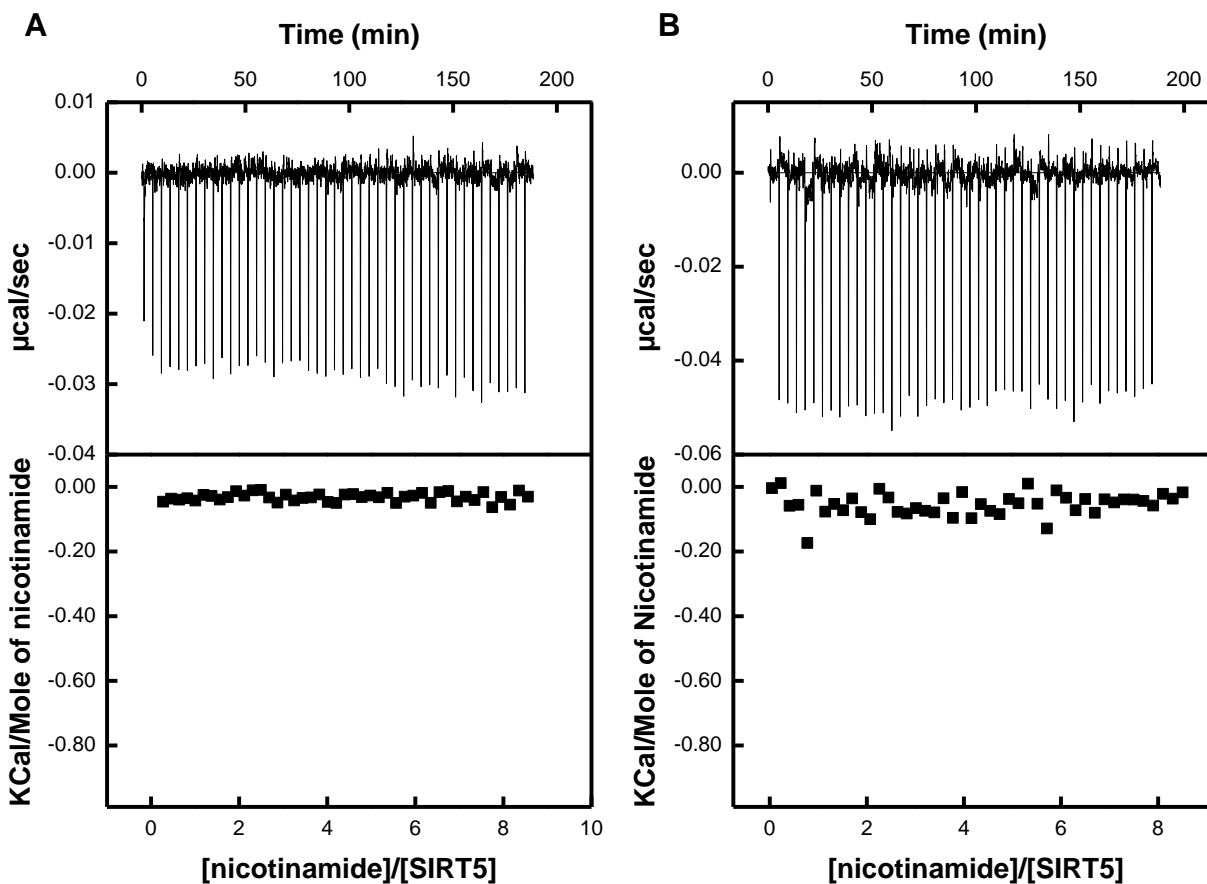


Figure 5.70. ITC profile for the binding of nicotinamide to SIRT5. (A) The top panels show the raw data generated by titration of 30  $\mu\text{M}$  SIRT5 by 45 injections (5  $\mu\text{l}$  each) of 10 mM nicotinamide. (B) The top panels show the raw data generated by titration of HEPES buffer by 45 injections (5  $\mu\text{l}$  each) of 2 mM. The area under each peak was integrated and plotted against the molar ratio of nicotinamide to SIRT5.

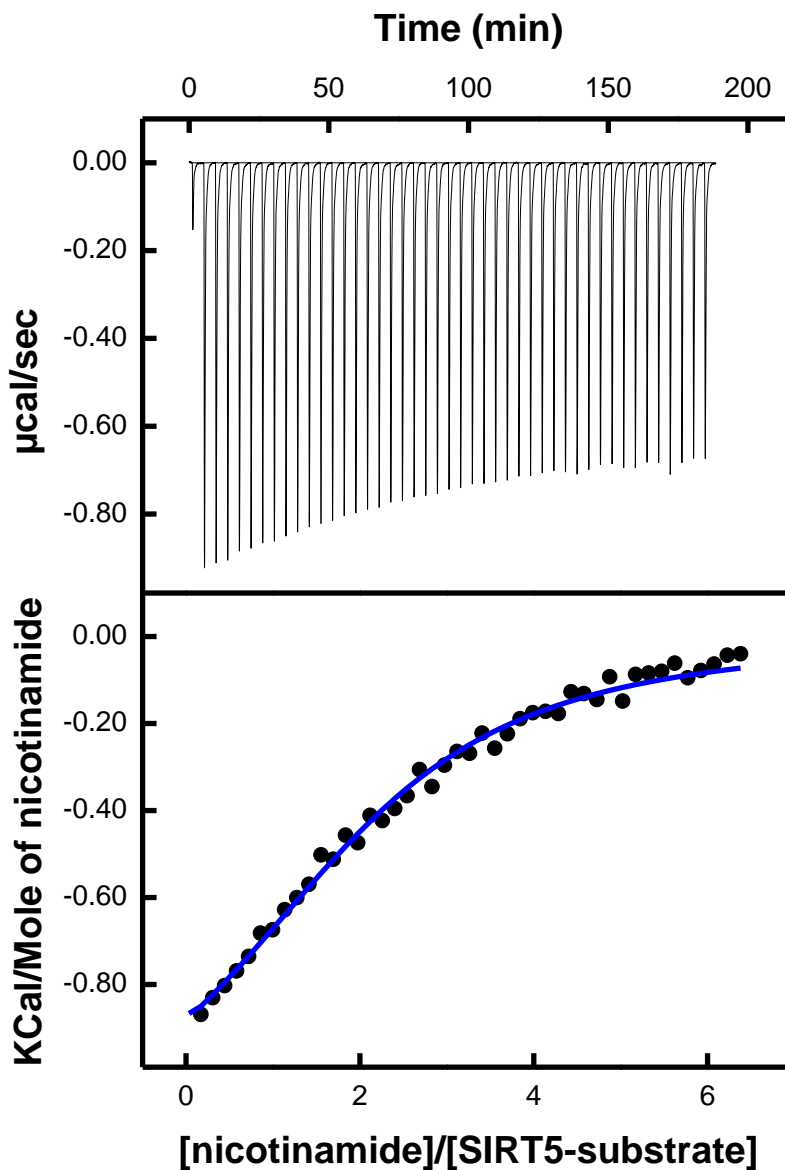


Figure 5.71. ITC profile for the binding of nicotinamide to SIRT5-substrate complex. The top panels show the raw data generated by titration of 40  $\mu\text{M}$  SIRT5 by 45 injections (5  $\mu\text{l}$  each) of 2 mM nicotinamide in the presence of 1 mM Ac-Suclys-AMC substrate. The area under each peak was integrated and plotted against the molar ratio of nicotinamide to SIRT5. The solid lines represent the best fit of the experimental data for the one binding site model, yielding the thermodynamic parameters of  $n$ ,  $K_a$  and  $\Delta H^\circ$  as  $2.1 \pm 0.1$ ,  $-(1.3 \pm 0.1) \text{ kcal/mol}$  and  $(2.7 \pm 0.2) \times 10^4 \text{ M}^{-1}$ , respectively.

#### 5.4.4. Binding of EX527 to SIRT5 variants

As described in section 5.3.7, the  $IC_{50}$  value of EX527 against the deacetylase activity of SIRT5 Y102A/R105I double mutant is much lower than SIRT5 wild type and its single mutants Y102A and R105I. Thus, it is reasonable to surmise that the enhanced inhibition potency is due to a tighter binding affinity of EX527 to SIRT5 Y102A/R105I double mutant. In order to probe the above hypothesis, isothermal titration calorimetry (ITC) studies were performed to determine the thermodynamic parameters for the binding of EX527 to SIRT5. Since previous studies suggest that the binding of EX527 is enhanced in the presence of  $NAD^+$  (45), the experiment was performed both in the absence and presence of  $NAD^+$ . Figure 5.70 shows the ITC profile for the titration of SIRT5 Y102A/R105I double mutant by increasing 45 aliquots of 1 mM EX527 in the absence and presence of 10 mM  $NAD^+$  in 50 mM HEPES buffer, pH 7.5, containing 100 mM NaCl, 10 % glycerol and 1 mM TCEP at 25 °C. The raw calorimetric data for the interaction of EX527 to SIRT5 Y102A/R105I double mutant and their binding isotherms are shown in the top and the bottom panels of the figures, respectively. Figure 5.70A shows that EX527 only binds weakly to SIRT5 Y102A/R105I mutant in the absence of  $NAD^+$ . However, in the presence of 10 mM  $NAD^+$  (Figure 5.70B), EX527 produces higher magnitude of the heat signal, suggesting tighter binding affinity of the inhibitor to the double mutant enzyme. The data of Figure 5.70B was analyzed for the single site binding model, yielding the magnitudes of  $n$ ,  $\Delta H^\circ$  and  $K_a$  as being equal to  $1.2 \pm 0.0$ ,  $-5.3 \pm 0.1$  kcal/mol and  $(2.5 \pm 0.2) \times 10^5 M^{-1}$ , respectively. The latter value translates to the  $\Delta G^\circ$  of binding as being equal to  $-7.3 \pm 0.1$  kcal/mol. Given the  $\Delta H^\circ$  and  $\Delta G^\circ$  values, the  $T\Delta S^\circ$  was calculated to be 2.03 kcal/mol. In view of these thermodynamic parameters, it is evident that the binding of EX527 to Y102A/R105 double mutant of SIRT5 is dominated by the enthalpic contribution to the overall binding free energy. When the same set of

experiments was performed for the binding of EX527 to the wild type SIRT5 under the identical condition, only miniscule heat signals were generated either in the absence or the presence of  $\text{NAD}^+$  (Figure 5.71). Hence, Y102 and R105 preclude the binding of EX527 to wild-type SIRT5.

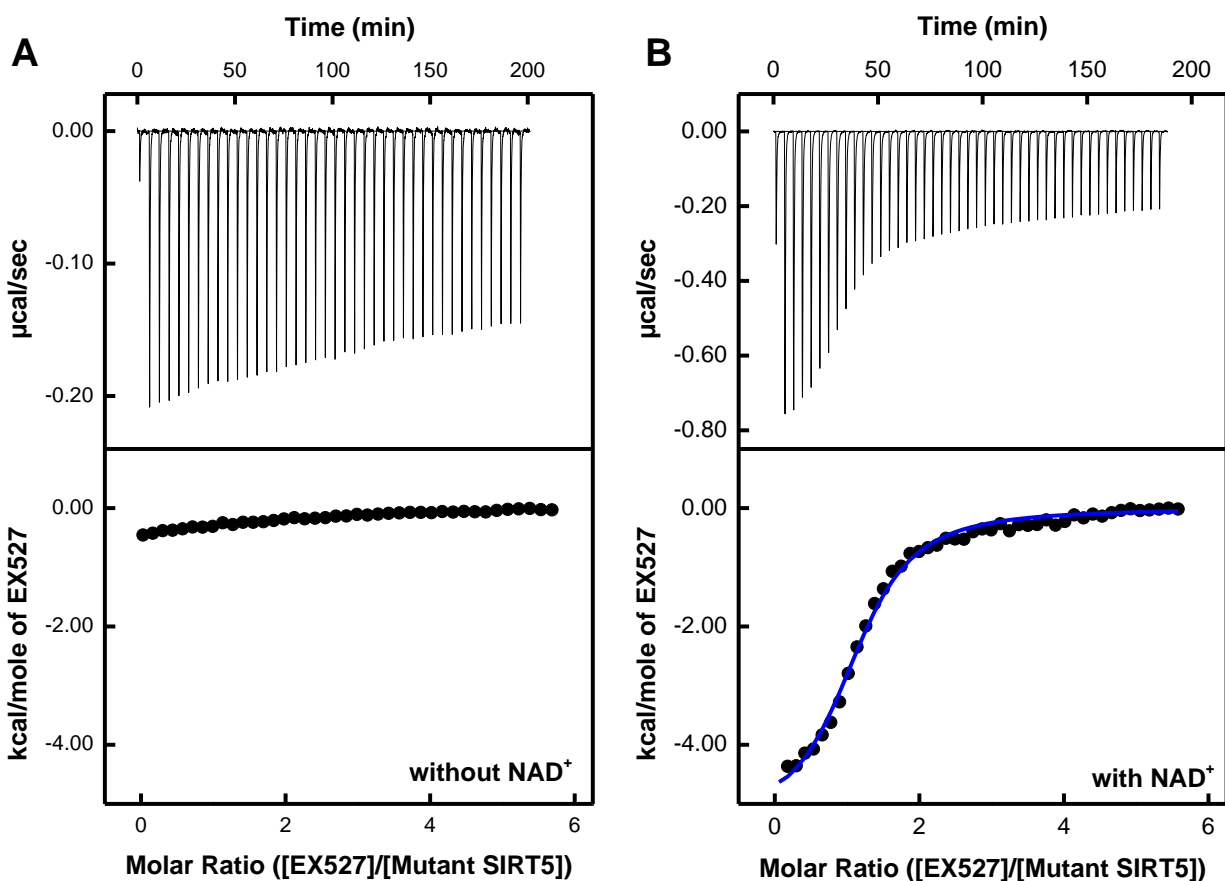


Figure 5.72. ITC profile for the binding of EX527 to SIRT5 Y102A/R105I in the absence (A) and presence (B) of 10 mM  $\text{NAD}^+$ . The top panels show the raw data generated by titration of 20  $\mu\text{M}$  SIRT5 Y102A/R105I by 45 injections (5  $\mu\text{l}$  each) of 500  $\mu\text{M}$  EX527. The area under each peak was integrated and plotted against the molar ratio of EX527 to SIRT5 Y102A/R105I. The solid lines (right panel) represent the best fit of the experimental data for the one binding site model, yielding the magnitudes of  $n$ ,  $K_a$  and  $\Delta H^\circ$  as being equal to  $1.2 \pm 0.0$ ,  $-5.3 \pm 0.1$  kcal/mol and  $(2.5 \pm 0.2) \times 10^5 \text{ M}^{-1}$ , respectively.

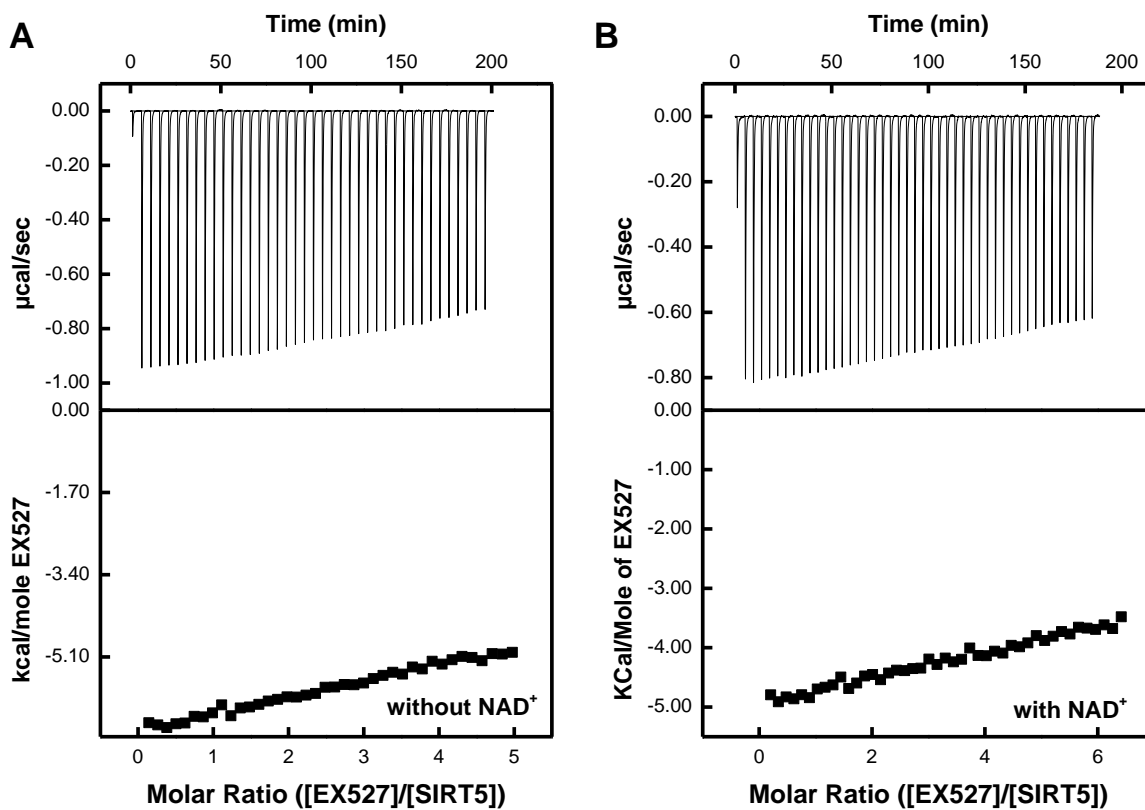


Figure 5.73. ITC profile for the binding of EX527 to SIRT5 in the absence (A) and presence (B) of 10 mM NAD<sup>+</sup>. The top panels show the raw data generated by titration of 20 µM SIRT5 by 45 injections (5 µl each) of 500 µM EX527. The area under each peak was integrated and plotted against the molar ratio of EX527 to SIRT5 Y102A/R105I.

## 5.5. Thermal Stabilities of SIRT1 and SIRT5 Variants

### 5.5.1. Thermal unfolding of SIRT1 and SIRT5 variants

The influence of three mutations of SIRT5, namely Y102A, R105I, and Y102A/R105I, on thermal stability of the enzyme was probed by performing comparative thermal unfolding studies. The latter were performed by measuring the loss in the secondary structural feature of the protein by CD spectroscopy. The latter approach was employed to monitor the ellipticity of the enzymes at 208 nm as a function of temperature. As shown in Figures 5.72 to 5.76., the increase in temperature increases the ellipticities of the enzymes at 208 nm in a sigmoidal manner, resulting in the attainment of plateau at high temperatures. A casual perusal of the data of Figures 5.72 to 5.75 reveal that while wild-type SIRT5 and Y102A mutant enzyme exhibit a single stage melting transition (Figure 5.72 and 5.73), R105I and Y102A/R105I mutant enzymes exhibit the two stage melting transitions (Figure 5.74 and 5.75). When the above experiment was performed with wild-type SIRT1 (Figure 5.76), the overall profile exhibited a single stage melting transition, similar to that observed with the wild-type SIRT5 (Figure 5.72) and its Y102A mutant variant (Figure 5.73). Depending on the nature of melting transition profiles of the enzymes, attempts were made to analyze the data of Figures 5.72 to 5.76 either by single (Eq. 4.15) or double (Eq. 4.16) transition Boltzmann equations as described in the Methods section (section §4.5.4). Since the analyses of the data of Figures 5.74 and 5.75 by two independent phases Boltzmann equation (Eq. 4.16) did not produce reliable results, recourse was made to analyze the individual melting transitions by the single phase Boltzmann equation (Eq 4.15). The derived  $T_m$  values (the temperature at which half of the proteins lost the secondary structural features) from the best fit of the data are summarized in Table 5.12. The data of Table 5.12 clearly shows that both wild-type SIRT1 and SIRT5 exhibit the single phase denaturation profile,

but the  $T_m$  value of SIRT1 ( $62.7 \pm 0.4$  °C) is about 10 degree higher than that of wild-type SIRT5 ( $52.9 \pm 0.04$  °C). On the other hand, the  $T_m$  value of the wild-type SIRT5 is about 11 degree higher than that of the Y102A mutant ( $41.8 \pm 0.03$ °C), suggesting that Y102A mutation destabilizes the enzyme structure. It is important to emphasize that of two  $T_m$  values of R105I mutant of SIRT5, while the  $T_m$  value of the first transition phase ( $58.1 \pm 1.0$  °C) resembles that of the wild-type SIRT5 ( $52.9 \pm 0.04$  °C), the  $T_m$  value of the second transition phase ( $72 \pm 0.1$  °C) is about 20 degree higher. On the other hand, while the  $T_m$  value of the first transition phase of Y102A/R105I double mutant ( $42.9 \pm 0.1$  °C) resembles that of Y102A mutant enzyme ( $41.8 \pm 0.03$  °C), the  $T_m$  value of the second transition phase ( $79.0 \pm 0.1$  °C) is about 5 degree higher than that of the second phase of R105I mutant ( $72.0 \pm 0.1$  °C). Clearly, Y102 and R105 residues exhibit differential effects on thermal stability of the enzyme.

To further investigate whether the fully denatured enzymes acquired the secondary structural features upon cooling to the room temperature (25 °C), the individual enzyme samples were heated to their final melting temperatures, cooled them to room temperature (25 °C), and recorded their CD spectra (Figure 5.77). Surprisingly, while the above treatment of wild-type SIRT5 resulted in nearly complete loss of the secondary structural feature that of the R105I mutant showed modest secondary structure. On the other hand, the Y102A/R105I mutant enzyme showed the secondary structural feature similar to that of the wild-type enzyme. However, none of the heat treated (and subsequently cooled) samples showed any enzyme activity.



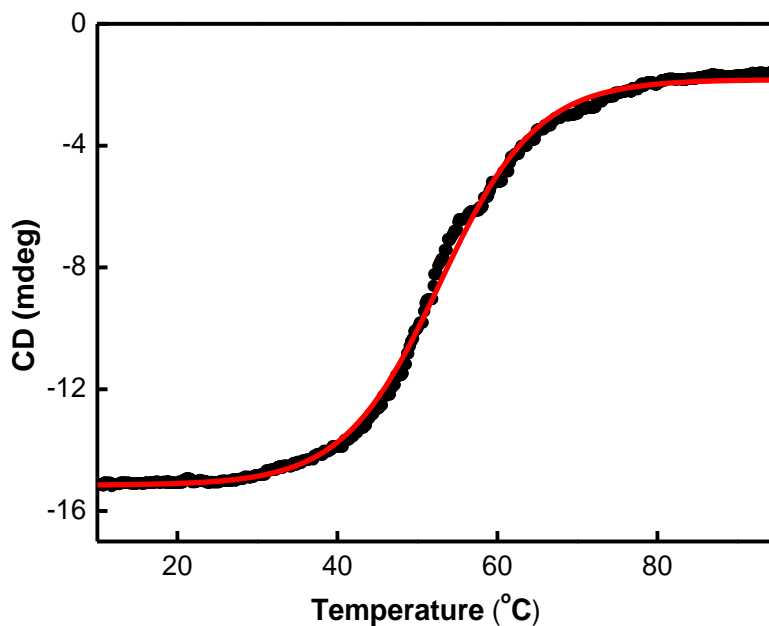


Figure 5.74. Thermal denaturation SIRT5. The ellipticity change of SIRT1 was monitored at 208 nm as a function of increasing temperatures. The scan was performed at a heating rate of  $1\text{ }^{\circ}\text{C min}^{-1}$  in 5 mM Tris-HCl buffer, pH 7.5 using a quartz cuvette of 1 mm path length.

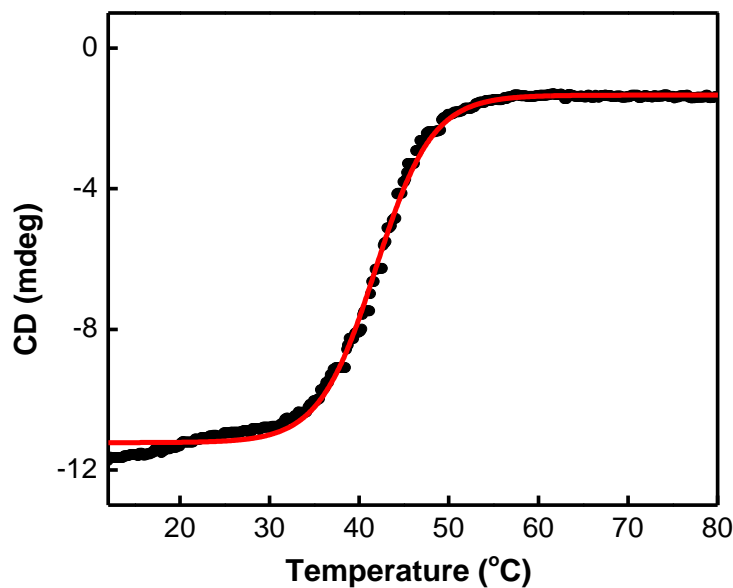


Figure 5.75. Thermal denaturation of SIRT5 Y102A. The ellipticity change of SIRT5 Y102A was monitored at 208 nm as a function of increasing temperatures. The scan was performed at a heating rate of  $1\text{ }^{\circ}\text{C min}^{-1}$  in 5 mM Tris-HCl buffer, pH 7.5 using a quartz cuvette of 1 mm path length.

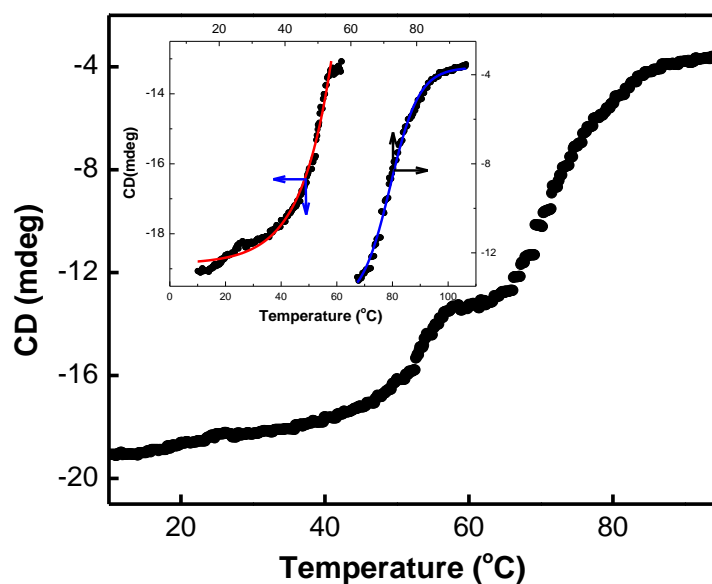


Figure 5.76. Thermal denaturation of SIRT5 R105I. The ellipticity change of SIRT5 R105I was monitored at 208 nm as a function of increasing temperatures. The scan was performed at a heating rate of  $1\text{ }^{\circ}\text{C min}^{-1}$  in 5 mM Tris-HCl buffer, pH 7.5 using a quartz cuvette of 1 mm path length.

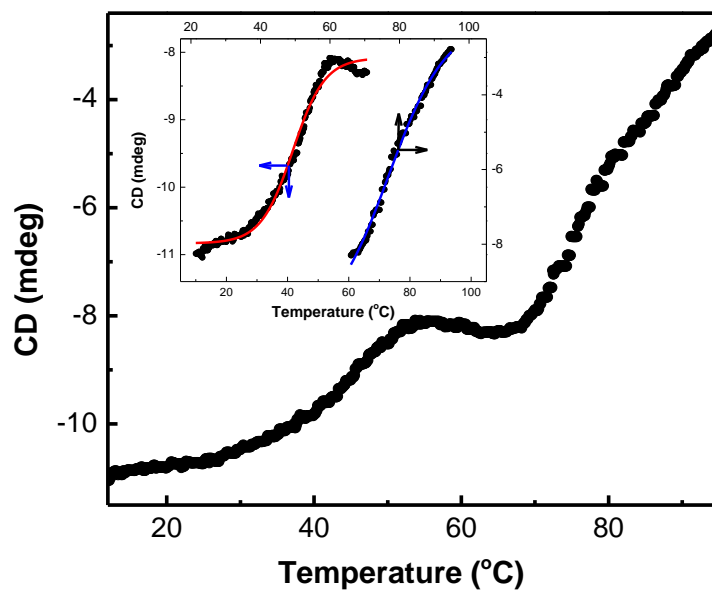


Figure 5.77. Thermal denaturation of SIRT5 Y102A/R105I. The ellipticity change of SIRT5 Y102A/R105I was monitored at 208 nm as a function of increasing temperatures. The scan was performed at a heating rate of  $1\text{ }^{\circ}\text{C min}^{-1}$  in 5 mM Tris-HCl buffer, pH 7.5 using a quartz cuvette of 1 mm path length.

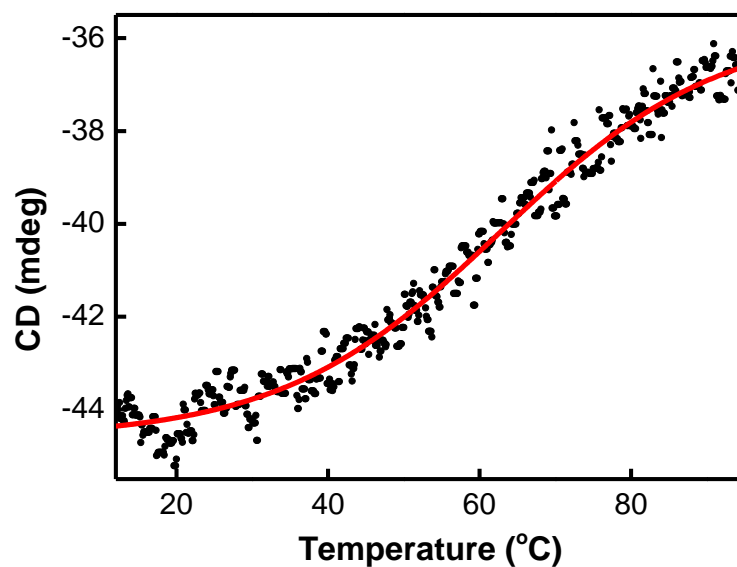


Figure 5.78. Thermal denaturation of SIRT1. The ellipticity change of SIRT1 was monitored at 208 nm as a function of increasing temperatures. The scan was performed at a heating rate of 1 °C min<sup>-1</sup> in 5 mM Tris-HCl buffer, pH 7.5 using a quartz cuvette of 1 mm path length.

Table 5.12. Melting temperatures of SIRT1 and SIRT5 variants

	T <sub>m</sub> (°C)
SIRT5 wild type	52.9 ± 0.04
SIRT5 Y102A	41.8 ± 0.03
SIRT5 R105I	58.1 ± 1.0
	72.0 ± 0.1
SIRT5 Y102A/R105I	42.9 ± 0.1
	79.0 ± 0.1
SIRT1	62.7 ± 0.4

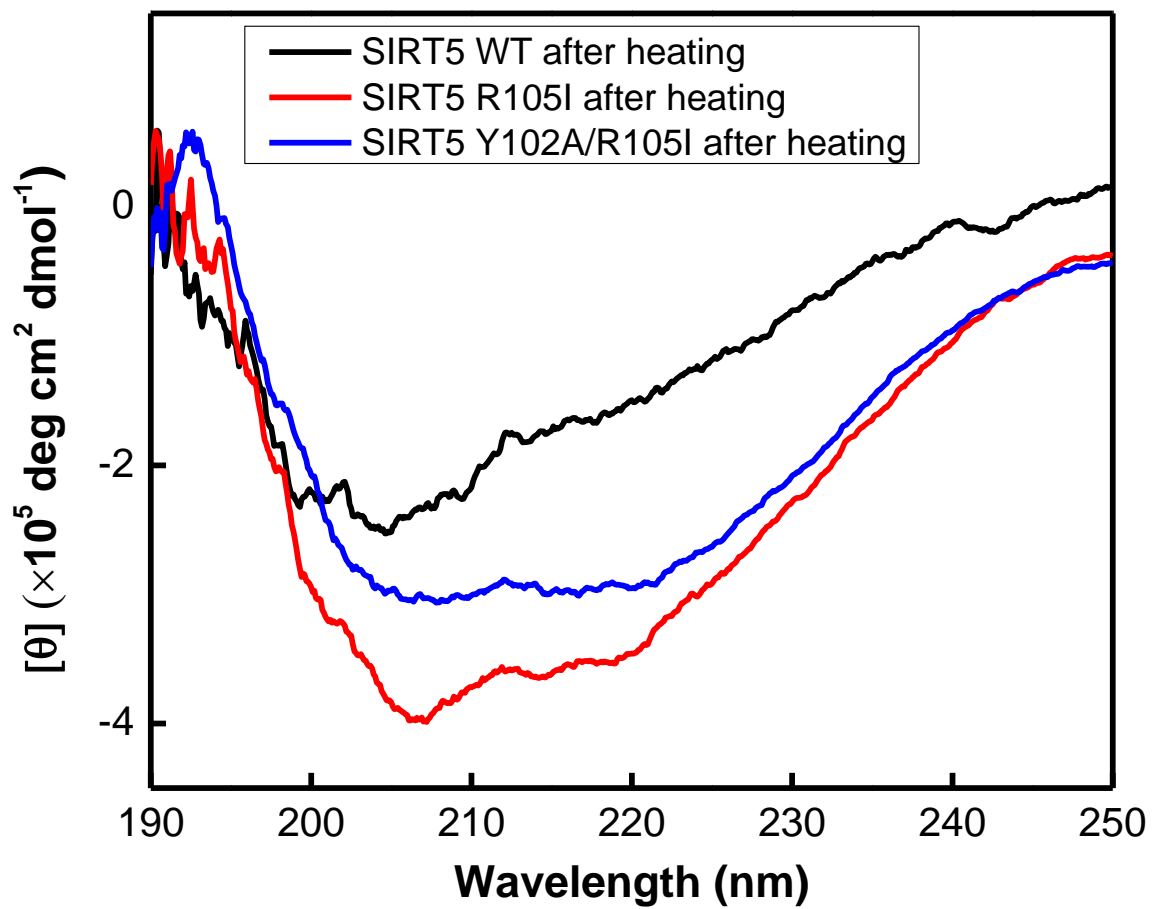


Figure 5.79. CD spectra of wild-type (black) and R105I (red) and Y102A (blue) mutants of SIRT5 after completion of the melting phases.

### 5.5.2. Thermal stability of SIRT5 in the presence of suramin

Binding of a ligand to protein is often associated with modulation in secondary structure of the protein. In order to investigate the change of the above feature for the binding of suramin to SIRT5, the CD spectra of SIRT5 in the absence and presence of suramin were recorded under the same experimental condition as described in the Method section. Figure 5.78 shows CD spectra of SIRT5 upon the binding of suramin (blue dashed line). The overall spectrum is comparable with the apo-SIRT5 except for a slight change between 210-220 nm, which is presumably due to the structural changes within the flexible loop connecting the Rossmann fold domain and the zinc binding domain (see Discussion section)(34).

In order to compare the thermal stability of SIRT5 when bound with suramin, the thermal stability of the suramin-bound form of SIRT5 was investigated by measuring the loss of the secondary structure (monitored by the ellipticity at 208 nm) as a function of temperature. as described in the Methods section (§4.3.4). Figure 5.79 shows the thermal unfolding curve of 10  $\mu$ M SIRT5 in the presence of 10  $\mu$ M suramin. The red smooth line represents the best fit of the data by the single phase Boltzmann equation (Eq 4.15), yielding the  $T_m$  value to be  $(62.7 \pm 0.4 \text{ }^\circ\text{C})$ . Note that the above value is about 10 degree higher the the  $T_m$  value of SIRT5 in the absence of suramin. The increased  $T_m$  suggests that the secondary structure of SIRT5 is stabilized upon the binding of suramin.

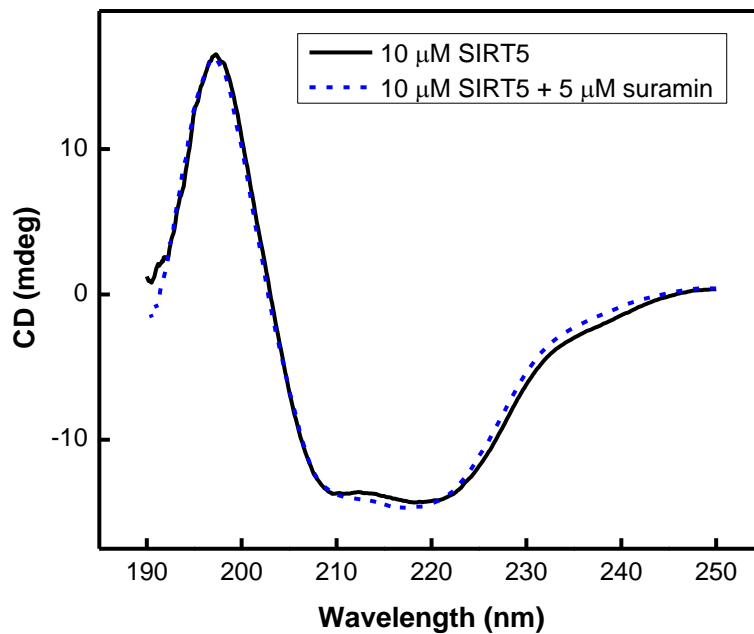


Figure 5.80. CD Spectra of SIRT5 in the absence and presence of suramin. The mean residue ellipticities of 10  $\mu\text{M}$  SIRT5 in the absence (black solid line) and presence (blue dashed line) of 5  $\mu\text{M}$  suramin as a function of wavelength are shown. The experiments were performed in 5 mM Tris-HCl buffer, pH 7.5 using a quartz cuvette of 1 mm path length.

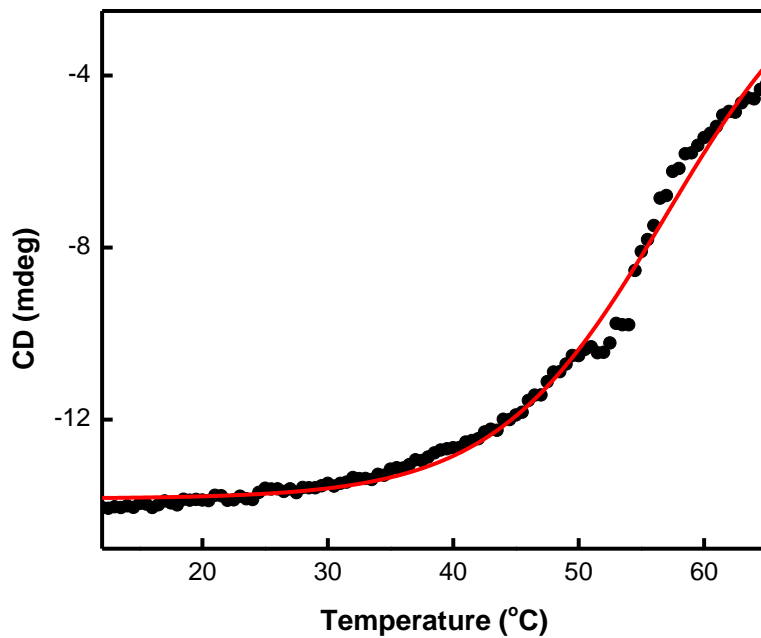


Figure 5.81. Thermal denaturation of SIRT5 in the presence of suramin. The ellipticity change of 10  $\mu\text{M}$  SIRT5 in the presence of 10  $\mu\text{M}$  suramin was monitored at 208 nm as a function of increasing temperatures. The scan was performed at a heating rate of 1  $^{\circ}\text{C min}^{-1}$  in 5 mM Tris-HCl buffer, pH 7.5 using a quartz cuvette of 1 mm path length.

## 6. DISCUSSION

### 6.1. Contribution of Y102 and R105 Residues of SIRT5 in Catalysis

Previous studies have shown that human SIRT5 has considerably lower deacetylase activity as compared to that of human SIRT1, SIRT2 and SIRT3 (272). While SIRT1 primarily catalyzes the deacetylation reaction (of acetylated lysine residues) in selected proteins, SIRT5 preferentially cleaves the negatively charged acyl moieties (viz., succinyl-, malonyl-, glutaryl-) from their lysine conjugates in enzymes and proteins (11, 257, 273). The above unique feature of SIRT5 appears to be encoded in the active site residues, Y102 and R105, of the enzyme, and these residues are substituted by A313 and I316 of SIRT1, respectively (Figure 5.5 of section §5.1.2). Whether the difference in the above residues between SIRT1 and SIRT5 served as the sole determinant of the substrate selectivity was probed by replacing Y102 and R105 residues of SIRT5 by corresponding Ala and Ile residues in SIRT1, respectively, via site directed mutagenesis. A detailed account of the kinetic data of wild-type SIRT1 and SIRT5 and Y102A, R105I, and Y102A/R105I mutants of the latter enzyme unraveled the fact that aside from the specific amino acid residues within the active site pockets, the overall structural features of the enzyme dictate the substrate specificity as well as the catalytic efficiencies of the enzymes. It has been widely accepted that sirtuin catalyzed reactions follow a sequential mechanism in which the acetylated peptide binds first followed by the binding of  $\text{NAD}^+$  to generate the enzyme-substrate- $\text{NAD}^+$  ternary complex, which undergoes the chemical transformation reaction to produce the reaction products (274). Since all sirtuins share a highly conserved catalytic core, it is not surprising that they utilize similar bi-substrate ternary complex mechanism. Although attempt was not made to differentiate among alternative bi-substrate reaction mechanisms with wild-type SIRT1 and SIRT5 and its mutants, the kinetic data (collected in a matrix format with varying



concentrations of the substrate(s) and  $\text{NAD}^+$ ) were analyzed by the sequential mechanism to derive the “true” (instead of “apparent”) kinetic parameters of the enzymes. The data of Table 5.1 clearly reveals that for structurally similar fluorogenic substrates, the specificity constant ( $k_{\text{cat}}/K_m$ ) for the SIRT5 catalyzed desuccinylation reaction is about one order of magnitude higher than that for the SIRT1 catalyzed deacetylation reaction, and none of the SIRT5 mutants (either catalyzing the desuccinylation or deacetylation reaction) yield the specificity constants similar to or higher than that of the wild-type enzyme.

Although the  $K_{m,\text{sub}}$  for the double mutant (SIRT5: Y102A/R105I) is comparable to that obtained for SIRT1, the  $k_{\text{cat}}$  value of the former enzyme was about 25 fold lower than that of the latter enzyme. Hence, although Y102A and/or R105I mutations in SIRT5 promote the deacetylase activity, the catalytic machinery of the mutant enzymes is not as efficient as that of SIRT1. Clearly, the substrate specificity of SIRT1 and SIRT5 is not manifested exclusively by the (above noted) “two” residues. Previous studies have shown that the conserved catalytic core of SIRT1 has very low catalytic activity toward several known protein substrates. The N- and C-terminal regions of SIRT1 increased the catalytic efficiency of SIRT1 by between 12- and 45-fold (56). Unlike SIRT1, SIRT5 does not possess the above two regions that potentiate the enzyme catalytic efficiency, which is at least the partial reason for explaining the different  $K_{\text{cat}}$  values between the double mutant SIRT5 (which mimics SIRT1 catalytic core) and SIRT1.

In the presence of high concentrations of  $\text{NAD}^+$  (found under certain physiological conditions), the latter interacts with non-mammalian sirtuins such as Sir2Af1 and Sir2Af2 in a nonproductive manner (29, 275). The binding affinities for  $\text{NAD}^+$  for SIRT1 and SIRT3 under in vitro condition have been found to be in the millimolar range (228). Of seven human sirtuins,

only SIRT6 has been shown to bind  $\text{NAD}^+$  tightly ( $K_d = 27 \mu\text{M}$ ) in the absence of acylated substrates (35).

However, it is becoming increasingly clear that the binding affinity of  $\text{NAD}^+$  in different sirtuins is modulated by the nature of the acylated substrates (15). Such difference in the substrate dependent changes in the binding affinity of  $\text{NAD}^+$  is evident from our kinetic data. As noted in the previous chapter, the  $K_m$  for  $\text{NAD}^+$  during the desuccinylation reaction (given by the wild-type SIRT5 and Y102A mutant) is lower than that for the deacetylation (given by SIRT1 and Y102A and Y102A/R105I mutants of SIRT5) reaction. Particularly in case of Y102A enzyme, which catalyzes both deacetylation and desuccinylation reactions, the  $K_m$  for  $\text{NAD}^+$  for the desuccinylation reaction is about 10 fold lower than that for the deacetylation reaction. This difference is presumably due to the electrostatic interaction between R105 and the phosphate moieties of  $\text{NAD}^+$  during the desuccinylation reaction.

## **6.2. Inhibition of Desuccinylase Activity of SIRT5**

Although several sirtuin inhibitors inhibit both deacetylase and desuccinylase reactions, their modes of action and mechanistic details have been found to be different for the above reactions as elaborated with respect to the following inhibitors.

### **6.2.1. Inhibition of nicotinamide**

In cases where the mode of nicotinamide inhibition could be reliably determined, only the deacetylation reaction (catalyzed by SIRT1 and SIRT5 Y102A/R015I mutant) showed the mixed inhibition of nicotinamide against  $\text{NAD}^+$ ; the desuccinylation reaction (catalyzed by wild-type SIRT5 and its SIRT5 Y102A mutant) unequivocally showed the competitive inhibition against  $\text{NAD}^+$ . Such inhibitory feature suggested that the “base-exchange” mechanism was either nonexistent or negligible during the desuccinylation reaction.

The model discrimination analysis for the wild-type SIRT5 and its Y012A mutant catalyzed reactions (section §5.3.5) unambiguously demonstrate that the nicotinamide inhibition (against NAD<sup>+</sup>) is purely “competitive” in nature, and the enzyme is nearly 100% inhibited in the presence of saturating concentration of the inhibitor. Based on the kinetic and modeling grounds, Guan et al. argued that “apparent competitive” inhibition of nicotinamide (against NAD<sup>+</sup>) in human SIRT3 catalyzed reaction may also involve the contribution of the base-exchange mechanism (267). However, it is non-intuitive as to how a “purely” competitive inhibitor, which inhibits the enzyme activity by nearly 100%, would reverse the deacylation step by exclusively interacting with the enzyme-acylimidate complex but not with the enzyme-substrate complex; the latter scenario could easily give rise to the pure competitive inhibition profile. The possibility of nicotinamide competitively displacing NAD<sup>+</sup> from the enzyme-substrate-NAD<sup>+</sup> complex is further supported by the isothermal titration calorimetric data (Figure 5.69) for the binding of nicotinamide to SIRT5-substrate complex. The ITC data shows that that only miniscule heat signals were generated as a result of heat dilution for the titration of nicotinamide to SIRT5 in the absence of Ac-Suclys-AMC substrate, while higher magnitude of the heat signal was generated in the presence of succinylated substrate. The K<sub>d</sub> value (41 μM) for the binding of nicotinamide to the enzyme-substrate complex is comparable to the K<sub>m</sub> value of NAD<sup>+</sup> (69 μM) during the wild-type SIRT5 catalyzed descuccinylation reaction. Unlike the descuccinylation reaction, the nicotinamide inhibition data for the deacetylation reaction shows the mixed non-competitive type of inhibition as observed with Sir2 enzymes in which the base-exchange mechanism has been unambiguously demonstrated (227).

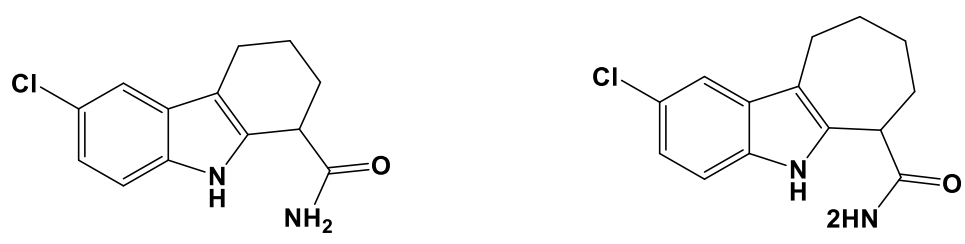
### 6.2.2. Inhibition of EX527

The fact that SIRT1 selective inhibitor, EX527, also inhibits the SIRT3 catalyzed reaction with reduced potency, but neither binds to wild-type SIRT5 nor inhibits its catalysis (45) is consistent with our finding that Y102 and R105 are responsible for precluding its avidity to the latter enzyme site. Since the magnitude of inhibition of SIRT5 R05I mutant by EX527 is higher than that determined with SIRT5 Y102A mutant (Figure 5.43), it appears logical to conclude that R105 in SIRT5 is a major contributor of resisting the inhibition. But this simplistic justification falls short in explaining a marked increase in the inhibitory potency of EX527 for Y012A/R105I double mutant enzyme. Evidently, Y102 and R105 coordinate with each other in controlling the accessibility (consequently inhibition) of the inhibitor to the enzyme. Interestingly, the inhibition constant of EX527 for Y102A/R105I mutant enzyme ( $21.7 \pm 1.0 \mu\text{M}$ ) is comparable to that obtained with the wild-type SIRT3, albeit it is still considerably higher than that obtained with SIRT1.

Previous studies have demonstrated that the binding affinities of EX527 to SIRT1 and SIRT3 are significantly higher in the presence of  $\text{NAD}^+$ , and the protein structure is more thermodynamically stable only in the presence of  $\text{NAD}^+$  (45, 268). Zhao et al. crystallized SIRT1 in complex with  $\text{NAD}^+$  and an EX527 analogue (Figure 6.1), providing insight into the mechanism for the binding and inhibition of EX527 to sirtuins (elaborated in section §1.7.2.2). Consistently, the isothermal titration calorimetric studies in section §5.4.4 suggest that the binding of EX527 to Y102A/R105I produced significantly higher heat signal in the presence of  $\text{NAD}^+$ , suggesting tighter binding affinity of the inhibitor to the double mutant enzyme in the presence of  $\text{NAD}^+$ . Furthermore, our ITC data for the binding of EX527 to Y102A/R105I double mutant enzyme reveals that the overall binding free energy is dominated by enthalpic rather than

entropic contribution. We conjecture that the lack of inhibition of wild-type SIRT5 by EX527 is contributed both by the steric hindrance (imposed by Y102 and R105 residues; see Figure 6.2) as well as by relatively higher level of solvation of the enzyme's active site pocket which is not conducive for binding of the predominantly hydrophobic molecules like EX527.

**A**



**B**

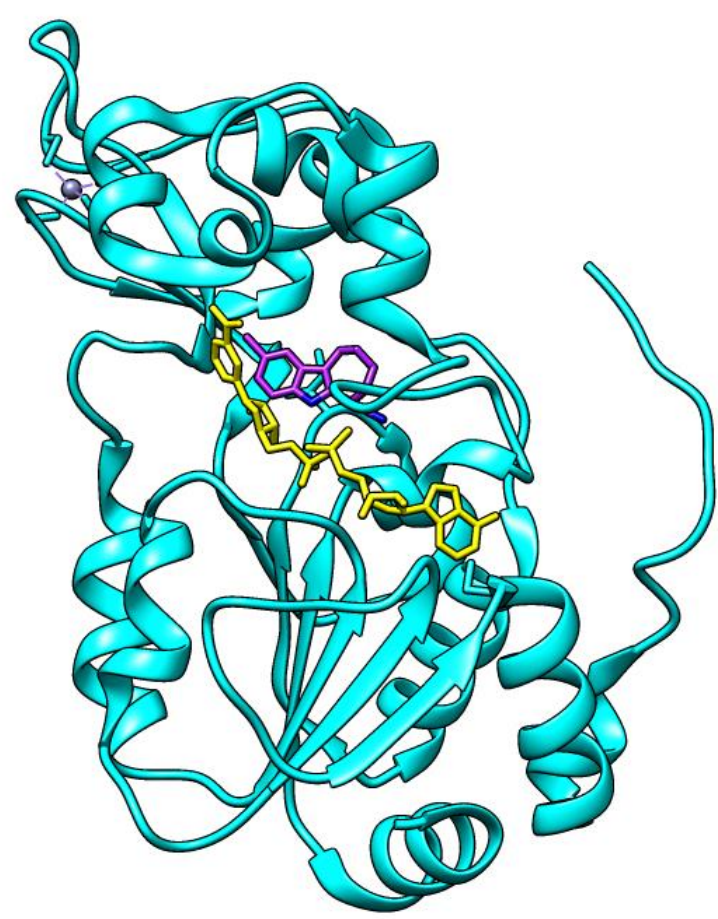


Figure 6.1. Structure of EX527, the analogue, and the catalytic domain of SIRT1 bound with EX527 analog and NAD<sup>+</sup>. (A) Schematic representation of EX527 to the left and the analogue to the right. (B) The crystal structure of SIRT1 bound to NAD<sup>+</sup> and the EX527 analogue. EX527 analogue and NAD<sup>+</sup> are presented in purple and yellow, respectively.

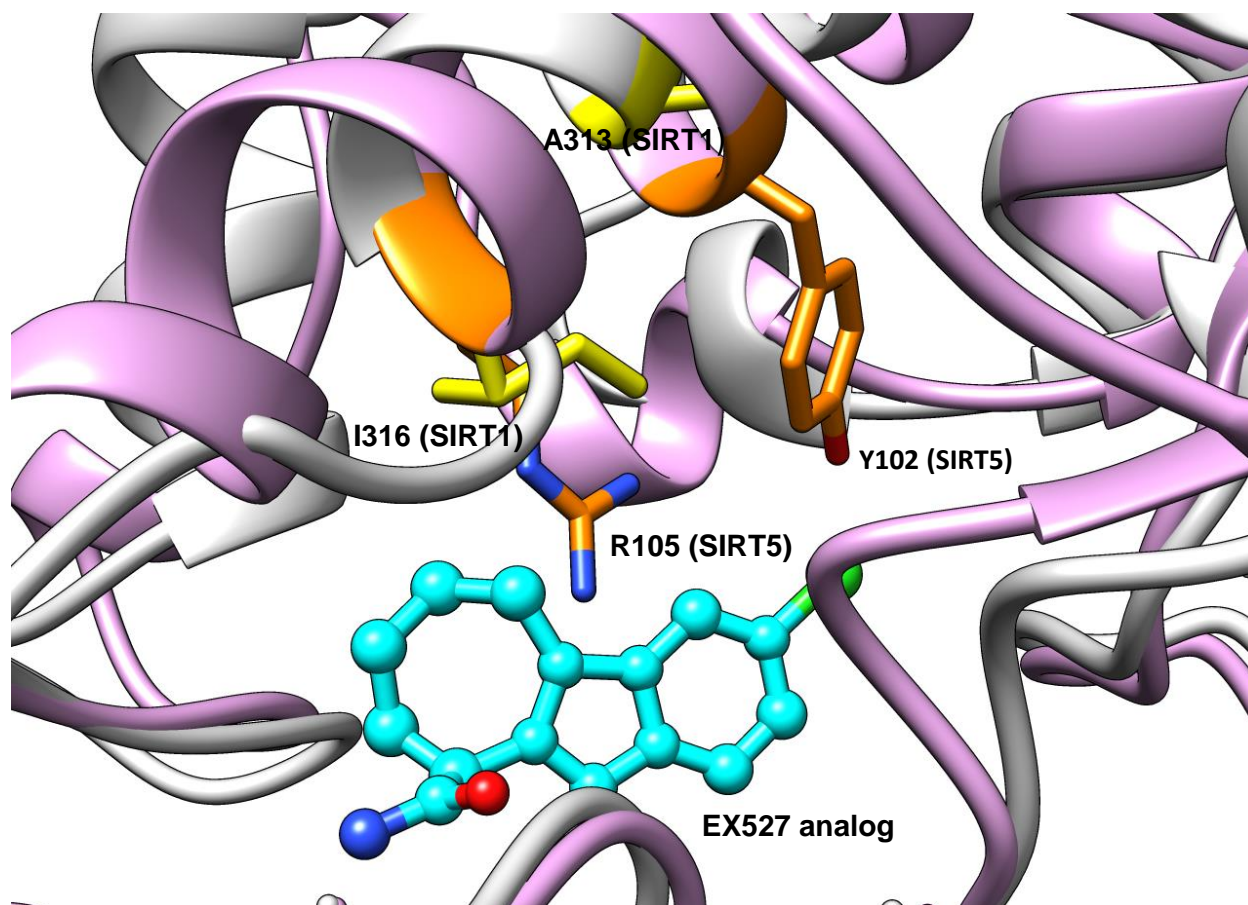


Figure 6.2. Superimposition of SIRT1 and SIRT5 showing the binding site of EX527. The crystal structure of SIRT1-EX527 analog complex was superimposed on the structure of SIRT5. SIRT1, SIRT5 and EX527 analog are shown in grey, pink, and cyan, respectively. Y102 and R105 in SIRT5 are labeled in orange, whereas A313 and I316 are labeled in yellow.

### 6.2.3. Inhibition of suramin

In view of the structural data that suramin occupies both the peptide and  $\text{NAD}^+$  binding sites in SIRT5, the suramin was expected to competitively inhibit the enzyme against both substrates. However, the kinetic analyses revealed that although the mode of inhibition of SIRT5 by suramin with respect to the succinylated substrate was competitive in nature, such inhibition with respect to  $\text{NAD}^+$  was unambiguously mixed type. The latter inhibitory mode led to the suggestion that suramin could, at the best, partially (but not fully) compete against the binding of  $\text{NAD}^+$ .

Further inhibition studies of suramin on single and double mutants (Y102A, R105I, and Y102A/R105I) of SIRT5 questioned the reliability of the structural data in predicting the mode of inhibition of suramin in SIRT5 catalysis. For example, although Y102 formed hydrogen bond with the sulfonate moiety of suramin in the crystal structure of SIRT5-suramin complex, Y102A mutation did not show any significant change in the inhibitory potency of suramin. The  $K_i$  values of suramin with respect to deacetylase and desuccinylase reactions of Y102A mutant enzyme being  $3.7 \pm 1.4 \mu\text{M}$  and  $6.8 \pm 1.7 \mu\text{M}$ , respectively, were found to be comparable to its  $K_d$  value ( $4.0 \mu\text{M}$ ). Clearly, the presence of enzyme substrates did not alter the intrinsic binding affinity of suramin to the active site pocket of the mutant enzyme. The kinetic and thermodynamic data for the binding of suramin to wild-type mutant SIRT5 further attests to the cooperative versus antagonistic roles of Y102 and R105 residues in binding of the inhibitor and its inhibitory potency. While Y102 and R105 residues mutually cooperate with each other in accommodating suramin (in the absence of substrates) within the active site pocket of SIRT5, the above residues play opposite roles during suramin mediated inhibition of the enzyme. While Y102 suppresses the inhibition of the enzyme by suramin, R105 promotes the inhibition.



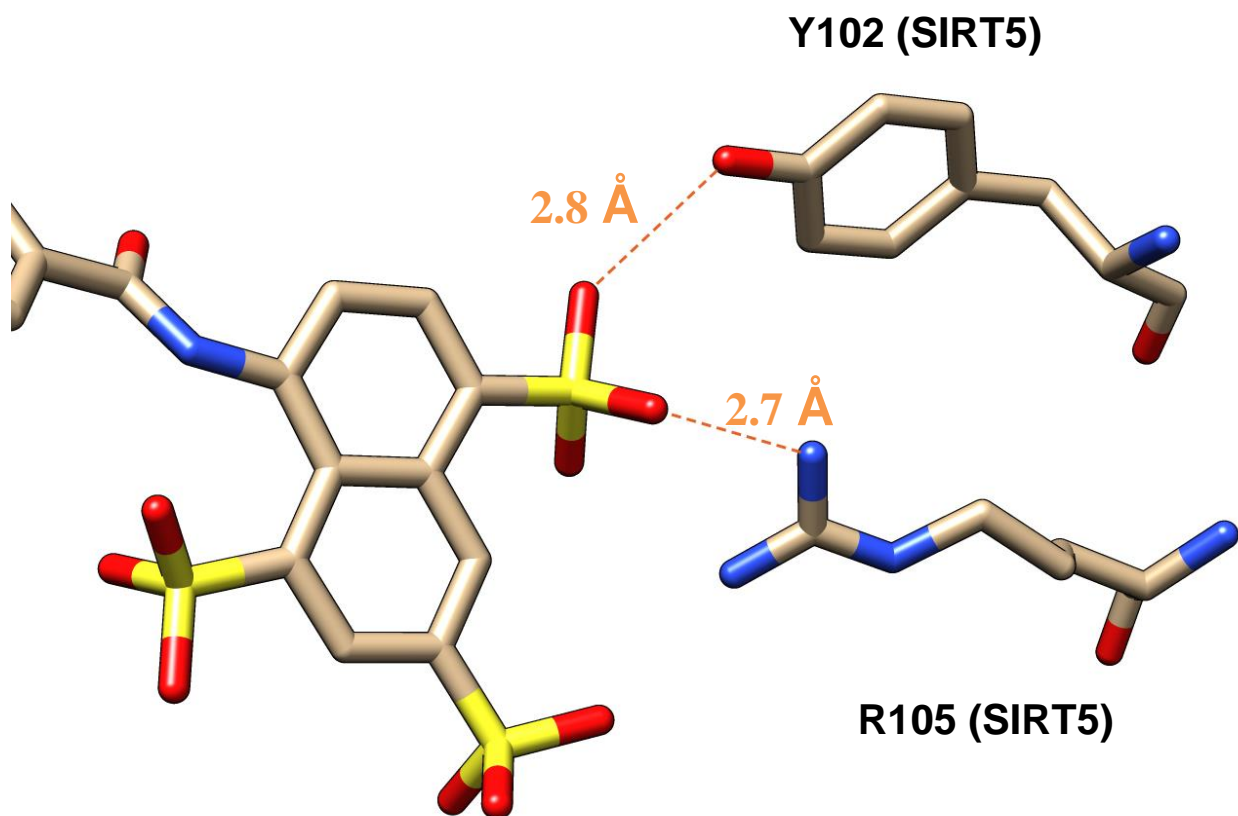


Figure 6.3. Coordination of Y102 and R105 with the sulfonate group of suramin. Hydrogen bonds are shown as dashed orange lines.

### 6.3. Mutation Induced Changes in the Secondary Structural Features of SIRT1 and SIRT5 and Its Mutant Variants

In view of the above discussion, it may imply that the differential substrate specificity as well as the inhibitory features of SIRT1 and SIRT5 are primarily modulated by the two specific amino acid residues within the active site pockets of the above enzymes. Whether such amino acid residues just alter the microenvironments of the enzyme's active site pockets or they modulate the global conformational states of the enzymes becomes evident by examining the secondary structural features of the wild-type SIRT1 and SIRT5 and its mutants. Although the

difference in the CD spectra between the wild-type SIRT1 and SIRT5 can be ascribed to the prevalence of the higher degree of random coil structure (due to extended N and C terminal residues) in case of the former enzyme, the difference in the CD spectral features among SIRT5 mutant enzymes clearly indicate to the subtle, albeit discernible, difference in the protein structures. The latter feature becomes more pronounced upon examining the temperature dependent changes in the secondary structures of the wild-type and mutant enzymes. It is explicitly evident that while wild-type SIRT1 and SIRT5 as well as Y102A mutant show the single step transition profile during the temperature dependent changes in the secondary structures of the protein, both Arg mutants (viz., R105I and Y102A/R105I) conform to the double step transitions with significantly different  $T_m$  values. It is noteworthy that Y102A mutation decreases the  $T_m$  value of the wild-type SIRT5 by about 11 degree, suggesting that the above mutation has destabilizing effect on the protein structure. While the  $T_m$  of the first phases of R105I and Y102A/R105I is similar to the  $T_m$  values of wild type and Y102A mutant enzymes, respectively, the  $T_m$  value of the second phases of the Arg mutants are both above 70 °C.

The question arises why R105 mutations in SIRT5 cause two sequential thermal transitions. Its origin may lie in two plausible scenarios: (1) the R105 mutation results in the reorganization of the protein domains such that they undergo independent thermal unfolding/transitions at two temperatures, (2) the R105 mutation creates two slowly interconvertible protein conformations which unfold differently. However, none of the above scenarios is consistent with the CD spectral data of the unfolded enzymes. The CD spectral data of wild-type SIRT5 as well as Y102A mutant enzymes show higher contribution of the random coil structure. But this is not the case with the R105I mutant enzyme. The CD spectra after heating of R105I and Y102A/R105I mutant enzymes show dominant  $\alpha$  helical and  $\beta$  sheet

structures, but rarely any contribution of the random coil structure (as observed with the heated samples of wild-type SIRT5 and its Y102 mutant; Figure 5.76). Hence, it is tempting to speculate that R105 mutant enzyme (cooperatively) acquires a more stable protein conformation (which melts at a much higher temperature) while undergoing unfolding of the native conformational state of the enzyme. This is presumably the reason why melting transition profile of the double mutant enzyme is not reliably fitted by the (independent) two-step Boltzmann equation (Eq. 4.16). Irrespectively, the denaturation does not preserve the active site pocket of the double mutant enzyme to facilitate catalysis.

In summary, the detailed comparative studies between SIRT1 and SIRT5 sheds light on the selectivity of the enzymes for different substrates and their distinct modes of inhibition by nicotinamide and EX527 inhibitors. The experimental data clearly suggest a marked cooperation/coordination between the Y102 and R105 residues in modulating the above features, and the latter appears to be facilitated by changes in the protein structure. Whether or not such structural differences are discernible via X-ray crystallographic analysis must await further studies.

#### **6.4. Barbiturate Derivative as Sirtuin Inhibitors**

Two barbiturate derivatives (MDS3-16 and MH5-75) were found to selectively inhibit SIRT5 with micromolar potency from the screening. MDS-3-16 did not show any inhibition against SIRT1, while 10  $\mu$ M concentration of MH5-75 exhibited only 20% inhibition against SRIT1.

The steady-state kinetic data revealed that MH5-75 served as the mixed inhibitor against succinylated substrate and the non-competitive inhibition against  $\text{NAD}^+$  during SIRT5 catalyzed reaction. The mixed inhibition of MH-5-75 against the Ac-Suclys-AMC may indicate that the

ligand partially occupies the active site where the succinylated substrate binds. Of the two inhibition constants derived from the mixed inhibition model,  $K_i'$  value was twofold higher than that of the  $K_i$  value, suggesting the binding of the inhibitor is weakened upon binding of the succinylated substrate, which is presumably due to the conformational change induced by enzyme-substrate interaction. The noncompetitive inhibition of MH5-75 with respect to  $\text{NAD}^+$  suggests that the conformational change upon the formation of the ternary complex does not further affect the binding of the inhibitor. Note that the three  $K_i$  values determined from the analysis are not significantly different, suggesting that the binding of MH5-75 is not apparently affected by the binding of the succinylated substrate and  $\text{NAD}^+$ . As mentioned in the Introduction section (§1.7.2.3), several thiobarbiturates have been identified as potent sirtuin inhibitors(245). The docking of the thiobarbiturates with SIRT5 by Maurer et al. shows that the thiobarbiturate ring mimicks the succinyl group of the substrate, forming hydrogen bonds with Tyr 102, Arg105 and Gln 140 (Figure 6.2). The interaction is stabilized by strong electrostatic interactions between acidic thiobarbiturate and basic guanidinium group of Arg105. This inhibition mode is supposed to generate competitive inhibition for the thiobarbiturate to SIRT5. However, such expected competitive feature is not observed in the inhibition of SIRT5 by MH5-75, which is a barbiturate derivative. The mixed inhibition model for the inhibition of SIRT5 desuccinylation reaction by MH5-75 with respect to the succinylated substrate suggests that the inhibitor at most partially occupied the active site pocket of the enzyme.

Combining the above analysis, the inhibition mechanism is depicted in Figure 6.4. The inhibitor binds to the enzyme both in the absence and presence of the succinylated substrate (presented as A) and  $\text{NAD}^+$  (presented as B), forming unproductive complexes SIRT5-MH5-75 (EI), SIRT5-MH5-75-substrate (EAI) and SIRT5-MH5-75-substrate- $\text{NAD}^+$  (EABI).

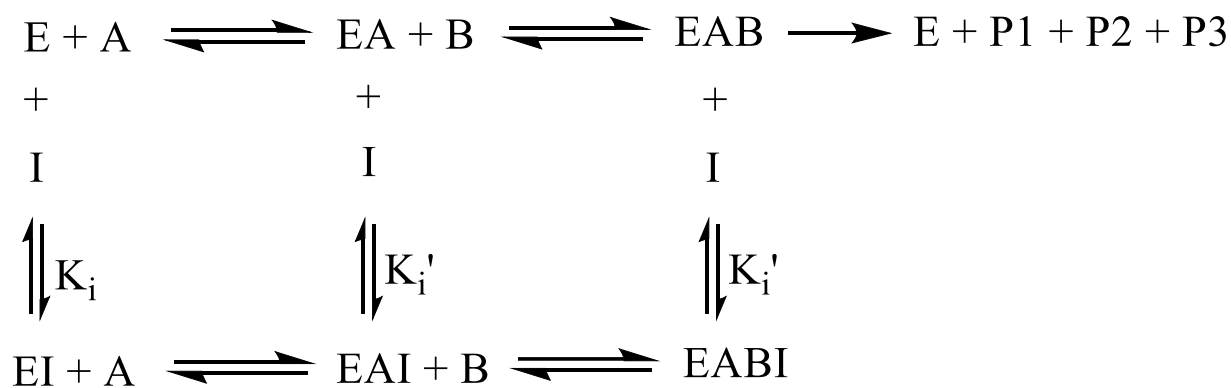
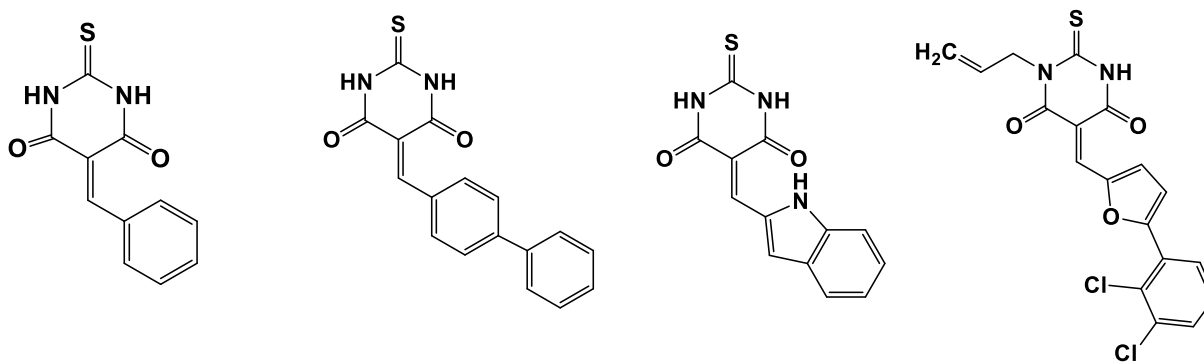
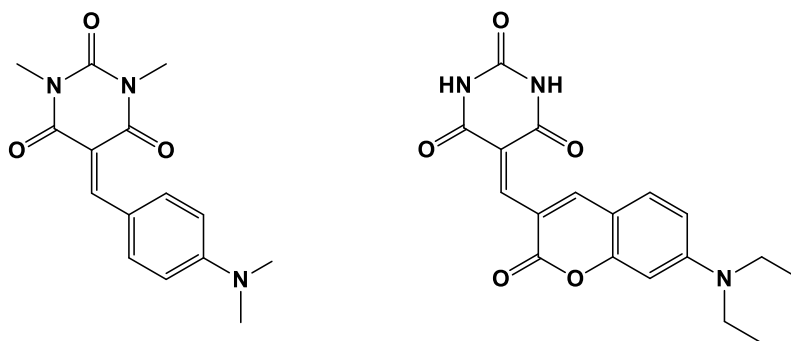


Figure 6.4. Binding and Inhibition mechanism of MH5-75 against SIRT5. A and B represent the succinylated substrate and NAD<sup>+</sup>. P1, P2, P3 represent the three products from SIRT5 catalyzed desuccinylation reaction. K<sub>i</sub> and K<sub>i</sub>' determined by steady-state kinetic experiment are 20 and 40 μM, respectively.



**Thiobarbiturates**



**Barbiturates (MDS3-16 and MH5-75)**

Figure 6.5. Sirtuin inhibitors with a barbiturate or thiobarbiturate scaffold.

A unique feature of MH5-75 is that the structure contains a coumarin group, which exhibits electronic spectroscopic properties. The absorption spectrum of MH5-75 is characterized by two peaks at 264 and 410 nm, respectively (section §5.4.1). Of these two peaks, the 410 nm peak is slowly red shifts to 445 nm upon binding of MH5-75 to the enzyme, suggesting that the enzyme induces an extended conjugation in the coumarin structure within the active site pocket of SIRT5. Based on the above results the binding mode of MH5-75 to SIRT5 is modified in Figure 6.5. However, due to the extremely poor solubility of the compound (0.56 g L<sup>-1</sup> in DMSO, and much lower in aqueous media), it could not be used for further experiments such as transient kinetic or isothermal titration calorimetric studies to further analyze the underlying mechanism for the enzyme-inhibitor interaction. Alternative approaches, such as prepare the inhibitor in complex with some solubilizing agent, need to be considered to solve this problem. By collaborating with Dr. Mallik, our lab used to develop two-pronged inhibitors with both improved solubility and selectivity (276-278), and similar approach could be utilized to develop more potent inhibitors for sirtuins.

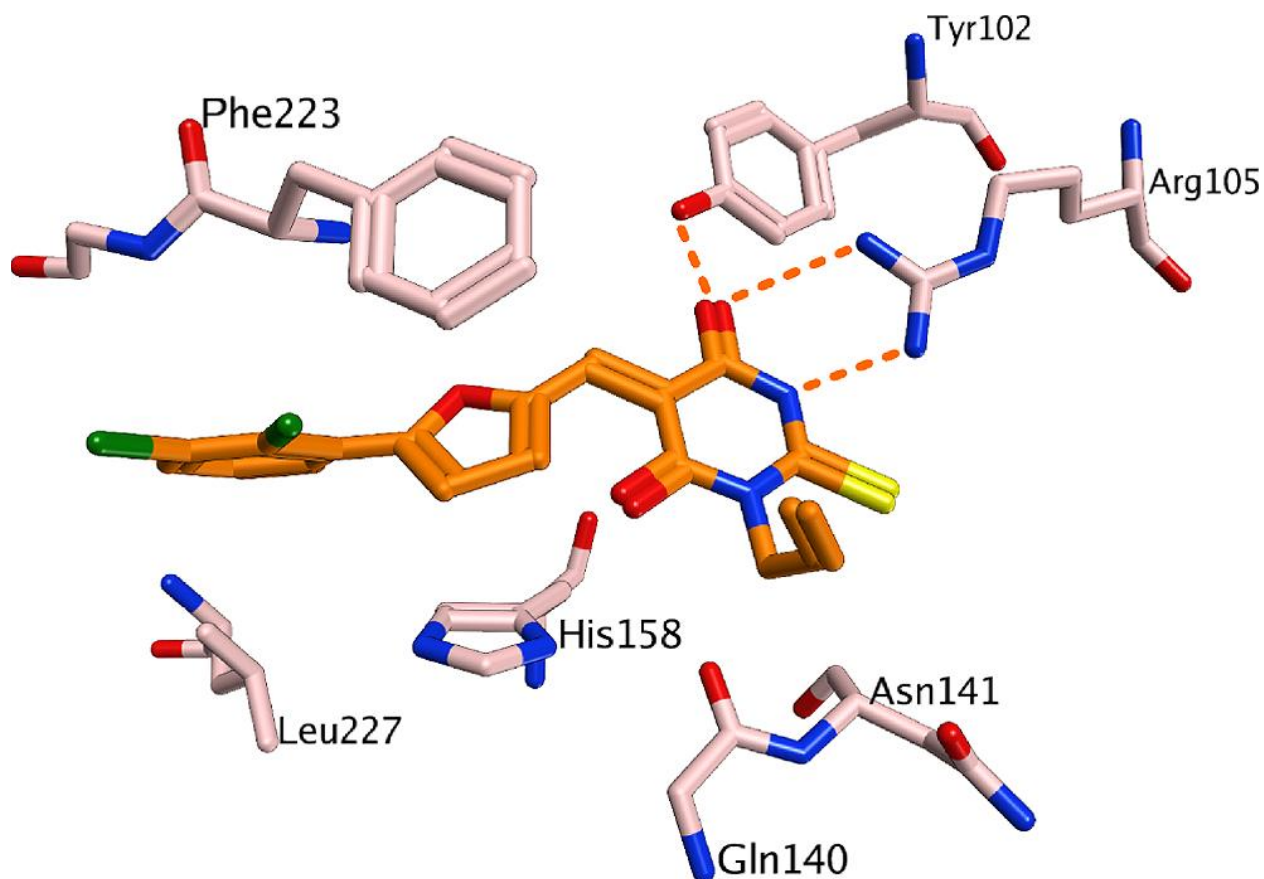


Figure 6.6. Docking result for one representative thiobarbiturate at SIRT5 active site pocket. Hydrogen bonds are shown as dashed orange lines.

## 6.5. Suramin-mediated Changes in the Structural Features of SIRT5

### 6.5.1. Suramin-mediated changes in the conformational states of SIRT5

The structure of apo-SIRT5 is not available, making it impossible to directly evaluate the structural changes of SIRT5 induced by the binding of suramin by crystallographic studies.

Hence, the direct binding studies of SIRT5 with suramin using spectroscopic approaches in the previous chapter provide valuable information for the conformational changes of the enzyme induced by the binding of suramin. First, comparison between the CD spectra of apo-SIRT5 and SIRT5- suramin complex (Figure 5.78) shows the overall spectrum is comparable with the apo-SIRT5 except for a slight change between 210-220 nm, suggesting that the overall secondary

structure of SIRT5 remains unchanged upon binding of suramin. Second, the  $T_m$  for the thermal denaturation of SIRT5 bound to suramin is about 10 degree higher ( $T_m = 62.7 \pm 0.4$  °C) than that of the apo enzyme ( $T_m = 52.9 \pm 0.04$  °C).

To explain the spectral change between 210-220 nm, three available crystal structures of SIRT5 (is compared with SIRT5-suramin complex (Figure 6.8): the structure of SIRT5 in complex with ADP-ribose (Figure 6.8B), the structure of SIRT5 in complex with H3K9(suc) peptide (Figure 6.8C) (279), and the ternary complex of SIRT5-H3K9(suc)-NAD<sup>+</sup> (Figure 6.8D). The spectral change between 210-220 nm as well as the increased thermal stability of the enzyme-ligand complex is presumably attributed by the structural change in the loop region connecting the Rossmann fold and the zinc-binding domain. Two significant structural changes could be observed. First, the flexible loop connecting the Rossmann fold and the zinc-binding domain (Val67-Tyr76) is partially disordered in the SIRT5-ADP ribose complex, but becomes ordered in the structure of SIRT5 bound to suramin (Figures 6.8A and B). Interestingly, this loop is disordered in the structure of SIRT5-H3K9(suc) peptide, but is ordered in the structure of SIRT5 bound with both H3K9(suc) peptide substrate and and NAD<sup>+</sup> (Figures 6.8C and D). The above observations suggest that the binding of suramin partially mimic the ternary complex of SIRT5-H3K9(suc) peptide-NAD<sup>+</sup>. Second, a C-terminal region (Glu277-Arg286) near the site A of the NAD<sup>+</sup> binding pocket is ordered in the SIRT-ADP ribose structure, but is disordered in the structure of SIRT5 bound to suramin. This region is ordered in both the SIRT5-H3K9(suc) peptide and SIRT5-H3K9(suc) peptide-NAD<sup>+</sup> complexes. Based on the above discussions, spectral change between 210-220 nm as well as the increased thermal stability of the enzyme-ligand complex is possibly attributed by the structural change in the loop region connecting the Rossmann fold and the zinc-binding domain.



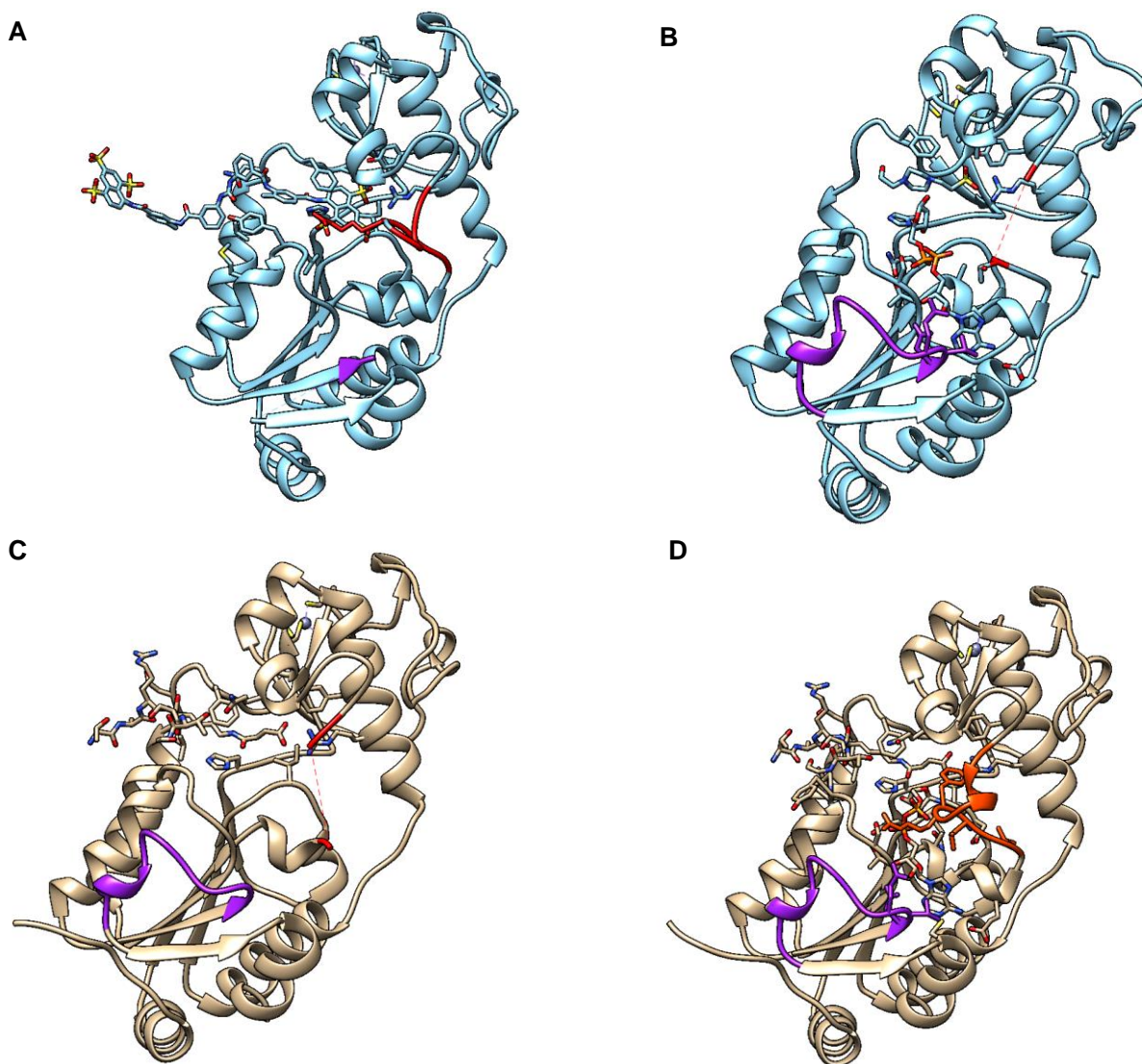


Figure 6.7. Crystal structures of SIRT5 in complex with suramin or substrates. (A) The structure of SIRT5 in complex with suramin. (B) The structure of SIRT5 in complex with ADP-ribose. (C) The structure of SIRT5 in complex with H3K9 peptide. (D) Ternary complex of SIRT5-H3K9-NAD<sup>+</sup>. Two regions, Val67-Tyr76 and Glu277-Arg286, are marked in red and purple, respectively.

The conformational modulation in the protein structure of SIRT5 induced by the binding of suramin is also reflected in the fluorescence spectroscopic studies in section §5.4.2.1. Upon the binding of suramin, the intrinsic protein fluorescence of SIRT5 was quenched without any shift in the fluorescence emission peak, and both the short and long lifetimes of SIRT5 were

reduced upon the binding of suramin. However, the precise deduction of the microenvironment of individual tryptophan moieties in SIRT5 could not be achieved due to the inherent complexity of the fluorescence decay curves.

Transient kinetic studies for the binding of suramin to SIRT5 using the signal from the fluorescence quenching of the intrinsic protein fluorescence suggest that the binding event conforms to the two-step binding model (Figure 6.9). While the fast phase was attributed to the initial binding/encounter of the inhibitor to the active site of the enzyme, the slow phase was due to the isomerization of the initial encounter complex. Due to technical difficulties in performing the transient kinetic experiments at lower concentrations of suramin while maintaining the pseudo-first condition, the individual microscopic rate constants for SIRT5-sruamin interactions could not be reliably determined. Nevertheless, since both of the two observed rate constants on suramin concentrations were almost constant (Figure 5.51), most likely the lowest concentration of suramin used in the experiment (4  $\mu\text{M}$ ) has almost been saturated for the binding of suramin to SIRT5. Hence, the estimated  $K_d$  based on this observation is in the nanomolar range (less than 10% of suramin concentrations). It is highly possible that the binding event studied by transient kinetics of the fluorescence change for the binding of suramin to SIRT5 represent the tighter binding site (0.1  $\mu\text{M}$  determined from the fluorescence quenching and isothermal titration calorimetric studies).

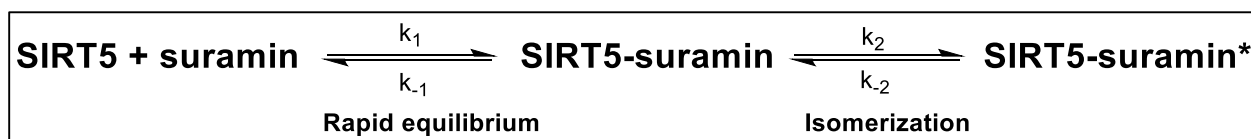


Figure 6.8. Two-step binding mechanism for the binding of suramin to SIRT5. The binding of the first step reaches rapid equilibration for association/dissociation of suramin to SIRT5, forming a transient intermediate which undergoes a slow isomerization/relaxation to produce the final ligand-protein complex

### 6.5.2. Suramin-mediated changes in the oligomeric states of SIRT5

The experimental data presented in section 5 provide, for the first time, a detailed account of suramin mediated changes in the oligomerization state of SIRT5, and such changes are encoded in the molar ratios of SIRT5 to suramin. SIRT5 exists both at monomeric and dimeric states at low and high molar ratios of SIRT5 to suramin, respectively, and the prevalence of such oligomeric states is demonstrable by isothermal titration calorimetric, size exclusion chromatographic, AFM imaging, and molecular modeling studies.

The experimental data presented herein does not support the crystallographically derived notion that SIRT5 exclusively exists in the dimeric state in the presence of suramin. Since the structural data are devoid of strong bonding interactions between two SIRT5 molecules (in the presence of suramin), and that the dimeric state appears to be induced by suramin, it is unlikely that the dimeric form of SIRT5 would be only thermodynamically stable in the presence of different concentrations of SIRT5. Our modeling data as well as those of Trapp et al clearly demonstrate that suramin can form both 1:1 and 1:2 complex with SIRT5 (as evident experimental), and thus it appears likely that only one of such complexes (i.e., 1:2 complex) predominates in the crystalline state for which the crystal structure was solved. This is one of the limitations of the crystallographic structure based predictions of molecular/mechanistic features in the aqueous solution.

The SEC data clearly demonstrates that even in the absence of suramin, SIRT5 exists in a dynamic equilibrium between the monomeric and dimeric forms albeit the monomeric form represent the most predominant enzyme species. Since the initial increase in suramin concentration predominates the dimeric over monomeric form of SIRT5, which reverts back to the monomeric vs. dimeric forms at further increase in suramin concentration, leads to the

suggestion that the oligomeric states of SIRT5 is dictated by the relative abundance of the enzyme and suramin in conjunction with their thermodynamic parameters. The ITC data clearly demonstrates that in titration of high concentration of SIRT5 by suramin (Figure 5.53; section §5.4.2.4), the first phase (ascribed to be due to the formation of the dimeric form of the enzyme) has considerably lower stoichiometry but much higher free energy than that observed with the second phase. On the other hand, the enthalpic contribution of the first phase is much lower than that of the second phase. Hence, it is not surprising that the first phase remains elusive when the ITC titration is performed at lower concentrations of the enzyme (Figure 5.54B; section §5.4.2.4). Consistently, the suramin induced formation of SIRT5 dimer (during the first phase) is an entropically driven process. We believe this is a result of desolvation of the surface of the monomeric SIRT5 involved in the formation of the dimeric form of the enzyme in the presence of suramin. This hypothesis is corroborated by the fact that there are no strong binding interactions between the SIRT5 surfaces involved in the dimer formation.

The demonstration that when the molar ratios of suramin to SIRT5 are high, the enzyme exists in the monomeric form, implying that half of the suramin molecule protrudes away from the enzyme's active site pocket as evident from the molecular modeling data of Trapp et al. as well as those presented in sections §5.4.2.4 to §5.4.2.8 (238). However, such model fails to explain as to why the binding affinity ( $K_d$ ) as well as the inhibition constant of half-suramin for SIRT5 is at least 2 orders of magnitude lower than that of full suramin. Evidently, it is unlikely that half of the suramin molecule (in full suramin structure), protruding away from the active site pocket of SIRT5, would be dangling in the solvent media. Hence, the only reasonable explanation of the marked difference in the binding affinity of full vs. half suramin for SIRT5 is that the protruded/dangling region of full suramin interacts on the surface of the enzyme. This

model is akin to the binding of the “two-prong” inhibitors to carbonic anhydrases and matrix metalloproteinases developed in our lab (276, 278). Both biophysical and crystallographic data unequivocally demonstrated that while one end of our two prong inhibitors interact at the active site pocket of carbonic anhydrase isozymes, the other end interacts on the enzymes’ surface. In fact, the two-prong binding mode suramin to SIRT5 is evident when the energy minimized structure of suramin molecule is docked to the monomeric form of SIRT5 by collaborating with Dr. Farukh Jabeen from Center for Computationally Assisted Science and Technology at University of North Dakota. As illustrated in Figure 5.69 (section §5.4.2.10), half of the suramin molecule, protruding from the enzyme’s active pocket, formed hydrogen bonds with bonding with Gln83 and Gly224 present on the surface of the protein. The latter binding mode justifies the experimental data that when  $[\text{suramin}] \gg [\text{SIRT5}]$ , only the monomeric form of the enzyme-ligand complex becomes predominant. The binding of half suramin structure on the surface of the SIRT5 monomer supports the experimental data that both binding affinity and inhibitory potency of full suramin is higher than that of the half suramin. This alternative mode of binding of suramin to SIRT5 leading to the formation of dimeric versus monomeric form of the enzyme is depicted as the cartoon of Figure 6.11.

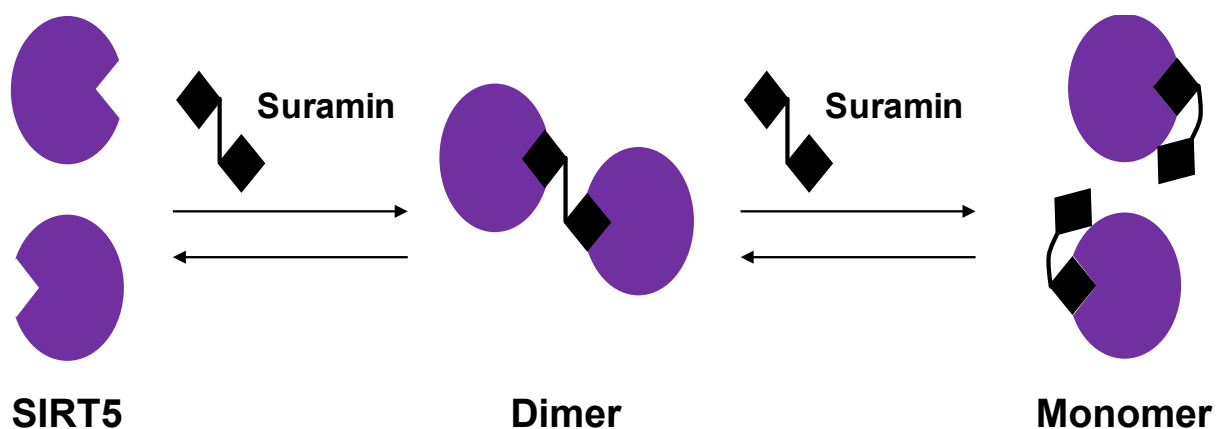


Figure 6.10. Proposed SIRT5-suramin binding mechanism.

The question arises whether the dimeric form of SIRT5 is “pre-existent” or it is exclusively “induced” by suramin in the aqueous solution. The fact that a small, albeit discernible, dimeric peak of SIRT5 is evident in our size exclusion chromatographic studies even in the absence of suramin suggests that a small fraction of the enzyme can pre-exist as dimer. In our attempt to probe whether the SIRT5 dimer (in the absence of suramin) exists in a dynamic equilibrium with the predominant monomeric form of SIRT5, we collected the monomeric peak fractions of SIRT5, concentrated them via amicon-concentrator, and re-chromatographed on the original size exclusion column. Interestingly, we noted the re-emergence of the dimeric peak of SIRT5 (data not shown), suggesting that there is a pre-existing equilibrium between the monomeric and dimeric forms of SIRT5, and such equilibrium is shifted to the dimeric form of the enzyme in the presence of suramin, particularly under the condition of lower molar ratios of suramin to SIRT5. The suramin induced increase in the dimeric form of SIRT5 appears to be thermodynamically favored as the carbonyl oxygen of urea (of full suramin) forms a hydrogen bond with interfacial Y255 (2.6 Å) in the dimer. It should be mentioned that suramin induced dimerization is not unique for SIRT5. The above feature has also been observed with other

suramin binding proteins such as aFGF and TNF $\alpha$  (280, 281). In case of aFGF, it has been noted that suramin induced the microaggregation of the protein (under physiological condition) prevents its aggregation to the cell surface receptors. However, at higher molecular ratios of suramin to aFGF, the latter reverts back to the monomeric form (similar to that observed with SIRT5) precluding its interaction with the cell surface receptors.

## REFERENCES

1. Stein, L. D. (2004) Human genome: End of the beginning, *Nature* 431, 915-916.
2. Lindahl, T., Satoh, M. S., Poirier, G. G., and Klungland, A. (1995) Post-translational modification of poly(ADP-ribose) polymerase induced by DNA strand breaks, *Trends in biochemical sciences* 20, 405-411.
3. Bode, A. M., and Dong, Z. (2004) Post-translational modification of p53 in tumorigenesis, *Nat Rev Cancer* 4, 793-805.
4. Bannister, A. J., and Kouzarides, T. (2011) Regulation of chromatin by histone modifications, *Cell Res* 21, 381-395.
5. Park, J., Chen, Y., Tishkoff, D. X., Peng, C., Tan, M., Dai, L., Xie, Z., Zhang, Y., Zwaans, B. M., Skinner, M. E., Lombard, D. B., and Zhao, Y. (2013) SIRT5-mediated lysine desuccinylation impacts diverse metabolic pathways, *Molecular cell* 50, 919-930.
6. Allfrey, V. G., Faulkner, R., and Mirsky, A. E. (1964) Acetylation and Methylation of Histones and Their Possible Role in the Regulation of RNA Synthesis, *Proceedings of the National Academy of Sciences of the United States of America* 51, 786-794.
7. Glozak, M. A., Sengupta, N., Zhang, X., and Seto, E. (2005) Acetylation and deacetylation of non-histone proteins, *Gene* 363, 15-23.
8. Roth, S. Y., Denu, J. M., and Allis, C. D. (2001) Histone Acetyltransferases, *Annual Review of Biochemistry* 70, 81-120.
9. Berndsen, C. E., and Denu, J. M. (2008) Catalysis and substrate selection by histone/protein lysine acetyltransferases, *Current Opinion in Structural Biology* 18, 682-689.
10. Du, J., Zhou, Y., Su, X., Yu, J. J., Khan, S., Jiang, H., Kim, J., Woo, J., Kim, J. H., Choi, B. H., He, B., Chen, W., Zhang, S., Cerione, R. A., Auwerx, J., Hao, Q., and Lin, H. (2011) Sirt5 is a NAD-dependent protein lysine demalonylase and desuccinylase, *Science* 334, 806-809.
11. Tan, M., Peng, C., Anderson, K. A., Chhoy, P., Xie, Z., Dai, L., Park, J., Chen, Y., Huang, H., Zhang, Y., Ro, J., Wagner, G. R., Green, M. F., Madsen, A. S., Schmiesing, J., Peterson, B. S., Xu, G., Ilkayeva, O. R., Muehlbauer, M. J., Braulke, T., Muhlhausen, C., Backos, D. S., Olsen, C. A., McGuire, P. J., Pletcher, S. D., Lombard, D. B., Hirschey, M. D., and Zhao, Y. (2014) Lysine glutarylation is a protein posttranslational modification regulated by SIRT5, *Cell metabolism* 19, 605-617.
12. Jiang, H., Khan, S., Wang, Y., Charron, G., He, B., Sebastian, C., Du, J., Kim, R., Ge, E., Mostoslavsky, R., Hang, H. C., Hao, Q., and Lin, H. (2013) SIRT6 regulates TNF-alpha secretion through hydrolysis of long-chain fatty acyl lysine, *Nature* 496, 110-113.



13. Chen, Y., Sprung, R., Tang, Y., Ball, H., Sangras, B., Kim, S. C., Falck, J. R., Peng, J., Gu, W., and Zhao, Y. (2007) Lysine Propionylation and Butyrylation Are Novel Post-translational Modifications in Histones, *Molecular & Cellular Proteomics* 6, 812-819.
14. Feldman, J. L., Baeza, J., and Denu, J. M. (2013) Activation of the protein deacetylase SIRT6 by long-chain fatty acids and widespread deacetylation by mammalian sirtuins, *The Journal of biological chemistry* 288, 31350-31356.
15. Feldman, J. L., Dittenhafer-Reed, K. E., Kudo, N., Thelen, J. N., Ito, A., Yoshida, M., and Denu, J. M. (2015) Kinetic and Structural Basis for Acyl-Group Selectivity and NAD(+) Dependence in Sirtuin-Catalyzed Deacetylation, *Biochemistry* 54, 3037-3050.
16. Klar, A. J. S., Fogel, S., and Macleod, K. (1979) MAR1—A Regulator of the HMa and HM $\alpha$  Loci in *saccharomyces cerevisiae*, *Genetics* 93, 37-50.
17. Rine, J., and Herskowitz, I. (1987) Four Genes Responsible for a Position Effect on Expression From HML and HMR in *Saccharomyces cerevisiae*, *Genetics* 116, 9-22.
18. Brachmann, C. B., Sherman, J. M., Devine, S. E., Cameron, E. E., Pillus, L., and Boeke, J. D. (1995) The SIR2 gene family, conserved from bacteria to humans, functions in silencing, cell cycle progression, and chromosome stability, *Genes & development* 9, 2888-2902.
19. Frye, R. A. (1999) Characterization of Five Human cDNAs with Homology to the Yeast SIR2 Gene: Sir2-like Proteins (Sirtuins) Metabolize NAD and May Have Protein ADP-Ribosyltransferase Activity, *Biochemical and Biophysical Research Communications* 260, 273-279.
20. Tanny, J. C., Dowd, G. J., Huang, J., Hilz, H., and Moazed, D. (1999) An Enzymatic Activity in the Yeast Sir2 Protein that Is Essential for Gene Silencing, *Cell* 99, 735-745.
21. Imai, S.-i., Armstrong, C. M., Kaeberlein, M., and Guarente, L. (2000) Transcriptional silencing and longevity protein Sir2 is an NAD-dependent histone deacetylase, *Nature* 403, 795-800.
22. Landry, J., Sutton, A., Tafrov, S. T., Heller, R. C., Stebbins, J., Pillus, L., and Sternglanz, R. (2000) The silencing protein SIR2 and its homologs are NAD-dependent protein deacetylases, *Proceedings of the National Academy of Sciences* 97, 5807-5811.
23. Lin, S.-J., Defossez, P.-A., and Guarente, L. (2000) Requirement of NAD and SIR2 for Life-Span Extension by Calorie Restriction in *Saccharomyces cerevisiae*, *Science* 289, 2126-2128.
24. Frye, R. A. (2000) Phylogenetic Classification of Prokaryotic and Eukaryotic Sir2-like Proteins, *Biochemical and Biophysical Research Communications* 273, 793-798.

25. Hirschev, Matthew D. (2011) Old Enzymes, New Tricks: Sirtuins Are NAD<sup>+</sup>-Dependent De-acylases, *Cell metabolism* 14, 718-719.
26. Zhao, K., Chai, X., and Marmorstein, R. (2004) Structure and substrate binding properties of cobB, a sir2 homolog protein deacetylase from *Escherichia coli*, *Journal of molecular biology* 337, 731-741.
27. Avalos, J. L., Bever, K. M., and Wolberger, C. (2005) Mechanism of sirtuin inhibition by nicotinamide: altering the NAD<sup>+</sup> cosubstrate specificity of a sir2 enzyme, *Molecular cell* 17, 855-868.
28. Hawse, W. F., Hoff, K. G., Fatkins, D. G., Daines, A., Zubkova, O. V., Schramm, V. L., Zheng, W., and Wolberger, C. (2008) Structural insights into intermediate steps in the Sir2 deacetylation reaction, *Structure* 16, 1368-1377.
29. Min, J., Landry, J., Sternglanz, R., and Xu, R.-M. (2001) Crystal Structure of a SIR2 Homolog–NAD Complex, *Cell* 105, 269-279.
30. Ringel, A. E., Roman, C., and Wolberger, C. (2014) Alternate deacylating specificities of the archaeal sirtuins Sir2Af1 and Sir2Af2, *Protein Science* 23, 1686-1697.
31. Zhao, K., Chai, X., and Marmorstein, R. (2003) Structure of the Yeast Hst2 Protein Deacetylase in Ternary Complex with 2' -O-Acetyl ADP Ribose and Histone Peptide, *Structure* 11, 1403-1411.
32. Finnin, M. S., Donigian, J. R., and Pavletich, N. P. (2001) Structure of the histone deacetylase SIRT2, *Nat Struct Mol Biol* 8, 621-625.
33. Jin, L., Wei, W., Jiang, Y., Peng, H., Cai, J., Mao, C., Dai, H., Choy, W., Bemis, J. E., Jirousek, M. R., Milne, J. C., Westphal, C. H., and Perni, R. B. (2009) Crystal structures of human SIRT3 displaying substrate-induced conformational changes, *The Journal of biological chemistry* 284, 24394-24405.
34. Schuetz, A., Min, J., Antoshenko, T., Wang, C. L., Allali-Hassani, A., Dong, A., Loppnau, P., Vedadi, M., Bochkarev, A., Sternglanz, R., and Plotnikov, A. N. (2007) Structural basis of inhibition of the human NAD<sup>+</sup>-dependent deacetylase SIRT5 by suramin, *Structure* 15, 377-389.
35. Pan, P. W., Feldman, J. L., Devries, M. K., Dong, A., Edwards, A. M., and Denu, J. M. (2011) Structure and Biochemical Functions of SIRT6, *Journal of Biological Chemistry* 286, 14575-14587.
36. Yuan, H., and Marmorstein, R. (2012) Structural Basis for Sirtuin Activity and Inhibition, *Journal of Biological Chemistry* 287, 42428-42435.

37. Avalos, J. L., Celic, I., Muhammad, S., Cosgrove, M. S., Boeke, J. D., and Wolberger, C. (2002) Structure of a Sir2 enzyme bound to an acetylated p53 peptide, *Molecular cell* *10*, 523-535.
38. Zhao, K., Chai, X., Clements, A., and Marmorstein, R. (2003) Structure and autoregulation of the yeast Hst2 homolog of Sir2, *Nat Struct Mol Biol* *10*, 864-871.
39. Zhao, K., Harshaw, R., Chai, X., and Marmorstein, R. (2004) Structural basis for nicotinamide cleavage and ADP-ribose transfer by NAD<sup>+</sup>-dependent Sir2 histone/protein deacetylases, *Proceedings of the National Academy of Sciences of the United States of America* *101*, 8563-8568.
40. Hawse, W. F., Hoff, K. G., Fatkins, D. G., Daines, A., Zubkova, O. V., Schramm, V. L., Zheng, W., and Wolberger, C. (2008) Structural insights into intermediate steps in the Sir2 deacetylation reaction, *Structure* *16*, 1368-1377.
41. Hawse, W. F., and Wolberger, C. (2009) Structure-based Mechanism of ADP-ribosylation by Sirtuins, *Journal of Biological Chemistry* *284*, 33654-33661.
42. Bheda, P., Wang, J. T., Escalante-Semerena, J. C., and Wolberger, C. (2011) Structure of Sir2Tm bound to a propionylated peptide, *Protein Science* *20*, 131-139.
43. Zhou, Y., Zhang, H., He, B., Du, J., Lin, H., Cerione, R. A., and Hao, Q. (2012) The bicyclic intermediate structure provides insights into the desuccinylation mechanism of human sirtuin 5 (SIRT5), *Journal of Biological Chemistry* *287*, 28307-28314.
44. Zhao, X., Allison, D., Condon, B., Zhang, F., Gheyi, T., Zhang, A., Ashok, S., Russell, M., MacEwan, I., Qian, Y., Jamison, J. A., and Luz, J. G. (2013) The 2.5 Å crystal structure of the SIRT1 catalytic domain bound to nicotinamide adenine dinucleotide (NAD<sup>+</sup>) and an indole (EX527 analogue) reveals a novel mechanism of histone deacetylase inhibition, *Journal of Medicinal Chemistry* *56*, 963-969.
45. Gertz, M., Fischer, F., Nguyen, G. T. T., Lakshminarasimhan, M., Schutkowski, M., Weyand, M., and Steegborn, C. (2013) Ex-527 inhibits Sirtuins by exploiting their unique NAD<sup>+</sup>-dependent deacetylation mechanism, *Proceedings of the National Academy of Sciences* *110*, E2772-E2781.
46. Davenport, A. M., Huber, F. M., and Hoelz, A. (2014) Structural and functional analysis of human SIRT1, *Journal of molecular biology* *426*, 526-541.
47. Sanders, B. D., Jackson, B., and Marmorstein, R. (2010) Structural basis for sirtuin function: What we know and what we don't, *Biochimica et Biophysica Acta (BBA) - Proteins and Proteomics* *1804*, 1604-1616.
48. Rossman, M. G., Liljas, A., Brändén, C.-I., and Banaszak, L. J. (1975) Evolutionary and Structural Relationships among Dehydrogenases, In *The Enzymes* (Paul, D. B., Ed.), pp 61-102, Academic Press.

49. Qian, X., Jeon, C., Yoon, H., Agarwal, K., and Weiss, M. A. (1993) Structure of a new nucleic-acid-binding motif in eukaryotic transcriptional elongation factor TFIIS, *Nature* 365, 277-279.
50. Zhu, W., Zeng, Q., Colangelo, C. M., Lewis, M., Summers, M. F., and Scott, R. A. (1996) The N-terminal domain of TFIIB from *Pyrococcus furiosus* forms a zinc ribbon, *Nat Struct Biol* 3, 122-124.
51. Wang, B., Jones, D. N. M., Kaine, B. P., and Weiss, M. A. (1998) High-resolution structure of an archaeal zinc ribbon defines a general architectural motif in eukaryotic RNA polymerases, *Structure* 6, 555-569.
52. Chakrabarty, S. P., and Balaram, H. (2010) Reversible binding of zinc in *Plasmodium falciparum* Sir2: Structure and activity of the apoenzyme, *Biochimica et Biophysica Acta (BBA) - Proteins and Proteomics* 1804, 1743-1750.
53. Davenport, A. M., Huber, F. M., and Hoelz, A. (2014) Structural and Functional Analysis of Human SIRT1, *Journal of Molecular Biology* 426, 526-541.
54. Li, J., Flick, F., Verheugd, P., Carloni, P., Lüscher, B., and Rossetti, G. (2015) Insight into the Mechanism of Intramolecular Inhibition of the Catalytic Activity of Sirtuin 2 (SIRT2), *PLoS ONE* 10, e0139095.
55. Dai, H., Case, A. W., Riera, T. V., Considine, T., Lee, J. E., Hamuro, Y., Zhao, H., Jiang, Y., Sweitzer, S. M., Pietrak, B., Schwartz, B., Blum, C. A., Disch, J. S., Caldwell, R., Szczepankiewicz, B., Oalman, C., Yee Ng, P., White, B. H., Casaubon, R., Narayan, R., Koppetsch, K., Bourbonais, F., Wu, B., Wang, J., Qian, D., Jiang, F., Mao, C., Wang, M., Hu, E., Wu, J. C., Perni, R. B., Vlasuk, G. P., and Ellis, J. L. (2015) Crystallographic structure of a small molecule SIRT1 activator-enzyme complex, *Nat Commun* 6.
56. Pan, M., Yuan, H., Brent, M., Ding, E. C., and Marmorstein, R. (2012) SIRT1 Contains N- and C-terminal Regions That Potentiate Deacetylase Activity, *Journal of Biological Chemistry* 287, 2468-2476.
57. Jackson, M. D., and Denu, J. M. (2002) Structural identification of 2'- and 3'-O-acetyl-ADP ribose as novel metabolites derived from the Sir2 family of beta-NAD<sup>+</sup>-dependant histone/protein deacetylases, *Journal of Biological Chemistry*.
58. Sauve, A. A. (2010) Sirtuin chemical mechanisms, *Biochimica et Biophysica Acta (BBA) - Proteins and Proteomics* 1804, 1591-1603.
59. Hoff, K. G., Avalos, J. L., Sens, K., and Wolberger, C. (2006) Insights into the sirtuin mechanism from ternary complexes containing NAD<sup>+</sup> and acetylated peptide, *Structure* 14, 1231-1240.

60. Smith, B. C., and Denu, J. M. (2007) Sir2 deacetylases exhibit nucleophilic participation of acetyl-lysine in NAD<sup>+</sup> cleavage, *Journal of the American Chemical Society* 129, 5802-5803.
61. Hu, P., Wang, S., and Zhang, Y. (2008) Highly dissociative and concerted mechanism for the nicotinamide cleavage reaction in Sir2Tm enzyme suggested by ab initio QM/MM molecular dynamics simulations, *Journal of the American Chemical Society* 130, 16721-16728.
62. Cen, Y., and Sauve, A. A. (2010) Transition state of ADP-Ribosylation of acetyllysine catalyzed by *Archaeoglobus fulgidus* Sir2 determined by kinetic isotope effects and computational approaches, *Journal of the American Chemical Society* 132, 12286-12298.
63. Sauve, A. A., and Youn, D. Y. (2012) Sirtuins: NAD<sup>+</sup>-dependent deacetylase mechanism and regulation, *Current Opinion in Chemical Biology* 16, 535-543.
64. Sauve, A. A., Celic, I., Avalos, J., Deng, H., Boeke, J. D., and Schramm, V. L. (2001) Chemistry of gene silencing: the mechanism of NAD<sup>+</sup>-dependent deacetylation reactions, *Biochemistry* 40, 15456-15463.
65. Smith, B. C., and Denu, J. M. (2006) Sir2 protein deacetylases: evidence for chemical intermediates and functions of a conserved histidine, *Biochemistry* 45, 272-282.
66. Smith, B. C., and Denu, J. M. (2007) Mechanism-based inhibition of Sir2 deacetylases by thioacetyl-lysine peptide, *Biochemistry* 46, 14478-14486.
67. Jackson, M. D., Schmidt, M. T., Oppenheimer, N. J., and Denu, J. M. (2003) Mechanism of nicotinamide inhibition and transglycosidation by Sir2 histone/protein deacetylases, *Journal of Biological Chemistry* 278, 50985-50998.
68. Sauve, A. A., and Schramm, V. L. (2003) Sir2 regulation by nicotinamide results from switching between base exchange and deacetylation chemistry, *Biochemistry* 42, 9249-9256.
69. Jackson, M. D., and Denu, J. M. (2002) Structural identification of 2'- and 3''-O-acetyl-ADP ribose as novel metabolites derived from the Sir2 family of beta-NAD<sup>+</sup>-dependant histone/protein deacetylases, *Journal of Biological Chemistry*.
70. Ahuja, N., Schwer, B., Carobbio, S., Waltregny, D., North, B. J., Castronovo, V., Maechler, P., and Verdin, E. (2007) Regulation of Insulin Secretion by SIRT4, a Mitochondrial ADP-ribosyltransferase, *Journal of Biological Chemistry* 282, 33583-33592.
71. Haigis, M. C., Mostoslavsky, R., Haigis, K. M., Fahie, K., Christodoulou, D. C., Murphy, Andrew J., Valenzuela, D. M., Yancopoulos, G. D., Karow, M., Blander, G., Wolberger, C., Prolla, T. A., Weindruch, R., Alt, F. W., and Guarente, L. (2006) SIRT4 inhibits

- glutamate dehydrogenase and opposes the effects of calorie restriction in pancreatic  $\beta$  cells, *Cell* 126, 941-954.
72. Liszt, G., Ford, E., Kurtev, M., and Guarente, L. (2005) Mouse Sir2 Homolog SIRT6 Is a Nuclear ADP-ribosyltransferase, *Journal of Biological Chemistry* 280, 21313-21320.
  73. Kowieski, T. M., Lee, S., and Denu, J. M. (2008) Acetylation-dependent ADP-ribosylation by *Trypanosoma brucei* Sir2, *Journal of Biological Chemistry* 283, 5317-5326.
  74. French, J. B., Cen, Y., and Sauve, A. A. (2008) Plasmodium falciparum Sir2 is an NAD<sup>+</sup>-dependent deacetylase and an acetyllysine-dependent and acetyllysine-independent NAD<sup>+</sup> glycohydrolase, *Biochemistry* 47, 10227-10239.
  75. Feldman, J. L., Dittenhafer-Reed, K. E., and Denu, J. M. (2012) Sirtuin catalysis and regulation, *The Journal of biological chemistry* 287, 42419-42427.
  76. Sasaki, T., Maier, B., Koclega, K. D., Chruszcz, M., Gluba, W., Stukenberg, P. T., Minor, W., and Scrable, H. (2008) Phosphorylation Regulates SIRT1 Function, *PloS one* 3, e4020.
  77. Nasrin, N., Kaushik, V. K., Fortier, E., Wall, D., Pearson, K. J., de Cabo, R., and Bordone, L. (2009) JNK1 Phosphorylates SIRT1 and Promotes Its Enzymatic Activity, *PloS one* 4, e8414.
  78. Gerhart-Hines, Z., Dominy, John E., Jr., Blättler, Sharon M., Jedrychowski, Mark P., Banks, Alexander S., Lim, J.-H., Chim, H., Gygi, Steven P., and Puigserver, P. (2011) The cAMP/PKA pathway rapidly activates SIRT1 to promote fatty acid oxidation independently of changes in NAD<sup>+</sup>, *Molecular cell* 44, 851-863.
  79. Pandithage, R., Lilischkis, R., Harting, K., Wolf, A., Jedamzik, B., Lüscher-Firzlauff, J., Vervoorts, J., Lasonder, E., Kremmer, E., Knöll, B., and Lüscher, B. (2008) The regulation of SIRT2 function by cyclin-dependent kinases affects cell motility, *The Journal of Cell Biology* 180, 915-929.
  80. Houtkooper, R. H., Canto, C., Wanders, R. J., and Auwerx, J. (2010) The secret life of NAD<sup>+</sup>: an old metabolite controlling new metabolic signaling pathways, *Endocrine reviews* 31, 194-223.
  81. Imai, S.-i. (2009) Nicotinamide phosphoribosyltransferase (Nampt): A link between NAD biology, metabolism, and diseases, *Current Pharmaceutical Design* 15, 20-28.
  82. Dan, L., Klimenkova, O., Klimiankou, M., Klusmann, J.-H., van den Heuvel-Eibrink, M. M., Reinhardt, D., Welte, K., and Skokowa, J. (2011) The role of Sirtuin 2 activation by nicotinamide phosphoribosyltransferase in the aberrant proliferation and survival of myeloid leukemia cells, *Haematologica*.

83. Canto, C., Gerhart-Hines, Z., Feige, J. N., Lagouge, M., Noriega, L., Milne, J. C., Elliott, P. J., Puigserver, P., and Auwerx, J. (2009) AMPK regulates energy expenditure by modulating NAD<sup>+</sup> metabolism and SIRT1 activity, *Nature* 458, 1056-1060.
84. Eskandarian, H. A., Impens, F., Nahori, M.-A., Soubigou, G., Coppée, J.-Y., Cossart, P., and Hamon, M. A. (2013) A role for SIRT2-dependent histone H3K18 deacetylation in bacterial infection, *Science* 341.
85. North, B. J., and Verdin, E. (2007) Interphase nucleo-cytoplasmic shuttling and localization of SIRT2 during mitosis, *PloS one* 2, e784.
86. Nakamura, Y., Ogura, M., Tanaka, D., and Inagaki, N. (2008) Localization of mouse mitochondrial SIRT proteins: Shift of SIRT3 to nucleus by co-expression with SIRT5, *Biochemical and Biophysical Research Communications* 366, 174-179.
87. Scher, M. B., Vaquero, A., and Reinberg, D. (2007) SirT3 is a nuclear NAD<sup>+</sup>-dependent histone deacetylase that translocates to the mitochondria upon cellular stress, *Genes & development* 21, 920-928.
88. Hallows, William C., Albaugh, Brittany N., and Denu, John M. (2008) Where in the cell is SIRT3? – functional localization of an NAD<sup>+</sup>-dependent protein deacetylase, *Biochemical Journal* 411, e11-e13.
89. Matsushita, N., Yonashiro, R., Ogata, Y., Sugiura, A., Nagashima, S., Fukuda, T., Inatome, R., and Yanagi, S. (2011) Distinct regulation of mitochondrial localization and stability of two human Sirt5 isoforms, *Genes to cells : devoted to molecular & cellular mechanisms* 16, 190-202.
90. Pfister, J. A., Ma, C., Morrison, B. E., and D'Mello, S. R. (2008) Opposing Effects of Sirtuins on Neuronal Survival: SIRT1-Mediated Neuroprotection Is Independent of Its Deacetylase Activity, *PloS one* 3, e4090.
91. Vaquero, A., Scher, M. B., Lee, D. H., Sutton, A., Cheng, H.-L., Alt, F. W., Serrano, L., Sternglanz, R., and Reinberg, D. (2006) SirT2 is a histone deacetylase with preference for histone H4 Lys 16 during mitosis, *Genes & development* 20, 1256-1261.
92. North, B. J., Marshall, B. L., Borra, M. T., Denu, J. M., and Verdin, E. (2003) The human Sir2 ortholog, SIRT2, is an NAD<sup>+</sup>-Dependent tubulin deacetylase, *Molecular cell* 11, 437-444.
93. Black, J. C., Mosley, A., Kitada, T., Washburn, M., and Carey, M. (2008) The SIRT2 deacetylase regulates autoacetylation of p300, *Molecular cell* 32, 449-455.
94. Kim, H.-S., Vassilopoulos, A., Wang, R.-H., Lahusen, T., Xiao, Z., Xu, X., Li, C., Veenstra, Timothy D., Li, B., Yu, H., Ji, J., Wang, Xin W., Park, S.-H., Cha, Yong I., Gius, D., and Deng, C.-X. (2011) SIRT2 maintains genome integrity and suppresses tumorigenesis through regulating APC/C activity, *Cancer Cell* 20, 487-499.

95. Nakagawa, T., Lomb, D. J., Haigis, M. C., and Guarente, L. (2009) SIRT5 Deacetylates carbamoyl phosphate synthetase 1 and regulates the urea cycle, *Cell* 137, 560-570.
96. Michishita, E., McCord, R. A., Berber, E., Kioi, M., Padilla-Nash, H., Damian, M., Cheung, P., Kusumoto, R., Kawahara, T. L. A., Barrett, J. C., Chang, H. Y., Bohr, V. A., Ried, T., Gozani, O., and Chua, K. F. (2008) SIRT6 is a histone H3 lysine 9 deacetylase that modulates telomeric chromatin, *Nature* 452, 492-496.
97. Kaidi, A., Weinert, B. T., Choudhary, C., and Jackson, S. P. (2010) Human SIRT6 promotes DNA end resection through CtIP deacetylation, *Science* 329, 1348-1353.
98. Barber, M. F., Michishita-Kioi, E., Xi, Y., Tasselli, L., Kioi, M., Moqtaderi, Z., Tennen, R. I., Paredes, S., Young, N. L., Chen, K., Struhl, K., Garcia, B. A., Gozani, O., Li, W., and Chua, K. F. (2012) SIRT7 links H3K18 deacetylation to maintenance of oncogenic transformation, *Nature* 487, 114-118.
99. Vakhrusheva, O., Smolka, C., Gajawada, P., Kostin, S., Boettger, T., Kubin, T., Braun, T., and Bober, E. (2008) Sirt7 increases stress resistance of cardiomyocytes and prevents apoptosis and inflammatory cardiomyopathy in mice, *Circulation Research* 102, 703-710.
100. Blander, G., Olejnik, J., Krzymanska-Olejnik, E., McDonagh, T., Haigis, M., Yaffe, M. B., and Guarente, L. (2005) SIRT1 shows no substrate specificity in vitro, *Journal of Biological Chemistry* 280, 9780-9785.
101. Khan, A. N., and Lewis, P. N. (2005) Unstructured conformations are a substrate requirement for the sir2 family of NAD-dependent protein deacetylases, *Journal of Biological Chemistry* 280, 36073-36078.
102. Garske, A. L., and Denu, J. M. (2006) SIRT1 top 40 hits: use of one-bead, one-compound acetyl-peptide libraries and quantum dots to probe deacetylase specificity, *Biochemistry* 45, 94-101.
103. Cosgrove, M. S., Bever, K., Avalos, J. L., Muhammad, S., Zhang, X., and Wolberger, C. (2006) The structural basis of sirtuin substrate affinity, *Biochemistry* 45, 7511-7521.
104. Rauh, D., Fischer, F., Gertz, M., Lakshminarasimhan, M., Bergbrede, T., Aladini, F., Kambach, C., Becker, C. F. W., Zerweck, J., Schutkowski, M., and Steegborn, C. (2013) An acetylome peptide microarray reveals specificities and deacetylation substrates for all human sirtuin isoforms, *Nature communications* 4.
105. Vaquero, A., Scher, M., Lee, D., Erdjument-Bromage, H., Tempst, P., and Reinberg, D. (2004) Human SirT1 interacts with histone H1 and promotes formation of facultative heterochromatin, *Molecular cell* 16, 93-105.
106. Vaziri, H., Dessain, S. K., Eaton, E. N., Imai, S.-I., Frye, R. A., Pandita, T. K., Guarente, L., and Weinberg, R. A. (2001) hSIR2/SIRT1 Functions as an NAD-Dependent p53 Deacetylase, *Cell* 107, 149-159.



107. Bouras, T., Fu, M., Sauve, A. A., Wang, F., Quong, A. A., Perkins, N. D., Hay, R. T., Gu, W., and Pestell, R. G. (2005) SIRT1 deacetylation and repression of p300 Involves lysine residues 1020/1024 within the cell cycle regulatory domain 1, *Journal of Biological Chemistry* 280, 10264-10276.
108. Hallows, W. C., Lee, S., and Denu, J. M. (2006) Sirtuins deacetylate and activate mammalian acetyl-CoA synthetases, *Proceedings of the National Academy of Sciences* 103, 10230-10235.
109. Gerhart - Hines, Z., Rodgers, J. T., Bare, O., Lerin, C., Kim, S. H., Mostoslavsky, R., Alt, F. W., Wu, Z., and Puigserver, P. (2007) Metabolic control of muscle mitochondrial function and fatty acid oxidation through SIRT1/PGC - 1  $\alpha$ , *The EMBO Journal* 26, 1913-1923.
110. Jeong, J., Juhn, K., Lee, H., Kim, S.-H., Min, B.-H., Lee, K.-M., Cho, M.-H., Park, G.-H., and Lee, K.-H. (2007) SIRT1 promotes DNA repair activity and deacetylation of Ku70, *Exp Mol Med* 39, 8-13.
111. Yang, Y., Hou, H., Haller, E. M., Nicosia, S. V., and Bai, W. (2005) Suppression of FOXO1 activity by FHL2 through SIRT1 - mediated deacetylation, *The EMBO Journal* 24, 1021-1032.
112. van der Horst, A., Tertoolen, L. G. J., de Vries-Smits, L. M. M., Frye, R. A., Medema, R. H., and Burgering, B. M. T. (2004) FOXO4 is acetylated upon peroxide stress and deacetylated by the longevity protein hSir2<sup>SIRT1</sup>, *Journal of Biological Chemistry* 279, 28873-28879.
113. Yeung, F., Hoberg, J. E., Ramsey, C. S., Keller, M. D., Jones, D. R., Frye, R. A., and Mayo, M. W. (2004) Modulation of NF -  $\kappa$  B - dependent transcription and cell survival by the SIRT1 deacetylase, *The EMBO Journal* 23, 2369-2380.
114. Pagans, S., Pedal, A., North, B. J., Kaehlcke, K., Marshall, B. L., Dorr, A., Hetzer-Egger, C., Henklein, P., Frye, R., McBurney, M. W., Hruby, H., Jung, M., Verdin, E., and Ott, M. (2005) SIRT1 Regulates HIV Transcription via Tat Deacetylation, *PLoS Biol* 3, e41.
115. Qiang, L., Lin, Hua V., Kim-Muller, Ja Y., Welch, Carrie L., Gu, W., and Accili, D. (2011) Proatherogenic abnormalities of lipid metabolism in SirT1 transgenic mice are mediated through Creb deacetylation, *Cell metabolism* 14, 758-767.
116. Narayan, N., Lee, I. H., Borenstein, R., Sun, J., Wong, R., Tong, G., Fergusson, M. M., Liu, J., Rovira, I. I., Cheng, H.-L., Wang, G., Gucek, M., Lombard, D., Alt, F. W., Sack, M. N., Murphy, E., Cao, L., and Finkel, T. (2012) The NAD-dependent deacetylase SIRT2 is required for programmed necrosis, *Nature* 492, 199-204.
117. Zhang, H., Park, S.-H., Pantazides, B. G., Karpiuk, O., Warren, M. D., Hardy, C. W., Duong, D. M., Park, S.-J., Kim, H.-S., Vassilopoulos, A., Seyfried, N. T., Johnsen, S. A., Gius, D., and Yu, D. S. (2013) SIRT2 directs the replication stress response through

- CDK9 deacetylation, *Proceedings of the National Academy of Sciences* 110, 13546-13551.
118. Iwahara, T., Bonasio, R., Narendra, V., and Reinberg, D. (2012) SIRT3 functions in the nucleus in the control of stress-related gene expression, *Molecular and Cellular Biology* 32, 5022-5034.
  119. Schwer, B., Bunkenborg, J., Verdin, R. O., Andersen, J. S., and Verdin, E. (2006) Reversible lysine acetylation controls the activity of the mitochondrial enzyme acetyl-CoA synthetase 2, *Proceedings of the National Academy of Sciences* 103, 10224-10229.
  120. Lombard, D. B., Alt, F. W., Cheng, H.-L., Bunkenborg, J., Streeper, R. S., Mostoslavsky, R., Kim, J., Yancopoulos, G., Valenzuela, D., Murphy, A., Yang, Y., Chen, Y., Hirschey, M. D., Bronson, R. T., Haigis, M., Guarente, L. P., Farese, R. V., Weissman, S., Verdin, E., and Schwer, B. (2007) Mammalian Sir2 homolog SIRT3 regulates global mitochondrial lysine acetylation, *Molecular and Cellular Biology* 27, 8807-8814.
  121. Sundaresan, N. R., Samant, S. A., Pillai, V. B., Rajamohan, S. B., and Gupta, M. P. (2008) SIRT3 Is a stress-responsive deacetylase in cardiomyocytes That protects cells from stress-mediated cell death by deacetylation of ku70, *Molecular and Cellular Biology* 28, 6384-6401.
  122. Cimen, H., Han, M.-J., Yang, Y., Tong, Q., Koc, H., and Koc, E. C. (2010) Regulation of succinate dehydrogenase activity by SIRT3 in mammalian mitochondria, *Biochemistry* 49, 304-311.
  123. Tao, R., Coleman, M. C., Pennington, J. D., Ozden, O., Park, S.-H., Jiang, H., Kim, H.-S., Flynn, C. R., Hill, S., Hayes McDonald, W., Olivier, A. K., Spitz, D. R., and Gius, D. (2010) Sirt3-mediated deacetylation of evolutionarily conserved lysine 122 regulates MnSOD activity in response to stress, *Molecular cell* 40, 893-904.
  124. Xue, L., Xu, F., Meng, L., Wei, S., Wang, J., Hao, P., Bian, Y., Zhang, Y., and Chen, Y. (2012) Acetylation-dependent regulation of mitochondrial ALDH2 activation by SIRT3 mediates acute ethanol-induced eNOS activation, *FEBS Letters* 586, 137-142.
  125. Shulga, N., Wilson-Smith, R., and Pastorino, J. G. (2010) Sirtuin-3 deacetylation of cyclophilin D induces dissociation of hexokinase II from the mitochondria, *Journal of cell science* 123, 894-902.
  126. Hirschey, M. D., Shimazu, T., Goetzman, E., Jing, E., Schwer, B., Lombard, D. B., Grueter, C. A., Harris, C., Biddinger, S., Ilkayeva, O. R., Stevens, R. D., Li, Y., Saha, A. K., Ruderman, N. B., Bain, J. R., Newgard, C. B., Farese Jr, R. V., Alt, F. W., Kahn, C. R., and Verdin, E. (2010) SIRT3 regulates mitochondrial fatty-acid oxidation by reversible enzyme deacetylation, *Nature* 464, 121-125.

127. Jiang, W., Wang, S., Xiao, M., Lin, Y., Zhou, L., Lei, Q., Xiong, Y., Guan, K.-L., and Zhao, S. (2011) Acetylation regulates gluconeogenesis by promoting PEPCK1 degradation via recruiting the UBR5 ubiquitin ligase, *Molecular cell* 43, 33-44.
128. Baur, J. A., Chen, D., Chini, E. N., Chua, K., Cohen, H. Y., Cabo, R. d., Deng, C., Dimmeler, S., Gius, D., Guarente, L. P., Helfand, S. L., Imai, S.-I., Itoh, H., Kadowaki, T., Koya, D., Leeuwenburgh, C., McBurney, M., Nabeshima, Y.-I., Neri, C., Oberdoerffer, P., Pestell, R. G., Rogina, B., Sadoshima, J., Sartorelli, V., Serrano, M., Sinclair, D. A., Steegborn, C., Tatar, M., Tissenbaum, H. A., Tong, Q., Tsubota, K., Vaquero, A., and Verdin, E. (2010) Dietary restriction: standing up for sirtuins, *Science* 329, 1012-1013.
129. Ramakrishnan, V. (1997) Histone structure and the organization of the nucleosome, *Annual Review of Biophysics and Biomolecular Structure* 26, 83-112.
130. Feige, J. N., and Auwerx, J. (2008) Transcriptional targets of sirtuins in the coordination of mammalian physiology, *Current Opinion in Cell Biology* 20, 303-309.
131. Imai, S.-i., and Guarente, L. (2014) NAD<sup>+</sup> and sirtuins in aging and disease, *Trends in Cell Biology* 24, 464-471.
132. Sebastián, C., Satterstrom, F. K., Haigis, M. C., and Mostoslavsky, R. (2012) From sirtuin biology to human diseases: an update, *Journal of Biological Chemistry* 287, 42444-42452.
133. Houtkooper, R. H., Pirinen, E., and Auwerx, J. (2012) Sirtuins as regulators of metabolism and healthspan, *Nature reviews. Molecular cell biology* 13, 225-238.
134. Rodgers, J. T., Lerin, C., Haas, W., Gygi, S. P., Spiegelman, B. M., and Puigserver, P. (2005) Nutrient control of glucose homeostasis through a complex of PGC-1 $\alpha$  and SIRT1, *Nature* 434, 113-118.
135. Liu, Y., Dentin, R., Chen, D., Hedrick, S., Ravnskjaer, K., Schenk, S., Milne, J., Meyers, D. J., Cole, P., Iii, J. Y., Olefsky, J., Guarente, L., and Montminy, M. (2008) A fasting inducible switch modulates gluconeogenesis via activator/coactivator exchange, *Nature* 456, 269-273.
136. Zhong, L., D'Urso, A., Toiber, D., Sebastian, C., Henry, R. E., Vadysirisack, D. D., Guimaraes, A., Marinelli, B., Wikstrom, J. D., Nir, T., Clish, C. B., Vaitheesvaran, B., Iliopoulos, O., Kurland, I., Dor, Y., Weissleder, R., Shirihai, O. S., Ellisen, L. W., Espinosa, J. M., and Mostoslavsky, R. (2010) The histone deacetylase Sirt6 regulates glucose homeostasis via Hif1 $\alpha$ , *Cell* 140, 280-293.
137. Feige, J. N., Lagouge, M., Canto, C., Strehle, A., Houten, S. M., Milne, J. C., Lambert, P. D., Matak, C., Elliott, P. J., and Auwerx, J. (2008) Specific SIRT1 activation mimics low energy levels and protects against diet-induced metabolic disorders by enhancing fat oxidation, *Cell metabolism* 8, 347-358.

138. Lagouge, M., Argmann, C., Gerhart-Hines, Z., Meziane, H., Lerin, C., Daussin, F., Messadeq, N., Milne, J., Lambert, P., Elliott, P., Geny, B., Laakso, M., Puigserver, P., and Auwerx, J. (2006) Resveratrol improves mitochondrial function and protects against metabolic disease by activating SIRT1 and PGC-1 $\alpha$ , *Cell* 127, 1109-1122.
139. Purushotham, A., Schug, T. T., Xu, Q., Surapureddi, S., Guo, X., and Li, X. (2009) Hepatocyte-specific deletion of SIRT1 alters fatty acid metabolism and results in hepatic steatosis and inflammation, *Cell metabolism* 9, 327-338.
140. Purushotham, A., Xu, Q., and Li, X. (2012) Systemic SIRT1 insufficiency results in disruption of energy homeostasis and steroid hormone metabolism upon high-fat-diet feeding, *The FASEB Journal* 26, 656-667.
141. Rodgers, J. T., and Puigserver, P. (2007) Fasting-dependent glucose and lipid metabolic response through hepatic sirtuin 1, *Proceedings of the National Academy of Sciences* 104, 12861-12866.
142. Chakrabarti, P., English, T., Karki, S., Qiang, L., Tao, R., Kim, J., Luo, Z., Farmer, S. R., and Kandror, K. V. (2011) SIRT1 controls lipolysis in adipocytes via FOXO1-mediated expression of ATGL, *Journal of Lipid Research* 52, 1693-1701.
143. Ponugoti, B., Kim, D.-H., Xiao, Z., Smith, Z., Miao, J., Zang, M., Wu, S.-Y., Chiang, C.-M., Veenstra, T. D., and Kemper, J. K. (2010) SIRT1 deacetylates and inhibits SREBP-1C activity in regulation of hepatic lipid metabolism, *Journal of Biological Chemistry* 285, 33959-33970.
144. Walker, A. K., Yang, F., Jiang, K., Ji, J.-Y., Watts, J. L., Purushotham, A., Boss, O., Hirsch, M. L., Ribich, S., Smith, J. J., Israelian, K., Westphal, C. H., Rodgers, J. T., Shioda, T., Elson, S. L., Mulligan, P., Najafi-Shoushtari, H., Black, J. C., Thakur, J. K., Kadyk, L. C., Whetstone, J. R., Mostoslavsky, R., Puigserver, P., Li, X., Dyson, N. J., Hart, A. C., and Näär, A. M. (2010) Conserved role of SIRT1 orthologs in fasting-dependent inhibition of the lipid/cholesterol regulator SREBP, *Genes & development* 24, 1403-1417.
145. Pfluger, P. T., Herranz, D., Velasco-Miguel, S., Serrano, M., and Tschöp, M. H. (2008) Sirt1 protects against high-fat diet-induced metabolic damage, *Proceedings of the National Academy of Sciences* 105, 9793-9798.
146. Wu, D., Qiu, Y., Gao, X., Yuan, X.-B., and Zhai, Q. (2011) Overexpression of SIRT1 in mouse forebrain impairs lipid/glucose metabolism and motor function, *PloS one* 6, e21759.
147. Hirschey, Matthew D., Shimazu, T., Jing, E., Grueter, Carrie A., Collins, Amy M., Aouizerat, B., Stančáková, A., Goetzman, E., Lam, Maggie M., Schwer, B., Stevens, Robert D., Muehlbauer, Michael J., Kakar, S., Bass, Nathan M., Kuusisto, J., Laakso, M., Alt, Frederick W., Newgard, Christopher B., Farese Jr, Robert V., Kahn, C. R., and

- Verdin, E. (2011) SIRT3 deficiency and mitochondrial protein hyperacetylation accelerate the development of the metabolic Syndrome, *Molecular cell* 44, 177-190.
148. Nasrin, N., Wu, X., Fortier, E., Feng, Y., Bare, O. C., Chen, S., Ren, X., Wu, Z., Streeper, R. S., and Bordone, L. (2010) SIRT4 regulates fatty acid oxidation and mitochondrial gene expression in liver and muscle cells, *Journal of Biological Chemistry* 285, 31995-32002.
149. Kim, H.-S., Xiao, C., Wang, R.-H., Lahusen, T., Xu, X., Vassilopoulos, A., Vazquez-Ortiz, G., Jeong, W.-I., Park, O., Ki, S. H., Gao, B., and Deng, C.-X. (2010) Hepatic-specific disruption of SIRT6 in mice results in fatty liver formation due to enhanced glycolysis and triglyceride synthesis, *Cell metabolism* 12, 224-236.
150. Finley, L. W. S., Haas, W., Desquiret-Dumas, V., Wallace, D. C., Procaccio, V., Gygi, S. P., and Haigis, M. C. (2011) Succinate dehydrogenase is a direct target of sirtuin 3 deacetylase activity, *PLoS ONE* 6, e23295.
151. Shimazu, T., Hirschey, M. D., Hua, L., Dittenhafer-Reed, K. E., Schwer, B., Lombard, D. B., Li, Y., Bunkenborg, J., Alt, F. W., Denu, J. M., Jacobson, M. P., and Verdin, E. (2010) SIRT3 deacetylates mitochondrial 3-hydroxy-3-methylglutaryl CoA synthase 2 and regulates ketone body production, *Cell Metabolism* 12, 654-661.
152. Hallows, W. C., Yu, W., Smith, B. C., Devires, M. K., Ellinger, J. J., Someya, S., Shortreed, M. R., Prolla, T., Markley, J. L., Smith, L. M., Zhao, S., Guan, K.-L., and Denu, J. M. (2011) Sirt3 promotes the urea cycle and fatty acid oxidation during dietary restriction, *Molecular Cell* 41, 139-149.
153. Finkel, T., Deng, C.-X., and Mostoslavsky, R. (2009) Recent progress in the biology and physiology of sirtuins, *Nature* 460, 587-591.
154. Choi, J.-E., and Mostoslavsky, R. (2014) Sirtuins, metabolism, and DNA repair, *Current Opinion in Genetics & Development* 26, 24-32.
155. Wang, R.-H., Sengupta, K., Li, C., Kim, H.-S., Cao, L., Xiao, C., Kim, S., Xu, X., Zheng, Y., Chilton, B., Jia, R., Zheng, Z.-M., Appella, E., Wang, X. W., Ried, T., and Deng, C.-X. (2008) Impaired DNA damage response, genome instability, and tumorigenesis in SIRT1 mutant mice, *Cancer Cell* 14, 312-323.
156. Yuan, Z., Zhang, X., Sengupta, N., Lane, W. S., and Seto, E. (2007) SIRT1 regulates the function of the nijmegen breakage syndrome protein, *Molecular cell* 27, 149-162.
157. Oberdoerffer, P., Michan, S., McVay, M., Mostoslavsky, R., Vann, J., Park, S.-K., Hartlerode, A., Stegmuller, J., Hafner, A., Loerch, P., Wright, S. M., Mills, K. D., Bonni, A., Yankner, B. A., Scully, R., Prolla, T. A., Alt, F. W., and Sinclair, D. A. (2008) SIRT1 redistribution on chromatin promotes genomic stability but alters gene expression during aging, *Cell* 135, 907-918.

158. Li, K., Casta, A., Wang, R., Lozada, E., Fan, W., Kane, S., Ge, Q., Gu, W., Orren, D., and Luo, J. (2008) Regulation of WRN protein cellular localization and enzymatic activities by SIRT1-mediated deacetylation, *Journal of Biological Chemistry* 283, 7590-7598.
159. Dobbin, M. M., Madabhushi, R., Pan, L., Chen, Y., Kim, D., Gao, J., Ahanonu, B., Pao, P.-C., Qiu, Y., Zhao, Y., and Tsai, L.-H. (2013) SIRT1 collaborates with ATM and HDAC1 to maintain genomic stability in neurons, *Nat Neurosci* 16, 1008-1015.
160. Fan, W., and Luo, J. (2010) SIRT1 regulates UV-induced DNA repair through deacetylating XPA, *Molecular cell* 39, 247-258.
161. Ming, M., Shea, C. R., Guo, X., Li, X., Soltani, K., Han, W., and He, Y.-Y. (2010) Regulation of global genome nucleotide excision repair by SIRT1 through xeroderma pigmentosum C, *Proceedings of the National Academy of Sciences* 107, 22623-22628.
162. Serrano, L., Martínez-Redondo, P., Marazuela-Duque, A., Vazquez, B. N., Dooley, S. J., Voigt, P., Beck, D. B., Kane-Goldsmith, N., Tong, Q., Rabanal, R. M., Fondevila, D., Muñoz, P., Krüger, M., Tischfield, J. A., and Vaquero, A. (2013) The tumor suppressor SirT2 regulates cell cycle progression and genome stability by modulating the mitotic deposition of H4K20 methylation, *Genes & development* 27, 639-653.
163. Bartkova, J., Horejsi, Z., Koed, K., Kramer, A., Tort, F., Zieger, K., Guldborg, P., Sehested, M., Nesland, J. M., Lukas, C., Orntoft, T., Lukas, J., and Bartek, J. (2005) DNA damage response as a candidate anti-cancer barrier in early human tumorigenesis, *Nature* 434, 864-870.
164. Chen, Y., Zhang, J., Lin, Y., Lei, Q., Guan, K. L., Zhao, S., and Xiong, Y. (2011) Tumour suppressor SIRT3 deacetylates and activates manganese superoxide dismutase to scavenge ROS, *EMBO reports* 12, 534-541.
165. Jeong, Seung M., Xiao, C., Finley, Lydia W. S., Lahusen, T., Souza, Amanda L., Pierce, K., Li, Y.-H., Wang, X., Laurent, G., German, Natalie J., Xu, X., Li, C., Wang, R.-H., Lee, J., Csibi, A., Cerione, R., Blenis, J., Clish, Clary B., Kimmelman, A., Deng, C.-X., and Haigis, Marcia C. (2013) SIRT4 has tumor-suppressive activity and regulates the cellular metabolic response to DNA damage by inhibiting mitochondrial glutamine metabolism, *Cancer Cell* 23, 450-463.
166. Csibi, A., Fendt, S.-M., Li, C., Poulogiannis, G., Choo, Andrew Y., Chapski, Douglas J., Jeong, Seung M., Dempsey, J. M., Parkhitko, A., Morrison, T., Henske, E. P., Haigis, Marcia C., Cantley, Lewis C., Stephanopoulos, G., Yu, J., and Blenis, J. (2013) The mTORC1 pathway stimulates glutamine metabolism and cell proliferation by repressing SIRT4, *Cell* 153, 840-854.
167. Mostoslavsky, R., Chua, K. F., Lombard, D. B., Pang, W. W., Fischer, M. R., Gellon, L., Liu, P., Mostoslavsky, G., Franco, S., Murphy, M. M., Mills, K. D., Patel, P., Hsu, J. T., Hong, A. L., Ford, E., Cheng, H.-L., Kennedy, C., Nunez, N., Bronson, R., Frenthewey,

- D., Auerbach, W., Valenzuela, D., Karow, M., Hottiger, M. O., Hursting, S., Barrett, J. C., Guarente, L., Mulligan, R., Demple, B., Yancopoulos, G. D., and Alt, F. W. (2006) Genomic instability and aging-like phenotype in the absence of mammalian SIRT6, *Cell* 124, 315-329.
168. McCord, R. A., Michishita, E., Hong, T., Berber, E., Boxer, L. D., Kusumoto, R., Guan, S., Shi, X., Gozani, O., and Burlingame, A. L. (2009) SIRT6 stabilizes DNA-dependent protein kinase at chromatin for DNA double-strand break repair, *Aging (Albany NY)* 1, 109-121.
169. Michishita, E., McCord, R. A., Boxer, L. D., Barber, M. F., Hong, T., Gozani, O., and Chua, K. F. (2009) Cell cycle-dependent deacetylation of telomeric histone H3 lysine K56 by human SIRT6, *Cell Cycle* 8, 2664-2666.
170. Mao, Z., Hine, C., Tian, X., Van Meter, M., Au, M., Vaidya, A., Seluanov, A., and Gorbunova, V. (2011) SIRT6 promotes DNA repair under stress by activating PARP1, *Science* 332, 1443-1446.
171. Toiber, D., Erdel, F., Bouazoune, K., Silberman, Dafne M., Zhong, L., Mulligan, P., Sebastian, C., Cosentino, C., Martinez-Pastor, B., Giacosa, S., D'Urso, A., Näär, Anders M., Kingston, R., Rippe, K., and Mostoslavsky, R. (2013) SIRT6 recruits SNF2H to DNA break sites, preventing genomic instability through chromatin remodeling, *Molecular cell* 51, 454-468.
172. Kominsky, D. J., Campbell, E. L., and Colgan, S. P. (2010) Metabolic shifts in immunity and inflammation, *The Journal of Immunology* 184, 4062-4068.
173. Schug, T. T., Xu, Q., Gao, H., Peres-da-Silva, A., Draper, D. W., Fessler, M. B., Purushotham, A., and Li, X. (2010) Myeloid deletion of SIRT1 induces inflammatory signaling in response to environmental stress, *Molecular and Cellular Biology* 30, 4712-4721.
174. Yoshizaki, T., Schenk, S., Imamura, T., Babendure, J. L., Sonoda, N., Bae, E. J., Oh, D. Y., Lu, M., Milne, J. C., Westphal, C., Bandyopadhyay, G., and Olefsky, J. M. (2010) SIRT1 inhibits inflammatory pathways in macrophages and modulates insulin sensitivity, *American Journal of Physiology - Endocrinology and Metabolism* 298, E419-E428.
175. Kauppinen, A., Suuronen, T., Ojala, J., Kaarniranta, K., and Salminen, A. (2013) Antagonistic crosstalk between NF- $\kappa$ B and SIRT1 in the regulation of inflammation and metabolic disorders, *Cellular Signalling* 25, 1939-1948.
176. Xu, H., Barnes, G. T., Yang, Q., Tan, G., Yang, D., Chou, C. J., Sole, J., Nichols, A., Ross, J. S., Tartaglia, L. A., and Chen, H. Chronic inflammation in fat plays a crucial role in the development of obesity-related insulin resistance, *The Journal of Clinical Investigation* 112, 1821-1830.

177. Li, P., Zhao, Y., Wu, X., Xia, M., Fang, M., Iwasaki, Y., Sha, J., Chen, Q., Xu, Y., and Shen, A. (2011) Interferon gamma (IFN- $\gamma$ ) disrupts energy expenditure and metabolic homeostasis by suppressing SIRT1 transcription, *Nucleic Acids Research*.
178. Zhang, Z., Lowry, S. F., Guarente, L., and Haimovich, B. (2010) Roles of SIRT1 in the acute and restorative phases following induction of inflammation, *Journal of Biological Chemistry* 285, 41391-41401.
179. Rothgiesser, K. M., Erener, S., Waibel, S., Lüscher, B., and Hottiger, M. O. (2010) SIRT2 regulates NF- $\kappa$ B-dependent gene expression through deacetylation of p65 Lys310, *Journal of cell science* 123, 4251-4258.
180. Kawahara, T. L. A., Rapicavoli, N. A., Wu, A. R., Qu, K., Quake, S. R., and Chang, H. Y. (2011) Dynamic chromatin localization of Sirt6 shapes stress- and aging-Related transcriptional networks, *PLoS Genet* 7, e1002153.
181. Kawahara, T. L. A., Michishita, E., Adler, A. S., Damian, M., Berber, E., Lin, M., McCord, R. A., Ongaigui, K. C. L., Boxer, L. D., Chang, H. Y., and Chua, K. F. (2009) SIRT6 links histone H3 lysine 9 deacetylation to NF- $\kappa$ B-dependent gene expression and organismal life span, *Cell* 136, 62-74.
182. Van Gool, F., Galli, M., Gueydan, C., Kruys, V., Prevot, P.-P., Bedalov, A., Mostoslavsky, R., Alt, F. W., De Smedt, T., and Leo, O. (2009) Intracellular NAD levels regulate tumor necrosis factor protein synthesis in a sirtuin-dependent manner, *Nat Med* 15, 206-210.
183. Kawashima, T., Inuzuka, Y., Okuda, J., Kato, T., Niizuma, S., Tamaki, Y., Iwanaga, Y., Kawamoto, A., Narazaki, M., Matsuda, T., Adachi, S., Takemura, G., Kita, T., Kimura, T., and Shioi, T. (2011) Constitutive SIRT1 overexpression impairs mitochondria and reduces cardiac function in mice, *Journal of Molecular and Cellular Cardiology* 51, 1026-1036.
184. Sundaresan, N. R., Pillai, V. B., Wolfgeher, D., Samant, S., Vasudevan, P., Parekh, V., Raghuraman, H., Cunningham, J. M., Gupta, M., and Gupta, M. P. (2011) The deacetylase SIRT1 promotes membrane localization and activation of Akt and PDK1 during tumorigenesis and cardiac hypertrophy, *Science Signaling* 4, ra46-ra46.
185. Alcendor, R. R., Gao, S., Zhai, P., Zablocki, D., Holle, E., Yu, X., Tian, B., Wagner, T., Vatner, S. F., and Sadoshima, J. (2007) Sirt1 Regulates Aging and Resistance to Oxidative Stress in the Heart, *Circulation Research* 100, 1512-1521.
186. Sundaresan, N. R., Gupta, M., Kim, G., Rajamohan, S. B., Isbatan, A., and Gupta, M. P. (2009) Sirt3 blocks the cardiac hypertrophic response by augmenting Foxo3a-dependent antioxidant defense mechanisms in mice, *The Journal of Clinical Investigation* 119, 2758-2771.



187. Pillai, V. B., Sundaresan, N. R., Kim, G., Gupta, M., Rajamohan, S. B., Pillai, J. B., Samant, S., Ravindra, P. V., Isbatan, A., and Gupta, M. P. (2010) Exogenous NAD blocks cardiac hypertrophic response via activation of the SIRT3-LKB1-AMP-activated kinase pathway, *Journal of Biological Chemistry* 285, 3133-3144.
188. Cai, Y., Yu, S.-S., Chen, S.-R., Pi, R.-B., Gao, S., Li, H., Ye, J.-T., and Liu, P.-Q. (2012) Nmnat2 protects cardiomyocytes from hypertrophy via activation of SIRT6, *FEBS Letters* 586, 866-874.
189. Sundaresan, N. R., Vasudevan, P., Zhong, L., Kim, G., Samant, S., Parekh, V., Pillai, V. B., Ravindra, P. V., Gupta, M., Jeevanandam, V., Cunningham, J. M., Deng, C.-X., Lombard, D. B., Mostoslavsky, R., and Gupta, M. P. (2012) The sirtuin SIRT6 blocks IGF-Akt signaling and development of cardiac hypertrophy by targeting c-Jun, *Nat Med* 18, 1643-1650.
190. Shen, P., Feng, X., Zhang, X., Huang, X., Liu, S., Lu, X., Li, J., You, J., Lu, J., and Li, Z. (2016) SIRT6 suppresses phenylephrine-induced cardiomyocyte hypertrophy through inhibiting p300, *Journal of Pharmacological Sciences*.
191. Roth, M., and Chen, W. Y. (2014) Sorting out functions of sirtuins in cancer, *Oncogene* 33, 1609-1620.
192. Deng, C.-X. (2009) SIRT1, is it a tumor promoter or tumor suppressor?, *International Journal of Biological Sciences* 5, 147-152.
193. Kim, H.-S., Patel, K., Muldoon-Jacobs, K., Bisht, K. S., Aykin-Burns, N., Pennington, J. D., van der Meer, R., Nguyen, P., Savage, J., Owens, K. M., Vassilopoulos, A., Ozden, O., Park, S.-H., Singh, K. K., Abdulkadir, S. A., Spitz, D. R., Deng, C.-X., and Gius, D. (2010) SIRT3 Is a Mitochondria-Localized Tumor Suppressor Required for Maintenance of Mitochondrial Integrity and Metabolism during Stress, *Cancer Cell* 17, 41-52.
194. Sebastián, C., Zwaans, Bernadette M. M., Silberman, Dafne M., Gymrek, M., Goren, A., Zhong, L., Ram, O., Truelove, J., Guimaraes, Alexander R., Toiber, D., Cosentino, C., Greenson, Joel K., MacDonald, Alasdair I., McGlynn, L., Maxwell, F., Edwards, J., Giacosa, S., Guccione, E., Weissleder, R., Bernstein, Bradley E., Regev, A., Shiels, Paul G., Lombard, David B., and Mostoslavsky, R. (2012) The Histone Deacetylase SIRT6 Is a Tumor Suppressor that Controls Cancer Metabolism, *Cell* 151, 1185-1199.
195. McCay, C., Crowell, M. F., and Maynard, L. A. (1935) The effect of retarded growth upon the length of life span and upon the ultimate body size, *J nutr* 10, 63-79.
196. Colman, R. J., Beasley, T. M., Kemnitz, J. W., Johnson, S. C., Weindruch, R., and Anderson, R. M. (2014) Caloric restriction reduces age-related and all-cause mortality in rhesus monkeys, *Nature communications* 5.
197. Weindruch, R. (1996) The retardation of aging by caloric restriction: studies in rodents and primates, *Toxicologic Pathology* 24, 742-745.

198. Masoro, E. J. (2005) Overview of caloric restriction and ageing, *Mechanisms of Ageing and Development* 126, 913-922.
199. Guarente, L. (2013) Calorie restriction and sirtuins revisited, *Genes & development* 27, 2072-2085.
200. Kanfi, Y., Naiman, S., Amir, G., Peshti, V., Zinman, G., Nahum, L., Bar-Joseph, Z., and Cohen, H. Y. (2012) The sirtuin SIRT6 regulates lifespan in male mice, *Nature* 483, 218-221.
201. Burnett, C., Valentini, S., Cabreiro, F., Goss, M., Somogyvari, M., Piper, M. D., Hoddinott, M., Sutphin, G. L., Leko, V., McElwee, J. J., Vazquez-Manrique, R. P., Orfila, A.-M., Ackerman, D., Au, C., Vinti, G., Riesen, M., Howard, K., Neri, C., Bedalov, A., Kaerberlein, M., Soti, C., Partridge, L., and Gems, D. (2011) Absence of effects of Sir2 overexpression on lifespan in *C. elegans* and *Drosophila*, *Nature* 477, 482-485.
202. Baur, J. A., Chen, D., Chini, E. N., Chua, K., Cohen, H. Y., de Cabo, R., Deng, C., Dimmeler, S., Gius, D., Guarente, L. P., Helfand, S. L., Imai, S., Itoh, H., Kadowaki, T., Koya, D., Leeuwenburgh, C., McBurney, M., Nabeshima, Y., Neri, C., Oberdoerffer, P., Pestell, R. G., Rogina, B., Sadoshima, J., Sartorelli, V., Serrano, M., Sinclair, D. A., Steegborn, C., Tatar, M., Tissenbaum, H. A., Tong, Q., Tsubota, K., Vaquero, A., and Verdin, E. (2010) Dietary restriction: standing up for sirtuins, *Science* 329, 1012-1013; author reply 1013-1014.
203. Howitz, K. T., Bitterman, K. J., Cohen, H. Y., Lamming, D. W., Lavu, S., Wood, J. G., Zipkin, R. E., Chung, P., Kisielewski, A., Zhang, L.-L., Scherer, B., and Sinclair, D. A. (2003) Small molecule activators of sirtuins extend *Saccharomyces cerevisiae* lifespan, *Nature* 425, 191-196.
204. Milne, J. C., Lambert, P. D., Schenk, S., Carney, D. P., Smith, J. J., Gagne, D. J., Jin, L., Boss, O., Perni, R. B., Vu, C. B., Bemis, J. E., Xie, R., Disch, J. S., Ng, P. Y., Nunes, J. J., Lynch, A. V., Yang, H., Galonek, H., Israelian, K., Choy, W., Iffland, A., Lavu, S., Medvedik, O., Sinclair, D. A., Olefsky, J. M., Jirousek, M. R., Elliott, P. J., and Westphal, C. H. (2007) Small molecule activators of SIRT1 as therapeutics for the treatment of type 2 diabetes, *Nature* 450, 712-716.
205. Dai, H., Kustigian, L., Carney, D., Case, A., Considine, T., Hubbard, B. P., Perni, R. B., Riera, T. V., Szczepankiewicz, B., Vlasuk, G. P., and Stein, R. L. (2010) SIRT1 activation by small molecules: kinetic and biophysical evidence for direct interaction of enzyme and activator, *Journal of Biological Chemistry* 285, 32695-32703.
206. Frémont, L. (2000) Biological effects of resveratrol, *Life Sciences* 66, 663-673.
207. Wood, J. G., Rogina, B., Lavu, S., Howitz, K., Helfand, S. L., Tatar, M., and Sinclair, D. (2004) Sirtuin activators mimic caloric restriction and delay ageing in metazoans, *Nature* 430, 686-689.

208. Valenzano, D. R., Terzibasi, E., Genade, T., Cattaneo, A., Domenici, L., and Cellarino, A. (2006) Resveratrol prolongs lifespan and retards the onset of age-related markers in a short-lived vertebrate, *Current Biology* 16, 296-300.
209. Rascón, B., Amdam, G. V., Hubbard, B. P., and Sinclair, D. A. (2012) The lifespan extension effects of resveratrol are conserved in the honey bee and may be driven by a mechanism related to caloric restriction.
210. Boily, G., He, X. H., Pearce, B., Jardine, K., and McBurney, M. W. (2009) SirT1-null mice develop tumors at normal rates but are poorly protected by resveratrol, *Oncogene* 28, 2882-2893.
211. Price, N. L., Gomes, A. P., Ling, A. J., Duarte, F. V., Martin-Montalvo, A., North, B. J., Agarwal, B., Ye, L., Ramadori, G., Teodoro, J. S., Hubbard, B. P., Varela, A. T., Davis, J. G., Varamini, B., Hafner, A., Moaddel, R., Rolo, A. P., Coppari, R., Palmeira, C. M., de Cabo, R., Baur, J. A., and Sinclair, D. A. (2012) SIRT1 is required for AMPK activation and the beneficial effects of resveratrol on mitochondrial function, *Cell metabolism* 15, 675-690.
212. Minor, R. K., Baur, J. A., Gomes, A. P., Ward, T. M., Csiszar, A., Mercken, E. M., Abdelmohsen, K., Shin, Y.-K., Canto, C., Scheibye-Knudsen, M., Krawczyk, M., Irusta, P. M., Martín-Montalvo, A., Hubbard, B. P., Zhang, Y., Lehmann, E., White, A. A., Price, N. L., Swindell, W. R., Pearson, K. J., Becker, K. G., Bohr, V. A., Gorospe, M., Egan, J. M., Talan, M. I., Auwerx, J., Westphal, C. H., Ellis, J. L., Ungvari, Z., Vlasuk, G. P., Elliott, P. J., Sinclair, D. A., and de Cabo, R. (2011) SRT1720 improves survival and healthspan of obese mice, *Scientific reports* 1, 70.
213. Hubbard, B. P., and Sinclair, D. A. (2014) Small molecule SIRT1 activators for the treatment of aging and age-related diseases, *Trends in pharmacological sciences* 35, 146-154.
214. Kaerberlein, M., McDonagh, T., Heltweg, B., Hixon, J., Westman, E. A., Caldwell, S. D., Napper, A., Curtis, R., DiStefano, P. S., Fields, S., Bedalov, A., and Kennedy, B. K. (2005) Substrate-specific activation of sirtuins by resveratrol, *Journal of Biological Chemistry* 280, 17038-17045.
215. Pacholec, M., Bleasdale, J. E., Chrnyk, B., Cunningham, D., Flynn, D., Garofalo, R. S., Griffith, D., Griffor, M., Loulakis, P., Pabst, B., Qiu, X., Stockman, B., Thanabal, V., Varghese, A., Ward, J., Withka, J., and Ahn, K. (2010) SRT1720, SRT2183, SRT1460, and resveratrol are not direct activators of SIRT1, *Journal of Biological Chemistry* 285, 8340-8351.
216. Dasgupta, B., and Milbrandt, J. (2007) Resveratrol stimulates AMP kinase activity in neurons, *Proceedings of the National Academy of Sciences* 104, 7217-7222.
217. Sinclair, D. A., and Guarente, L. (2014) Small-molecule allosteric activators of sirtuins, *Annual Review of Pharmacology and Toxicology* 54, 363-380.

218. Hubbard, B. P., Gomes, A. P., Dai, H., Li, J., Case, A. W., Considine, T., Riera, T. V., Lee, J. E., E, S. Y., Lamming, D. W., Pentelute, B. L., Schuman, E. R., Stevens, L. A., Ling, A. J. Y., Armour, S. M., Michan, S., Zhao, H., Jiang, Y., Sweitzer, S. M., Blum, C. A., Disch, J. S., Ng, P. Y., Howitz, K. T., Rolo, A. P., Hamuro, Y., Moss, J., Perni, R. B., Ellis, J. L., Vlasuk, G. P., and Sinclair, D. A. (2013) Evidence for a common mechanism of SIRT1 regulation by allosteric activators, *Science* 339, 1216-1219.
219. Kim, E.-J., Kho, J.-H., Kang, M.-R., and Um, S.-J. (2007) Active regulator of SIRT1 cooperates with SIRT1 and facilitates suppression of p53 activity, *Molecular cell* 28, 277-290.
220. Liu, B., Ghosh, S., Yang, X., Zheng, H., Liu, X., Wang, Z., Jin, G., Zheng, B., Kennedy, Brian K., Suh, Y., Kaerberlein, M., Tryggvason, K., and Zhou, Z. (2012) Resveratrol rescues SIRT1-dependent adult stem cell decline and alleviates progeroid features in laminopathy-based progeria, *Cell metabolism* 16, 738-750.
221. Ghosh, S., Liu, B., and Zhou, Z. (2013) Resveratrol activates SIRT1 in a Lamin A-dependent manner, *Cell Cycle* 12, 872-876.
222. Sauve, A. A., Moir, R. D., Schramm, V. L., and Willis, I. M. (2005) Chemical Activation of Sir2-Dependent Silencing by Relief of Nicotinamide Inhibition, *Molecular cell* 17, 595-601.
223. Smoliga, J. M., Baur, J. A., and Hausenblas, H. A. (2011) Resveratrol and health – A comprehensive review of human clinical trials, *Molecular Nutrition & Food Research* 55, 1129-1141.
224. Hoffmann, E., Wald, J., Lavu, S., Roberts, J., Beaumont, C., Haddad, J., Elliott, P., Westphal, C., and Jacobson, E. (2013) Pharmacokinetics and tolerability of SRT2104, a first-in-class small molecule activator of SIRT1, after single and repeated oral administration in man, *British Journal of Clinical Pharmacology* 75, 186-196.
225. Baksi, A., Kraydashenko, O., Zalevkaya, A., Stets, R., Elliott, P., Haddad, J., Hoffmann, E., Vlasuk, G. P., and Jacobson, E. W. (2014) A phase II, randomized, placebo-controlled, double-blind, multi-dose study of SRT2104, a SIRT1 activator, in subjects with type 2 diabetes, *British Journal of Clinical Pharmacology* 78, 69-77.
226. Bitterman, K. J., Anderson, R. M., Cohen, H. Y., Latorre-Esteves, M., and Sinclair, D. A. (2002) Inhibition of silencing and accelerated aging by nicotinamide, a putative negative regulator of yeast sir2 and human SIRT1, *The Journal of biological chemistry* 277, 45099-45107.
227. Jackson, M. D., Schmidt, M. T., Oppenheimer, N. J., and Denu, J. M. (2003) Mechanism of nicotinamide inhibition and transglycosidation by Sir2 histone/protein deacetylases, *The Journal of biological chemistry* 278, 50985-50998.

228. Fischer, F., Gertz, M., Suenkel, B., Lakshminarasimhan, M., Schutkowski, M., and Steegborn, C. (2012) Sirt5 deacylation activities show differential sensitivities to nicotinamide inhibition, *PLoS one* 7, e45098.
229. Guan, X., Lin, P., Knoll, E., and Chakrabarti, R. (2014) Mechanism of inhibition of the human sirtuin enzyme SIRT3 by nicotinamide: computational and experimental studies, *PLoS one* 9, e107729.
230. Slama, J. T., and Simmons, A. M. (1989) Inhibition of NAD glycohydrolase and ADP-ribosyl transferases by carbocyclic analogs of oxidized nicotinamide adenine dinucleotide, *Biochemistry* 28, 7688-7694.
231. Szczepankiewicz, B. G., Dai, H., Koppetsch, K. J., Qian, D., Jiang, F., Mao, C., and Perni, R. B. (2012) Synthesis of carba-NAD and the structures of its ternary complexes with SIRT3 and SIRT5, *The Journal of Organic Chemistry* 77, 7319-7329.
232. Fatkins, D. G., Monnot, A. D., and Zheng, W. (2006) N $\epsilon$ -Thioacetyl-lysine: a multi-facet functional probe for enzymatic protein lysine N $\epsilon$ -deacetylation, *Bioorganic & medicinal chemistry letters* 16, 3651-3656.
233. Kiviranta, P. H., Suuronen, T., Wallén, E. A. A., Leppänen, J., Tervonen, J., Kyrölenko, S., Salminen, A., Poso, A., and Jarho, E. M. (2009) N $\epsilon$ -Thioacetyl-lysine-containing tri-, tetra-, and pentapeptides as SIRT1 and SIRT2 inhibitors, *Journal of medicinal chemistry* 52, 2153-2156.
234. He, B., Du, J., and Lin, H. (2012) Thiosuccinyl peptides as Sirt5-specific inhibitors, *Journal of the American Chemical Society* 134, 1922-1925.
235. McGeary, R. P., Bennett, A. J., Tran, Q. B., Cosgrove, K. L., and Ross, B. P. (2008) Suramin: Clinical Uses and Structure-Activity Relationships, *Mini-Rev Med Chem* 8, 1384-1394.
236. Mirza, M. R., Jakobsen, E., Pfeiffer, P., Lindebjerg-Clasen, B., Bergh, J., and Rose, C. (1997) Suramin in Non-small Cell Lung Cancer and Advanced Breast Cancer: Two Parallel Phase II Studies, *Acta Oncologica* 36, 171-174.
237. Small, E. J., Meyer, M., Marshall, M. E., Reyno, L. M., Meyers, F. J., Natale, R. B., Lenehan, P. F., Chen, L., Slichenmyer, W. J., and Eisenberger, M. (2000) Suramin Therapy for Patients With Symptomatic Hormone-Refractory Prostate Cancer: Results of a Randomized Phase III Trial Comparing Suramin Plus Hydrocortisone to Placebo Plus Hydrocortisone, *Journal of Clinical Oncology* 18, 1440-1450.
238. Trapp, J., Meier, R., Hongwiset, D., Kassack, M. U., Sippl, W., and Jung, M. (2007) Structure-Activity Studies on Suramin Analogues as Inhibitors of NAD<sup>+</sup>-Dependent Histone Deacetylases (Sirtuins), *ChemMedChem* 2, 1419-1431.

239. Napper, A. D., Hixon, J., McDonagh, T., Keavey, K., Pons, J.-F., Barker, J., Yau, W. T., Amouzegh, P., Flegg, A., Hamelin, E., Thomas, R. J., Kates, M., Jones, S., Navia, M. A., Saunders, J. O., DiStefano, P. S., and Curtis, R. (2005) Discovery of Indoles as Potent and Selective Inhibitors of the Deacetylase SIRT1, *J Med Chem* 48, 8045-8054.
240. Grozinger, C. M., Chao, E. D., Blackwell, H. E., Moazed, D., and Schreiber, S. L. (2001) Identification of a class of small molecule inhibitors of the sirtuin family of NAD-dependent deacetylases by phenotypic screening, *Journal of Biological Chemistry* 276, 38837-38843.
241. Mai, A., Massa, S., Lavu, S., Pezzi, R., Simeoni, S., Ragno, R., Mariotti, F. R., Chiani, F., Camilloni, G., and Sinclair, D. A. (2005) Design, synthesis, and biological evaluation of sirtinol analogues as class III histone/protein deacetylase (Sirtuin) inhibitors, *Journal of medicinal chemistry* 48, 7789-7795.
242. Heltweg, B., Gatbonton, T., Schuler, A. D., Posakony, J., Li, H., Goehle, S., Kollipara, R., DePinho, R. A., Gu, Y., Simon, J. A., and Bedalov, A. (2006) Antitumor activity of a small-molecule inhibitor of human silent information regulator 2 enzymes, *Cancer research* 66, 4368-4377.
243. Maurer, B., Rumpf, T., Scharfe, M., Stolfa, D. A., Schmitt, M. L., He, W., Verdin, E., Sippl, W., and Jung, M. (2012) Inhibitors of the NAD<sup>+</sup>-dependent protein desuccinylase and demalonylase Sirt5, *ACS medicinal chemistry letters* 3, 1050-1053.
244. Medda, F., Russell, R. J. M., Higgins, M., McCarthy, A. R., Campbell, J., Slawin, A. M. Z., Lane, D. P., Lain, S., and Westwood, N. J. (2009) Novel cambinol analogs as sirtuin inhibitors: synthesis, biological evaluation, and rationalization of activity, *Journal of medicinal chemistry* 52, 2673-2682.
245. Uciechowska, U., Schemies, J., Neugebauer, R. C., Huda, E.-M., Schmitt, M. L., Meier, R., Verdin, E., Jung, M., and Sippl, W. (2008) Thiobarbiturates as sirtuin inhibitors: virtual screening, free-energy calculations, and biological testing, *ChemMedChem* 3, 1965-1976.
246. Hirao, M., Posakony, J., Nelson, M., Hruby, H., Jung, M., Simon, J. A., and Bedalov, A. (2003) Identification of selective inhibitors of NAD<sup>+</sup>-dependent deacetylases using phenotypic screens in yeast, *Journal of Biological Chemistry* 278, 52773-52782.
247. Neugebauer, R. C., Uchiechowska, U., Meier, R., Hruby, H., Valkov, V., Verdin, E., Sippl, W., and Jung, M. (2008) Structure–activity studies on splitomicin derivatives as sirtuin inhibitors and computational prediction of binding mode, *Journal of medicinal chemistry* 51, 1203-1213.
248. He, B., Du, J., and Lin, H. (2012) Thiosuccinyl peptides as Sirt5-specific inhibitors, *Journal of the American Chemical Society* 134, 1922-1925.

249. Lawson, M., Uciechowska, U., Schemies, J., Rumpf, T., Jung, M., and Sippl, W. (2010) Inhibitors to understand molecular mechanisms of NAD<sup>+</sup>-dependent deacetylases (sirtuins), *Biochimica et Biophysica Acta (BBA) - Gene Regulatory Mechanisms* 1799, 726-739.
250. Madsen, A. S., and Olsen, C. A. (2012) Substrates for efficient fluorometric screening employing the NAD-dependent sirtuin 5 lysine deacylase (KDAC) enzyme, *Journal of medicinal chemistry* 55, 5582-5590.
251. Cabrita, L., Dai, W., and Bottomley, S. (2006) A family of E. coli expression vectors for laboratory scale and high throughput soluble protein production, *BMC Biotechnology* 6, 12.
252. Kuzmič, P. (1996) Program DYNAFIT for the Analysis of Enzyme Kinetic Data: Application to HIV Proteinase, *Analytical Biochemistry* 237, 260-273.
253. Burnham, K. anderson Dr (2002) Model selection and multimodel inference: a practical information-theoretic approach, springer, new york.
254. Myung, J. I., Tang, Y., and Pitt, M. A. (2009) Chapter 11 Evaluation and Comparison of Computational Models, In *Methods in Enzymology*, pp 287-304, Academic Press.
255. (MOE), M. O. E. (2013.08) Chemical Computing Group Inc., 1010 Sherbooke St. West, Suite #910, Montreal, QC, Canada, H3A 2R7, 2015.
256. Halgren, T. A. (1996) Merck molecular force field. I. Basis, form, scope, parameterization, and performance of MMFF94, *Journal of Computational Chemistry* 17, 490-519.
257. Du, J., Zhou, Y., Su, X., Yu, J. J., Khan, S., Jiang, H., Kim, J., Woo, J., Kim, J. H., Choi, B. H., He, B., Chen, W., Zhang, S., Cerione, R. A., Auwerx, J., Hao, Q., and Lin, H. (2011) Sirt5 is a NAD-dependent protein lysine demalonylase and desuccinylase, *Science* 334, 806-809.
258. Gill, S. C., and von Hippel, P. H. (1989) Calculation of protein extinction coefficients from amino acid sequence data, *Analytical Biochemistry* 182, 319-326.
259. Eftink, M. R., and Ghiron, C. A. (1981) Fluorescence quenching studies with proteins, *Analytical Biochemistry* 114, 199-227.
260. Lakowicz, J. R. (2013) *Principles of fluorescence spectroscopy*, Springer Science & Business Media.
261. Borra, M. T., Langer, M. R., Slama, J. T., and Denu, J. M. (2004) Substrate Specificity and Kinetic Mechanism of the Sir2 Family of NAD<sup>+</sup>-Dependent Histone/Protein Deacetylases†, *Biochemistry* 43, 9877-9887.

262. Pan, P. W., Feldman, J. L., Devries, M. K., Dong, A., Edwards, A. M., and Denu, J. M. (2011) Structure and biochemical functions of SIRT6, *The Journal of biological chemistry* 286, 14575-14587.
263. Madsen, A. S., and Olsen, C. A. (2012) Substrates for Efficient Fluorometric Screening Employing the NAD-Dependent Sirtuin 5 Lysine Deacetylase (KDAC) Enzyme, *Journal of medicinal chemistry* 55, 5582-5590.
264. Cleland, W. W. (1979) Optimizing coupled enzyme assays, *Analytical Biochemistry* 99, 142-145.
265. Langley, E., Pearson, M., Faretta, M., Bauer, U. M., Frye, R. A., Minucci, S., Pelicci, P. G., and Kouzarides, T. (2002) Human SIR2 deacetylates p53 and antagonizes PML/p53 - induced cellular senescence, *The EMBO Journal* 21, 2383-2396.
266. Amengual, J. E., Clark-Garvey, S., Kalac, M., Scotto, L., Marchi, E., Neylon, E., Johannet, P., Wei, Y., Zain, J., and O'Connor, O. A. (2013) Sirtuin and pan-class I/II deacetylase (DAC) inhibition is synergistic in preclinical models and clinical studies of lymphoma, *Blood* 122, 2104-2113.
267. Guan, D., Lim, J. H., Peng, L., Liu, Y., Lam, M., Seto, E., and Kao, H. Y. (2014) Deacetylation of the tumor suppressor protein PML regulates hydrogen peroxide-induced cell death, *Cell death & disease* 5, e1340.
268. Zhao, X., Allison, D., Condon, B., Zhang, F., Gheyi, T., Zhang, A., Ashok, S., Russell, M., MacEwan, I., Qian, Y., Jamison, J. A., and Luz, J. G. (2013) The 2.5 Å Crystal Structure of the SIRT1 Catalytic Domain Bound to Nicotinamide Adenine Dinucleotide (NAD<sup>+</sup>) and an Indole (EX527 Analogue) Reveals a Novel Mechanism of Histone Deacetylase Inhibition, *Journal of medicinal chemistry* 56, 963-969.
269. Jung, Y. J., Lee, J. E., Lee, A. S., Kang, K. P., Lee, S., Park, S. K., Lee, S. Y., Han, M. K., Kim, D. H., and Kim, W. (2012) SIRT1 overexpression decreases cisplatin-induced acetylation of NF-κB p65 subunit and cytotoxicity in renal proximal tubule cells, *Biochemical and Biophysical Research Communications* 419, 206-210.
270. Çakir, I. i., Perello, M., Lansari, O., Messier, N. J., Vaslet, C. A., and Nillni, E. A. (2009) Hypothalamic Sirt1 Regulates Food Intake in a Rodent Model System, *PloS one* 4, e8322.
271. Kettenes-van den Bosch, J. J., Hop, E., Overbeek, W., Underberg, W. J. M., Beijnen, J. H., and Bult, A. (1997) Degradation of suramin in aqueous solutions, *International Journal of Pharmaceutics* 155, 27-34.
272. Landry, J., and Sternglanz, R. (2003) Enzymatic assays for NAD-dependent deacetylase activities, *Methods* 31, 33-39.
273. Peng, C., Lu, Z., Xie, Z., Cheng, Z., Chen, Y., Tan, M., Luo, H., Zhang, Y., He, W., Yang, K., Zwaans, B. M. M., Tishkoff, D., Ho, L., Lombard, D., He, T.-C., Dai, J.,



- Verdin, E., Ye, Y., and Zhao, Y. (2011) The First Identification of Lysine Malonylation Substrates and Its Regulatory Enzyme, *Molecular & Cellular Proteomics* 10.
274. Borra, M. T., Langer, M. R., Slama, J. T., and Denu, J. M. (2004) Substrate Specificity and Kinetic Mechanism of the Sir2 Family of NAD<sup>+</sup>-Dependent Histone/Protein Deacetylases, *Biochemistry* 43, 9877-9887.
275. Avalos, J. L., Boeke, J. D., and Wolberger, C. (2004) Structural basis for the mechanism and regulation of Sir2 enzymes, *Molecular cell* 13, 639-648.
276. Roy, B. C., Banerjee, A. L., Swanson, M., Jia, X. G., Haldar, M. K., Mallik, S., and Srivastava, D. K. (2004) Two-prong inhibitors for human carbonic anhydrase II, *Journal of the American Chemical Society* 126, 13206-13207.
277. Roy, B. C., Hegge, R., Rosendahl, T., Jia, X., Lareau, R., Mallik, S., and Srivastava, D. K. (2003) Conjugation of poor inhibitors with surface binding groups: a strategy to improve inhibition, *Chem Commun (Camb)*, 2328-2329.
278. Banerjee, A. L., Tobwala, S., Haldar, M. K., Swanson, M., Roy, B. C., Mallik, S., and Srivastava, D. K. (2005) Inhibition of matrix metalloproteinase-9 by "multi-prong" surface binding groups, *Chem Commun (Camb)*, 2549-2551.
279. Zhou, Y., Zhang, H., He, B., Du, J., Lin, H., Cerione, R. A., and Hao, Q. (2012) The bicyclic intermediate structure provides insights into the desuccinylation mechanism of human sirtuin 5 (SIRT5), *The Journal of biological chemistry* 287, 28307-28314.
280. Middaugh, C. R., Mach, H., Burke, C. J., Volkin, D. B., Dabora, J. M., Tsai, P. K., Bruner, M. W., Ryan, J. A., and Marfia, K. E. (1992) Nature of the interaction of growth factors with suramin, *Biochemistry* 31, 9016-9024.
281. Alzani, R., Cozzi, E., Corti, A., Temponi, M., Trizio, D., Gigli, M., and Rizzo, V. (1995) Mechanism of suramin-induced deoligomerization of tumor necrosis factor .alpha., *Biochemistry* 34, 6344-6350.